The Inversion of the Radon Transform on the Rotational Group and Its Application to Texture Analysis

Der Fakultät für Mathematik und Informatik
der Technischen Universität Bergakademie Freiberg
eingereichte

DISSERTATION

zur Erlangung des akademischen Grades

doctor rerum naturalium
Dr. rer. nat.

vorgelegt

von Dipl.-Math. Ralf Hielscher
geboren am 09.06.1977 in Löbau

Freiberg, den 12.12.2006

Contents

1 Introduction

Radon Transforms. Tomographic methods like computed tomography, positron emission tomography, and X–ray tomography are well established and frequently used techniques in material science and medicine . They all base on the inversion of the one–dimensional Radon transform in $\mathbb{R}^d$, $d \in \mathbb{N}$,

$$\mathcal{R}\colon C_c(\mathbb{R}^d) \to C(\mathbb{R}^d \times \mathbb{S}^{d-1}), \quad \mathcal{R}f(\mathbf{x}, \boldsymbol{\xi}) = \int_{\mathbb{R}} f(\mathbf{x} + \tau\boldsymbol{\xi})\,\mathrm{d}\tau.$$

The inversion of the Radon transform in $\mathbb{R}^d$ is a classical ill–posed problem and has been analyzed by numerous authors (e.g. by Natterer, 1986; Gardner, 1995; Ramm and Katsevich, 1996).

A generalization of the one–dimensional Radon transform for the Lie–group SO(3) of all rotations in the three–dimensional Euclidean space is defined by

$$\mathcal{R}\colon C(\mathrm{SO}(3)) \to C(\mathbb{S}^2 \times \mathbb{S}^2), \quad \mathcal{R}f(\mathbf{h}, \mathbf{r}) = \int_{G(\mathbf{h},\mathbf{r})} f(\mathbf{g})\,\mathrm{d}\mathbf{g}$$

where

$$G(\mathbf{h}, \mathbf{r}) = \{\, \mathbf{g} \in \mathrm{O}(3) \mid \mathbf{g}\mathbf{h} = \mathbf{r} \,\}, \quad \mathbf{h}, \mathbf{r} \in \mathbb{S}^2,$$

defines a parameterization of all geodesics in SO(3). Its inversion is a key problem in *quantitative texture analysis* (QTA).

Quantitative Texture Analysis. The goal of QTA is the quantification of crystallographic preferred orientations in polycrystalline materials. In QTA two functions are used to describe crystallographic preferred orientations in a specimen — the *orientation density function* (ODF) $f \in C(\mathrm{SO}(3))$ and the *pole density function* (PDF) $P \in C(\mathbb{S}^2 \times \mathbb{S}^2)$. We assume here that the ODF and the PDF are continuous functions to avoid the problem of undefined pointwise evaluation for functions in $L^1(\mathrm{SO}(3))$ and $L^1(\mathbb{S}^2 \times \mathbb{S}^2)$. This issue is discussed in more detail in Section 4.2. The ODF $\mathbf{g} \to f(\mathbf{g})$ is used to model the distribution of crystal orientations $\mathbf{g} \in \mathrm{SO}(3)$ by volume within the polycrystalline specimen whereas the PDF $(\mathbf{h}, \mathbf{r}) \mapsto P(\mathbf{h}, \mathbf{r})$ is used to model the distribution of the crystal lattice plane normal vectors $\mathbf{h} \in \mathbb{S}^2$ that are in line with the direction $\mathbf{r} \in \mathbb{S}^2$ by volume. Updating the rather symbolic notation by Roe (1965) and Bunge (1965) the relationship between the ODF f and the PDF P assigned to a specific specimen has been expressed in terms of the one–dimensional Radon transform on SO(3)

$$P(\mathbf{h}, \mathbf{r}) = \mathcal{X}f(\mathbf{h}, \mathbf{r}) = \frac{1}{2}\big(\mathcal{R}f(\mathbf{h}, \mathbf{r}) + \mathcal{R}f(-\mathbf{h}, \mathbf{r})\big), \tag{1.1}$$

by Schaeben and v.d. Boogaart (2003).

Since the PDF $P(\mathbf{h}_i, \mathbf{r}_{ij})$ is experimental accessible for discrete directions $\mathbf{h}_i, \mathbf{r}_{ij} \in \mathbb{S}^2$, $i = 1, \ldots, N$, $j = 1, \ldots, N_i$ by diffraction techniques an estimate of the ODF can be obtained by solving the inverse problem

$$\mathcal{X}f(\mathbf{h}_i, \mathbf{r}_{ij}) = P(\mathbf{h}_i, \mathbf{r}_{ij}), \quad i = 1, \ldots, N,\ j = 1, \ldots, N_i. \tag{1.2}$$

However, the exact values for $P(\mathbf{h}_i, \mathbf{r}_{ij})$ are generally not known and only diffraction counts are available. These diffraction counts differ from the exact values of $P(\mathbf{h}_i, \mathbf{r}_{ij})$ by unknown measurement errors, an in general known background radiation and unknown normalization coefficients. The latter depend only on the specific crystal lattice plane $\mathbf{h}_i$, $i = 1, \ldots, N$ but not on the direction $\mathbf{r}_{ij}$, $j = 1, \ldots, N_i$.

The objective of this thesis is to analyze whether and to which extent an ODF can be reconstructed from those diffraction counts. Eventually we derive an algorithm for ODF estimation that allows for arbitrary measurement designs, robust estimation of the normalization coefficients and the estimation of ODFs with very sharp peaks, i.e. with peaks that have a halfwidth less then five degrees. For these purposes the following road map was processed.

Functions on $\mathbb{S}^2$ and SO(3). In Chapter 2 we introduce harmonic functions on the domains $\mathbb{S}^2$, $\mathbb{S}^2 \times \mathbb{S}^2$, SO(3) and O(3) with special emphasis on their relationships. Moreover we construct Sobolev–Hilbert spaces over these domains following the approach of Freeden (1998), characterize them in terms of the Laplace–Beltrami operator and formulate the corresponding lemma of Sobolev.

The Radon Transform on SO(3). Chapter 3 compiles the basic properties of the Radon transform on SO(3). Based on the Fourier representation of the Radon transform on SO(3) we characterize it in Theorem 3.10 as an isomorphism between specific Sobolev–Hilbert spaces on the domains SO(3) and $\mathbb{S}^2 \times \mathbb{S}^2$ and clarify the ill posedness of the inversion problem (1.2) according to Louis (1989). In Proposition 3.11 we extend the characterization of the range of the Radon transform as given by Nikolayev and Schaeben (1999) to the case of Sobolev–Hilbert spaces. In Theorem 3.16 we characterize the adjoint operator of the Radon transform as an integral operator and derive a classical inversion formula for the Radon transform on SO(3) (cf. Helgason, 1984, Theorem 3.13). Moreover we prove in Theorem 3.19 that the inversion of the Radon transform is not a local operator. Finally, we extend the Radon transform on SO(3) to the class of absolute integrable functions $L^1(\mathrm{SO}(3))$ (cf. Theorem 3.20) and to quotient spaces $\mathrm{SO}(3)/Q$, where $Q \subseteq \mathrm{SO}(3)$ is a finite subgroup. The subgroup Q is later used to model crystal symmetries.

A second point in Chapter 3 are radially symmetric functions on the domains $\mathbb{S}^2$ and SO(3). It is well known that the Radon transform maps radially symmetric functions on SO(3) onto radially symmetric functions on $\mathbb{S}^2$. This relationship can be expressed

either by an integral equation (cf. Lemma 3.7) or in terms of Chebyshev and Legendre coefficients (cf. Lemma 3.13). In combination both of the connections provide a mean to derive explicit formulae and recurrence formulae for radially symmetric function on one of the domain if the corresponding explicit formulae and recurrence formulae on the just other domain are known. This method has been applied in Section 3.4 to the Abel–Poisson kernel, the de la Vallée Poussin kernel, the von Mises–Fisher kernel and the locally supported kernel. This way we extend the the list of pairs of radially symmetric functions on SO(3) and $\mathbb{S}^2$ given by Matthies et al. (1987), Schaeben and v.d. Boogaart (2003) and others.

The PDF–to–ODF Inversion Problem. In Sections 4.1 and 4.2 we give a brief account to diffraction at crystallographic lattice planes and derive a simple statistical model for diffraction at polycrystalline specimen based on the Poisson distribution (cf. equation (4.6)). Based on this model we formulate the PDF–to–ODF inversion problem as a parameter estimation problem for a given random sample of diffraction counts.

In Section 4.3 we discuss the inherent ambiguity of the PDF–to–ODF inversion problem. In particular, we analyze the impact of distinct origins for its ambiguity which are: Friedel's law, the kernel of the Radon transform on O(3), the clustered sampling design, superposed pole figures, unknown normalization coefficients, and measurement errors (cf. Wenk et al., 1987) and illustrate them by examples. In particular, we show in Proposition 3.11 that the range of ODFs that corresponds to a specific PDF is in general unbounded with respect to the maximum norm and the L^2–norm, but bounded with respect to the L^1–norm.

In Section 4.4 we are concerned with the question about the variation width of solutions of the inverse problem (1.1) for a given number of complete and exact pole figures $P(\mathbf{h}_i, \circ)$, $i = 1, \ldots, N$. This question was first posed by Matthies (1982) and first numerical results where obtained by Schaeben (1994). Our approach is based on the concept of the *concentration* of a density function in a certain subset of its domain with respect to a weighting function (cf. Definition 4.13). In Theorem 4.14 we give lower and upper bounds for the concentration of an ODF in terms of concentrations of corresponding pole figures. In the subsequent paragraphs Theorem 4.14 is applied to the cases of triclinic and orthorhombic crystal symmetry and explicit inequalities about the variance of the ODF and about its mass that is concentrated in a neighborhood of a specific orientation are given (cf. Proposition 4.21 and 4.22).

In Section 4.5 a statistical approach to the PDF–to–ODF inversion problem is discussed. The ODF estimator that is derived in this section differs from the non negatively constrained, regularized least squares approach (cf. Bernier and Miller, 2006) only by some weights that are chosen according to the variance of the measurement error of the diffraction counts. Moreover, the presented estimator (4.32) incorporates the normalization coefficients as unknown parameters, i.e. they are estimated simultaneously. We call this estimator *modified least squares ODF estimator* (MLS ODF estimator).

Implementation of the MLS ODF Estimator. Chapter 5 is devoted to the numerical implementation of the MLS ODF estimator presented in Section 4.5. In contrast to the commonly chosen discretisations of the function space of ODFs by harmonic functions (Bunge, 1969), indicator functions (Schaeben, 1994), or finite elements (Bernier and Miller, 2006) we propose a discretisation by radially symmetric functions. Based on this discretisation we adapt the modified steepest descent algorithm to the MLS ODF estimator (4.32) and derive Algorithm 5. In Theorem 5.17 we prove that Algorithm 5 has the numerical complexity $\mathcal{O}(\bar{N} + M + L^3 \ln^2 L)$ per iteration where $\bar{N}$ denotes the total number of measured diffraction counts, M denotes the total number of ansatz functions of the discretisation, and L denotes the bandwidth of the ansatz functions. Algorithm 5 makes use of the non–equispaced fast Fourier transform on the domains SO(3) and $\mathbb{S}^2$. These Fourier techniques are introduced in Section 5.1 following the works of Potts and Steidl (2003); Keiner (2005); Vollrath (2006).

In the final Sections 5.4 and 5.5 Algorithm 5 is tested for various settings of input data and parameters. In particular we show that Algorithm 5 is well suited for the estimation of sharp ODFs and diffraction data measured for highly irregular sampling layouts. Case studies of Algorithm 5 applied to two real world problems, presented in Section 5.5, complete the thesis.

Danksagung. Die Arbeit wäre nicht zustande gekommen ohne die tolle Betreuung durch Prof. Dr. H. Schaeben. Er war nicht nur der Initiator der Arbeit, sondern hat auch in vielen fruchtbaren Diskussionen immer neue Ideen und Richtungen aufgezeigt. Insbesondere habe ich es Prof. Dr. H. Schaeben zu verdanken, dass die Arbeit auch unter Geologen und Materialwissenschaftlern Interesse und Anwendung findet. Nicht zu vergessen ist außerdem sein nimmermüder Kampf mit dem Ralf'schen Englisch und die Tatsache, dass er mir in unglaublicher Weise den Rücken freigehalten hat, so dass ich mich in den vergangenen Jahren ausschließlich der Promotion widmen konnte.

Entscheidend zum Gelingen der Arbeit hat das Dreigespann Prof. Dr. J. Prestin, Prof. Dr. D. Potts und Prof. Dr. K. G. van den Boogaart beigetragen. Die Diskussionen mit ihnen waren für mich immer eine große Bereicherung und ein großes Vergnügen. Sich haben mich vor allem dazu angeregt, dass Problem aus vielen verschiedenen Blickwinkeln zu betrachten. Der Lübecker und Chemnitzer Arbeitsgruppe möchte ich weiterhin für die Bereitstellung der `NFFT`–Bibliothek danken, sowie für alle Diskussionen über schnelle Algorithmen. Ohne ihr algorithmisches und softwaretechnisches Knowhow wäre die Implementierung der in der Arbeit vorgestellten Methode nicht möglich gewesen.

Entscheidend zum theoretischen Teil dieser Arbeit haben außerdem Dr. S. Bernstein und Dr. J. Wirth beigetragen, denen ich für die erhellenden Diskussionen danken möchte.

I was very glad to cooperate with Dr. D. Chateigner, Dr. J. Fundenberger, Dr. U. Garbe, Dr. F. Heilbronner, Dr. D. Nikolaev, Dr. C. Scheffzück and Dr. K. Walter. As

material scientists, geologists and physicists they gave me an understanding about the practical point of texture analysis. In particular, they provided me with real world data to test my algorithm.

Danken möchte ich auch allen Bewohnern der 3. Etage des Humboldt–Baus für all die lustigen Zeiten zwischendurch und insbesondere allen Essengehern und Frisbeespielern, welche mich immer wieder der Krake Computer entrissen haben.

Zu großem Dank bin ich der Deutschen Forschungsgesellschaft für die finanzielle Unterstützung meiner Dissertation im Rahmen des Projektes "Hochauflösende Texturanalyse" SCHA 465/15 und PR 331/11 verpflichtet.

2 Functions on $\mathbb{S}^2$ and SO(3)

In this introductory chapter we provide some basic notations concerning the two–dimensional sphere $\mathbb{S}^2$ *and the rotational group in three dimensions* SO(3)*, and compile some basic facts about special functions on both domains. The major special functions on the sphere* $\mathbb{S}^2$ *are the spherical harmonics which are closely related to the Legendre polynomials on the interval* $[-1, 1]$*. Following the books by Freeden (1998) and Müller (1966) we give an outline of their basic properties. Analogously we proceed with the Chebyshev polynomials and the Wigner functions on* SO(3)*. Here our approach is based on representation theory as presented in the books by Helgason (1999), Gurarie (1992) or Vilenkin and Klimyk (1991). We complete this chapter by introducing the Laplace–Beltrami operator on the domains* $\mathbb{S}^2$ *and* SO(3) *which leads us to Sobolev spaces and pseudodifferential operators.*

2.1 Parameterization of the Domains $\mathbb{S}^2$ and SO(3)

The Sphere. All through this thesis we denote by $\mathbf{e}_1, \mathbf{e}_2, \mathbf{e}_3 \in \mathbb{R}^3$ the canonical basis in $\mathbb{R}^3$ and by $\mathbb{S}^2 = \{\, \boldsymbol{\xi} \in \mathbb{R}^3 \mid \|\boldsymbol{\xi}\| = 1 \,\}$ the two–dimensional unit sphere. Every element $\boldsymbol{\xi} = \xi_1\mathbf{e}_1 + \xi_2\mathbf{e}_2 + \xi_3\mathbf{e}_3 \in \mathbb{S}^2$ of the two–dimensional sphere can be described by its polar coordinates $(\theta, \rho) \in [0, \pi] \times [0, 2\pi)$ which are defined by the equality

$$\boldsymbol{\xi} = \sin\theta\cos\rho\,\mathbf{e}_1 + \sin\theta\sin\rho\,\mathbf{e}_2 + \cos\theta\,\mathbf{e}_3.$$

Let $\boldsymbol{\xi}, \boldsymbol{\xi}' \in \mathbb{S}^2$ be two unit vectors and $(\theta, \rho), (\theta', \rho') \in [0, \pi] \times [0, 2\pi)$ its polar coordinates. Then the inner product $\boldsymbol{\xi} \cdot \boldsymbol{\xi}'$ and the angle $\measuredangle(\boldsymbol{\xi}, \boldsymbol{\xi}')$ between both vectors are related to each other by

$$\boldsymbol{\xi} \cdot \boldsymbol{\xi}' = \cos\measuredangle(\boldsymbol{\xi}, \boldsymbol{\xi}') = \cos\theta\cos\theta' + \sin\theta\sin\theta'\cos(\rho - \rho'). \tag{2.1}$$

Let $S_1, S_2 \subseteq \mathbb{S}^2$ be two subsets of $\mathbb{S}^2$. Then we define the angle between both sets as the minimal angle between any two points of both sets

$$\measuredangle(S_1, S_2) = \inf_{\boldsymbol{\xi} \in S_1,\, \boldsymbol{\xi}' \in S_2} \measuredangle(\boldsymbol{\xi}, \boldsymbol{\xi}').$$

The canonical surface element $\mathrm{d}\boldsymbol{\xi}$ of the two–dimensional sphere reads in polar coordinates as $\mathrm{d}\boldsymbol{\xi} = \mathrm{d}\rho \wedge \sin\theta\,\mathrm{d}\theta$ and one verifies

$$\int_{\mathbb{S}^2} 1\,\mathrm{d}\boldsymbol{\xi} = \int_0^{\pi}\int_0^{2\pi} 1\,\mathrm{d}\rho\sin\theta\,\mathrm{d}\theta = 4\pi. \tag{2.2}$$

The Rotational Group. We denote the group of real valued, orthogonal 3×3 matrixes by O(3) and the subgroup of all matrixes with determinant 1 by $\mathrm{SO}(3) \subseteq \mathrm{O}(3)$. The elements of SO(3) can be interpreted as proper rotations in $\mathbb{R}^3$. The group O(3) additionally contains the concatenations of proper rotations and the inversion $-\mathrm{Id} \in \mathrm{O}(3)$ which are sometimes called *improper rotations*.

Parameterization of the group SO(3) can be done in various ways. The most intuitive possibility of parameterization is to specify a rotation $\mathbf{g} \in \mathrm{SO}(3)$ by a rotational axis $\boldsymbol{\eta} \in \mathbb{S}^2$ and a rotational angle $\omega \in [0, \pi]$. We will write $\mathbf{g} = \mathrm{Rot}_{\boldsymbol{\eta}}(\omega)$ in this case. Let $\mathbf{g} \in \mathrm{SO}(3)$. Then the rotational angle $\measuredangle\mathbf{g}$ of $\mathbf{g}$ is well defined and satisfies

$$\measuredangle\mathbf{g} = \arccos \frac{-1 + \operatorname{Tr} \mathbf{g}}{2},$$

where $\operatorname{Tr} \mathbf{g}$ denotes the trace of the matrix $\mathbf{g}$.

Let $\mathrm{Rot}_{\boldsymbol{\eta}_1}(\omega_1)$ and $\mathrm{Rot}_{\boldsymbol{\eta}_2}(\omega_2)$ be two rotations with rotational axes $\boldsymbol{\eta}_1, \boldsymbol{\eta}_2 \in \mathbb{S}^2$ and rotational angles $\omega_1, \omega_2 \in [0, \pi]$, respectively. Then the concatenation of both rotations yields a rotation

$$\mathrm{Rot}_{\boldsymbol{\eta}_3}(\omega_2) = \mathrm{Rot}_{\boldsymbol{\eta}_1}(\omega_1)\mathrm{Rot}_{\boldsymbol{\eta}_2}(\omega_2)$$

with rotational axis $\boldsymbol{\eta}_3 \in \mathbb{S}^2$ and rotational angle $\omega_3 \in [0, \pi]$ given by

$$\boldsymbol{\eta}_3 = \sin\frac{\omega_1}{2}\cos\frac{\omega_2}{2}\boldsymbol{\eta}_2 + \sin\frac{\omega_2}{2}\cos\frac{\omega_1}{2}\boldsymbol{\eta}_1 + \cos\frac{\omega_1}{2}\cos\frac{\omega_2}{2}\boldsymbol{\eta}_1 \times \boldsymbol{\eta}_2, \tag{2.3}$$

$$\cos\frac{\omega_3}{2} = \cos\frac{\omega_1}{2}\cos\frac{\omega_2}{2} - \sin\frac{\omega_1}{2}\sin\frac{\omega_2}{2}\boldsymbol{\eta}_1 \cdot \boldsymbol{\eta}_2. \tag{2.4}$$

The rotational angle between two rotations $\mathbf{g}_1, \mathbf{g}_2 \in \mathrm{SO}(3)$

$$\measuredangle(\mathbf{g}_1, \mathbf{g}_2) := \measuredangle\mathbf{g}_1^{-1}\mathbf{g}_2$$

defines a metric on the group SO(3). Analogously to the spherical case we define the distance of two subset $S_1, S_2 \subseteq \mathrm{SO}(3)$ as

$$\measuredangle(S_1, S_2) = \inf_{\mathbf{g}_1 \in S_1,\, \mathbf{g}_2 \in S_2} \measuredangle(\mathbf{g}_1, \mathbf{g}_2).$$

Application of a rotation $\mathbf{g} \in \mathrm{SO}(3)$ to a three–dimensional unit vector $\boldsymbol{\xi} \in \mathbb{S}^2$ yields a three–dimensional unit vector $\mathbf{g}\boldsymbol{\xi} \in \mathbb{S}^2$ and we have for any two rotations $\mathbf{g}_1, \mathbf{g}_2 \in \mathrm{SO}(3)$ and for any two unit vectors $\boldsymbol{\xi}_1, \boldsymbol{\xi}_2 \in \mathbb{S}^2$ the continuity inequality

$$\measuredangle(\mathbf{g}_1\boldsymbol{\xi}_1, \mathbf{g}_2\boldsymbol{\xi}_2) \leq \measuredangle(\mathbf{g}_1, \mathbf{g}_2) + \measuredangle(\boldsymbol{\xi}_1, \boldsymbol{\xi}_2). \tag{2.5}$$

Using the parameterization in terms of a rotational axis $\boldsymbol{\eta} \in \mathbb{S}^2$ and a rotational angle $\omega \in [0, \pi]$ the vector $\mathrm{Rot}_{\boldsymbol{\eta}}(\omega)\,\boldsymbol{\xi}$ can be expressed as

$$\mathrm{Rot}_{\boldsymbol{\eta}}(\omega)\,\boldsymbol{\xi} = \cos\omega\,\boldsymbol{\xi} + \sin\omega\,\boldsymbol{\eta} \times \boldsymbol{\xi} + (1 - \cos\omega)(\boldsymbol{\eta} \cdot \boldsymbol{\xi})\,\boldsymbol{\eta}.$$

The canonical volume element on SO(3) given by $\mathrm{d}\mathbf{g} = 4\,\mathrm{d}\boldsymbol{\eta} \wedge \sin^2 \frac{\omega}{2}\,\mathrm{d}\omega$ in terms of the rotational axis rotational – angle parameterization $\mathbf{g} = \mathrm{Rot}_{\boldsymbol{\eta}}(\omega)$ establishes a rotational invariant measure on SO(3) which due to

$$\int_{\mathrm{SO}(3)} 1\,\mathrm{d}\mathbf{g} = 4 \int_0^\pi \int_{\mathbb{S}^2} 1\,\mathrm{d}\boldsymbol{\eta} \sin^2 \frac{\omega}{2}\,\mathrm{d}\omega = 8\pi^2 \tag{2.6}$$

is normalized to $8\pi^2$ in contrast to the classical chosen normalization of Haar measures.

Euler angles provide an alternative parameterization of rotations. In our paper we utilize them for an explicit formula of the Wigner functions on SO(3) (cf. Section 2.5) and for the visualization of functions defined on SO(3). Since there are miscellaneous conventions of Euler angles we have to stick to a specific one. In our work we will follow the convention by Matthies et al. (1987), Varshalovich et al. (1988) or Kostelec and Rockmore (2003) where the Euler angles (α, β, γ) with $\alpha, \gamma \in [0, 2\pi)$ and $\beta \in [0, \pi]$ of a rotation $\mathbf{g} \in \mathrm{SO}(3)$ are defined such that the following equation is satisfied

$$\mathbf{g} = \mathrm{Rot}_{\mathbf{e}_3}(\alpha)\mathrm{Rot}_{\mathbf{e}_2}(\beta)\mathrm{Rot}_{\mathbf{e}_3}(\gamma).$$

One verifies this convention of Euler angles is consistent with polar coordinates in $\mathbb{S}^2$ in the sense that the vector $\mathrm{Rot}_{\mathbf{e}_3}(\alpha)\mathrm{Rot}_{\mathbf{e}_1}(\beta)\mathrm{Rot}_{\mathbf{e}_3}(\gamma)\,\mathbf{e}_3$ is given in polar coordinates by (β, α).

There are a lot of other parameterizations of SO(3) like Rodriguez parameters, Cayley–Klein parameters, quaternions and Miller indices each of which has its special advantages. However since we will not make explicit use of them we rather refer to the works of Morawiec (2004, Sec. 2) and Meister and Schaeben (2004).

2.2 Legendre Polynomials

The *Legendre polynomials* $\mathcal{P}_l \colon [-1, 1] \to \mathbb{R}$, $l \in \mathbb{N}_0$, are the key special functions in harmonic analysis on the two–dimensional sphere. They are characterized as classical orthogonal polynomials on the interval $[-1, 1]$ by the properties

1. $\mathcal{P}_l$ is a polynomial of degree l,
2. $\int_{-1}^1 \mathcal{P}_l(t)\mathcal{P}_{l'}(t)\,\mathrm{d}t = \frac{2}{2l+1}\delta_{l,l'}$ for $l, l' \in \mathbb{N}_+$

and hence establish an orthogonal basis in $L^2([-1, 1])$. Let $f \in L^2([-1, 1])$. Then f has a well defined series expansion

$$f = \sum_{l=0}^{\infty} \hat{f}(l)\mathcal{P}_l$$

with *Legendre coefficients* $\hat{f}(l)$, $l \in \mathbb{N}_0$, determined by

$$\hat{f}(l) = \frac{2}{2l+1} \int_{-1}^1 f(t)\mathcal{P}_l(t)\,\mathrm{d}t. \tag{2.7}$$

By property 2 the Legendre polynomials are normed to $\mathcal{P}_l(1) = 1$, $l \in \mathbb{N}_0$. The three–term recurrence satisfied by the Legendre Polynomials reads

$$(l+1)\mathcal{P}_{l+1}(t) + l\mathcal{P}_{l-1}(t) = (2l+1)t\mathcal{P}_l(t), \quad t \in [-1,1],\ l \in \mathbb{N}_0, \tag{2.8}$$

with initial polynomials $\mathcal{P}_{-1} = \mathcal{P}_0 = 1$. The derivatives of the Legendre polynomials satisfy the recurrence formula (cf. Freeden, 1998, Sec. 3.2)

$$\frac{\mathrm{d}}{\mathrm{d}t}\Big(\mathcal{P}_{l+1}(t) - \mathcal{P}_{l-1}(t)\Big) = (2l+1)\mathcal{P}_l(t), \quad t \in [-1,1]. \tag{2.9}$$

In the next section we will also need the *associated Legendre Polynomials* $\mathcal{P}_l^k \colon [-1,1] \to \mathbb{R}$, $l, k \in \mathbb{N}_0$, $k \le l$, which are defined as the derivatives of the Legendre polynomials by

$$\mathcal{P}_l^k(t) = \left(\frac{(l-k)!}{(l+k)!}\right)^{1/2} (1-t^2)^{k/2} \frac{d^k}{dt^k}\mathcal{P}_l(t), \quad t \in [-1,1].$$

2.3 Spherical Harmonics

The following summary on spherical harmonics is taken from the monograph by Freeden (1998). Let $\boldsymbol{\xi} \in \mathbb{S}^2$ and let $(\theta, \rho) \in [0,\pi] \times [0, 2\pi)$ be its polar coordinates. Then for any $l \in \mathbb{N}_0$ and $k = -l, \ldots, l$, the *spherical harmonics* of degree l are defined as

$$\mathcal{Y}_l^k(\boldsymbol{\xi}) = \sqrt{\frac{2l+1}{4\pi}}\mathcal{P}_l^{|k|}(\cos\theta)e^{ik\rho}.$$

The subspace $\mathrm{Harm}_l(\mathbb{S}^2) = \mathrm{span}\left\{\mathcal{Y}_l^{-l}, \ldots, \mathcal{Y}_l^l\right\}$ of all spherical harmonics with a fixed degree $l \in \mathbb{N}_0$ is called *harmonic space* of degree l. The harmonic spaces $\mathrm{Harm}_l(\mathbb{S}^2)$, $l \in \mathbb{N}_0$ provide a complete system of rotational invariant, irreducible subspaces of $L^2(\mathbb{S}^2)$, i.e.

$$L^2(\mathbb{S}^2) = \mathrm{clos}_{L^2} \bigoplus_{l=0}^{\infty} \mathrm{Harm}_l(\mathbb{S}^2)$$

and for every rotation $\mathbf{g} \in \mathrm{SO}(3)$ and every function $f \in \mathrm{Harm}_l(\mathbb{S}^2)$, $l \in \mathbb{N}_0$, we have $f(\mathbf{g}\circ) \in \mathrm{Harm}_l(\mathbb{S}^2)$. Moreover, the spherical harmonics satisfy the orthogonality relationship

$$\int_{\mathbb{S}^2} \mathcal{Y}_l^k(\boldsymbol{\xi})\overline{\mathcal{Y}_{l'}^{k'}(\boldsymbol{\xi})}\,\mathrm{d}\boldsymbol{\xi} = \delta_{ll'}\delta_{kk'},$$

and hence, the function system $\mathcal{Y}_l^k$, $l \in \mathbb{N}_0$, $k = -l, \ldots, l$ forms an orthonormal basis of $L^2(\mathbb{S}^2)$. We define the Fourier coefficients $\hat{f}(l,k)$ of a function $f \in L^2(\mathbb{S}^2)$ as the coefficients with respect to the basis of spherical harmonics, i.e.

$$\hat{f}(l,k) = \int_{\mathbb{S}^2} f(\boldsymbol{\xi})\overline{\mathcal{Y}_l^k(\boldsymbol{\xi})}\,\mathrm{d}\boldsymbol{\xi}, \quad l \in \mathbb{N}_0, k = -l, \ldots, l.$$

For the vector of functions $(\mathcal{Y}_l^{-l}, \ldots, \mathcal{Y}_l^l)^T$ we will write just $\mathcal{Y}_l$. The well known addition theorem can now be expressed as

$$\frac{2l+1}{4\pi}\mathcal{P}_l(\boldsymbol{\xi}\cdot\boldsymbol{\eta}) = \mathcal{Y}_l(\boldsymbol{\xi})^T\overline{\mathcal{Y}_l(\boldsymbol{\eta})}, \quad \boldsymbol{\eta},\boldsymbol{\xi}\in\mathbb{S}^2,\ l\in\mathbb{N}_0. \tag{2.10}$$

Definition 2.1. A function $f\colon \mathbb{S}^2\to\mathbb{R}$ is called *radially symmetric* with center $\boldsymbol{\xi}_0\in\mathbb{S}^2$ if it exists a function $F\colon [-1,1]\to\mathbb{R}$ such that

$$f(\boldsymbol{\xi}) = F(\boldsymbol{\xi}\cdot\boldsymbol{\xi}_0), \quad \boldsymbol{\xi}\in\mathbb{S}^2,$$

i.e. if $f(\boldsymbol{\xi})$ depends only on the angle between $\boldsymbol{\xi}$ and $\boldsymbol{\xi}_0$.

Lemma 2.2. *For any radially symmetric function $Y_l\in\mathrm{Harm}_l(\mathbb{S}^2)$ with center $\boldsymbol{\xi}_0\in\mathbb{S}^2$ we have*

$$Y_l(\boldsymbol{\xi}) = Y_l(\boldsymbol{\xi}_0)\mathcal{P}_l(\boldsymbol{\xi}\cdot\boldsymbol{\xi}_0), \quad \boldsymbol{\xi}\in\mathbb{S}^2. \tag{2.11}$$

Let $f\in L^2(\mathbb{S}^2)$ be a radially symmetric function with center $\boldsymbol{\xi}_0\in\mathbb{S}^2$. Then

$$F(\boldsymbol{\xi}\cdot\boldsymbol{\xi}_0) = f(\boldsymbol{\xi}), \quad \boldsymbol{\xi}\in\mathbb{S}^2, \tag{2.12}$$

defines a square integrable function $F\in L^2(\mathbb{S}^2)$ and the mapping $f\mapsto F$ defines an isomorphism between the subspace of radially symmetric functions in $L^2(\mathbb{S}^2)$ with center $\boldsymbol{\xi}_0$ and the space $L^2([-1,1])$. In particular, f has a well defined expansion into Legendre polynomials

$$f(\boldsymbol{\xi}) = \left(\sum_{l=0}^{\infty}\hat{F}(l)\mathcal{P}_l\right)(\boldsymbol{\xi}\cdot\boldsymbol{\xi}_0), \quad \boldsymbol{\xi}\in\mathbb{S}^2, \tag{2.13}$$

where $\hat{F}(l)$, $l\in\mathbb{N}_0$ are the Legendre coefficients of the F.

Proof. Since the harmonic space $\mathrm{Harm}_l(\mathbb{S}^2)$ is irreducible the subspace of radially symmetric functions with center $\boldsymbol{\xi}_0\in\mathbb{S}^2$ in $\mathrm{Harm}_l(\mathbb{S}^2)$ is one–dimensional. Due to the addition theorem this subspaces is spanned by the Legendre polynomial $\mathcal{P}_l(\boldsymbol{\xi}_0\cdot\circ)$ which implies equation (2.11).

With $F\colon[-1,1]\to\mathbb{R}$ as defined in equation (2.12) we have

$$\int_{\mathbb{S}^2}|f(\boldsymbol{\xi})|^2\,\mathrm{d}\boldsymbol{\xi} = \int_{\mathbb{S}^2}|F(\boldsymbol{\xi}\cdot\boldsymbol{\xi}_0)|^2\,\mathrm{d}\boldsymbol{\xi} = \int_0^{\pi}|F(\cos\theta)|^2\sin\theta\,\mathrm{d}\theta = \int_{-1}^{1}|F(t)|^2\,\mathrm{d}t$$

and hence $f\mapsto F$ is the described isomorphism. □

An important consequence of Lemma 2.2 is the following spherical mean value theorem (cf. Freeden, 1998, equation 3.6.15).

Theorem 2.3 (spherical mean value theorem)**.** *Let $l \in \mathbb{N}_0$ and $\boldsymbol{\xi}, \boldsymbol{\xi}_0 \in \mathbb{S}^2$. Then every harmonic function $Y_l \in \mathrm{Harm}_l(\mathbb{S}^2)$ of order $l \in \mathbb{N}_0$ satisfies*

$$\frac{1}{2\pi} \int_0^{2\pi} Y_l(\mathrm{Rot}_{\boldsymbol{\xi}_0}(\omega)\boldsymbol{\xi}) \,\mathrm{d}\omega = \mathcal{P}_l(\boldsymbol{\xi} \cdot \boldsymbol{\xi}_0) Y_l(\boldsymbol{\xi}_0). \tag{2.14}$$

Proof. The integral on the left hand side of equation (2.14) defines a radially symmetric function in $\mathrm{Harm}_l(\mathbb{S}^2)$ with center $\boldsymbol{\xi}_0$. Now the assertion follows from equation (2.11). □

The Funk–Hecke formula generalizes the spherical mean value theorem to convolutions with arbitrary absolutely integrable, radially symmetric functions. However, we will formulate it only for square integrable functions and refer for a complete proof to Freeden (1998, Theorem 3.6.1).

Theorem 2.4 (Funk–Hecke)**.** *Let $f \in L^2(\mathbb{S}^2)$ be a radially symmetric function with center $\boldsymbol{\xi}_0 \in \mathbb{S}^2$ and let $F\colon [-1,1] \to \mathbb{R}$ be defined by $F(\boldsymbol{\xi}_0 \cdot \boldsymbol{\xi}) = f(\boldsymbol{\xi})$. Then for any $l \in \mathbb{N}_0$, $k = -l, \ldots, l$ we have*

$$\frac{2l+1}{4\pi} \int_{\mathbb{S}^2} F(\boldsymbol{\xi}_0 \cdot \boldsymbol{\xi}) \mathcal{Y}_l^k(\boldsymbol{\xi}) \,\mathrm{d}\boldsymbol{\xi} = \hat{F}(l) \mathcal{Y}_l^k(\boldsymbol{\xi}_0), \tag{2.15}$$

where $\hat{F}$ denotes the Legendre coefficients of F. Let $\boldsymbol{\eta} \in \mathbb{S}^2$ be some unit vector. Then the Funk–Hecke formula reads as

$$\frac{2l+1}{4\pi} \int_{\mathbb{S}^2} F(\boldsymbol{\xi} \cdot \boldsymbol{\xi}_0) \mathcal{P}_l(\boldsymbol{\xi} \cdot \boldsymbol{\eta}) \,\mathrm{d}\boldsymbol{\xi} = \hat{F}(l) \mathcal{P}_l(\boldsymbol{\eta} \cdot \boldsymbol{\xi}_0). \tag{2.16}$$

Proof. By the addition theorem we have for all $l \in \mathbb{N}_0$, $k = -l, \ldots, l$ the equality

$$\frac{2l+1}{4\pi} \int_{\mathbb{S}^2} \mathcal{P}_l(\boldsymbol{\xi} \cdot \boldsymbol{\xi}_0) \mathcal{Y}_l^k(\boldsymbol{\xi}) \,\mathrm{d}\boldsymbol{\xi} = \int_{\mathbb{S}^2} \left(\sum_{k'=-l}^{l} \mathcal{Y}_l^{k'}(\boldsymbol{\xi}_0) \overline{\mathcal{Y}_l^{k'}(\boldsymbol{\xi})} \right) \mathcal{Y}_l^k(\boldsymbol{\xi}) \,\mathrm{d}\boldsymbol{\xi} = \mathcal{Y}_l^k(\boldsymbol{\xi}_0).$$

Expanding F into its Legendre series and taking into account the orthogonality of the harmonic spaces $\mathrm{Harm}_l(\mathbb{S}^2)$ we obtain equation (2.15).

Equation (2.16) follows directly from equation (2.15) by multiplication with $\mathcal{Y}_l^k(\boldsymbol{\eta})$ and summation over all $k = -l, \ldots, l$. □

2.4 Chebyshev Polynomials

The *Chebyshev polynomials of second kind* $\mathcal{U}_l\colon [-1,1] \to \mathbb{R}$ are of similar importance for harmonic analysis on the rotational group SO(3) as the Legendre polynomials are for harmonic analysis on the two–dimensional sphere. They are defined as orthogonal polynomials on the interval $[-1,1]$ with respect to the weighting function $t \mapsto \sqrt{1-t^2}$, i.e. the Chebyshev polynomials of second kind are defined by the properties

1. $\mathcal{U}_l\colon [-1,1] \to \mathbb{R}$ is a polynomial of degree l,
2. $\int_{-1}^{1} \mathcal{U}_l(t)\mathcal{U}_{l'}(t)\sqrt{1-t^2}\,\mathrm{d}t = \frac{\pi}{2}\delta_{l,l'}$ for $l, l' \in \mathbb{N}_+$.

Consequently, any function $f \in L^2([-1,1], \sqrt{1-t^2})$ has a well defined series expansion

$$F = \sum_{l=0}^{\infty} \hat{F}(l)\mathcal{U}_l$$

with *Chebyshev coefficients* $\hat{F}(l)$, $l \in \mathbb{N}_0$ determined by

$$\hat{F}(l) = \frac{2}{\pi}\int_{-1}^{1} F(t)\mathcal{U}_l(t)\sqrt{1-t^2}\,\mathrm{d}t. \tag{2.17}$$

Substituting t by $\cos\omega$ the Chebyshev polynomials have a simple representation in terms of trigonometric functions

$$\mathcal{U}_l(\cos\omega) = \frac{\sin(l+1)\omega}{\sin\omega}. \tag{2.18}$$

In particular, we have for the Chebyshev polynomials of odd degree $l \in 2\mathbb{N}_0 + 1$

$$\mathcal{U}_l(0) = 0, \quad \mathcal{U}_l(1) = l+1, \quad \mathcal{U}_l(-1) = -(l+1),$$

and for the Chebyshev polynomials of even degree $l \in 2\mathbb{N}_0$

$$\mathcal{U}_l(0) = (-1)^{\frac{l}{2}}, \quad \mathcal{U}_l(1) = l+1, \quad \mathcal{U}_l(-1) = l+1.$$

Moreover, the Chebyshev polynomials satisfy the following recurrence formulae (cf. Szegö, 1992, Sec. 4.5)

$$\mathcal{U}_{l+1}(t) = 2t\mathcal{U}_l(t) - \mathcal{U}_{l-1}(t), \tag{2.19}$$
$$\mathcal{U}_{l+2}(t) = (4t^2-2)\mathcal{U}_l(t) - \mathcal{U}_{l-2}(t), \tag{2.20}$$
$$(1-t^2)\frac{\mathrm{d}}{\mathrm{d}t}\mathcal{U}_l(t) = -lt\mathcal{U}_l(t) + (l+1)\mathcal{U}_{l-1}(t), \tag{2.21}$$
$$2t(1-t^2)\frac{\mathrm{d}}{\mathrm{d}t}\mathcal{U}_l(t) = (l+1-2lt^2)\mathcal{U}_l(t) + (l+1)\mathcal{U}_{l-2}(t) \tag{2.22}$$

with initial polynomials $\mathcal{U}_0 = 1$ and $\mathcal{U}_1(t) = 2t$.

The subspace of even functions in $L^2([-1,1], \sqrt{1-t^2})$ can be identified with the space of radially symmetric functions in $L^2(\mathrm{SO}(3))$.

Definition 2.5. A function $f\colon \mathrm{SO}(3) \to \mathbb{R}$ is called *radially symmetric* with center $\mathbf{g}_0 \in \mathrm{SO}(3)$ if $f(\mathbf{g}) = f(\mathbf{g}')$ for all $\mathbf{g}, \mathbf{g}' \in \mathrm{SO}(3)$ satisfying $\measuredangle(\mathbf{g}, \mathbf{g}_0) = \measuredangle(\mathbf{g}', \mathbf{g}_0)$, i.e. if $f(\mathbf{g})$ depends only on the rotational distance of $\mathbf{g}$ to $\mathbf{g}_0$. A radially symmetric function on SO(3) with center $\mathbf{g}_0 = \mathrm{Id}$ is called *conjugate invariant*.

Lemma 2.6. *Let for any radially symmetric function $f \in L^2(\mathrm{SO}(3))$ with center $\mathbf{g}_0 \in \mathrm{SO}(3)$ the function $F\colon [-1,1] \to \mathbb{R}$ be defined by*

$$F(t) = f(\mathbf{g}), \quad t \in [-1,1],\ \mathbf{g} \in \mathrm{SO}(3),\ \text{with } |t| = \cos \tfrac{\measuredangle(\mathbf{g},\mathbf{g}_0)}{2}.$$

Then the mapping $f \mapsto F$ defines an isomorphism between the subspace of radially symmetric functions in $L^2(\mathrm{SO}(3))$ with center $\mathbf{g}_0$ and the subspace of even functions in $L^2([-1,1], \sqrt{1-t^2})$. In particular f allows for the series expansion

$$f(\mathbf{g}) = \left(\sum_{l=0}^{\infty} \hat{F}(2l) \mathcal{U}_{2l} \right) \left(\cos \tfrac{\measuredangle(\mathbf{g},\mathbf{g}_0)}{2} \right), \quad \mathbf{g} \in \mathrm{SO}(3), \tag{2.23}$$

where $\hat{F}(2l)$, $l \in \mathbb{N}_0$ are the even order Chebyshev coefficients of F.

Proof. Let $f \in L^2(\mathrm{SO}(3))$ and $F \in L^2([-1,1])$ be defined as above. Then we have

$$\int_{\mathrm{SO}(3)} |f(\mathbf{g})|^2 \, \mathrm{d}\mathbf{g} = 16\pi \int_0^{\pi} \left| F(\cos \tfrac{\omega}{2}) \right|^2 \sin^2 \tfrac{\omega}{2} \, \mathrm{d}\boldsymbol{\omega} = 16\pi \int_{-1}^{1} |F(t)|^2 \sqrt{1-t^2} \, \mathrm{d}t.$$

Since F is an even function in $L^2([-1,1])$ all odd order Chebyshev coefficients are zero and we obtain representation (2.23). □

2.5 Wigner Functions

This section gives a short summary about harmonic analysis on the rotational group SO(3). Although most of the results presented in this section are known in the much more general context of Lie–groups we give an elementary outline close to the approach in Gurarie (1992, Sec. 4.4) with special emphasis on the relationship to the spherical harmonics. The reader interested in the general theory is referred to the books Vilenkin and Klimyk (1991) and Helgason (1984).

The central concept in harmonic analysis are group representations.

Definition 2.7. A *representation* of a group G on a vector space V is a group homomorphism from G to $\mathrm{GL}(V)$, the general linear group over V.

Let V, V_1 and V_2 be vector spaces over the field K. Two representations $\pi\colon G \to \mathrm{GL}(V_1)$ and $\pi'\colon G \to \mathrm{GL}(V_2)$ are called *equivalent* $\pi \sim \pi'$ if there is an isomorphism $A\colon V_1 \to V_2$ such that $\pi \circ A = A \circ \pi'$. A subspace $U \subseteq V$ is called *invariant* with respect to a representation $\pi\colon G \to \mathrm{GL}(V)$ if $\pi(g)U \subseteq U$ for all $g \in G$. A representation is called *irreducible* if $\mathrm{GL}(V)$ does not contain any nontrivial invariant subspace. A central problem in harmonic analysis is to find all irreducible representations of a certain group G modulo equivalence, i.e. to find a *complete system of irreducible representations* of the group G.

Let $\{ \mathbf{v}_i \in V \mid i = 1, \dots, \dim V \}$ be some basis in V. Then the *matrix entries* of a representation $\pi \colon G \to \mathrm{GL}(V)$ are defined by

$$\pi_{ij}(g) = \langle \pi(g)\mathbf{v}_j, \mathbf{v}_i \rangle , \quad i, j = 1, \dots, \dim V,\ g \in G$$

and the character of π is defined by

$$\chi_\pi(g) = \sum_{i=1}^{\dim V} \pi_{ii}(g), \quad g \in G.$$

We note that the matrix entries $\pi_{ij} \colon G \to K$ as well as the character $\chi_\pi \colon G \to K$ are functions from G into the field K of the vector space V. Additionally the character χ_π of a representation π is *conjugate invariant*, i.e. $\chi_\pi(gg'g^{-1}) = \chi_\pi(g')$.

The question for all irreducible representations of a group G becomes significantly easier if G is compact. In this case there exists a unique (up to multiplication by a positive constant) left invariant Haar measure μ on G. The crucial point is to treat the matrix elements and the characters of representations of the group G as functions in $L^2(G, \mu)$. The following Peter–Weyl theorem provides a complete characterization of the orthogonality relations of matrix elements and characters in $L^2(G, \mu)$.

Theorem 2.8 (Peter–Weyl)**.** *Let G be a compact group and let μ be a Haar measure on G. Then it applies*

1. *Any irreducible representation of G is finite dimensional.*
2. *The matrix entries of two representations π, π' of the group G satisfy the orthogonality relation*

$$\int_G \pi_{ij}(g)\overline{\pi'_{mn}(g)}\,\mathrm{d}\mu(g) = \begin{cases} \frac{\mu(g)}{\dim \pi}\delta_{ij}\delta_{mn}, & \text{if } \pi \sim \pi', \\ 0 & \text{if } \pi \neq \pi'. \end{cases}$$

3. *The characters of two representation π, π' of the group G satisfy the orthogonality relation*

$$\int_G \chi_\pi(g)\overline{\chi_{\pi'}(g)}\,\mathrm{d}\mu(g) = \begin{cases} \mu(G) & \text{if } \pi \sim \pi', \\ 0 & \text{if } \pi \neq \pi'. \end{cases}$$

4. *The matrix entries π_{ij} of all representations π of the group G form a complete, orthogonal system in $L^2(G, \mu)$. Its characters χ_π form a complete system in the subspace of conjugate invariant functions.*

For a proof of the Peter–Weyl theorem 2.8 we refer the reader to Vilenkin and Klimyk (1991, Chap. 7) or Gurarie (1992, Sec. 3.1). Our next objective is to use the Peter–Weyl theorem to characterize a complete system of irreducible representations of SO(3). This is a well studied problem in harmonic analysis and the reader can find complete investigations in the above mentioned books. However, in view of its simplicity we prove the next characterization lemma directly.

Lemma 2.9. *Let $l \in \mathbb{N}_0$ and $\mathcal{T}_l$ be the left regular representation of* SO(3) *into the space of spherical harmonics of order l, i.e.*

$$\begin{aligned} &\mathcal{T}_l \colon \mathrm{SO}(3) \to \mathrm{GL}(\mathrm{Harm}_l(\mathbb{S}^2)), \\ &\mathcal{T}_l(\mathbf{g}) f(\boldsymbol{\xi}) = f(\mathbf{g}^{-1}\boldsymbol{\xi}). \end{aligned} \tag{2.24}$$

Then $\mathcal{T}_l$, $l \in \mathbb{N}_0$, is a complete system of irreducible representations. Its characters are given by

$$\chi_l(\mathbf{g}) = \mathcal{U}_{2l}(\cos \tfrac{\measuredangle \mathbf{g}}{2}), \quad \mathbf{g} \in \mathrm{SO}(3),\ l \in \mathbb{N}_0. \tag{2.25}$$

Proof. Irreducibility of the representation $\mathcal{T}_l$, $l \in \mathbb{N}_0$ follows from the fact that the harmonic spaces $\mathrm{Harm}_l(\mathbb{S}^2)$ are minimal rotational invariant subspaces of $L^2(\mathbb{S}^2)$. Let us fix the spherical harmonics $\mathcal{Y}_l^k$, $k = -l, \dots, l$, as an orthonormal basis in $\mathrm{Harm}_l(\mathbb{S}^2)$. Then the diagonal matrix entries T_l^{kk}, $k = -l, \dots, l$, of $\mathcal{T}_l$ satisfy for $\omega \in [0, 2\pi]$,

$$T_l^{kk}(\mathrm{Rot}_{\mathbf{e}_3}(\omega)) = \int_{\mathbb{S}^2} \mathcal{Y}_l^k(\mathrm{Rot}_{\mathbf{e}_3}(-\omega)\boldsymbol{\xi}) \overline{\mathcal{Y}_l^k(\boldsymbol{\xi})} \,\mathrm{d}\boldsymbol{\xi} = e^{-ik\omega} \int_{\mathbb{S}^2} \mathcal{Y}_l^k(\boldsymbol{\xi}) \overline{\mathcal{Y}_l^k(\boldsymbol{\xi})} \,\mathrm{d}\boldsymbol{\xi} = e^{-ik\omega}.$$

Since the characters of $\mathcal{T}_l$ are conjugate invariant, i.e. depend only on the rotational angle of $\mathbf{g}$ we have

$$\chi_l(\mathbf{g}) = \chi_l(\mathrm{Rot}_{\mathbf{e}_3}(\measuredangle \mathbf{g})) = \mathrm{Tr}\, T_l(\mathrm{Rot}_{\mathbf{e}_3}(\measuredangle \mathbf{g})) = \sum_{k=-l}^{l} e^{-ik\measuredangle \mathbf{g}} = \frac{\sin(\frac{2l+1}{2}\measuredangle \mathbf{g})}{\sin(\frac{1}{2}\measuredangle \mathbf{g})} = \mathcal{U}_{2l}(\cos \tfrac{\measuredangle \mathbf{g}}{2}).$$

By Lemma 2.6 the functions $\mathbf{g} \mapsto \mathcal{U}_{2l}(\cos \frac{\measuredangle \mathbf{g}}{2})$, $l \in \mathbb{N}_0$, form a complete, orthogonal system in the space of conjugate invariant, square integrable functions on SO(3). We conclude by the Peter–Weyl Theorem 2.8 that the regular representations $\mathcal{T}_l$ of SO(3) into the harmonic spaces $\mathrm{Harm}_l(\mathbb{S}^2)$, $l \in \mathbb{N}_0$, form a complete system of irreducible representations of the group SO(3). □

Definition 2.10. Let $l \in \mathbb{N}_0$ and denote $\mathcal{T}_l \colon \mathrm{SO}(3) \to \mathrm{GL}(\mathrm{Harm}_l(\mathbb{S}^2))$ the left regular representations of SO(3) into the harmonic space $\mathrm{Harm}_l(\mathbb{S}^2)$. Then the matrix entries

$$T_l^{kk'}(\mathbf{g}) = \left\langle \mathcal{Y}_l^{k'}(\mathbf{g}^{-1} \circ), \mathcal{Y}_l^k \right\rangle_{L^2(\mathbb{S}^2)} = \int_{\mathbb{S}^2} \mathcal{Y}_l^{k'}(\mathbf{g}^{-1}\boldsymbol{\xi}) \overline{\mathcal{Y}_l^k(\boldsymbol{\xi})} \,\mathrm{d}\boldsymbol{\xi}, \quad \mathbf{g} \in \mathrm{SO}(3), \tag{2.26}$$

$k, k' = -l, \dots, l$, of $\mathcal{T}_l$ with respect to the basis of spherical harmonics $\mathcal{Y}_l^k$, $k = -l, \dots, l$, are called *Wigner–D functions* of degree l.

The Wigner–D functions are also known as *generalized spherical harmonics* (Bunge, 1969). By the Peter–Weyl Theorem 2.8 they form an orthogonal basis in $L^2(\mathrm{SO}(3))$. Hence, every function $f \in L^2(\mathrm{SO}(3))$ has a unique series expansion in terms of Wigner–D functions

$$f = \sum_{l=0}^{\infty} \sum_{k,k'=-l}^{l} \frac{(l+\frac{1}{2})^{\frac{1}{2}}}{2\pi} \hat{f}(l,k,k') T_l^{kk'} \tag{2.27}$$

with coefficients $\hat{f}(l,k,k')$ given by the integral

$$\hat{f}(l,k,k') = \frac{(l+\frac{1}{2})^{\frac{1}{2}}}{2\pi} \int_{\mathrm{SO}(3)} f(\mathbf{g}) \overline{T_l^{kk'}(\mathbf{g})} \, \mathrm{d}\mathbf{g}.$$

Note that the Wigner–D functions $T_l^{kk'}$ are not normalized in the L^2–sense but satisfy

$$\left\| T_l^{kk'} \right\|^2_{L^2(\mathrm{SO}(3))} = \frac{4\pi^2}{l+\frac{1}{2}}.$$

The constants in the above definition are chosen such that the coefficients $\hat{f}(l,k,k')$ of f correspond to the coefficients with respect to an L^2–basis.

For abbreviation we denote by $T_l = (T_l^{kk'})_{k,k'=-l}^{l}$ the matrix formed by the matrix elements $T_l^{kk'}$, $k,k' = -l,\ldots,l$ and arrange the symbols $\hat{f}(l,k,k')$ of f in matrix form $\hat{f}(l) = (\hat{f}(l,k,k'))_{k,k'=-l,\ldots,l}$, accordingly. Now the representation properties of $\mathcal{T}_l$ may be rewritten in matrix notation.

Corollary 2.11. *Let $\mathbf{g},\mathbf{g}' \in \mathrm{SO}(3)$, $\boldsymbol{\xi} \in \mathbb{S}^2$ and $l \in \mathbb{N}_0$. Then the Wigner–D functions are characterized by the following properties*

$$\begin{aligned} T_l^T(\mathbf{g}) \mathcal{Y}_l(\boldsymbol{\xi}) &= \mathcal{Y}_l(\mathbf{g}^{-1}\,\boldsymbol{\xi}), \\ T_l(\mathbf{g}) T_l(\mathbf{g}') &= T_l(\mathbf{g}\mathbf{g}'), \\ \overline{T_l(\mathbf{g})}^T &= T_l(\mathbf{g}^{-1}). \end{aligned} \tag{2.28}$$

Furthermore, the Fourier coefficients $\widehat{f}$ and $\widehat{P}$ satisfy for any function $f \in L^2(\mathrm{SO}(3))$ and $P \in L^2(\mathbb{S}^2)$ the equalities

$$\widehat{f(\mathbf{g}^{-1}\circ)}(l) = T_l(\mathbf{g})\hat{f}(l) \text{ and } \widehat{f(\circ\,\mathbf{g}^{-1})}(l) = \hat{f}(l) T_l(\mathbf{g}),$$

and

$$\widehat{P(\mathbf{g}^{-1}\circ)}(l) = T_l(\mathbf{g})\widehat{P}(l),$$

respectively.

Analogously to the spherical case we define the harmonic spaces in $L^2(\mathrm{SO}(3))$.

Definition 2.12. Let $l \in \mathbb{N}_0$. Then the *harmonic space* $\mathrm{Harm}_l(\mathrm{SO}(3))$ of degree l is defined as

$$\mathrm{Harm}_l(\mathrm{SO}(3)) = \mathrm{span}\left\{ T_l^{kk'} \;\middle|\; k,k' = -l,\ldots,l \right\}.$$

Lemma 2.13. *The harmonic spaces $\mathrm{Harm}_l(\mathrm{SO}(3))$, $l \in \mathbb{N}_0$, are rotational invariant and irreducible in the sense that for any function $f \in \mathrm{Harm}_l(\mathrm{SO}(3))$ we have*

$$\mathrm{Harm}_l(\mathrm{SO}(3)) = \mathrm{span}\left\{ \mathbf{g} \mapsto f(\mathbf{g}_1\,\mathbf{g}\,\mathbf{g}_2) \;\middle|\; \mathbf{g}_1,\mathbf{g}_2 \in \mathrm{SO}(3) \right\}.$$

In particular, the harmonic spaces $\mathrm{Harm}_l(\mathrm{SO}(3))$ *provide a decomposition of* $L^2(\mathrm{SO}(3))$ *into a direct sum of rotational invariant, irreducible subspaces, i.e.*

$$L^2(\mathrm{SO}(3)) = \mathrm{clos}_{L^2} \bigoplus_{l=0}^{\infty} \mathrm{Harm}_l(\mathrm{SO}(3)).$$

Proof. The rotational invariance and irreducibility is a direct consequence of the defining equation (2.26) and the rotational invariance and irreducibility of the spherical harmonic spaces $\mathrm{Harm}_l(\mathbb{S}^2)$. □

We have already proven the rotational analogous to the spherical addition theorem when calculating the characters of the representations $\mathcal{T}_l$ in Lemma 2.9. More precisely, we have shown

Theorem 2.14 (Addition Theorem)**.** *Let* $l \in \mathbb{N}_0$ *and let* T_l *be the matrix representation as defined in equation* (2.26)*. Then the trace* $\mathrm{Tr}\, T_l(\mathbf{g})$ *depends on the rotational angle* $\measuredangle\mathbf{g}$ *of* $\mathbf{g}$ *only. In particular, we have for any* $\mathbf{g}_1, \mathbf{g}_2 \in \mathrm{SO}(3)$ *the equality*

$$\sum_{k,k'=-l}^{l} T_l^{kk'}(\mathbf{g}_1)\overline{T_l^{kk'}(\mathbf{g}_2)} = \mathrm{Tr}\, T_l(\mathbf{g}_1\mathbf{g}_2^{-1}) = \mathcal{U}_{2l}\Big(\cos\tfrac{\measuredangle(\mathbf{g}_1,\mathbf{g}_2)}{2}\Big).$$

Combining Addition Theorem 2.14 with Lemma 2.6 we obtain the following characterization of radially symmetric, square integrable functions on SO(3).

Proposition 2.15. *For any function* $f \in L^2(\mathrm{SO}(3))$ *and any rotation* $\mathbf{g}_0 \in \mathrm{SO}(3)$ *the following conditions are equivalent.*

1. *The function* f *is radially symmetric with center* $\mathbf{g}_0 \in \mathrm{SO}(3)$*.*
2. *There is an even function* $F \in L^2([-1,1], \sqrt{1-t^2})$ *such that*

$$f(\mathbf{g}) = F\left(\cos\tfrac{\measuredangle(\mathbf{g},\mathbf{g}_0)}{2}\right), \quad \mathbf{g} \in \mathrm{SO}(3).$$

3. *There are coefficients* $\hat{F}(2l)$*,* $l \in \mathbb{N}_0$ *such that* f *has the Fourier expansions*

$$f = \sum_{l=0}^{\infty} \hat{F}(2l) \sum_{k,k'=-l}^{l} T_l^{kk'}(\mathbf{g}_0) T_l^{kk'}.$$

4. *There are coefficients* $\hat{F}(2l)$*,* $l \in \mathbb{N}_0$ *such that* f *has the series expansions*

$$f(\mathbf{g}) = \left(\sum_{l=0}^{\infty} \hat{F}(2l)\mathcal{U}_{2l}\right)\left(\cos\tfrac{\measuredangle(\mathbf{g}_0,\mathbf{g})}{2}\right), \quad \mathbf{g} \in \mathrm{SO}(3). \tag{2.29}$$

Moreover, if one assertion holds true then the coefficients $\hat{F}(2l)$, $l \in \mathbb{N}_0$ are the even order Chebyshev coefficients of F and we have the following equivalent to the Funk Hecke formula

$$\hat{F}(2l) = \int_{\mathrm{SO}(3)} F\Big(\cos \tfrac{\measuredangle(\mathbf{g},\mathbf{g}_0)}{2}\Big) \mathcal{U}_{2l}\Big(\cos \tfrac{\measuredangle(\mathbf{g},\mathbf{g}_0)}{2}\Big) \,\mathrm{d}\mathbf{g}.$$

By equation (2.29) the subspace of radially symmetric functions of a certain harmonic degree $l \in \mathbb{N}_0$ and with fixed center $\mathbf{g}_0 \in \mathrm{SO}(3)$ has dimension one and is spanned by the functions $\mathbf{g} \mapsto \mathcal{U}_{2l}(\cos \frac{\measuredangle(\mathbf{g}_0,\mathbf{g})}{2})$. This implies the following analogue to the spherical mean value theorem 2.3.

Lemma 2.16. *Let $\mathbf{g}_0, \mathbf{g} \in \mathrm{SO}(3)$. Then the following equality is satisfied for any function $f \in \mathrm{Harm}_l(\mathrm{SO}(3))$, $l \geq 0$,*

$$\frac{1}{4\pi} \int_{\mathbb{S}^2} f\left(\mathrm{Rot}_{\boldsymbol{\eta}}(\measuredangle(\mathbf{g}_0, \mathbf{g}))\mathbf{g}_0\right) \,\mathrm{d}\boldsymbol{\eta} = \frac{1}{2l+1} \mathcal{U}_{2l}\left(\cos \tfrac{\measuredangle(\mathbf{g}_0,\mathbf{g})}{2}\right) f(\mathbf{g}_0). \tag{2.30}$$

In particular, we have for $\measuredangle(\mathbf{g}, \mathbf{g}_0) = \pi$

$$\frac{1}{4\pi} \int_{\mathbb{S}^2} f(\mathrm{Rot}_{\boldsymbol{\eta}}(\pi)\mathbf{g}_0) \,\mathrm{d}\boldsymbol{\eta} = \frac{(-1)^l}{2l+1} f(\mathbf{g}_0). \tag{2.31}$$

Proof. We mention that the integral on the left hand side of equation (2.30) defines a radially symmetric harmonic function in $\mathbf{g}$ that has order l and center $\mathbf{g}_0$. Hence it is the product of the Chebyshev function $\mathcal{U}_{2l}(\cos \frac{\measuredangle(\mathbf{g}_0,\mathbf{g})}{2})$ with some factor $\lambda \in \mathbb{R}$. Since $\mathcal{U}_{2l}(1) = 2l + 1$ we conclude

$$\lambda = \frac{1}{2l+1} f(\mathbf{g}_0).$$

Equation (2.31) follows from $\mathcal{U}_{2l}(0) = (-1)^l$. □

Let $f, h \in L^2(\mathrm{SO}(3))$. Then the *convolution* of f and h is defined by

$$(f * h)(\mathbf{g}) = \int_{\mathrm{SO}(3)} f(\mathbf{g}\mathbf{q}^{-1})\, h(\mathbf{q}) \,\mathrm{d}\mathbf{q}, \quad \mathbf{g} \in \mathrm{SO}(3). \tag{2.32}$$

By the Cauchy–Schwartz inequality we have $f * h \in L^2(\mathrm{SO}(3))$ and the Fourier coefficients of $f * h$ satisfy

$$\widehat{f * h}(l) = 2\pi \left(l + \frac{1}{2}\right)^{-\frac{1}{2}} \hat{f}(l)\hat{h}(l), \quad l \in \mathbb{N}_0. \tag{2.33}$$

In fact, equality (2.33) holds true in any convolution algebra $L^2(G)$ of a compact group G (cf. Gurarie, 1992, Sec. 3.1.4)

For the numerical evaluation of the Wigner–D functions the defining equation (2.26) is not well suited. Fast algorithms mainly rely on representations of the Wigner–D functions with respect to Euler angles (Kostelec and Rockmore, 2003; Vollrath, 2006). The following representation is taken from Varshalovich et al. (1988, Chap. 4).

Remark 2.17. Denote for some rotation $\mathbf{g} = \mathrm{Rot}_{\mathbf{e}_3}(\alpha)\mathrm{Rot}_{\mathbf{e}_1}(\beta)\mathrm{Rot}_{\mathbf{e}_3}(\gamma)$ the decomposition into Euler angles (α, β, γ). Then the Wigner–D functions $T_l^{kk'}$ factorize into the *Wigner–d functions* $d_l^{kk'}$ depending on β only and the exponential function depending on α and γ:

$$T_l^{kk'}(\alpha, \beta, \gamma) = e^{-ik\alpha} d_l^{kk'}(\cos\beta) e^{-ik'\gamma}. \tag{2.34}$$

The Wigner–d functions $d_l^{kk'} : [-1, 1] \to \mathbb{R}$, $l \in \mathbb{N}_0$, $k, k' = -l, \ldots, l$ are defined as

$$d_l^{kk'}(t) = \frac{(-1)^{l-k}}{2^l} \sqrt{\frac{(l+k')!}{(l-k')!(l+k)!(l-k)!}} \sqrt{\frac{(1-t)^{k-k'}}{(1+t)^{k+k'}}} \frac{\mathrm{d}^{l-k'}}{\mathrm{d}t^{l-k'}} (1-t)^{l-k}(1+t)^{l+k}.$$

2.6 The Laplace–Beltrami Operator and Sobolev Spaces

The Laplace–Beltrami Operator. Let (Ω, d) be a Riemannian manifold. Then the *Laplace–Beltrami operator* $\triangle_\Omega$ on (Ω, d) is defined in local coordinates by

$$\triangle_\Omega f = \operatorname{div} \operatorname{grad} f = \frac{1}{\sqrt{|d|}} \sum_{ij} \partial_i \sqrt{|d|} d^{ij} \partial_j f, \quad f \in C^2(\Omega), \tag{2.35}$$

where $|d|$ denotes the determinant of metric tensor d and d^{ij} the entries of its inverse. One verifies that the definition of the Laplace–Beltrami operator does not depend on the particular choice of the coordinate system (cf. Helgason, 1984, Sec. 2.4.2). Moreover, the Laplace–Beltrami operator is invariant under symmetries $\Phi \colon (\Omega, d) \to (\Omega, d)$, i.e. $\triangle(f \circ \Phi) = (\triangle f) \circ \Phi$ (cf. Helgason, 1984, Prop. 2.4). For the domains of our special interest $\Omega = \mathbb{S}^2$ and $\Omega = \mathrm{SO}(3)$ this implies rotational invariance of the Laplace–Beltrami operator.

Explicit calculation of the Laplace–Beltrami operator $\triangle_{\mathbb{S}^2}$ on the sphere $\mathbb{S}^2$ in terms of polar coordinates (θ, ρ) yields (cf. Jähnich, 1992, Sec. 13.9)

$$\triangle_{\mathbb{S}^2} = \frac{1}{\sin^2\theta} \partial_\rho^2 + \frac{1}{\sin\theta} \partial_\theta (\sin\theta\, \partial_\theta). \tag{2.36}$$

The rotational invariance of the Laplace–Beltrami operator $\triangle_{\mathbb{S}^2}$ implies that the harmonic spaces $\mathrm{Harm}_l(\mathbb{S}^2)$ are invariant with respect to $\triangle_{\mathbb{S}^2}$. Moreover, the spherical harmonics are the eigenfunctions of $\triangle_{\mathbb{S}^2}$ (cf. Freeden, 1998, Sec. 3.5).

Lemma 2.18. *Let $l \in \mathbb{N}_0$ and $k = -l, \ldots, l$. Then*

$$\triangle_{\mathbb{S}^2} \mathcal{Y}_l^k = -l(l+1) \mathcal{Y}_l^k. \tag{2.37}$$

Next we want to achieve an analogous characterization of the Laplace–Beltrami operator on the rotational group SO(3). Therefore we first note that the the metric tensor

$d(\alpha, \beta, \gamma)$ of the Riemannian manifold SO(3) using Euler angle parameterization has the form (cf. Morawiec, 2004, Sec. 3.1)

$$d = \begin{pmatrix} 1 & 0 & \cos\beta \\ 0 & 1 & 0 \\ \cos\beta & 0 & 1 \end{pmatrix}. \tag{2.38}$$

Combining equation (2.38) and equation (2.35) we obtain the following Euler angle representation of the Laplace–Beltrami operator on SO(3)

$$\triangle_{\mathrm{SO}(3)} = \frac{1}{\sin^2\beta}\partial_\alpha^2 + \frac{1}{\sin^2\beta}\partial_\gamma^2 + \frac{1}{\sin\beta}\partial_\beta(\sin\beta\,\partial_\beta) - 2\frac{\cos\beta}{\sin^2\beta}\partial_\alpha\partial_\gamma. \tag{2.39}$$

This representation allows us to prove

Lemma 2.19. *Let $l \in \mathbb{N}_0$, $k = -l, \ldots, l$ and denote $\mathcal{Y}_l^k(\circ\,\boldsymbol{\eta})\colon \mathrm{SO}(3) \to \mathbb{R}$ the function $\mathbf{g} \mapsto \mathcal{Y}_l^k(\mathbf{g}\boldsymbol{\eta})$. Then*

$$\triangle_{\mathrm{SO}(3)}\mathcal{Y}_l^k(\circ\,\boldsymbol{\eta}) = -l(l+1)\mathcal{Y}_l^k(\circ\,\boldsymbol{\eta}). \tag{2.40}$$

Moreover, we have for all $l \in \mathbb{N}_0$ and $k, k' = -l, \ldots, l$,

$$\triangle_{\mathrm{SO}(3)}T_l^{kk'} = -l(l+1)T_l^{kk'}. \tag{2.41}$$

Proof. Due to the rotational invariance of the Laplace–Beltrami operator we can assume without loss of generality that $\boldsymbol{\eta} = \mathbf{e}_3$. Using Euler angles $\mathbf{q} = (\alpha, \beta, \gamma)$ we have $\mathbf{q}\mathbf{e}_3 = (\beta, \alpha)$ in polar coordinates. Consequently $\partial_\gamma\mathcal{Y}_l^k(\circ\,\mathbf{e}_3) = 0$ and by equation (2.39) and equation (2.36) we obtain

$$\begin{aligned}\triangle_{\mathrm{SO}(3)}\mathcal{Y}_l^k(\beta,\alpha) &= \Big(\frac{1}{\sin^2\beta}\partial_\alpha^2 + \frac{1}{\sin\beta}\partial_\beta(\sin\beta\,\partial_\beta)\Big)\mathcal{Y}_l^k(\beta,\alpha) \\ &= \triangle_{\mathbb{S}^2}\mathcal{Y}_l^k(\beta,\alpha) = -l(l+1)\mathcal{Y}_l^k(\beta,\alpha).\end{aligned}$$

Application to the defining equation (2.26) of the Wigner–D functions proves the assertion

$$\triangle_{\mathrm{SO}(3)}T_l^{kk'} = \triangle_{\mathrm{SO}(3)}\int_{\mathbb{S}^2}\mathcal{Y}_l^{k'}(\circ^{-1}\boldsymbol{\eta})\overline{\mathcal{Y}_l^k(\boldsymbol{\eta})}\,\mathrm{d}\boldsymbol{\eta} = \int_{\mathbb{S}^2}\mathcal{Y}_l^{k'}(\boldsymbol{\eta})\triangle_{\mathrm{SO}(3)}\overline{\mathcal{Y}_l^k(\circ\,\boldsymbol{\eta})}\,\mathrm{d}\boldsymbol{\eta} = -l(l{+}1)T_l^{kk'}.$$

□

Sobolev Spaces. Now we are ready to define Sobolev–Hilbert spaces on the domains $\Omega = \mathbb{S}^2$ and $\Omega = \mathrm{SO}(3)$. For a more general definition the reader is referred to Freeden (1998, Sec. 5.1) and Cheney and Light (1999, Section32).

Definition 2.20 (Sobolev–spaces on $\mathbb{S}^2$ and SO(3))**.** Let $s \in \mathbb{R}$. Then we define the *Sobolev–Hilbert space* $\mathcal{H}_s(\mathbb{S}^2)$ to be the closure of the linear span of all spherical harmonics $\mathcal{Y}_l^k$, $l \in \mathbb{N}_0$, $k = -l, \ldots, l$, with respect to the inner product

$$\left\langle \mathcal{Y}_l^k, \mathcal{Y}_{l'}^{k'} \right\rangle_{\mathcal{H}_s(\mathbb{S}^2)} = (l + \tfrac{1}{2})^{2s} \delta_{l,l'} \delta_{k,k'}.$$

By the *Sobolev–Hilbert space* $\mathcal{H}_s(\mathrm{SO}(3))$ on the rotational group we mean the completion of the linear span of all Wigner–D functions $T_l^{kk'}$, $l \in \mathbb{N}_0$, $k, k' = -l, \ldots, l$ with respect to the inner product

$$\left\langle \frac{(l+\frac{1}{2})^{\frac{1}{2}}}{2\pi} T_l^{kk'}, \frac{(l+\frac{1}{2})^{\frac{1}{2}}}{2\pi} T_{l'}^{mm'} \right\rangle_{\mathcal{H}_s(\mathrm{SO}(3))} = (l + \tfrac{1}{2})^{2s} \delta_{l,l'} \delta_{k,m} \delta_{k',m'}.$$

Remark 2.21. In the case that $s = 0$ we have $\mathcal{H}_0(\mathbb{S}^2) = L^2(\mathbb{S}^2)$ and $\mathcal{H}_0(\mathrm{SO}(3)) = L^2(\mathrm{SO}(3))$.

A major result in the theory of Sobolev spaces is the Lemma of Sobolev which relates the order s of the Sobolev spaces $\mathcal{H}_s(\Omega)$ to continuity properties of its functions. The following spherical variant is proven in Freeden (1998, Lemma 5.2.3). The assertion with respect to the Sobolev spaces on SO(3) might be proven using the same ideas.

Lemma 2.22 (Lemma of Sobolev)**.** *Let $f \in \mathcal{H}_s(\mathbb{S}^2)$ and $s, k \in \mathbb{N}_0$ with $s > k + 1$. Then f corresponds to a function of class $C^{(k)}(\mathbb{S}^2)$.*

Let $f \in \mathcal{H}_s(\mathrm{SO}(3))$ and $s, k \in \mathbb{N}_0$ with $s > k + \frac{3}{2}$. Then f corresponds to a function of class $C^{(k)}(\mathrm{SO}(3))$.

Sobolev spaces are intimately related to the Laplace–Beltrami operator on the specific domain.

Lemma 2.23. *Let $s, t \in \mathbb{R}$ and $\Omega = \mathbb{S}^2$ or $\Omega = \mathrm{SO}(3)$. Then $(-\triangle_\Omega + \frac{1}{4})^{s/2}$ defines an isometric operator between the Sobolev spaces $\mathcal{H}_{t+s}(\Omega)$ and $\mathcal{H}_t(\Omega)$. In particular, the inner product in $\mathcal{H}_s(\Omega)$ can be written as*

$$\langle f, g \rangle_{\mathcal{H}_s(\Omega)} = \left\langle (-\triangle_\Omega + \tfrac{1}{4})^{s/2} f, (-\triangle_\Omega + \tfrac{1}{4})^{s/2} g \right\rangle_{L^2(\Omega)}.$$

Proof. From Lemma 2.18 and Lemma 2.19 we conclude for any $l \in \mathbb{N}_0$ and $k, k' = -l, \ldots, l$ that

$$(-\triangle_{\mathbb{S}^2} + \tfrac{1}{4}) \mathcal{Y}_l^k = (l + \tfrac{1}{2})^2 \mathcal{Y}_l^k \quad \text{and} \quad (-\triangle_{\mathrm{SO}(3)} + \tfrac{1}{4}) T_l^{kk'} = (l + \tfrac{1}{2})^2 T_l^{kk'}.$$

By Definition 2.20 this implies the assertions. □

The Laplace–Beltrami operator is the prototype of any invariant differential operator. A more general class of invariant operators is formed by the pseudodifferential operators which we define analogously to Freeden (cf. Freeden, 1998, def. 5.1.2).

Definition 2.24. Let $s, t \in \mathbb{R}$ and let $\hat{A}(l)$, $l \in \mathbb{N}_0$ be a real valued sequence satisfying

$$\lim_{l\to\infty} \frac{\left|\hat{A}(l)\right|}{(l+\frac{1}{2})^T} = const \neq 0.$$

Moreover, denote $\Pi_l \colon \mathcal{H}_s(\Omega) \to \mathrm{Harm}_l(\Omega)$ the projection onto the harmonic space of order $l \in \mathbb{N}_0$. Then the operator $A \colon \mathcal{H}_s(\Omega) \to \mathcal{H}_{s-t}(\Omega)$ defined by

$$Af = \sum_{l=0}^{\infty} \hat{A}(l)\Pi_l f$$

is called *invariant pseudodifferential operator of order t*.

Sobolev Spaces over $\mathbb{S}^2 \times \mathbb{S}^2$. In this section we introduce Sobolev spaces over $\mathbb{S}^2 \times \mathbb{S}^2$. They will become useful in Section 3 when we analyze the Radon transform on SO(3).

Following equation (2.35) the Laplace – Beltrami operator on $\mathbb{S}^2 \times \mathbb{S}^2$ is defined as

$$\triangle_{\mathbb{S}^2\times\mathbb{S}^2} P = \triangle_{\mathbb{S}^2,1} P + \triangle_{\mathbb{S}^2,2} P, \quad P \in C^2(\mathbb{S}^2 \times \mathbb{S}^2).$$

Here $\triangle_{\mathbb{S}^2,1}$ and $\triangle_{\mathbb{S}^2,2}$ denote the application of the spherical Laplace – Beltrami operator to the first and second argument of a function on $\mathbb{S}^2 \times \mathbb{S}^2$, respectively.

Analogously to Definition 2.20 and Lemma 2.23 we define the Sobolev space over $\mathbb{S}^2 \times \mathbb{S}^2$ by

Definition 2.25. Let $s \in \mathbb{R}$. Then the *Sobolev space* $\mathcal{H}_s(\mathbb{S}^2 \times \mathbb{S}^2)$ is defined as the completion of the linear span of the spherical harmonics $\mathcal{Y}_l^k(\circ_1)\overline{\mathcal{Y}_{l'}^{k'}(\circ_2)}$, $l, l' \in \mathbb{N}_0$, $k, k' = -l, \ldots, l$ on $\mathbb{S}^2 \times \mathbb{S}^2$ with respect to the inner product

$$\langle P_1, P_2 \rangle_{\mathcal{H}_s(\mathbb{S}^2\times\mathbb{S}^2)} = \left\langle (-\triangle_{\mathbb{S}^2\times\mathbb{S}^2} + \tfrac{1}{4})^{s/2} P_1, (-\triangle_{\mathbb{S}^2\times\mathbb{S}^2} + \tfrac{1}{4})^{s/2} P_2 \right\rangle_{L^2(\mathbb{S}^2\times\mathbb{S}^2)}.$$

Remark 2.26. By Lemma 2.18 we have

$$\triangle_{\mathbb{S}^2\times\mathbb{S}^2} \mathcal{Y}_l^k(\circ_1)\overline{\mathcal{Y}_{l'}^{k'}(\circ_2)} = -\big(l(l+1) + l'(l'+1)\big)\mathcal{Y}_l^k(\circ_1)\overline{\mathcal{Y}_{l'}^{k'}(\circ_1)}.$$

Hence, an orthonormal basis of $\mathcal{H}_s(\mathbb{S}^2 \times \mathbb{S}^2)$ is given by the list of functions

$$\big((l+\tfrac{1}{2})^s + (l'+\tfrac{1}{2})^s\big)^{-1} \mathcal{Y}_l^k(\circ_1)\overline{\mathcal{Y}_{l'}^{k'}(\circ_2)}, \quad l, l' \in \mathbb{N}_0,\ k = -l, \ldots, l,\ k' = -l', \ldots, l'.$$

Lemma 2.27 (Lemma of Sobolev)**.** *Let $P \in \mathcal{H}_s(\mathbb{S}^2 \times \mathbb{S}^2)$ and let $s, k \in \mathbb{N}_0$ with $s > k+2$. Then P corresponds to a function of class $C^{(k)}(\mathbb{S}^2 \times \mathbb{S}^2)$.*

If the Fourier coefficients of $P \in \mathcal{H}_s(\mathbb{S}^2 \times \mathbb{S}^2)$ satisfy $\hat{P}(l, l', k, k') = 0$ whenever $l \neq l'$ then the condition $s > k + \frac{3}{2}$ is already sufficient for P to correspond to a function in $C^{(k)}(\mathbb{S}^2 \times \mathbb{S}^2)$.

Proof. Let $s > 2$ and $P \in \mathcal{H}_s(\mathbb{S}^2 \times \mathbb{S}^2)$. We show that the Fourier series

$$P(\boldsymbol{\xi}, \boldsymbol{\eta}) = \sum_{l,l'=0}^{\infty} \sum_{k=-l}^{l} \sum_{k'=-l'}^{l'} \hat{P}(l, l', k, k') \mathcal{Y}_l^k(\boldsymbol{\xi}) \overline{\mathcal{Y}_{l'}^{k'}(\boldsymbol{\eta})}$$

of P is uniformly convergent. Let $L \in \mathbb{N}$. Then we have for any $\boldsymbol{\xi}, \boldsymbol{\eta} \in \mathbb{S}^2$

$$\begin{aligned}
&\left| \sum_{l,l'=L}^{\infty} \sum_{k=-l}^{l} \sum_{k'=-l'}^{l'} \hat{P}(l, l', k, k') \mathcal{Y}_l^k(\boldsymbol{\xi}) \overline{\mathcal{Y}_{l'}^{k'}(\boldsymbol{\eta})} \right|^2 \\
&\leq \left(\sum_{l,l'=L}^{\infty} \sum_{k=-l}^{l} \sum_{k'=-l'}^{l'} \left((l+\tfrac{1}{2})^s + (l+\tfrac{1}{2})^s \right)^2 \left| \hat{P}(l, l', k, k') \right|^2 \right) \\
&\quad \left(\sum_{l,l'=L}^{\infty} \sum_{k=-l}^{l} \sum_{k'=-l'}^{l'} \frac{\left| \mathcal{Y}_l^k(\boldsymbol{\xi}) \right|^2 \left| \mathcal{Y}_{l'}^{k'}(\boldsymbol{\eta}) \right|^2}{\left((l+\tfrac{1}{2})^s + (l'+\tfrac{1}{2})^s \right)^2} \right) \\
&\leq \|P\|_{\mathcal{H}_s(\mathbb{S}^2 \times \mathbb{S}^2)} \sum_{l,l'=L}^{\infty} (l+\tfrac{1}{2})^{1-s} (l'+\tfrac{1}{2})^{1-s}.
\end{aligned}$$

Since the last sum converges to zero as L converges to infinity the Fourier series of P is uniformly convergent.

If the Fourier coefficients of P satisfy $\hat{P}(l, l', k, k') = 0$ whenever $l \neq l'$ the last sum simplifies to $\sum_{l=L}^{\infty} (l+\frac{1}{2})^{2-2s}$, which converges already for $s > \frac{3}{2}$.

In order to obtain the assertion of Lemma 2.27 for higher orders of differentiability $k \in \mathbb{N}$ one has to show uniformly convergence of the Fourier series of $P^{(k)}$. This can be done analogously. □

We will need also the following trace theorem.

Theorem 2.28 (trace theorem)**.** *Let $s \in \mathbb{R}$ and $\boldsymbol{\eta} \in \mathbb{S}^2$. Then the trace operator*

$$\tau_{\circ_1 \mapsto \boldsymbol{\xi}} \colon \mathcal{H}_{s+\frac{1}{2}}(\mathbb{S}^2 \times \mathbb{S}^2) \to \mathcal{H}_s(\mathbb{S}^2), \quad (\tau_{\circ_1 \mapsto \boldsymbol{\xi}} P)(\boldsymbol{\eta}) = P(\boldsymbol{\xi}, \boldsymbol{\eta})$$

defines a linear, bounded operator for all $P \in C(\mathbb{S}^2 \times \mathbb{S}^2)$ and hence has a well defined linear, bounded extension to the entire space $\mathcal{H}_{s+\frac{1}{2}}(\mathbb{S}^2 \times \mathbb{S}^2)$.

Proof. For any $\boldsymbol{\xi} \in \mathbb{S}^2$ and any $l, l' \in \mathbb{N}$, $k = -l, \ldots, l$, $k' = -l', \ldots, l'$ we have

$$\begin{aligned}
\left\| \tau_{\circ_1 \mapsto \boldsymbol{\xi}} \mathcal{Y}_l^k(\circ_1) \overline{\mathcal{Y}_{l'}^{k'}(\circ_2)} \right\|_{\mathcal{H}_s(\mathbb{S}^2)} &= \left| \mathcal{Y}_l^k(\boldsymbol{\xi}) \right| \|\mathcal{Y}_{l'}^{k'}\|_{\mathcal{H}_s(\mathbb{S}^2)} \leq \sqrt{\frac{2l+1}{4\pi}} (l'+\tfrac{1}{2})^s \\
&\leq (l+\tfrac{1}{2})^{s+\frac{1}{2}} + (l'+\tfrac{1}{2})^{s+\frac{1}{2}} = \|\mathcal{Y}_l^k(\circ_1) \overline{\mathcal{Y}_{l'}^{k'}(\circ_2)}\|_{\mathcal{H}_{s+\frac{1}{2}}(\mathbb{S}^2 \times \mathbb{S}^2)}
\end{aligned}$$

and hence $\tau_{\circ_1 \mapsto \boldsymbol{\xi}}$ is bounded. □

3 The Radon Transform on SO(3)

After the Radon transform was first defined for the domains $\Omega = \mathbb{S}^2$ (cf. Funk, 1913, 1916) and $\Omega = \mathbb{R}^2$ (cf. Radon, 1917), as the linear operator that relates each continuous function $f \in C_c(\Omega)$ to its integrals along all great circles or straight lines, respectively, numerous generalizations have been considered. A generalization in terms of homogeneous spaces was given by Helgason (1999) whereas a generalization in terms of dual manifolds was given by Gurarie (1992). The one–dimensional Radon transform on SO(3) *perfectly fits into both frameworks and some basic results (e.g. Lemma 3.15) could be derived directly from the abstract framework. However, we obtain most of the results presented in this section much easier relying on the specific setting.*

3.1 Definition and Basic Properties

Let (Ω, d) be a Riemannian manifold. A one–dimensional submanifold of Ω is called *geodesic* if it is locally the shortest path between two points. On SO(3) the shortest path connecting the identity $\mathrm{Id} \in \mathrm{SO}(3)$ with any other rotation $\mathrm{Rot}_{\boldsymbol{\eta}_0}(\omega_0)$ is $\omega \mapsto \mathrm{Rot}_{\boldsymbol{\eta}_0}(\omega)$, $\omega \in [0, \omega_0]$ (cf. Morawiec, 2004, Sec. 3.1). Using the rotational symmetry of SO(3) we conclude that any closed geodesic on SO(3) can be written in the form

$$G = \{\, \mathbf{g}_0 \mathrm{Rot}_{\boldsymbol{\eta}_0}(\omega) \mid \omega \in [0, 2\pi) \,\},$$

where $\mathbf{g}_0 \in \mathrm{SO}(3)$ is some arbitrary rotation and $\boldsymbol{\eta}_0 \in \mathbb{S}^2$ is some arbitrary rotational axis. In texture analysis it is common to call the geodesics of SO(3) *fibres*. The next lemma provides a useful parameterization of all fibres on SO(3), i.e. of all geodesics of SO(3).

Lemma 3.1. *Let $G \subseteq \mathrm{SO}(3)$ be a geodesic of the Riemannian manifold* SO(3)*. Then there are two unit vectors $\mathbf{h}, \mathbf{r} \in \mathbb{S}^2$ such that*

$$G = G(\mathbf{h}, \mathbf{r}) := \{\, \mathbf{g} \in \mathrm{SO}(3) \mid \mathbf{gh} = \mathbf{r} \,\}.$$

The unit vectors $\mathbf{h}, \mathbf{r} \in \mathbb{S}^2$ are uniquely defined modulo the symmetry $G(\mathbf{h}, -\mathbf{r}) = G(-\mathbf{h}, \mathbf{r})$.

Proof. Let $\mathbf{g}_0 \in \mathrm{SO}(3)$, $\boldsymbol{\eta} \in \mathbb{S}^2$ and let $G = \{\, \mathbf{g}_0 \mathrm{Rot}_{\boldsymbol{\eta}}(\omega) \mid \omega \in [0, 2\pi) \,\}$ be a geodesic submanifold of SO(3). Then $G = G(\boldsymbol{\eta}, \mathbf{g}_0\boldsymbol{\eta})$. In order to show uniqueness we set without loss of generality $G = \{\, \mathrm{Rot}_{\mathbf{e}_3}(\omega) \mid \omega \in [0, 2\pi) \,\}$. For this geodesic it is clear that $G(\mathbf{e}_3, \mathbf{e}_3)$ and $G(-\mathbf{e}_3, -\mathbf{e}_3)$ are the only possible choices for $\mathbf{h} \in \mathbb{S}^2$ and $\mathbf{r} \in \mathbb{S}^2$. □

Fixing any unit vectors $\mathbf{h}_0, \mathbf{r}_0 \in \mathbb{S}^2$, the sets of geodesics $G(\mathbf{h}_0, \mathbf{r})$, $\mathbf{r} \in \mathbb{S}^2$ and $G(\mathbf{h}, \mathbf{r}_0)$, $\mathbf{h} \in \mathbb{S}^2$ are disjoint coverages of SO(3) (cf. Meister and Schaeben, 2004). Moreover, given two different rotations $\mathbf{g}_1, \mathbf{g}_2 \in \mathrm{SO}(3)$ there is a unique geodesic $G = G(\mathbf{h}, \mathbf{g}_1\mathbf{h})$ containing both rotations. Here $\mathbf{h} \in \mathbb{S}^2$ denotes the rotational axis of $\mathbf{g}_1^{-1}\mathbf{g}_2$. Manifolds with this property are called *geodesically complete*.

Let $f \in C(\mathrm{SO}(3))$ be a continuous function on SO(3). Then the integral of f along the geodesic $G(\mathbf{h}, \mathbf{r})$ exists for all $\mathbf{h}, \mathbf{r} \in \mathbb{S}^2$ and depends continuously on $\mathbf{h}$ and $\mathbf{r}$. Hence, we are able to define:

Definition 3.2. The *(one–dimensional) Radon transform on* SO(3) is defined as the integral operator

$$\begin{aligned} &\mathcal{R}\colon C(\mathrm{SO}(3)) \to C(\mathbb{S}^2 \times \mathbb{S}^2), \\ &(\mathcal{R}f)(\mathbf{h}, \mathbf{r}) = \frac{1}{2\pi} \int_{G(\mathbf{h},\mathbf{r})} f(\mathbf{g})\, \mathrm{d}\mathbf{g} = \frac{1}{2\pi} \int_0^{2\pi} f(\mathrm{Rot}_{\mathbf{r}}(\omega)\mathbf{g}_{\mathbf{h},\mathbf{r}})\, \mathrm{d}\boldsymbol{\omega}, \end{aligned}$$

where $\mathbf{g}_{\mathbf{h},\mathbf{r}} \in G(\mathbf{h}, \mathbf{r})$ is an arbitrary rotation that maps $\mathbf{h}$ onto $\mathbf{r}$.

In order to study invariance under group actions of the Radon transform we define the following actions.

Definition 3.3. For any pair $(\mathbf{g}_1, \mathbf{g}_2) \in \mathrm{SO}(3) \times \mathrm{SO}(3)$ we define an action $\star$ on SO(3) and on $\mathbb{S}^2 \times \mathbb{S}^2$ by

$$(\mathbf{g}_1, \mathbf{g}_2) \star \mathbf{g} = \mathbf{g}_2\mathbf{g}\mathbf{g}_1^{-1} \quad \text{and} \quad (\mathbf{g}_1, \mathbf{g}_2) \star (\mathbf{h}, \mathbf{r}) = (\mathbf{g}_1\mathbf{h}, \mathbf{g}_2\mathbf{r}),$$

with $\mathbf{g} \in \mathrm{SO}(3)$ and $\mathbf{h}, \mathbf{r} \in \mathbb{S}^2$.

Lemma 3.4. *The Radon transform on* SO(3) *is invariant under the action* $\star$ *of the group* SO(3) × SO(3)*, i.e. we have for any pair* $\mathbf{g}_1, \mathbf{g}_2 \in \mathrm{SO}(3)$ *and any function* $f \in C(\mathrm{SO}(3))$ *the equality*

$$(\mathbf{g}_1, \mathbf{g}_2) \star (\mathcal{R}f) = \mathcal{R}\big((\mathbf{g}_1, \mathbf{g}_2) \star f\big).$$

Proof. Lemma 3.4 follows by substitution from

$$\int_{G(\mathbf{g}_1\mathbf{h},\mathbf{g}_2\mathbf{r})} f(\mathbf{g})\, \mathrm{d}\mathbf{g} = \int_{G(\mathbf{h},\mathbf{r})} f(\mathbf{g}_2\mathbf{g}\mathbf{g}_1^{-1})\, \mathrm{d}\mathbf{g}.$$

□

As a direct consequence of Lemma 3.4 and the irreducibility of the harmonic spaces $\mathrm{Harm}_l(\mathbb{S}^2)$ and $\mathrm{Harm}_l(\mathrm{SO}(3))$ the Radon transform maps a harmonic function on SO(3) of a certain degree either to zero or to a harmonic function on $\mathbb{S}^2 \times \mathbb{S}^2$ of the same degree. More precisely, we have the following fundamental lemma about the Radon transform on SO(3) which was already mentioned by Bunge (1969, Section 11.5.2).

Lemma 3.5. *Let $l \in \mathbb{N}_0$ and $k, k' = -l, \dots, l$. The Radon transform of the Wigner-D function $T_l^{kk'}$ is*

$$\mathcal{R}T_l^{kk'}(\mathbf{h}, \mathbf{r}) = \frac{2\pi}{l + \frac{1}{2}} \mathcal{Y}_l^{k'}(\mathbf{h}) \overline{\mathcal{Y}_l^k(\mathbf{r})}, \quad (\mathbf{h}, \mathbf{r} \in \mathbb{S}^2). \tag{3.1}$$

Proof. For arbitrary $l \in \mathbb{N}_0$, $k, k' = -l, \dots, l$ we obtain by equation (2.26)

$$\begin{aligned} \mathcal{R}T_l^{kk'}(\mathbf{h}, \mathbf{r}) &= \frac{1}{2\pi} \int_{G(\mathbf{h},\mathbf{r})} T_l^{kk'}(\mathbf{g}) \, \mathrm{d}\mathbf{g} \\ &= \frac{1}{2\pi} \int_{G(\mathbf{h},\mathbf{r})} \int_{\mathbb{S}^2} \mathcal{Y}_l^{k'}(\mathbf{g}^{-1}\boldsymbol{\eta}) \overline{\mathcal{Y}_l^k(\boldsymbol{\eta})} \, \mathrm{d}\boldsymbol{\eta} \, \mathrm{d}\mathbf{g} \\ &= \frac{1}{2\pi} \int_{\mathbb{S}^2} \mathcal{Y}_l^{k'}(\boldsymbol{\eta}) \int_{G(\mathbf{h},\mathbf{r})} \overline{\mathcal{Y}_l^k(\mathbf{g}\boldsymbol{\eta})} \, \mathrm{d}\mathbf{g} \, \mathrm{d}\boldsymbol{\eta}. \end{aligned} \tag{3.2}$$

Since we have for any $\boldsymbol{\eta}, \mathbf{h}, \mathbf{r} \in \mathbb{S}^2$ and $\mathbf{g}_0 \in G(\mathbf{h}, \mathbf{r})$

$$\{ \, \mathbf{g}\boldsymbol{\eta} \mid \mathbf{g} \in G(\mathbf{h}, \mathbf{r}) \, \} = \{ \, \mathrm{Rot}_{\mathbf{r}}(\omega)\mathbf{g}_0\boldsymbol{\eta} \in \mathbb{S}^2 \mid \omega \in [0, 2\pi) \, \}$$

the inner integral rewrites as

$$\frac{1}{2\pi} \int_{G(\mathbf{h},\mathbf{r})} \overline{\mathcal{Y}_l^k(\mathbf{g}\boldsymbol{\eta})} \, \mathrm{d}\mathbf{g} = \frac{1}{2\pi} \int_0^{2\pi} \overline{\mathcal{Y}_l^k(\mathrm{Rot}_{\mathbf{r}}(\omega)\mathbf{g}_0\boldsymbol{\eta})} \, \mathrm{d}\omega = \mathcal{P}_l(\mathbf{r} \cdot \mathbf{g}_0\boldsymbol{\eta}) \overline{\mathcal{Y}_l^k(\mathbf{r})}.$$

Here we have applied the spherical mean value theorem 2.3. Together with equation (3.2) and the Funk–Hecke theorem 2.4 we obtain

$$\mathcal{R}T_l^{kk'}(\mathbf{h}, \mathbf{r}) = \int_{\mathbb{S}^2} \mathcal{Y}_l^{k'}(\boldsymbol{\eta}) \mathcal{P}_l(\mathbf{h} \cdot \boldsymbol{\eta}) \overline{\mathcal{Y}_l^k(\mathbf{r})} \, \mathrm{d}\boldsymbol{\eta} = \frac{2\pi}{l + \frac{1}{2}} \mathcal{Y}_l^{k'}(\mathbf{h}) \overline{\mathcal{Y}_l^k(\mathbf{r})}.$$

□

Remark 3.6. Let $l \in \mathbb{N}_0$. Using the matrix representation $T_l = (T_l^{kk'})$ of the Wigner–D functions Lemma 3.5 may be written as

$$\mathcal{R}T_l(\mathbf{h}, \mathbf{r}) = \frac{2\pi}{l + \frac{1}{2}} \overline{\mathcal{Y}_l(\mathbf{r})} \mathcal{Y}_l(\mathbf{h})^T, \quad \mathbf{h}, \mathbf{r} \in \mathbb{S}^2. \tag{3.3}$$

Applying the trace operator to equation (3.3) we obtain for any $\mathbf{h}, \mathbf{r} \in \mathbb{S}^2$

$$(\mathcal{R} \operatorname{Tr} T_l)(\mathbf{h}, \mathbf{r}) = \frac{2\pi}{l + \frac{1}{2}} \sum_{k=-l}^{l} \mathcal{Y}_l^k(\mathbf{h}) \overline{\mathcal{Y}_l^k(\mathbf{r})} = \mathcal{P}_l(\mathbf{h} \cdot \mathbf{r}). \tag{3.4}$$

The next two lemmas provide representations of the Radon transform for the class of radially symmetric and the class of fibre symmetric functions on SO(3).

Lemma 3.7. *Let $f \in C(\mathrm{SO}(3))$ be a radially symmetric function with center $\mathbf{g}_0 \in \mathrm{SO}(3)$ and denote $F\colon [0,1] \to \mathbb{R}$ the function defined by*

$$f(\mathbf{g}) = F\left(\cos\frac{\measuredangle(\mathbf{g},\mathbf{g}_0)}{2}\right), \quad \mathbf{g} \in \mathrm{SO}(3).$$

Then its Radon transform $\mathcal{R}f$ has the integral representation

$$\mathcal{R}f(\mathbf{h},\mathbf{r}) = \frac{2}{\pi}\int_0^{\pi/2} F\left(\cos(\theta)\cos\frac{\measuredangle(\mathbf{g}_0\mathbf{h},\mathbf{r})}{2}\right)\mathrm{d}\theta, \quad \mathbf{h},\mathbf{r} \in \mathbb{S}^2, \tag{3.5}$$

and hence depends only on the angular distance $\measuredangle(\mathbf{g}_0\mathbf{h},\mathbf{r})$. In particular, for any $\mathbf{h},\mathbf{r} \in \mathbb{S}^2$ the trace functions $\mathcal{R}f(\mathbf{h},\circ)$ and $\mathcal{R}f(\circ,\mathbf{r})$ are radially symmetric with centers $\mathbf{g}_0\mathbf{h}$ and $\mathbf{g}_0^{-1}\mathbf{r}$, respectively.

Proof. A proof of equation (3.5) can be found in Schaeben (1997). □

Definition 3.8. Let $\mathbf{h}_0,\mathbf{r}_0 \in \mathbb{S}^2$. A function $f\colon \mathrm{SO}(3) \to \mathbb{R}$ that depends only on the angular distance $\measuredangle(\mathbf{g}\mathbf{h}_0,\mathbf{r}_0)$, $\mathbf{g} \in \mathrm{SO}(3)$ is called *fibre symmetric* with respect to the fibre $G(\mathbf{h}_0,\mathbf{r}_0)$.

Lemma 3.9. *Let $f \in C(\mathrm{SO}(3))$ be a fibre symmetric function and let $F\colon [-1,1] \to \mathbb{R}$ be defined by*

$$F(\mathbf{g}\mathbf{h}_0\cdot\mathbf{r}_0) = f(\mathbf{g}), \quad \mathbf{g} \in \mathrm{SO}(3).$$

Then the Radon transform of f has the integral representation

$$\mathcal{R}f(\mathbf{h},\mathbf{r}) = \frac{1}{\pi}\int_0^{\pi} F(\cos\measuredangle(\mathbf{h},\mathbf{h}_0)\cos\measuredangle(\mathbf{r},\mathbf{r}_0) + \sin\measuredangle(\mathbf{h},\mathbf{h}_0)\sin\measuredangle(\mathbf{r},\mathbf{r}_0)\cos\theta)\,\mathrm{d}\theta. \tag{3.6}$$

In particular, the trace functions $\mathcal{R}f(\circ,\mathbf{r}), \mathcal{R}f(\mathbf{h},\circ) \in C(\mathbb{S}^2)$ are radially symmetric functions with center $\mathbf{h}_0$ and $\mathbf{r}_0$, respectively.

Proof. Let $\mathbf{h},\mathbf{r} \in \mathbb{S}^2$ and let $\mathbf{g}_0 \in \mathrm{SO}(3)$ be the rotation mapping $\mathbf{h}$ onto $\mathbf{r}$ such that $\mathbf{g}_0\mathbf{h}_0$ is on one geodesic with $\mathbf{r}$ and $\mathbf{r}_0$. Then $G(\mathbf{h},\mathbf{r}) = \{\,\mathrm{Rot}_{\mathbf{r}}(\omega)\mathbf{g}_0 \mid \omega \in [0,2\pi)\,\}$ and we have

$$\mathcal{R}f(\mathbf{h},\mathbf{r}) = \frac{1}{2\pi}\int_0^{2\pi} f\big(\mathrm{Rot}_{\mathbf{r}}(\omega)\mathbf{g}_0\big)\,\mathrm{d}\omega = \frac{1}{2\pi}\int_0^{2\pi} F\big(\mathbf{g}_0\mathbf{h}_0\cdot\mathrm{Rot}_{\mathbf{r}}(\omega)\,\mathbf{r}_0\big)\,\mathrm{d}\omega.$$

Treating $\mathbf{r}$ as the north pole of a polar coordinate system and observing

$$\measuredangle(\mathbf{g}_0\mathbf{h}_0,\mathbf{r}) = \measuredangle(\mathbf{h}_0,\mathbf{g}_0^{-1}\mathbf{r}) = \measuredangle(\mathbf{h}_0,\mathbf{h})$$

we obtain from equation (2.1)

$$\cos\measuredangle(\mathbf{g}_0\mathbf{h}_0,\mathrm{Rot}_{\mathbf{r}}(\omega)\mathbf{r}_0) = \cos\measuredangle(\mathbf{h},\mathbf{h}_0)\cos\measuredangle(\mathbf{r},\mathbf{r}_0) + \sin\measuredangle(\mathbf{h},\mathbf{h}_0)\sin\measuredangle(\mathbf{r},\mathbf{r}_0)\cos(\omega),$$

which proves equation (3.6). □

3.2 The Radon Transform in Sobolev–Hilbert Spaces

In this section we are going to extend the Radon transform on SO(3) to a bounded operator acting between Sobolev spaces. A more detailed analysis of the Radon transform on SO(3) between Sobolev spaces can be found in van den Boogaart et al. (2006).

Theorem 3.10. *Let $s \in \mathbb{R}$. Then there is a well defined extension of the Radon transform $\mathcal{R}\colon C(\mathrm{SO}(3)) \to C(\mathbb{S}^2 \times \mathbb{S}^2)$ to an isometric operator*

$$\mathcal{R}_{\mathcal{H}_s}\colon \mathcal{H}_s(\mathrm{SO}(3)) \to \mathcal{H}_{s+\frac{1}{2}}(\mathbb{S}^2 \times \mathbb{S}^2).$$

Proof. For any unit basis function $\frac{1}{2\pi}(l+\frac{1}{2})^{\frac{1}{2}-s}T_l^{kk'}$ in $\mathcal{H}_s(\mathrm{SO}(3))$ we have by Lemma 3.5

$$\frac{1}{2\pi}(l+\tfrac{1}{2})^{\frac{1}{2}-s}\,\mathcal{R}T_l^{kk'} = 2(l+\tfrac{1}{2})^{-\frac{1}{2}-s}\mathcal{Y}_l^{k'}(\circ_1)\overline{\mathcal{Y}_l^{k}(\circ_2)}.$$

Hence, $\mathcal{R}_{\mathcal{H}_s}$ defines an $\mathcal{H}_s(\mathrm{SO}(3))$–$\mathcal{H}_{s+\frac{1}{2}}(\mathbb{S}^2 \times \mathbb{S}^2)$ isometric operator on a dense subset of $\mathcal{H}_s(\mathrm{SO}(3))$. This implies the existence of an isometric extension. □

The next proposition characterizes the range of $\mathcal{H}_s(\mathrm{SO}(3))$ under the Radon transform (cf. Nikolayev and Schaeben, 1999).

Proposition 3.11. *The range of the spherical Radon transform $\mathcal{R}_{\mathcal{H}_s}$, $s \in \mathbb{R}$ is the subspace of all functions $P \in \mathcal{H}_{s+\frac{1}{2}}(\mathbb{S}^2 \times \mathbb{S}^2)$ that satisfy the ultrahyperbolic differential equation*

$$\triangle_{\mathbb{S}^2,1}P = \triangle_{\mathbb{S}^2,2}P,$$

where $\triangle_{\mathbb{S}^2,i}P$, $i = 1, 2$, denotes the application of the spherical Laplace–Beltrami operator to P with respect to its i-th free variable.

Proof. By Lemma 3.5 we have for all $l \in \mathbb{N}_0$ and $k, k' = -l, \ldots, l$ the equality

$$\triangle_{\mathbb{S}^2,1}\mathcal{R}T_l^{kk'} = \frac{2\pi}{l+\frac{1}{2}}(\triangle_{\mathbb{S}^2}\mathcal{Y}_l^{k'})(\circ_1)\overline{\mathcal{Y}_l^{k}}(\circ_2) = \frac{2\pi}{l+\frac{1}{2}}\mathcal{Y}_l^{k'}(\circ_1)\triangle_{\mathbb{S}^2}\overline{\mathcal{Y}_l^{k'}}(\circ_2) = \triangle_{\mathbb{S}^2,2}\mathcal{R}T_l^{kk'}.$$

Together with Theorem 3.10 this proves the assertion. □

Remark 3.12. Theorem 3.10 implies in particular that there is a well defined bounded operator

$$\mathcal{R}_{L^2}\colon L^2(\mathrm{SO}(3)) \to L^2(\mathbb{S}^2 \times \mathbb{S}^2)$$

that extends the Radon transform. Moreover, we have by Theorem 3.24 that $\mathcal{R}f \in \mathcal{H}_{\frac{1}{2}}(\mathbb{S}^2 \times \mathbb{S}^2)$ for any $f \in L^2(\mathrm{SO}(3))$. Applying the trace theorem 2.28 we obtain that the trace functions $\mathcal{R}f(\boldsymbol{\eta}, \circ), \mathcal{R}f(\circ, \boldsymbol{\eta}) \in L^2(\mathbb{S}^2)$ are well defined for any $\boldsymbol{\eta} \in \mathbb{S}^2$.

The next two lemma extend Lemma 3.7 and Lemma 3.9 by characterizing the Radon transform of radially and fibre symmetric functions on SO(3) by its Fourier coefficients.

Lemma 3.13. *Let $f \in L^2(\mathrm{SO}(3))$ be a radially symmetric function with center $\mathbf{g}_0 \in \mathrm{SO}(3)$ and let the function $F \in L^2([-1,1], \sqrt{1-t^2})$ be defined by*

$$F(t) = f(\mathbf{g}), \quad t \in [-1,1],\ \mathbf{g} \in \mathrm{SO}(3),\ |t| = \cos \tfrac{\measuredangle(\mathbf{g},\mathbf{g}_0)}{2}.$$

Then the function $P \in L^2([-1,1])$,

$$P(\mathbf{g}_0\mathbf{h} \cdot \mathbf{r}) = \mathcal{R}f(\mathbf{h},\mathbf{r}), \quad \mathbf{h},\mathbf{r} \in \mathbb{S}^2,$$

has the Legendre expansion

$$P = \sum_{l=0}^{\infty} \hat{F}(2l)\mathcal{P}_l,$$

where $\hat{F}(2l)$, $l \in \mathbb{N}_0$, are the even order Chebyshev coefficients of F.

Proof. Combining Lemma 3.7 and Remark 3.12 we conclude that $\mathcal{R}f(\circ,\mathbf{r}) \in L^2(\mathbb{S}^2)$ defines a radially symmetric function with center $\mathbf{g}_0^{-1}\mathbf{r}$. By Lemma 2.2 this implies $P \in L^2([-1,1])$ and hence P has a well defined expansion into Legendre polynomials. The fact that the Legendre coefficients of P coincides with the even order Chebyshev coefficients of F is due to Proposition 2.15 and the equations (3.4) and (2.25). □

Lemma 3.14. *Let $f \in L^2(\mathrm{SO}(3))$ be a fibre symmetric function with respect to the fibre $G(\mathbf{h}_0,\mathbf{r}_0)$, $\mathbf{h}_0,\mathbf{r}_0 \in \mathbb{S}^2$. Then f has the Fourier representation*

$$f = \sum_{l=0}^{\infty} \frac{2\pi}{l+\frac{1}{2}} \widehat{F}(l) \sum_{kk'=-l}^{l} \mathcal{Y}_l^k(\mathbf{h}_0)\overline{\mathcal{Y}_l^{k'}(\mathbf{r}_0)}T_l^{kk'}, \tag{3.7}$$

where $\hat{F}(l)$, $l \in \mathbb{N}_0$ are the Legendre coefficients of the function $F \in L^2([-1,1])$ defined by

$$F(\mathbf{g}\mathbf{h}_0 \cdot \mathbf{r}_0) = f(\mathbf{g}), \quad \mathbf{g} \in \mathrm{SO}(3).$$

Its Radon transform $\mathcal{R}f \in L^2(\mathbb{S}^2 \times \mathbb{S}^2)$ has the series expansion

$$\mathcal{R}f(\mathbf{h},\mathbf{r}) = \sum_{l=0}^{\infty} \widehat{F}(l)\mathcal{P}_l(\mathbf{h}_0 \cdot \mathbf{h})\mathcal{P}_l(\mathbf{r}_0 \cdot \mathbf{r}), \quad \mathbf{h},\mathbf{r} \in \mathbb{S}^2 \tag{3.8}$$

where convergence is meant in the sense of $L^2(\mathbb{S}^2 \times \mathbb{S}^2)$.

Proof. Let $f \in L^2(\mathrm{SO}(3))$ and $F\colon [-1,1] \to \mathbb{R}$ be as defined in the Lemma. Then we have

$$\int_{\mathrm{SO}(3)} |f(\mathbf{g})|^2 \,\mathrm{d}\mathbf{g} = \int_{\mathrm{SO}(3)} |F(\mathbf{g}\mathbf{h}_0 \cdot \mathbf{r}_0)|^2 \,\mathrm{d}\mathbf{g} = 2\pi \int_{\mathbb{S}^2} |F(\mathbf{r} \cdot \mathbf{r}_0)|^2 \,\mathrm{d}\mathbf{r} = 2\pi \int_{-1}^{1} |F(t)|^2 \,\mathrm{d}\mathbf{t}$$

and hence $F \in L^2([-1,1])$.

Let

$$F = \sum_{l=0}^{\infty} \hat{F}(l)\mathcal{P}_l$$

be the Legendre expansion of F. By the spherical addition theorem we have for all $\mathbf{g} \in \mathrm{SO}(3)$,

$$\frac{2l+1}{4\pi}\mathcal{P}_l(\mathbf{g}\mathbf{h}_0 \cdot \mathbf{r}_0) = \mathcal{Y}_l(\mathbf{r}_0)^T\overline{\mathcal{Y}_l(\mathbf{g}\mathbf{h}_0)} = \mathcal{Y}_l(\mathbf{r}_0)^T\overline{T_l(\mathbf{g}^{-1})^T\mathcal{Y}_l(\mathbf{h}_0)} = \mathcal{Y}_l(\mathbf{r}_0)^T T_l(\mathbf{g})\overline{\mathcal{Y}_l(\mathbf{h}_0)},$$

which proves equation (3.7). Applying the Radon transform to the last term we obtain by Remark 3.6 and the spherical addition theorem

$$\begin{aligned}\big(\mathcal{R}\,\mathcal{Y}_l(\mathbf{r}_0)^T T_l(\circ)\overline{\mathcal{Y}_l(\mathbf{h}_0)}\big)(\mathbf{h},\mathbf{r}) &= \frac{4\pi}{2l+1}\mathcal{Y}_l(\mathbf{r}_0)^T\overline{\mathcal{Y}_l(\mathbf{r})}\mathcal{Y}_l(\mathbf{h})^T\overline{\mathcal{Y}_l(\mathbf{h}_0)} \\ &= \frac{2l+1}{4\pi}\mathcal{P}_l(\mathbf{r}_0 \cdot \mathbf{r})\mathcal{P}_l(\mathbf{h} \cdot \mathbf{h}_0),\end{aligned}$$

which implies equation (3.8). □

Thanks to Lemma 3.5 the operator $\mathcal{R}_{L^2}$ is a multiplication operator in Fourier space and hence its adjoint operator $\mathcal{R}^*_{L^2}$ is a multiplication operator Fourier space as well. In the next lemma we show that the adjoint operator $\mathcal{R}^*_{L^2}$ has also a representation as an integral operator.

Lemma 3.15. *The adjoint operator to the one–dimensional Radon transform $\mathcal{R}_{L^2}$ on* $\mathrm{SO}(3)$ *is the integral operator*

$$\begin{aligned}\mathcal{R}^*_{L^2} &\colon L^2(\mathbb{S}^2 \times \mathbb{S}^2) \to L^2(\mathrm{SO}(3)), \\ \mathcal{R}^*_{L^2}P(\mathbf{g}) &= \frac{1}{2\pi}\int_{\mathbb{S}^2} \overline{P(\mathbf{h}, \mathbf{g}\mathbf{h})}\,\mathrm{d}\mathbf{h}.\end{aligned} \tag{3.9}$$

Moreover, we have for all $l \in \mathbb{N}_0$ and $k, k' = -l, \ldots, l$,

$$\mathcal{R}^*_{L^2}\mathcal{Y}_l^{k'}(\circ_1)\overline{\mathcal{Y}_l^k(\circ_2)} = \frac{1}{2\pi}T_l^{kk'}. \tag{3.10}$$

Proof. For every $f \in L^2(\mathrm{SO}(3))$ and $P \in L^2(\mathbb{S}^2 \times \mathbb{S}^2)$ we calculate

$$\begin{aligned}\big\langle f, \mathcal{R}^*_{L^2}P\big\rangle_{L^2(\mathrm{SO}(3))} &= \big\langle \mathcal{R}_{L^2}f, P\big\rangle_{L^2(\mathbb{S}^2\times\mathbb{S}^2)} \\ &= \int_{\mathbb{S}^2}\int_{\mathbb{S}^2}\frac{1}{2\pi}\int_{G(\mathbf{h},\mathbf{r})} f(\mathbf{g})\,\mathrm{d}\mathbf{g}\overline{P(\mathbf{h},\mathbf{r})}\,\mathrm{d}\mathbf{h}\,\mathrm{d}\mathbf{r} \\ &= \int_{\mathrm{SO}(3)} f(\mathbf{g})\frac{1}{2\pi}\int_{\mathbb{S}^2}\overline{P(\mathbf{h},\mathbf{g}\mathbf{h})}\,\mathrm{d}\mathbf{h}\,\mathrm{d}\mathbf{g}.\end{aligned}$$

Equation (3.10) is a direct consequence of

$$\left\langle \mathcal{R}_{L^2} T_l^{kk'}, \mathcal{Y}_l^{k'}(\circ_1)\overline{\mathcal{Y}_l^{k}(\circ_2)} \right\rangle_{L^2(\mathbb{S}^2\times\mathbb{S}^2)} = \frac{2\pi}{l+\frac{1}{2}} = \left\langle T_l^{kk'}, \mathcal{R}^*_{L^2}\mathcal{Y}_l^{k'}(\circ_1)\overline{\mathcal{Y}_l^{k}(\circ_2)} \right\rangle_{L^2(\mathrm{SO}(3))}.$$

□

In fact, integral formula (3.9) defines the *dual Radon transform* to the one–dimensional Radon transform on SO(3) and one can show that in the general setting of homogeneous spaces the dual Radon transform always coincides with the L^2–adjoint Radon transform (cf. Helgason, 1999, Proposition 2.2). Moreover, one can show that the Radon transform as well as its dual are rotational invariant and hence their concatenation is so, too. Since for nice manifolds the algebra of rotational invariant operators is generated by the Laplace–Beltrami operator (cf. Vilenkin and Klimyk, 1991, Chap. 6, Thm. 2) one concludes that $\mathcal{R}^*\mathcal{R}$ is a function of the Laplace–Beltrami operator (cf. Gurarie, 1992, Sec. 2.5). In particular, this holds true for the Radon transform on SO(3).

Theorem 3.16. *The concatenation* $\mathcal{R}^*_{L^2}\mathcal{R}_{L^2}\colon \mathcal{H}_0(\mathrm{SO}(3)) \to \mathcal{H}_1(\mathrm{SO}(3))$ *of the Radon transform and the adjoint Radon transform is an invariant, pseudodifferential operator of order* -1*. The inverse operator* $(\mathcal{R}^*_{L^2}\mathcal{R}_{L^2})^{-1}\colon \mathcal{H}_1(\mathrm{SO}(3)) \to \mathcal{H}_0(\mathrm{SO}(3))$ *is an invariant, pseudodifferential operator of order* 1 *and can be expressed in terms of the Laplace–Beltrami operator on* SO(3) *by*

$$(\mathcal{R}^*_{L^2}\mathcal{R}_{L^2})^{-1} = (-\triangle_{\mathrm{SO}(3)} + \tfrac{1}{4})^{1/2}. \tag{3.11}$$

In particular, we have for all $f \in L^2(\mathrm{SO}(3))$ *the inversion formula*

$$f = (-\triangle_{\mathrm{SO}(3)} + \tfrac{1}{4})^{1/2}\mathcal{R}^*_{L^2}\mathcal{R}_{L^2} f. \tag{3.12}$$

Proof. By Lemma 3.5 and Lemma 3.15 we have for all $l \in \mathbb{N}_0$ and $k, k' = -l, \dots, l$

$$\mathcal{R}^*\mathcal{R} T_l^{kk'} = (l+\tfrac{1}{2})^{-1} T_l^{kk'},$$

and consequently $\widehat{\mathcal{R}^*_{L^2}\mathcal{R}_{L^2}}(l) = (l+\frac{1}{2})^{-1}$. Using Definition 2.24 one verifies that $\mathcal{R}^*_{L^2}\mathcal{R}_{L^2}$ as well as $(\mathcal{R}^*_{L^2}\mathcal{R}_{L^2})^{-1}$ are pseudodifferential operators. On the other hand we know from Lemma 2.19 that

$$\triangle_{\mathrm{SO}(3)} T_l^{kk'} = -l(l+1) T_l^{kk'}$$

for all $l \in \mathbb{N}_0$ and $k, k' = -l, \dots, l$. Since $(l(l+1)+\frac{1}{4})^{\frac{1}{2}} = l + \frac{1}{2}$ we have equation (3.11). □

There exists also other inversion formulae for the one–dimensional Radon transform on SO(3). A concise representation of the inversion formulae of the one–dimensional Radon transform on SO(3) can be found in (Bernstein and Schaeben, 2005).

Finally we are concerned with the question whether the inversion of the Radon transform is local or not. Loosely spoken the inversion of the Radon transform is said to be local if for the reconstruction of $f(\mathbf{g}_0)$, $\mathbf{g}_0 \in \mathrm{SO}(3)$ it is sufficient to know $\mathcal{R}f(\mathbf{h}, \mathbf{r})$ for all geodesics $G(\mathbf{h}, \mathbf{r})$ passing through an arbitrary small neighborhood of $\mathbf{g}_0$. Formally this property is defined in the next Definition.

Definition 3.17. The inversion of the Radon transform $\mathcal{R}\colon \mathcal{H}_0(\mathrm{SO}(3)) \to \mathcal{H}_{\frac{1}{2}}(\mathbb{S}^2 \times \mathbb{S}^2)$ is *local* if for any open set $U \subseteq \mathrm{SO}(3)$ the constraint $\mathcal{R}f(\mathbf{h}, \mathbf{r}) = 0$ for all $(\mathbf{h}, \mathbf{r}) \in \mathbb{S}^2 \times \mathbb{S}^2$ satisfying $G(\mathbf{h}, \mathbf{r}) \cap U \neq \emptyset$ implies $f|_U = 0$.

Before we prove that the Radon transform on SO(3) is not local we first prove the following series representation of the function $t \mapsto \sqrt{2-2t}$ in terms of Legendre polynomials.

Proposition 3.18. *The series*

$$\sum_{l=0}^{\infty} \frac{4}{(2l-1)(2l+3)} \mathcal{P}_l(t) = -\sqrt{2-2t}, \quad t \in [-1, 1] \tag{3.13}$$

converges uniformly on the interval $[-1, 1]$ *to the given function.*

Proof. Uniform convergence of the sum follows from $|\mathcal{P}_l(t)| \leq 1$ for $t \in [-1, 1]$ and $l \in \mathbb{N}_0$.

Let $a, b \in \mathbb{R}$ such that $a + b, b > -1$. Then we have the following expression for the Beta function $B(b+1, a+b+1)$

$$\begin{aligned} B(b+1, a+b+1) &= \int_0^1 (1-t)^{a+b}(1+t)^b \,\mathrm{d}t = 2^{-(a+2b+1)} \int_{-1}^1 (1-t)^{a+b}(1+t)^b \,\mathrm{d}t \\ &= 2^{-(a+2b+1)} \int_{-1}^1 (1-t)^a (1-t^2)^b \,\mathrm{d}t. \end{aligned}$$

Combining this equality with the Rodriguez formula (cf. Freeden, 1998, Equ. 3.2.15) we obtain

$$\begin{aligned} -\int_{-1}^1 \sqrt{2-2t}\mathcal{P}_l(t) \,\mathrm{d}t &= \frac{1}{2^l l!} \int_{-1}^1 \Big(\frac{\mathrm{d}^l}{\mathrm{d}t^l} \sqrt{2-2t}\Big)(1-t^2)^l \,\mathrm{d}t \\ &= \frac{(2l-3)!}{2^{2l-2}(l-2)!l!} \int_{-1}^1 (2-2t)^{-\frac{2l-1}{2}} (1-t^2)^l \,\mathrm{d}t \\ &= \frac{(2l-3)!}{2^{3l-5/2}(l-2)!l!} \int_{-1}^1 (1-t)^{-\frac{2l-1}{2}} (1-t^2)^l \,\mathrm{d}t \\ &= \frac{(2l-3)!}{2^{2l-4}(l-2)!l!} B(l+1, \tfrac{3}{2}). \end{aligned}$$

Using the representation of the Beta function in terms of the Gamma function and the duplication formula for the Gamma function we find

$$\begin{aligned}\frac{(2l-3)!}{2^{2l-4}(l-2)!l!}B(l+1,\tfrac{3}{2}) &= \frac{\Gamma(2l-2)\Gamma(l+1)\Gamma(\frac{3}{2})}{2^{2l-4}\Gamma(l-1)\Gamma(l+1)\Gamma(l+5/2)}\\ &= \frac{\Gamma(2l-2)\Gamma(\frac{3}{2})}{2^{2l-1}\Gamma(l-1)\Gamma(l-1/2)(2l-1)(2l+1)(2l+3)}\\ &= \frac{\Gamma(2l-2)\Gamma(\frac{3}{2})}{2^2\sqrt{\pi}\Gamma(2l-2)(2l-1)(2l+1)(2l+3)}\\ &= \frac{8}{(2l-1)(2l+1)(2l+3)}\end{aligned}$$

and consequently we have for all $l \in \mathbb{N}_0$,

$$-\frac{2l+1}{2}\int_{-1}^{1}\sqrt{2-2t}\mathcal{P}_l(t)\,\mathrm{d}t = \frac{4}{(2l-1)(2l+3)}.$$

Since the Legendre polynomials provide an orthogonal function system in $L^2([-1,1])$ this implies the assertion. □

Now we are ready to prove that the inversion of the Radon transform on SO(3) is not local.

Theorem 3.19. *The inversion of the one–dimensional Radon transform on* SO(3) *is not local.*

Proof. Let $\psi \in C^\infty([-1,1])$ be an infinitely often differentiable test function such that -1 and 1 are not contained in the closure of the support of ψ. Then

$$P(\mathbf{h},\mathbf{r}) = \psi(\mathbf{h}\cdot\mathbf{r}), \quad \mathbf{h},\mathbf{r}\in\mathbb{S}^2$$

defines the Radon transform of a radially symmetric function $f = \mathcal{R}^{-1}P \in C^\infty(\mathrm{SO}(3))$ with center $\mathrm{Id} \in \mathrm{SO}(3)$. Moreover, there is a neighborhood U of Id such that $P(\mathbf{h},\mathbf{r}) = 0$ for all $\mathbf{h},\mathbf{r}\in\mathbb{S}^2$ with $G(\mathbf{h},\mathbf{r})\cap U \neq \emptyset$. We show that ψ can be chosen such that $f(\mathrm{Id}) \neq 0$.

By Lemma 2.2 the function ψ has a well defined expansion into Legendre polynomials. Applying Lemma 3.13 we obtain by partial integration

$$\begin{aligned}\mathcal{R}^{-1}P(\mathrm{Id}) &= \sum_{l=0}^{\infty}\frac{2l+1}{2}\int_{-1}^{1}\psi(t)\mathcal{P}_l(t)\,\mathrm{d}t\,\mathcal{U}_{2l}(\mathrm{Id})\\ &= \sum_{l=0}^{\infty}\frac{2l+1}{2}\int_{-1}^{1}\psi'(t)\big(\mathcal{P}_{l-1}(t)-\mathcal{P}_{l+1}(t)\big)\,\mathrm{d}t\\ &= \sum_{l=1}^{\infty}2\int_{-1}^{1}\psi'(t)\mathcal{P}_l(t)\,\mathrm{d}t\end{aligned}$$

$$= -\sum_{l=1}^{\infty} 2 \int_{-1}^{1} \psi''(t) \frac{\mathcal{P}_{l+1}(t) - \mathcal{P}_{l-1}(t)}{2l+1} \, \mathrm{d}t$$
$$= 2 \int_{-1}^{1} \psi''(t) \Big(\frac{1}{3} + \frac{1}{5} t - \sum_{l=2}^{\infty} \frac{4}{(2l-1)(2l+3)} \mathcal{P}_l(t) \Big) \, \mathrm{d}t.$$

By Proposition 3.18 the sum in the integral converges uniformly for $t \in [-1, 1]$ to

$$\frac{1}{3} + \frac{1}{5} t - \sum_{l=2}^{\infty} \frac{4}{(2l-1)(2l+3)} \mathcal{P}_l(t) = 1 + t + \sqrt{2 - 2t}.$$

Substituting this formula back to the integral and applying partial integration the other way round we obtain

$$\begin{aligned} f(\mathrm{Id}) = \mathcal{R}^{-1} P(\mathrm{Id}) &= 2 \int_{-1}^{1} \psi''(t) \big(1 + t + \sqrt{2 - 2t} \big) \, \mathrm{d}t \\ &= -2 \int_{-1}^{1} \psi'(t) \Big(1 - \frac{1}{\sqrt{2 - 2t}} \Big) \, \mathrm{d}t \\ &= -2 \int_{-1}^{1} \psi(t) (2 - 2t)^{-\frac{3}{2}} \, \mathrm{d}t. \end{aligned}$$

Since, $(2 - 2t)^{-\frac{3}{2}} > 0$ for $t \in [-1, 1)$ we find a function ψ such that $f(\mathrm{Id}) \neq 0$. □

Theorem 3.19 may be interpreted that in order to reconstruct a function $f \in C(\mathrm{SO}(3))$ at a single point $\mathbf{g} \in \mathrm{SO}(3)$ the integral along all one–dimensional geodesic manifolds of SO(3) has to be known. The question whether the inverse Radon transform is local is central in the analysis of the Radon transform since it strongly effects the choice of an appropriate algorithm that has to be used for its numerical treatment (cf. Ramm and Katsevich, 1996).

3.3 Generalizations of the Radon Transform

The Radon Transform in $L^1(\mathrm{SO}(3))$. First are going to extend the Radon transform to the space of absolutely integrable function on SO(3).

Theorem 3.20. *The one–dimensional Radon transform $\mathcal{R} \colon C(\mathrm{SO}(3)) \to C(\mathbb{S}^2 \times \mathbb{S}^2)$ has a well defined extension to a linear, bounded operator*

$$\mathcal{R}_{L^1} \colon L^1(\mathrm{SO}(3)) \to L^1(\mathbb{S}^2 \times \mathbb{S}^2).$$

Moreover, the trace functions $\mathcal{R}_{L^1} f(\mathbf{h}, \circ), \mathcal{R}_{L^1} f(\circ, \mathbf{r}) \in L^1(\mathbb{S}^2)$ are well defined for any unit vectors $\mathbf{h}, \mathbf{r} \in \mathbb{S}^2$.

Proof. For any $f \in C(\mathrm{SO}(3))$ and any unit vector $\mathbf{h} \in \mathbb{S}^2$ we have

$$\begin{aligned}\|\mathcal{R}f(\mathbf{h},\circ)\|_{L^1(\mathbb{S}^2)} \leq \big\|\mathcal{R}\,|f(\mathbf{h},\circ)|\big\|_{L^1(\mathbb{S}^2)} &= \int_{\mathbb{S}^2} \frac{1}{2\pi} \int_{G(\mathbf{h},\mathbf{r})} |f(\mathbf{g})| \,\mathrm{d}\mathbf{g}\,\mathrm{d}\mathbf{r} \\ &= \frac{1}{2\pi} \int_{\mathrm{SO}(3)} |f(\mathbf{g})| \,\mathrm{d}\mathbf{g} = \frac{1}{2\pi} \|f\|_{L^1(\mathrm{SO}(3))}.\end{aligned}$$

Consequently, the mappings $f \mapsto \mathcal{R}f(\mathbf{h},\circ)$ and $f \mapsto \mathcal{R}f(\circ,\mathbf{r})$ constitute $L^1(\mathrm{SO}(3))$–$L^1(\mathbb{S}^2)$ bounded operators on a dense subset of $L^1(\mathrm{SO}(3))$. Hence, there exists a well defined extension to a bounded operator acting on the whole space $L^1(\mathrm{SO}(3))$.

By the inequality

$$\|\mathcal{R}f\|_{L^1(\mathbb{S}^2\times\mathbb{S}^2)} = \int_{\mathbb{S}^2} \|\mathcal{R}f(\mathbf{h},\circ)\|_{L^1(\mathbb{S}^2)} \,\mathrm{d}\mathbf{h} \leq 2\,\|f\|_{L^1(\mathrm{SO}(3))}$$

this applies to the Radon transform $f \mapsto \mathcal{R}f$ as well. □

Radon Transforms on O(3). Next we are going to define a Radon transform on the orthogonal group O(3). In order to reuse most of the results obtained for the rotational group SO(3) we introduce the following notations.

Definition 3.21. Let $\mathbf{g} \in \mathrm{O}(3)$. Then we denote by $-\mathbf{g} = -\mathrm{Id}\,\mathbf{g}$ the concatenation of $\mathbf{g}$ with the inversion and define the rotational part $|\mathbf{g}|$ and the signum $\mathrm{sign}(\mathbf{g})$ of $\mathbf{g}$ by

$$|\mathbf{g}| := \begin{cases} \mathbf{g} & \text{if } \mathbf{g} \in \mathrm{SO}(3), \\ -\mathbf{g} & \text{if } \mathbf{g} \notin \mathrm{SO}(3), \end{cases} \quad \text{and} \quad \operatorname{sign}\mathbf{g} := \begin{cases} 1 & \text{if } g \in \mathrm{SO}(3), \\ -1 & \text{if } g \notin \mathrm{SO}(3). \end{cases}$$

Using these notations we characterize an orthogonal basis in $L^2(\mathrm{O}(3))$.

Lemma 3.22. *The system of functions*

$$T_l^{kk'} \otimes 1(\mathbf{g}) := T_l^{kk'}(|\mathbf{g}|) \quad \textit{and} \quad T_l^{kk'} \otimes \bar{1} := \mathrm{sign}(\mathbf{g}) T_l^{kk'}(|\mathbf{g}|),$$

$l \in \mathbb{N}_0$, $k, k' = -l, \ldots, l$, forms an orthogonal basis in $L^2(\mathrm{O}(3))$.

Remember that the geodesics in SO(3) are

$$G(\mathbf{h},\mathbf{r}) = \{\, \mathbf{g} \in \mathrm{SO}(3) \mid \mathbf{g}\mathbf{h} = \mathbf{r} \,\}, \quad \mathbf{h},\mathbf{r} \in \mathbb{S}^2.$$

Since O(3) is topologically the disjoint sum of two copies of the group SO(3) the geodesics of O(3) are the geodesics $G(\mathbf{h},\mathbf{r})$, $\mathbf{h},\mathbf{r} \in \mathbb{S}^2$ of SO(3) plus the geodesics

$$-G(\mathbf{h},\mathbf{r}) = \{\, -\mathbf{g} \mid \mathbf{g} \in G(\mathbf{h},\mathbf{r}) \,\} \subseteq \mathrm{O}(3)\backslash\mathrm{SO}(3), \quad \mathbf{h},\mathbf{r} \in \mathbb{S}^2$$

of $\mathrm{O}(3)\backslash\mathrm{SO}(3) = -\mathrm{SO}(3)$.

Consequently, the one–dimensional Radon transform on O(3) is defined as

$$\begin{aligned}\mathcal{R}\colon C(\mathrm{O}(3)) &\to C\left(\mathbb{S}^2\times\mathbb{S}^2\times\{\mathrm{Id},-\mathrm{Id}\}\right),\\ \mathcal{R}f(\mathbf{h},\mathbf{r},\mathbf{q}) &= \frac{1}{4\pi}\int_{\mathbf{q}G(\mathbf{h},\mathbf{r})} f(\mathbf{g})\,\mathrm{d}\mathbf{g}.\end{aligned}$$

It is not hard to prove that all main properties of the Radon transform on SO(3) remain true for the Radon transform on O(3) as well.

In the remainder of this section we focus on a symmetrized version of the Radon transform on O(3) which will be our central subject during the next chapters.

Definition 3.23. We define the operator $\mathcal{X}$ as

$$\begin{aligned}\mathcal{X}\colon C(\mathrm{O}(3)) &\to C\left(\mathbb{S}^2\times\mathbb{S}^2\right),\\ \mathcal{X}f(\mathbf{h},\mathbf{r}) &= \frac{1}{2}\big(\mathcal{R}f(\mathbf{h},\mathbf{r},\mathrm{Id})+\mathcal{R}f(\mathbf{h},\mathbf{r},-\mathrm{Id})\big).\end{aligned}\tag{3.14}$$

The next theorem is the counterpart to the characterization theorem 3.10 of the Radon transform on SO(3) in Sobolev spaces.

Theorem 3.24. *Let $s\in\mathbb{R}$. Then the operator $\mathcal{X}$ extends uniquely to a linear, bounded operator*

$$\mathcal{X}_{\mathcal{H}_s(\mathrm{O}(3))}\colon \mathcal{H}_s(\mathrm{O}(3))\to\mathcal{H}_{s+\frac{1}{2}}(\mathbb{S}^2\times\mathbb{S}^2)$$

with kernel

$$\ker\mathcal{X}_{\mathcal{H}_s(\mathrm{O}(3))}=\mathrm{clos}_{\mathcal{H}_s}\,\mathrm{span}\left\{T_{2l}^{kk'}\otimes 1,\ T_{2l+1}^{kk'}\otimes\bar{1}\ \mid\ l\in\mathbb{N}_0,\ k,k'=-l,\dots,l\right\}.$$

In particular, the restriction of the operator $\mathcal{X}_{\mathcal{H}_s(\mathrm{O}(3))}$ to its cokernel and image is an isometric operator.

Moreover, there is a well defined extension of the operator $\mathcal{X}$ to a linear, bounded operator

$$\mathcal{X}_{L^1(\mathrm{O}(3))}\colon L^1(\mathrm{O}(3))\to L^1(\mathbb{S}^2\times\mathbb{S}^2).$$

Proof. By Lemma 3.5 we have for any $l\in\mathbb{N}_0$ and $k,k'=-l,\dots,l$

$$\begin{aligned}\mathcal{X}T_l^{kk'}\otimes 1(\mathbf{h},\mathbf{r}) &= \frac{1}{2}\Big(\mathcal{R}T_l^{kk'}(\mathbf{h},\mathbf{r})+\mathcal{R}T_l^{kk'}(-\mathbf{h},\mathbf{r})\Big)\\ &= \frac{\pi}{l+\frac{1}{2}}\Big(\mathcal{Y}_l^{k'}(\mathbf{h})\overline{\mathcal{Y}_l^{k}(\mathbf{r})}+\mathcal{Y}_l^{k'}(-\mathbf{h})\overline{\mathcal{Y}_l^{k}(\mathbf{r})}\Big)\\ &= \begin{cases}\frac{2\pi}{l+\frac{1}{2}}\mathcal{Y}_l^{k'}(\mathbf{h})\overline{\mathcal{Y}_l^{k}(\mathbf{r})} & \text{if } l \text{ even},\\ 0 & \text{if } l \text{ odd}\end{cases}\end{aligned}$$

and, analogously,

$$\mathcal{X}T_l^{kk'} \otimes \bar{1}(\mathbf{h},\mathbf{r}) = \begin{cases} 0 & \text{if } l \text{ even,} \\ \frac{2\pi}{l+\frac{1}{2}} \mathcal{Y}_l^{k'}(\mathbf{h})\overline{\mathcal{Y}_l^{k}(\mathbf{r})} & \text{if } l \text{ odd.} \end{cases}$$

Now Theorem 3.24 follows from Theorem 3.10 and Theorem 3.20. □

Let $\Pi\colon \mathcal{H}_s(\mathrm{O}(3)) \to \mathcal{H}_s(\mathrm{SO}(3))$ the canonical mapping that projects the cokernel of $\mathcal{X}_{\mathcal{H}(\mathrm{O}(3))}$ onto $\mathcal{H}_s(\mathrm{SO}(3))$. Then $\mathcal{X}_{\mathcal{H}_s(\mathrm{O}(3))} = \mathcal{R}_{\mathcal{H}_s(\mathrm{SO}(3))}\Pi$ and the results of Chapter 3 apply to the operator $\mathcal{X}$ as well.

The Radon Transform on Quotient Spaces. Let $s \in \mathbb{R}$. Then we define for any finite subgroup $Q \subseteq \mathrm{O}(3)$ the symmetrization operators

$$S_Q\colon \mathcal{H}_s(\mathrm{O}(3)) \to \mathcal{H}_s(\mathrm{O}(3)/Q), \qquad S_Q f(\mathbf{g}) = \frac{1}{|Q|}\sum_{\mathbf{q}\in Q} f(\mathbf{gq})$$

and

$$S_Q\colon \mathcal{H}_s(\mathbb{S}^2\times\mathbb{S}^2) \to \mathcal{H}_s(\mathbb{S}^2/Q\times\mathbb{S}^2), \qquad S_Q P(\mathbf{h},\mathbf{r}) = \frac{1}{|Q|}\sum_{\mathbf{q}\in Q} P(\mathbf{qh},\mathbf{r}).$$

In Lemma 3.4 we have shown that the Radon transform commutes with S_Q. Hence, there is a well defined restriction of the operator $\mathcal{X}_{\mathcal{H}_s(\mathrm{O}(3))}$ to a bounded operator $\mathcal{X}_{\mathcal{H}_s(\mathrm{O}(3)/Q)}$ such that the diagram

$$\begin{array}{ccc} \mathcal{H}_s(\mathrm{O}(3)) & \xrightarrow{\mathcal{X}_{\mathcal{H}_s(\mathrm{O}(3))}} & \mathcal{H}_{s+\frac{1}{2}}(\mathbb{S}^2\times\mathbb{S}^2) \\ \big\downarrow S_Q & & \big\downarrow S_Q \\ \mathcal{H}_s(\mathrm{O}(3)/G) & \xrightarrow{\mathcal{X}_{\mathcal{H}_s(\mathrm{O}(3)/Q)}} & \mathcal{H}_{s+\frac{1}{2}}(\mathbb{S}^2/Q\times\mathbb{S}^2) \end{array}$$

commutes. The same holds true if the Sobolev Hilbert spaces are replaced by the corresponding spaces of absolutely integrable functions.

Remark 3.25. Let $Q \subseteq \mathrm{O}(3)$ be a finite subgroup that contains the inversion, i.e. $-\mathrm{Id} \in Q$. Since $G(\mathbf{h},\mathbf{r}) = G(-\mathbf{h},-\mathbf{r})$ we have for any $f \in C(\mathrm{O}(3)/S_{\mathrm{Laue}})$ and any $\mathbf{h},\mathbf{r} \in \mathbb{S}^2$ the equality

$$\mathcal{X}f(Q\mathbf{h},\mathbf{r}) = \mathcal{X}f(-Q\mathbf{h},\mathbf{r}) = \mathcal{X}f(Q\mathbf{h},-\mathbf{r}).$$

In particular, the trace function $\mathcal{X}(Q\mathbf{h},\circ)$ is an even function for any $\mathbf{h} \in \mathbb{S}^2$.

3.4 Radially Symmetric Functions on $\mathbb{S}^2$ and SO(3)

Let $K \in L^2(\mathrm{SO}(3))$ be a radially symmetric function on SO(3) with center $\mathbf{g}_0 \in \mathrm{SO}(3)$. Then Lemma 2.6 defines a function $\tilde{K} \in L^2([0,1],\sqrt{1-t^2})$ such that

$$\tilde{K}\left(\cos\frac{\measuredangle(\mathbf{g}_0,\mathbf{g})}{2}\right) = K(\mathbf{g}), \quad \mathbf{g} \in \mathrm{SO}(3).$$

On the other hand it exists by Lemma 2.2 for any radially symmetric function $P \in L^2(\mathbb{S}^2)$ with center $\boldsymbol{\eta}_0 \in \mathbb{S}^2$ a function $\tilde{P} \in L^2([-1,1])$ such that

$$\tilde{P}(\boldsymbol{\eta} \cdot \boldsymbol{\eta}_0) = P(\boldsymbol{\eta}), \quad \boldsymbol{\eta} \in \mathbb{S}^2.$$

Since the Radon transform is a bounded operator that maps radially symmetric functions in $L^2(\mathrm{SO}(3))$ onto radially symmetric functions in $L^2(\mathbb{S}^2)$ it defines a bounded operator

$$\begin{aligned} \tilde{\mathcal{R}} \colon L^2\big([0,1], \sqrt{1-t^2}\big) &\to L^2([-1,1]), \\ \tilde{\mathcal{R}}\tilde{K}(\mathbf{g}_0\mathbf{h} \cdot \mathbf{r}) &= \mathcal{R}K(\mathbf{h}, \mathbf{r}), \quad \mathbf{h}, \mathbf{r} \in \mathbb{S}^2. \end{aligned}$$

In Lemma 3.7 we have shown that $\tilde{\mathcal{R}}$ is in fact the integral operator

$$\tilde{\mathcal{R}}\tilde{K}(t) = \int_0^\pi \tilde{K}\left(\cos\theta \sqrt{\tfrac{1+t}{2}}\right) \mathrm{d}\theta.$$

On the other hand, we have shown in Lemma 3.13 that $\tilde{\mathcal{R}}$ provides a one to one relation between the even order Chebyshev coefficients of $\tilde{K}$ and the Legendre coefficients of $\tilde{\mathcal{R}}\tilde{K}$, i.e.

$$\widehat{\tilde{K}}(2l) = \widehat{\tilde{\mathcal{R}}\tilde{K}}(l), \quad l \in \mathbb{N}_0.$$

In this section we are going to make use of this two fold relationship between radially symmetric functions in $L^2(\mathrm{SO}(3))$ and radially symmetric function in $L^2(\mathbb{S}^2)$ to derive representations of some important (radially symmetric) kernel functions on $\mathrm{SO}(3)$ and $\mathbb{S}^2$. Moreover, we give formulae for the relationship between the free parameter of the kernel functions and their *halfwidth*, i.e. the angle $b \in [0, \pi]$ where the kernel function $\tilde{K}$ satisfies

$$\tilde{K}(\cos\tfrac{b}{2}) = \frac{1}{2}\tilde{K}(1).$$

Predecessors of the following compilation of kernel functions can be found in Matthies et al. (1987), Freeden (1998), Schaeben and v.d. Boogaart (2003) and many others.

The Abel–Poisson Kernel. Our compilation starts with the *Abel–Poisson kernel* which is for any $\kappa \in (0,1)$ characterized by the Legendre coefficients

$$\widehat{\tilde{K}}(2l) = \widehat{\tilde{\mathcal{R}}\tilde{K}}(l) = (2l+1)\kappa^{2l}, \quad l \in \mathbb{N}_0.$$

For $\tilde{\mathcal{R}}\tilde{K}$ we have the well known representation (cf. Freeden, 1998, Sec. 6.5)

$$\tilde{\mathcal{R}}\tilde{K}(t) = \frac{1-\kappa^4}{(1-2\kappa^2 t + \kappa^4)^{3/2}}, \quad t \in [-1,1].$$

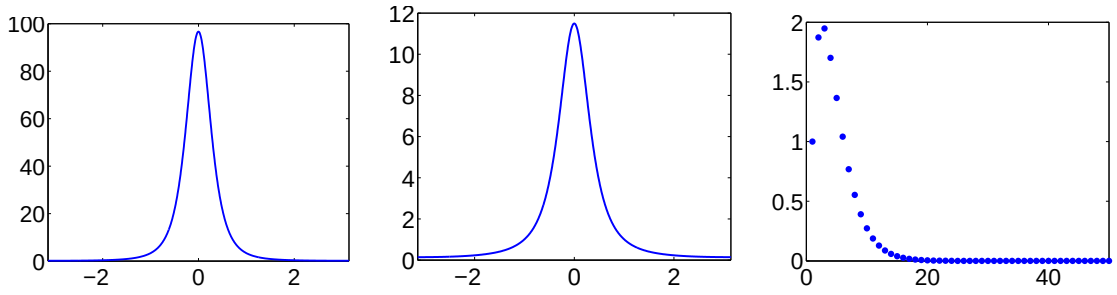

Figure 3.1: The Abel–Poisson kernel for $\kappa = 0.79$.

The corresponding kernel function K on SO(3) was investigated in Matthies et al. (1987, Sec. 17) where it is called *Lorentz function*. In particular, there it is shown

$$\tilde{K}(t) = \frac{1-\kappa^2}{(1+2\kappa t+\kappa^2)^2} + \frac{1-\kappa^2}{(1-2\kappa t+\kappa^2)^2}, \quad t \in [0,1]$$

and the following relation between the parameter $\kappa \in (0,1)$ and the halfwidth b of the kernel is given

$$b = 4 \arccos \sqrt{c}, \tag{3.15}$$

where

$$c = \frac{(2\tau^2 - \tau + 1) - \sqrt{5\tau^4 - 8\tau^3 + 2\tau^2 + 1}}{1+\tau} \quad \text{and} \quad \tau = \frac{(1+\kappa^2)^2}{4\kappa^2}.$$

A visual illustration of the Abel–Poisson kernel together with its Radon transform, and its even order Chebyshev coefficients can be found in Figure 3.1.

The de la Vallée Poussin Kernel. The second radially symmetric function we mention here is the *de la Vallée Poussin kernel*. On SO(3) it is defined by

$$\tilde{K}(t) = \frac{B(\frac{3}{2}, \frac{1}{2})}{B(\frac{3}{2}, \kappa + \frac{1}{2})} t^{2\kappa}, \quad t \in [0,1]$$

where B denotes the Beta function. The parameter $\kappa > 0$ is related to the halfwidth $b \in (0, \pi)$ of the kernel by

$$\kappa \ln \cos \frac{b}{2} = -\ln \sqrt{2}.$$

The main features of the de la Vallée Poussin kernel are its non–negativity and its non–negative finite Fourier series (cf. Schaeben, 1997). More precisely, we have $\widehat{\tilde{K}}(2l) = 0$ for $l \geq \kappa$. Using integration formula (3.5) Schaeben (1997) proves the following explicit formula for the Radon transformed de la Vallée Poussin Kernel on $\mathbb{S}^2$.

Lemma 3.26. *Let $\kappa > 0$ and let $\tilde{K}\colon [0,1] \to \mathbb{R}$ be the de la Vallée Poussin kernel. Then its Radon transformed kernel $\tilde{\mathcal{R}}\tilde{K}$ is given by the formula*

$$\tilde{\mathcal{R}}\tilde{K}(t) = \frac{1+\kappa}{2^\kappa}(1+t)^\kappa, \quad t \in [-1,1] \tag{3.16}$$

An explicit formula for the Chebyshev coefficients of the de la Vallée Poussin kernel can be found once again in Schaeben (1997). However, the following three term recurrence is more applicable for numerical issues.

Lemma 3.27. *Let $\kappa > 0$. Then the even order Chebyshev coefficients $C_l(\kappa) = \widehat{\tilde{K}}(2l)$ of the de la Vallée Poussin kernel satisfy the three term recurrence formula*

$$\frac{l+\kappa+2}{2l+3}C_{l+1}(\kappa) + C_l(\kappa) + \frac{l-\kappa-1}{2l-1}C_{l-1}(\kappa) = 0, \quad l \in \mathbb{N}\backslash\{0\}.$$

The first two Chebyshev coefficients are given by $C_0(\kappa) = 1$ and $C_1(\kappa) = \frac{3\kappa}{\kappa+2}$.

Proof. Let $l \in \mathbb{N}_0$. By Lemma equation (2.7) the Legendre coefficients of $\tilde{\mathcal{R}}\tilde{K}$ and hence the even order Chebyshev coefficients of $\tilde{K}$ satisfy

$$C_l(\kappa) = \frac{2l+1}{2}\int_{-1}^{1} \frac{1+\kappa}{2^\kappa}(1+t)^\kappa \mathcal{P}_l(t)\,\mathrm{d}t.$$

Now we can proceed as in Freeden (1998, Lemma 5.8.1) for the locally supported kernel on the sphere. The three term recurrence formula (2.8) of the Legendre polynomials implies

$$\frac{l+1}{2l+3}C_{l+1}(\kappa) + C_l(\kappa) + \frac{l}{2l-1}C_{l-1}(\kappa) = C_l(\kappa+1).$$

By partial integration and the derivation rule (2.9) we find

$$\begin{aligned} C_l(\kappa+1) &= \frac{2l+1}{2}\int_{-1}^{1} \frac{1+\kappa}{2^\kappa}(1+t)^{\kappa+1}\frac{\mathrm{d}}{\mathrm{d}t}\frac{\mathcal{P}_{l+1}(t)-\mathcal{P}_{l-1}(t)}{2l+1}\,\mathrm{d}t \\ &= -\frac{(1+\kappa)^2}{2^{\kappa+1}}\int_{-1}^{1}(1+t)^\kappa(\mathcal{P}_{l+1}(t)-\mathcal{P}_{l-1}(t))\,\mathrm{d}t \\ &= (1+\kappa)\Big(\frac{1}{2l-1}C_{l-1}(\kappa) - \frac{1}{2l+3}C_{l+1}(\kappa)\Big). \end{aligned}$$

In combination both recurrence formulae prove the recurrence formula of the Lemma. □

Remark 3.28. It is more convenient to write the de la Vallée Poussin kernel as a function of the angle, i.e. for $\mathbf{g}_0 \in \mathrm{SO}(3)$ and $\kappa > 0$ we have

$$K(\mathbf{g}) = \frac{B(\frac{3}{2},\frac{1}{2})}{B(\frac{3}{2},\kappa+\frac{1}{2})}\cos^{2\kappa}\frac{\measuredangle(\mathbf{g}_0,\mathbf{g})}{2} \text{ and } \mathcal{R}K(\mathbf{h},\mathbf{r}) = (1+\kappa)\cos^{2\kappa}\frac{\measuredangle(\mathbf{g}_0\mathbf{h},\mathbf{r})}{2}.$$

The graph of the de la Vallée Poussin kernel, its Radon transform, and its Legendre coefficients are plotted in Figure 3.2.

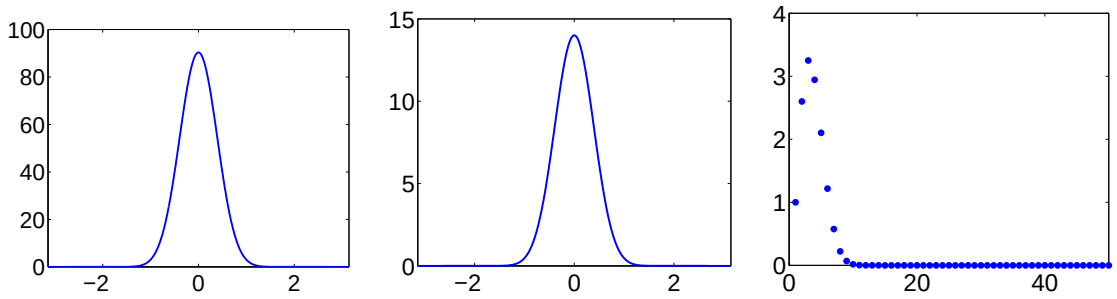

Figure 3.2: The de la Vallée Poussin kernel for $\kappa = 13$.

The von Mises–Fisher Kernel. For any $\kappa > \frac{1}{2}\ln 2$ the *von Mises–Fisher kernel* (cf. Schaeben and v.d. Boogaart, 2003) or *Gaussian kernel* (cf. Matthies et al., 1987, Sec. 16.1) on SO(3) is defined as

$$\tilde{K}\left(\cos\frac{\omega}{2}\right) = \frac{1}{\mathcal{I}_0(\kappa) - \mathcal{I}_1(\kappa)} e^{\kappa\cos\omega}, \quad \omega \in [0,\pi], \tag{3.17}$$

where $\mathcal{I}_n$, $n \in \mathbb{N}_0$ denote the modified Bessel functions of first kind

$$\mathcal{I}_n(\kappa) = \frac{1}{\pi}\int_0^\pi e^{\kappa\cos\omega}\cos n\omega \,\mathrm{d}\omega, \quad \kappa \in \mathbb{R}_+.$$

One verifies that $\tilde{K}(t)$ is positive and monotonically increasing for all $t \in [0,1]$ (cf. Matthies et al., 1987, Sec. 16.1). Furthermore, we have for the halfwidth $b \in [0,\pi]$ of the von Mises–Fischer kernel the simple formula

$$\cos b = 1 - \frac{\ln 2}{\kappa}.$$

Explicit formulae for the Chebyshev coefficients of the von Mises–Fischer kernel as well as for its Radon transform are given in the next lemma.

Lemma 3.29. *The even order Chebyshev coefficients of the von Mises–Fischer kernel $\tilde{K}$ with parameter $\kappa > \frac{1}{2}\ln 2$ satisfy*

$$\widehat{\tilde{K}}(2l) = \frac{\mathcal{I}_l(\kappa) - \mathcal{I}_{l+1}(\kappa)}{\mathcal{I}_0(\kappa) - \mathcal{I}_1(\kappa)}, \quad l \in \mathbb{N}_0.$$

The Radon transformed kernel of $\tilde{K}$ has the representation

$$\tilde{\mathcal{R}}\tilde{K}(\cos\omega) = \frac{\mathcal{I}_0(\frac{\kappa}{2}(1+\cos\omega))}{\mathcal{I}_0(\kappa) - \mathcal{I}_1(\kappa)} e^{\frac{\kappa}{2}(\cos\omega - 1)}, \quad \omega \in [0,\pi].$$

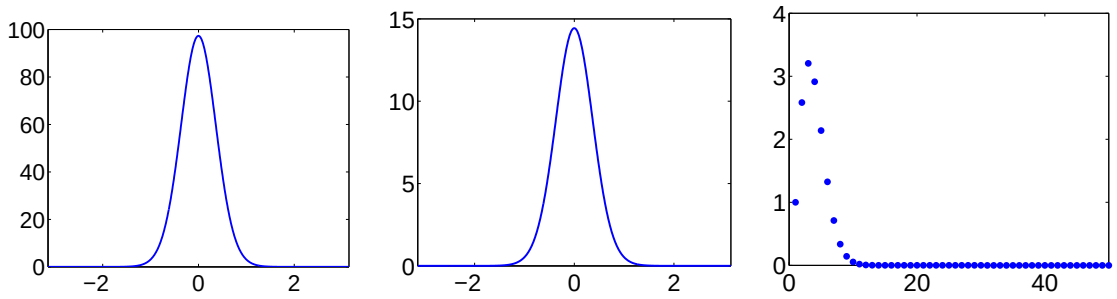

Figure 3.3: The von Mises–Fisher kernel for $\kappa = 7.5$.

Proof. By equation (2.17) the even order Chebyshev coefficients $\widehat{\tilde{K}}(2l), l \in \mathbb{N}_0$ of $\tilde{K}$ are given by

$$\begin{aligned}
\big(\mathcal{I}_0(\kappa) - \mathcal{I}_1(\kappa)\big)\widehat{\tilde{K}}(2l) &= \big(\mathcal{I}_0(\kappa) - \mathcal{I}_1(\kappa)\big)\frac{2}{\pi}\int_0^\pi \tilde{K}(\cos\tfrac{\omega}{2})\mathcal{U}_{2l}(\cos\tfrac{\omega}{2})\sin^2\tfrac{\omega}{2}\,\mathrm{d}\omega \\
&= \frac{2}{\pi}\int_0^\pi e^{\kappa\cos\omega}\sin\tfrac{2l+1}{2}\sin\tfrac{\omega}{2}\,\mathrm{d}\omega \\
&= \frac{1}{\pi}\int_0^\pi e^{\kappa\cos\omega}\big(\cos l\omega - \cos(l+1)\omega\big)\,\mathrm{d}\omega = \mathcal{I}_l(\kappa) - \mathcal{I}_{l+1}(\kappa).
\end{aligned}$$

In order to calculate the Radon transform of the von Mises–Fischer kernel we apply Lemma 3.7 and obtain

$$\begin{aligned}
\big(\mathcal{I}_0(\kappa) - \mathcal{I}_1(\kappa)\big)\tilde{\mathcal{R}}\tilde{K}(\cos\omega) &= \frac{1}{\pi}\int_0^\pi \tilde{K}(\cos\theta\cos\tfrac{\omega}{2})\,\mathrm{d}\theta \\
&= \frac{1}{\pi}\int_0^\pi e^{\kappa\cos 2\arccos\left(\cos\theta\cos\frac{\omega}{2}\right)}\,\mathrm{d}\theta \\
&= \frac{1}{\pi}\int_0^\pi e^{\kappa\left(-1+(1+\cos 2\theta)\cos^2\frac{\omega}{2}\right)}\,\mathrm{d}\theta \\
&= e^{\kappa(\cos^2\frac{\omega}{2}-1)}\frac{1}{\pi}\int_0^\pi e^{\kappa\cos^2\frac{\omega}{2}\cos 2\theta}\,\mathrm{d}\theta \\
&= \mathcal{I}_0(\tfrac{\kappa}{2}(1+\cos\omega))e^{\frac{\kappa}{2}(\cos\omega-1)}.
\end{aligned}$$

□

Figure 3.3 includes a graphical illustration of the von Mises–Fischer kernel, its Radon transformed kernel, and its Legendre coefficients.

The Locally Supported Kernel. By the locally supported kernel on SO(3) we mean a radially symmetric function that is polynomial within a certain neighborhood of its center and that is equal to zero outside of this neighborhood. Denote $p \in \mathbb{N}_+$ the

polynomial degree and $b \in (0,1)$ the width at which the kernel vanishes. Then we define the *locally supported kernel* on SO(3) by

$$\tilde{K}(t) = \begin{cases} (t-b)^p & t \in [b,1], \\ 0 & t < [0,b). \end{cases} \tag{3.18}$$

For a small polynomial degree p the Radon transform of the locally supported kernel on SO(3) can be calculated explicitly. However, for numerical work recurrence formulae for the Chebyshev coefficients of the locally supported kernel seem to be more appropriate. The remainder of the section is devoted to this objective. As a first step we prove a recurrence formula for the zero order Chebyshev coefficients.

Lemma 3.30. *Let $b \in (0,1)$ and $p \in \mathbb{N}$. Then the integrals*

$$I_p = \int_b^1 (t-b)^p \sqrt{1-t^2}\,\mathrm{d}t \quad \text{and} \quad J_p = \int_b^1 (t-b)^p \arcsin t\,\mathrm{d}t$$

satisfy the recurrence formulae

$$(p+2)I_p = \frac{\pi}{2}(1-b)^p - p(bI_{p-1} + J_{p-1}), \tag{3.19}$$

$$(p+1)J_p = \frac{\pi}{2}(1-b)^p - p(I_{p-1} + bJ_{p-1}). \tag{3.20}$$

Initial values are given by $I_{-1} = \sqrt{1-b^2}$ and $J_{-1} = \arcsin b$.

Proof. Partial integration yields

$$\begin{aligned} I_p =& \int_b^1 (t-b)^p \sqrt{1-t^2}\,\mathrm{d}t \\ =& \frac{\pi}{4}(1-b)^p - \int_b^1 \frac{p}{2}(t-b)^{p-1}\big(t\sqrt{1-t^2} + \arcsin t\big)\,\mathrm{d}t \\ =& \frac{\pi}{4}(1-b)^p - \frac{p}{2}\int_b^1 (t-b)^{p-1}\arcsin t\,\mathrm{d}t \\ & - \frac{p}{2}\int_b^1 (t-b)^p\sqrt{1-t^2}\,\mathrm{d}t + \frac{pb}{2}\int_b^1 (t-b)^{p-1}\sqrt{1-t^2}\,\mathrm{d}t \\ =& \frac{\pi}{4}(1-b)^p - \frac{p}{2}J_{p-1} - \frac{p}{2}I_p - \frac{pb}{2}I_{p-1}. \end{aligned}$$

This proves formula (3.19). For formula (3.20) we again apply partial integration and obtain

$$\begin{aligned} J_p =& \int_b^1 (t-b)^p \arcsin t\,\mathrm{d}t \\ =& \frac{\pi}{2}(1-b)^p - \int_b^1 p(t-b)^{p-1}\big(\sqrt{1-t^2} + t\arcsin t\big)\,\mathrm{d}t \end{aligned}$$

$$
\begin{aligned}
=&\frac{\pi}{2}(1-b)^p p\int_b^1 (t-b)^{p-1}\sqrt{1-t^2}\,\mathrm{d}t \\
&- p\int_b^1 (t-b)^p \arcsin t\,\mathrm{d}t + pb\int_b^1 (t-b)^{p-}\arcsin t\,\mathrm{d}t \\
=&\frac{\pi}{2}(1-b)^p - pI_{p-1} - pJ_p + pbJ_{p-1}.
\end{aligned}
$$

□

Lemma 3.31. *Let $b \in (0,1)$ and $p \in \mathbb{N}$. Then the Chebyshev coefficients*

$$\widehat{\widehat{K}}(l) = I_{l,p} = \int_0^{2\arccos(b)} (\cos\tfrac{\omega}{2} - b)^2 \mathcal{U}_l(\cos\tfrac{\omega}{2})\,\mathrm{d}\omega = \int_b^1 (t-b)^p\sqrt{1-t^2}\mathcal{U}_l(t)\,\mathrm{d}t, \quad l \in \mathbb{N}_0$$

of the locally supported kernel satisfy for all $l \in \mathbb{N}\backslash\{0\}$ the recurrence formulae

$$I_{l+1,p} = 2I_{l,p+1} + 2bI_{l,p} - I_{l-1,p}$$

and

$$(l+p+3)I_{l,p+1} + b(l+2p+3)I_{l,p} + (b^2-1)pI_{l,p-1} - (l+1)I_{l-1,p} = 0.$$

For $p = 0$ and $l \in \mathbb{N}_0$ we have

$$I_{l,0} = \frac{\sin(l\arccos b)}{l} - \frac{\sin((l+2)\arccos b)}{l+2}.$$

Proof. Let $b \in (0,1)$, $p \in \mathbb{N}$ and $l \in \mathbb{N}_0$. Then we have for the Chebyshev coefficients of the first and the second momentum of the locally supported kernel the expressions

$$\int_b^1 (t-b)^p t\mathcal{U}_l(t)\sqrt{1-t^2}\,\mathrm{d}t = I_{l,p+1} + bI_{l,p} \tag{3.21}$$

and

$$\int_b^1 (t-b)^p t^2\mathcal{U}_l(t)\sqrt{1-t^2}\,\mathrm{d}t = I_{l,p+2} + 2bI_{l,p+1} + b^2 I_{l,p}. \tag{3.22}$$

Together with the three term recurrence formula (2.19) we derive the equality

$$
\begin{aligned}
I_{l+1,p} &= \int_b^1 (t-b)^p \mathcal{U}_{l+1}(t)\,\mathrm{d}t \\
&= \int_b^1 (t-b)^p \big(2t\mathcal{U}_l(t) - \mathcal{U}_{l-1}(t)\big)\,\mathrm{d}t \\
&= 2I_{l,p+1} + 2bI_{l,p} - I_{l-1,p}.
\end{aligned} \tag{3.23}
$$

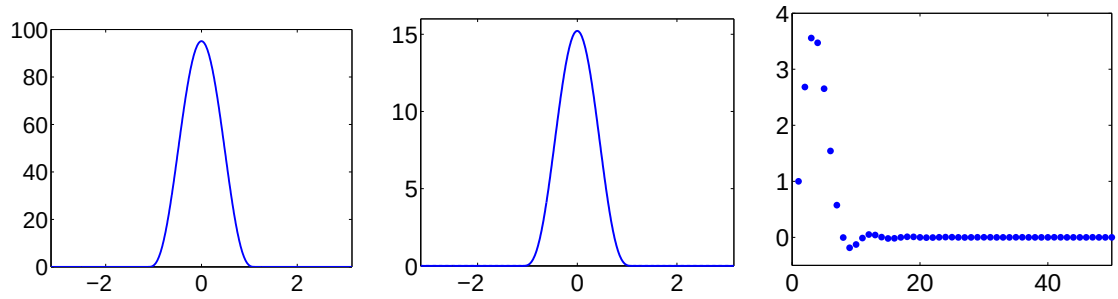

Figure 3.4: The locally supported kernel for $\kappa = 0.85$.

Applying subsequently equation (3.21), derivations rule (2.21), partial integration, and equations (3.21) and (3.22) we obtain

$$\begin{aligned}
-lI_{l,p+1} - lbI_{l,p} + (l+1)I_{l-1,p} &= \int_b^1 (t-b)^p \big(-lt\mathcal{U}_l(t) + (l+1)\mathcal{U}_{l-1}(t)\big)\sqrt{1-t^2}\,\mathrm{d}t \\
&= \int_b^1 (t-b)^p (1-t^2)\left(\frac{\mathrm{d}}{\mathrm{d}t}\mathcal{U}_l(t)\right)\sqrt{1-t^2}\,\mathrm{d}t \\
&= \int_b^1 (t-b)^p 3t\mathcal{U}_l(t)\sqrt{1-t^2}\,\mathrm{d}t \\
&\quad - \int_b^1 p(t-b)^{p-1}(1-t^2)\mathcal{U}_l(t)\sqrt{1-t^2}\,\mathrm{d}t \\
&= 3I_{l,p+1} + 3bI_{l,p} - pI_{l,p-1} + pI_{l,p+1} + 2bpI_{l,p} + b^2pI_{l,p-1} \\
&= (p+3)I_{l,p+1} + b(2p+3)I_{l,p} + (b^2-1)pI_{l,p-1}
\end{aligned}$$

and consequently

$$(l+p+3)I_{l,p+1} + b(l+2p+3)I_{l,p} + (b^2-1)pI_{l,p-1} - (l+1)I_{l-1,p} = 0. \tag{3.24}$$

Multiplying equation (3.23) by $(l+p+3)$ and equation (3.24) by -2 and summing them results in the recurrence formula

$$(l+p+3)I_{l+1,p} + 2bpI_{l,p} + (p-l+1)I_{l-1,p} - 2p(1-b^2)I_{l,p-1} = 0.$$

□

A plot of the locally supported kernel of polynomial degree three together with its Radon transform and its Legendre coefficients can be found in Figure 3.4.

4 The PDF–to–ODF Inversion Problem

In this chapter we are concerned with the central problem of quantitative texture analysis — the estimation of an orientation density function (ODF) of a specimen from diffraction measurements. Starting with a brief summary of crystallographic terminology and diffraction at crystals we derive a statistical model for diffraction in polycrystalline materials. Based on the statistical model we formulate the problem of ODF estimation by means of diffraction measurements as a parameter estimation problem and analyze its inherent indeterminateness and ill–posedness. The canonical question about the reliability of ODF estimation is addressed in Section 4.3 and in Section 4.4. Eventually we take advantage of the statistical model and derive a least squares ODF estimator from on diffraction data.

4.1 Crystallographic Background

In this section only the most basic notations of crystallography are introduced. For a more comprehensive introduction into crystallography including diffraction the reader is referred to Schwarzenbach (2001) or Hammond (1997).

Crystal Geometry. The characterizing property of all crystals is the three–dimensional periodic alignment of their atoms, in other words their atoms form a regular lattice. The common way to describe the regularity of an atom lattice is to extend it periodically to the three–dimensional Euclidean space $\mathbb{R}^3$ and to consider its symmetries. Symmetries are isometric mappings of the three–dimensional space that leave the extended atom lattice invariant. The set of all symmetries of the extended atom lattice forms a group, the so called *space group* $S_{\text{space}} \subseteq \mathrm{O}(3) \otimes \mathrm{T}(3)$ of the crystal. Here $\mathrm{O}(3)$ denotes the group of all orthogonal transformations in $\mathbb{R}^3$ and $\mathrm{T}(3)$ denotes the group of all translations in $\mathbb{R}^3$. The orthogonal part $S_{\text{point}} = S_{\text{space}}/\mathrm{T}(3) \subseteq \mathrm{O}(3)$ of the space group is called *point group* of the crystal.

Every crystal allows for a conventional assignment of an orthonormal coordinate system which is well defined modulo the crystal symmetries described by the space group S_{space}. Such a coordinate system is called *crystal coordinate system*. A direction specified

by coordinates relative to a crystal coordinate system is called *crystal direction*. Following the general convention we denote crystal directions by the letter $\mathbf{h} \in \mathbb{S}^2$. Two crystal directions $\mathbf{h}_1, \mathbf{h}_2 \in \mathbb{S}^2$ are called *crystallographically equivalent* if it exists a symmetry $\mathbf{q} \in S_{\text{point}}$ of the crystal such that $\mathbf{h}_1 = \mathbf{q}\mathbf{h}_2$. We denote by

$$S_{\text{point}}\mathbf{h} = \{\, \mathbf{q}\mathbf{h} \mid \mathbf{q} \in S_{\text{point}} \,\} \in \mathbb{S}^2/S_{\text{point}}$$

the class of all crystal directions crystallographically equivalent to a given crystal direction $\mathbf{h} \in \mathbb{S}^2$ and by $\mathbb{S}^2/S_{\text{point}}$ the set of all classes of crystallographically equivalent directions.

Let us consider a specimen and a *specimen coordinate system* fixed to it according to some convention. A direction specified by its coordinate vector relative to the specimen coordinate system is called *specimen direction* and is usually denoted by the letter $\mathbf{r} \in \mathbb{S}^2$.

Crystal directions and specimen directions are connected via the coordinate transformation from the crystal coordinate system to the specimen coordinate system. This coordinate transformation can be represented by an orthogonal 3×3–matrix which is commonly denoted by the letter $\mathbf{g} \in \mathrm{O}(3)$. With this notation a crystal direction $\mathbf{h} \in \mathbb{S}^2$ and a specimen direction $\mathbf{r} \in \mathbb{S}^2$ represent the same physical direction if and only if

$$\mathbf{r} = \mathbf{g}\mathbf{h}.$$

Moreover, the matrix $\mathbf{g} \in \mathrm{O}(3)$ can be interpreted as a (possibly improper) rotation with respect to the specimen coordinate system that brings the specimen coordinate system in coincidence with the crystal coordinate system. Hence, the matrix $\mathbf{g} \in \mathrm{O}(3)$ describes the orientation of the crystal relative to the specimen.

Let $\mathbf{g}_1, \mathbf{g}_2 \in \mathrm{O}(3)$ be two coordinate transformations. Then $\mathbf{g}_1$ and $\mathbf{g}_2$ describe two crystallographically equivalent orientations if and only if it exists a symmetry $\mathbf{q} \in S_{\text{point}}$ such that $\mathbf{g}_1 = \mathbf{g}_2\mathbf{q}$. The class

$$\mathbf{g}S_{\text{point}} = \{\, \mathbf{g}\mathbf{q} \mid \mathbf{q} \in S_{\text{point}} \,\} \in \mathrm{O}(3)/S_{\text{point}}$$

of all coordinate transformations that are crystallographically equivalent to a given coordinate transformation $\mathbf{g} \in \mathrm{O}(3)$ is called *crystal orientation* and the factor group $\mathrm{O}(3)/S_{\text{point}}$ of all crystal orientations is called *orientation space*. Let $\mathbf{g}S_{\text{point}} \in \mathrm{O}(3)/S_{\text{point}}$ be a crystal orientation, $S_{\text{point}}\mathbf{h} \in \mathbb{S}^2$ a class of crystallographically equivalent crystal directions and $\mathbf{r} \in \mathbb{S}^2$ a specimen direction. Then $\mathbf{r}$ represents a direction identical to one of the directions represented by the class $S_{\text{point}}\mathbf{h}$ if and only if

$$S_{\text{point}}\mathbf{h} = (\mathbf{g}S_{\text{point}})^{-1}\mathbf{r}.$$

Textures. Let us consider a mono–phase, polycrystalline specimen, i.e. a compound of identical crystals all possessing the same point group $S_{\text{point}} \subseteq \mathrm{O}(3)$. Next we assume that each crystal has a well defined crystal orientation $\mathbf{g}S_{\text{point}} \in \mathrm{O}(3)/S_{\text{point}}$ relative to the

specimen thus neglecting e.g. internal crystal defects. Then the distribution of crystal orientations by volume within the specimen is called *texture* and can be modelled by a probability measure on the orientation space $\mathrm{O}(3)/S_{\mathrm{point}}$. Its quantitative investigation is called *quantitative texture analysis* (QTA). The central idea of QTA is to describe this probability measure on $\mathrm{O}(3)/S_{\mathrm{point}}$ by a probability density function. Such a probability density function is called *orientation density function* of the specimen. More abstractly we define

Definition 4.1. Let $S_{\mathrm{point}} \subseteq \mathrm{O}(3)$ be a point group and let

$$f\colon \mathrm{O}(3)/S_{\mathrm{point}} \to \mathbb{R}_+$$

be a non–negative, integrable function on $\mathrm{O}(3)/S_{\mathrm{point}}$ normalized to

$$\frac{1}{16\pi^2}\int_{\mathrm{O}(3)} f(\mathbf{g}S_{\mathrm{point}})\,\mathrm{d}\mathbf{g} = 1.$$

Then f is called *orientation density function* (ODF).

Beside the distribution of crystal orientations within a specimen one can also ask for the distribution of crystal directions that are in line with a certain specimen direction modulo crystal symmetry. To be more precisely let us fix a specimen direction $\mathbf{r} \in \mathbb{S}^2$. Then any distribution of crystal orientations $\mathbf{g}S_{\mathrm{point}} \in \mathrm{O}(3)/S_{\mathrm{point}}$ constitutes by virtue of the mapping $\mathbf{g}S_{\mathrm{point}} \mapsto (\mathbf{g}S_{\mathrm{point}})^{-1}\mathbf{r}$ a distribution on the classes of crystallographically equivalent crystal directions $\mathbb{S}^2/S_{\mathrm{point}}$.

Lemma 4.2 (fundamental equation of texture analysis)**.** *Let $S_{point} \subseteq \mathrm{O}(3)$ be some point group and let $f \in L^1(\mathrm{O}(3)/S_{point})$ be the ODF of a probability measure μ on $\mathrm{O}(3)/S_{point}$. Then the mapping*

$$\Pi_{\mathbf{r}}\colon \mathrm{O}(3)/S_{point} \to \mathbb{S}^2/S_{point}, \quad \mathbf{g}S_{point} \mapsto (\mathbf{g}S_{point})^{-1}\mathbf{r}$$

is measurable for any $\mathbf{r} \in \mathbb{S}^2$ and the induced measure $\mu \circ \Pi_{\mathbf{r}}^{-1}$ on $\mathbb{S}^2/S_{point}$ has the probability density function

$$\mathcal{X}f(\circ, \mathbf{r}) \in L^1(\mathbb{S}^2/S_{point}). \tag{4.1}$$

Here the operator $\mathcal{X}$ is defined as in Definition 3.23 and Theorem 3.24.

Proof. First of all we notice that by Remark 3.20 the trace function $\mathcal{X}f(\circ, \mathbf{r}) \in L^1(\mathbb{S}^2/S_{\mathrm{point}})$ is well defined for any $\mathbf{r} \in \mathbb{S}^2$. Since we have for any function $\phi \in C(\mathbb{S}^2/S_{\mathrm{point}})$ and any unit vector $\mathbf{r} \in \mathbb{S}^2$ the equality

$$\begin{aligned}\frac{1}{16\pi^2}\int_{\mathrm{O}(3)} \phi\left(\Pi_{\mathbf{r}}(\mathbf{g}S_{\mathrm{point}})\right) f(\mathbf{g})\,\mathrm{d}\mathbf{g} &= \frac{1}{4\pi}\int_{\mathbb{S}^2}\frac{1}{4\pi}\int_{\{\,\mathbf{g}\in\mathrm{O}(3)\,|\,\mathbf{g}\mathbf{h}=\mathbf{r}\,\}} \phi(\Pi_{\mathbf{r}}\mathbf{g}S_{\mathrm{point}}) f(\mathbf{g}S_{\mathrm{point}})\,\mathrm{d}\mathbf{g}\,\mathrm{d}\mathbf{h} \\ &= \frac{1}{4\pi}\int_{\mathbb{S}^2} \phi(S_{\mathrm{point}}\mathbf{h})\mathcal{X}f(S_{\mathrm{point}}\mathbf{h}, \mathbf{r})\,\mathrm{d}\mathbf{h}\end{aligned}$$

we conclude that $\mathcal{X}f(\circ, \mathbf{r})$ is the density function of $\mu \circ \Pi_{\mathbf{r}}^{-1}$. □

For the practical problem of QTA Lemma 4.2 can be read as follows. If the distribution of crystal orientations within a specimen is modelled by an ODF $f \in L^1(\mathrm{O}(3)/S_{\mathrm{point}})$, then the distribution of crystal directions that are in line with a fixed specimen direction $\mathbf{r} \in \mathbb{S}^2$ modulo crystal symmetry is modelled by the probability density function $\mathcal{X}f(\circ, \mathbf{r}) \in L^1(\mathbb{S}^2/S_{\mathrm{point}})$.

Definition 4.3. Let $f \in L^1(\mathrm{O}(3)/S_{\mathrm{point}})$ be an ODF. Then the function $\mathcal{X}f \in L^1(\mathbb{S}^2/S_{\mathrm{point}} \times \mathbb{S}^2)$ is called *pole density function* (PDF) corresponding to f. For any $\mathbf{h}, \mathbf{r} \in \mathbb{S}^2$ the trace functions $\mathcal{X}f(S_{\mathrm{point}}\mathbf{h}, \circ) \in L^1(\mathbb{S}^2)$ and $\mathcal{X}f(\circ, \mathbf{r}) \in L^1(\mathbb{S}^2/S_{\mathrm{point}})$ are called *pole figure* and *inverse pole figure*, respectively.

The PDF defined by an ODF $f \in L^1(\mathrm{O}(3)/S_{\mathrm{point}})$ is commonly denoted by the letter $P = \mathcal{X}f$. The relationship (4.1) between an ODF and its PDF is known as the *fundamental equation of texture analysis* and is due to Bunge (1965), Roe (1965) and others.

Setting $\phi = 1$ in the proof of Lemma 4.2 we obtain the following normalization properties of the PDF.

Remark 4.4. Let $S_{\mathrm{point}} \subseteq \mathrm{O}(3)$ be an arbitrary point group, $f \in L^1(\mathrm{O}(3)/S_{\mathrm{point}})$ an ODF and let $P = \mathcal{X}f \in L^1(\mathbb{S}^2/S_{\mathrm{point}} \times \mathbb{S}^2)$ be the corresponding PDF. Then we have for all unit vectors $\mathbf{h}, \mathbf{r} \in \mathbb{S}^2$ the normalizations

$$\frac{1}{4\pi} \int_{\mathbb{S}^2} P(S_{\mathrm{point}}\mathbf{h}, \mathbf{r}) \, \mathrm{d}\mathbf{r} = 1, \quad \frac{1}{4\pi} \int_{\mathbb{S}^2} P(S_{\mathrm{point}}\mathbf{h}, \mathbf{r}) \, \mathrm{d}\mathbf{h} = 1$$

and

$$\frac{1}{16\pi^2} \int_{\mathbb{S}^2} \int_{\mathbb{S}^2} P(S_{\mathrm{point}}\mathbf{h}, \mathbf{r}) \, \mathrm{d}\mathbf{r} \, \mathrm{d}\mathbf{h} = 1.$$

Remark 4.5. Although the ODF and the PDF are defined on the factor spaces $\mathrm{O}(3)/S_{\mathrm{point}}$ and $\mathbb{S}^2/S_{\mathrm{point}} \times \mathbb{S}^2$, respectively, we will treat them sometimes as functions defined on $\mathrm{O}(3)$ and $\mathbb{S}^2 \times \mathbb{S}^2$ possessing for any $\mathbf{g} \in \mathrm{O}(3)$, $\mathbf{h}, \mathbf{r} \in \mathbb{S}^2$ and $\mathbf{q} \in S_{\mathrm{point}}$ the symmetry properties $f(\mathbf{g}) = f(\mathbf{gq})$ and $P(\mathbf{h}, \mathbf{r}) = P(\mathbf{qh}, \mathbf{r})$, respectively.

While the ODF of an specimen is not directly accessible, the PDF $P(\mathbf{h}, \mathbf{r})$ of a specimen can be determined for specific crystal and specimen direction $\mathbf{h}, \mathbf{r} \in \mathbb{S}^2$ by diffraction techniques. This issue is discussed in the next section.

4.2 The Diffraction Experiment

Diffraction at Single Crystals. Let us start with diffraction at a single crystal. We assume that the bisecting line between the initial and the diffracted beam is represented by the crystal direction $\mathbf{h} \in \mathbb{S}^2$ and denote by $\lambda \in \mathbb{R}_+$ the wavelength of the beam. The angle $\theta \in (0, \frac{\pi}{2})$ between the initial beam and the plane perpendicular to the crystal

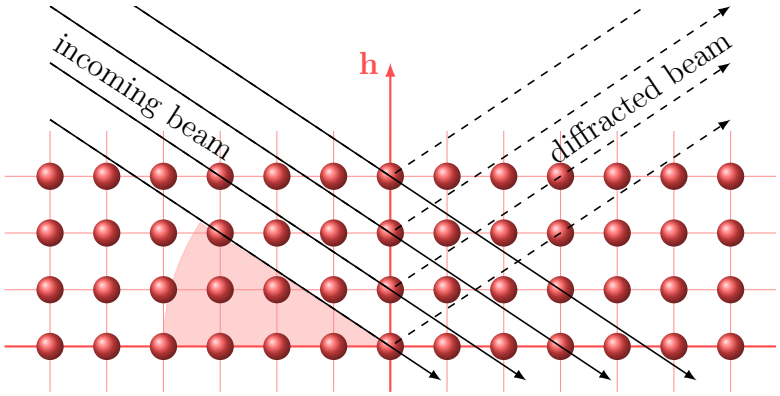

Figure 4.1: Diffraction at a single crystal.

direction $\mathbf{h}$ is called *Bragg angle*. See Figure 4.1 for an illustration of this setting. The question for which specific combinations of a wavelength $\lambda \in \mathbb{R}_+$, a crystal direction $\mathbf{h} \in \mathbb{S}^2$, and a Bragg angle $\theta \in (0, \frac{\pi}{2})$ diffraction occurs is answered by Bragg's law (cf. Schwarzenbach, 2001, Section 3.4.2). However, in our work we simply define the set $H(\lambda, \theta)$ as the set of all crystal directions $\mathbf{h} \in \mathbb{S}^2$ for which diffraction intensities with respect to the Bragg angle θ ant the wavelength λ are experimentally detectable.

Let (λ, θ) be a combination of a wavelength and a Bragg angle such that the set $H(\lambda, \theta)$ is not empty. Then we define the function

$$\rho_{\lambda,\theta} \colon H(\lambda, \theta) \to \mathbb{R}_+$$

as the relative diffraction intensities $\rho_{\lambda,\theta}(\mathbf{h})$ of the crystal directions $\mathbf{h} \in H(\lambda, \theta)$ normalized to

$$\sum_{\mathbf{h} \in H(\lambda,\theta)} \rho(\mathbf{h}) = 1.$$

Remark 4.6. A direct consequence of the crystal symmetry described by the point group $S_{\text{point}} \subseteq \mathrm{O}(3)$ is that

$$S_{\text{point}} H(\lambda, \theta) = H(\lambda, \theta)$$

for any combination of a wavelength λ and a Bragg angle θ. Moreover, we have

$$\rho_{\lambda,\theta}(\mathbf{h}') = \rho_{\lambda,\theta}(\mathbf{h})$$

for all crystallographic equivalent directions $S_{\text{point}}\mathbf{h} = S_{\text{point}}\mathbf{h}'$.

It should be noted that the set $H(\lambda, \theta)$ is not empty only for roughly about 20 specific combinations of the parameters λ and θ and that the function $\rho_{\lambda,\theta}$ is not constant only in the rare cases that the set $H(\lambda, \theta)$ contains more then one class of crystallographic equivalent directions. The relative diffraction intensities $\rho_{\lambda,\theta}(\mathbf{h})$ are due to the crystal structure and can be calculated theoretically.

Diffraction at Polycrystalline Specimen. We are now going to generalize Bragg's law for monophase, polycrystalline specimen. Let us consider a beam with wavelength $\lambda \in \mathbb{R}_+$, Bragg angle $\theta \in (0, \frac{\pi}{2})$, and let the intersecting line between the initial and the diffracted beam be represented by the specimen direction $\mathbf{r} \in \mathbb{S}^2$. Then the intensity of the diffracted beam depends on the volume fraction of crystals with crystal orientation $\mathbf{g}S_{\text{point}} \in \mathrm{O}(3)/S_{\text{point}}$ such that

$$\mathbf{gh} = \mathbf{r}.$$

for some crystal direction $\mathbf{h} \in H(\lambda, \theta)$, i.e. of those crystals such that the specimen direction $\mathbf{r}$ coincides with one of the crystal directions in $H(\lambda, \theta)$ subject to the crystal orientation.

Let the distribution of crystal orientations in the specimen be modelled by an ODF $f_{\text{true}} \in C(\mathrm{O}(3)/S_{\text{point}})$. Then the diffraction intensities can be quantitatively modelled by superpositions of the corresponding PDF $P_{\text{true}} = \mathcal{X} f_{\text{true}} \in C(\mathbb{S}^2/S_{\text{point}} \times \mathbb{S}^2)$. Denote $I(\lambda, \theta, \mathbf{r})$ the intensity of the diffracted beam with respect to the parameters $(\lambda, \theta, \mathbf{r})$. Then we have the model

$$I(\lambda, \theta, \mathbf{r}) = \alpha(\lambda, \theta) \sum_{\mathbf{h} \in H(\lambda,\theta)} \rho_{\lambda,\theta}(\mathbf{h}) P_{\text{true}}(\mathbf{h}, \mathbf{r}) \tag{4.2}$$

with relative diffraction intensities $\rho_{\lambda,\theta}(\mathbf{h}) \in \mathbb{R}_+$ and normalization coefficients $\alpha(\lambda, \theta) \in \mathbb{R}_+$. The normalization coefficients $\alpha(\lambda, \theta)$ are in general not experimentally accessible and will considered as unknown parameters.

Remark 4.7. In model (4.2) we have assumed $f \in C(\mathrm{O}(3)/S_{\text{point}})$ since the pointwise evaluation $\mathcal{X} f(\mathbf{h}, \mathbf{r})$, $\mathbf{h}, \mathbf{r} \in \mathbb{S}^2$ of the corresponding PDF is not defined in the canonical space of ODFs $L^1(\mathrm{O}(3)/S_{\text{point}})$.

In practice the measurement of diffraction intensities is affected by background radiation and measurement errors. We denote the background intensity for the specific parameters $\lambda, \theta \in \mathbb{R}$ and $\mathbf{r} \in \mathbb{S}^2$ by $I^b(\lambda, \theta, \mathbf{r}) \in \mathbb{R}_+$ and assume that it is known. Since the diffraction intensities are measured by particle counting we model them as random samples $\mathbf{I}(\lambda, \theta, \mathbf{r}) \in \mathbb{R}$ of the Poisson distribution

$$\mathcal{I}(\lambda, \theta, \mathbf{r}) = \mathrm{Poiss}\big(I(\lambda, \theta, \mathbf{r}) + I^b(\lambda, \theta, \mathbf{r})\big) \tag{4.3}$$

with mean value equal to the sum of the intensity of the diffracted beam and the background radiation. We refer to the random sample $\mathbf{I}(\lambda, \theta, \mathbf{r})$ as the *diffraction counts* and write

$$\mathbf{I}(\lambda, \theta, \mathbf{r}) \sim \mathcal{I}(\lambda, \theta, \mathbf{r}).$$

It should be noted that equation (4.3) does not represent a complete model for experimental diffraction counts. First of all Bragg's law itself is only a rough simplification of much more sophisticated models explaining diffraction (cf. Cowley, 1995). Second, the diffraction counts commonly used for texture determination are obtained by processing a spectrum of diffraction counts for varying Bragg angle θ or wavelength λ (cf. Hammond, 1997).

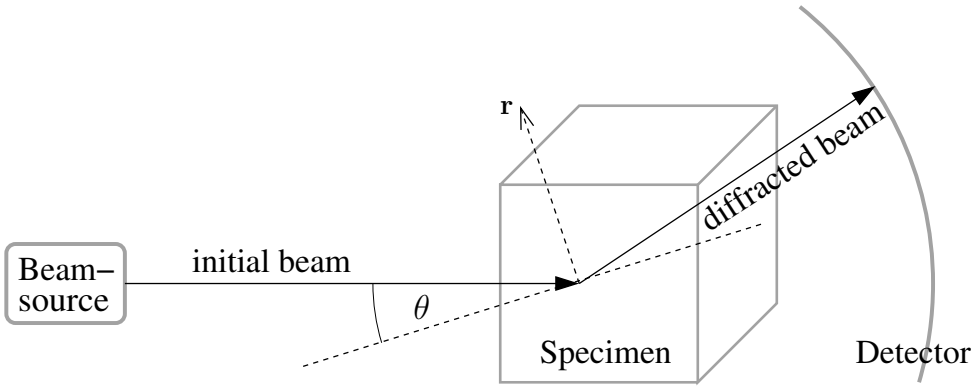

Figure 4.2: The diffraction experiment.

Texture Determination. Figure 4.2 shows the general setting of a diffraction experiment. It consists of a beam source, a detector, and the specimen in line with them. The beam source emits a coherent, monochromatic beam of a certain wavelength. Any detector position constitutes a certain Bragg angle $\theta \in (0, \frac{\pi}{2})$ and a certain specimen direction $\mathbf{r} \in \mathbb{S}^2$ defined as the bisecting line between initial and diffracted beam.

In a usual diffraction experiment for the purpose of texture determination a list of wavelengths $\lambda_i \in \mathbb{R}_+$ and Bragg angles $\theta_i \in (0, \frac{\pi}{2})$, $i = 1, \ldots, N$, is chosen such that the corresponding sets of crystal directions $H_i = H(\lambda_i, \theta_i)$ that cause diffraction is not empty. Moreover, a list of specimen directions $\mathbf{r}_{ij} \in \mathbb{S}^2$, $j = 1, \ldots, N_i$, is chosen for each pair (λ_i, θ_i). Relative to these specimen directions and parameters $(\lambda_i, \theta_i, \mathbf{r}_{ij})$, $i = 1, \ldots, N$, $j = 1, \ldots, N_i$ diffraction counts $\mathbf{I}_{ij} = \mathbf{I}(\lambda_i, \theta_i, \mathbf{r}_{ij}) \in \mathbb{R}_+$ and background intensities $\mathbf{I}^b_{ij} = I^b(\lambda_i, \theta_i, \mathbf{r}_{ij}) \in \mathbb{R}_+$, are measured. The number N of chosen combinations (λ_i, θ_i), $i = 1, \ldots, N$, of wavelengths and Bragg angles usually varies between three and twenty whereas the number N_i of measured diffraction counts $\mathbf{I}_{ij}$ for a fixed combination (λ_i, θ_i) may vary between 250 and 1,000,000.

In order to adapt equation (4.3) such that it serves as a model for a complete diffraction experiment we introduce the following vector notations. First we abbreviate the unknown normalization coefficients by the vector $\boldsymbol{\alpha}_{\text{true}} \in \mathbb{R}^N_+$, $[\boldsymbol{\alpha}_{\text{true}}]_i = \alpha(\lambda_i, \theta_i)$ and the relative diffraction intensities by the functions $\rho_i = \rho_{\lambda_i, \theta_i}$, $i = 1, \ldots, N$. Furthermore, we will frequently use the vector notations

$$\mathbf{I} = (\underbrace{\mathbf{I}_{11}, \ldots, \mathbf{I}_{1N_1}}_{\mathbf{I}_1^T}, \underbrace{\mathbf{I}_{21}, \ldots, \mathbf{I}_{2N_2}}_{\mathbf{I}_2^T}, \ldots, \underbrace{\mathbf{I}_{N1}, \ldots, \mathbf{I}_{NN_N}}_{\mathbf{I}_N^T})^T \in \mathbb{R}^{\bar{N}}, \tag{4.4}$$

where $\mathbf{I}_i = (\mathbf{I}_{i1}, \ldots, \mathbf{I}_{iN_i})^T \in \mathbb{R}^{N_i}_+$ are the diffraction counts corresponding to the i–th pole figure and $\bar{N} = \sum_{i=1}^N N_i$ denotes the total number of measured diffraction data. Finally, we define for any ODF $f \in C(\mathrm{O}(3)/S_{\text{point}})$ the notation

$$\mathcal{X}f(H_i, \mathbf{r}_{ij}) = \sum_{\mathbf{h} \in H_i} \rho_i(\mathbf{h})\ \mathcal{X}f(\mathbf{h}, \mathbf{r}_{ij}). \tag{4.5}$$

Symbol	Description
$N \in \mathbb{N}$	number of pole figures
$N_i \in \mathbb{N}, i = 1, \dots, N$	number of specimen directions
$S_{\text{point}} \subseteq \mathrm{O}(3)$	point group of the specimen
$H_i = H(\lambda_i, \theta_i) \subseteq \mathbb{S}^2/S_{\text{point}}, i = 1, \dots, N$	superposed crystal directions
$\rho_i \colon H_i \to \mathbb{R}_+$	relative reflection intensities
$\mathbf{r}_{ij} \in \mathbb{S}^2, i = 1 \dots, N,\ j = 1, \dots, N_i$	specimen directions
$\mathbf{I}_{ij} \in \mathbb{R}_+, i = 1, \dots, N,\ j = 1, \dots, N_i$	diffraction counts
$\mathbf{I}^b_{ij} \in \mathbb{R}_+, i = 1, \dots, N,\ j = 1, \dots, N_i$	background intensities

Table 4.1: List of parameters of a diffraction experiment.

Assuming that the distribution of crystal orientations in the specimen is modelled by an ODF $f_{\text{true}} \in C(\mathrm{O}(3)/S_{\text{point}})$ we obtain by the fundamental equation of texture analysis (4.1) and the equations (4.2) and (4.3) the following statistical relationship between the measured diffraction counts $\mathbf{I} \in \mathbb{R}_+^{\bar{N}}$ and the model ODF $f_{\text{true}} \in C(\mathrm{O}(3)/S_{\text{point}})$

$$\mathbf{I}_{ij} \sim \mathrm{Poiss}\Big(\mathbf{I}^b_{ij} + [\boldsymbol{\alpha}_{\text{true}}]_i \, \mathcal{X} f_{\text{true}}(H_i, \mathbf{r}_{ij})\Big), \quad i = 1, \dots, N, j = 1, \dots, N. \tag{4.6}$$

A complete overview about all parameters of a diffraction experiment is given in Table 4.1. From the point of view of Equation (4.6) the measured diffraction counts $\mathbf{I} \in \mathbb{R}^{\bar{N}}$ occur as an one–element random sample of a family of a parameterized Poisson distributions. Then the objective of quantitative texture analysis is to retrieve information about the unknown parameters f_{true} and $\boldsymbol{\alpha}_{\text{true}}$ from the random sample $\mathbf{I}$. The problem of estimation of the true ODF f_{true} is known as the *PDF–to–ODF inversion problem*. The analysis of this problem will be our main challenge during the remainder of this thesis.

4.3 The Ill–Posedness of the PDF–to–ODF Inversion Problem

Although the problem of ODF estimation dates back to the works of Bunge (1965) and Roe (1965) its inherent indeterminateness was first explained by Matthies (1979) only 15 years later. The indeterminateness of the PDF–to–ODF inversion problem has several reasons. In this section we attempt to give an almost complete list of these reasons (cf. Matthies et al. (1987, Sec. 12), Wenk et al. (1987)).

The Ambiguity Due to Friedel's Law. Friedel's law states that antipodal crystal directions $\mathbf{h} \in \mathbb{S}^2$ and $-\mathbf{h} \in \mathbb{S}^2$ are indistinguishable by diffraction experiments, i.e. we have $H_i = -H_i$, $i = 1, \dots, N$. In turn, Friedel's law implies that it is impossible to

distinguish between a crystal orientation $\mathbf{g}S_{\text{point}} \in \mathrm{O}(3)/S_{\text{point}}$ and the corresponding inverse crystal orientation $-\mathbf{g}S_{\text{point}}$ of a single crystal by diffraction experiments. Hence, $\mathbf{g}S_{\text{point}}$ and $-\mathbf{g}S_{\text{point}}$ should be treated as orientations symmetrically equivalent with respect to diffraction properties. Symmetry with respect to diffraction is described by the so called *Laue group* $S_{\text{Laue}} \subseteq \mathrm{O}(3)$ of the crystal. It is related to the point group S_{point} of the crystal by the equation

$$S_{\text{Laue}} = S_{\text{point}} \otimes \{\mathrm{Id}, -\mathrm{Id}\}.$$

In this thesis we deal with diffraction data only. Hence, the appropriate symmetry we have to work with is the symmetry with respect to diffraction $S_{\text{Laue}} \subseteq \mathrm{O}(3)$.

Remark 4.8. In Lemma 3.25 we have shown that the PDF of any ODF $f \in L^1(\mathrm{O}(3)/S_{\text{Laue}})$ possessing the symmetry $f(\mathbf{g}) = f(-\mathbf{g})$ satisfies

$$\mathcal{X}f(\mathbf{h}, \mathbf{r}) = \mathcal{X}f(\mathbf{h}, -\mathbf{r}), \quad \mathbf{h}, \mathbf{r} \in \mathbb{S}^2.$$

In other words all pole figures $\mathcal{X}f(\mathbf{h}, \circ)$ of f are even functions and hence, it is sufficient to sample them only at specimen directions located on the upper hemisphere $\mathbb{S}^2_+$.

The Ambiguity of the Operator $\mathcal{X}$. Let $S_{\text{Laue}} \subseteq \mathrm{O}(3)$ be some Laue group. From Section 2.5 we know that any ODF $f_{\text{true}} \in L^2(\mathrm{O}(3)/S_{\text{Laue}})$ has a Fourier expansion of the form

$$f_{\text{true}}(\mathbf{g}) = \sum_{l=0}^{\infty} \sum_{k,k'=-l}^{l} \frac{(l+\frac{1}{2})^{\frac{1}{2}}}{2\pi} \hat{f}_{\text{true}}(l,k,k') T_l^{kk'}(|\mathbf{g}|), \quad \mathbf{g} \in \mathrm{O}(3),$$

where $|\mathbf{g}| = \mathbf{g}$ if $\mathbf{g} \in \mathrm{SO}(3)$ and $|\mathbf{g}| = -\mathbf{g}$ if $\mathbf{g} \in \mathrm{O}(3) \backslash \mathrm{SO}(3)$. By the fundamental equation of texture analysis (4.1) and Theorem 3.24 we have for the corresponding PDF $P_{\text{true}} = \mathcal{X}f_{\text{true}}$

$$\mathcal{X}f_{\text{true}}(\mathbf{h}, \mathbf{r}) = \sum_{l \in 2\mathbb{N}_0} \sum_{k,k'=-l}^{l} \frac{1}{(l+\frac{1}{2})^{\frac{1}{2}}} \hat{f}_{\text{true}}(l,k,k') \mathcal{Y}_l^{k'}(\mathbf{h}) \overline{\mathcal{Y}_l^{k}(\mathbf{r})}, \quad \mathbf{h}, \mathbf{r} \in \mathbb{S}^2.$$

We mention that the true PDF P_{true} does not contain any information about the odd order Fourier coefficients of the true ODF f_{true}. Consequently any ODF

$$f(\mathbf{g}) = \sum_{l=0}^{\infty} \sum_{k,k'=-l}^{l} \frac{(l+\frac{1}{2})^{\frac{1}{2}}}{2\pi} \hat{f}(l,k,k') T_l^{kk'}(|\mathbf{g}|), \quad \mathbf{g} \in \mathrm{O}(3)$$

with $\hat{f}(l,k,k') = \hat{f}_{\text{true}}(l,k,k')$ for $l = 0, 2, \ldots$ and $k, k' = -l, \ldots, l$ defines the same PDF as the true ODF f_{true}, i.e. $\mathcal{X}f = \mathcal{X}f_{\text{true}}$ and hence causes the same diffraction behavior.

This ambiguity of the PDF–to–ODF inversion problem is called *ghost effect* and was first explained by Matthies (1979).

In the following we provide the reader with two examples illustrating the ghost effect. In both examples we consider triclinic crystal symmetry, i.e $S_{\text{Laue}} = S_{\text{tric}} = \{\text{Id}, -\text{Id}\}$. In the case of triclinic crystal symmetry the ODF $f\colon \text{O}(3)/S_{\text{tric}} \to \mathbb{R}_+$ can be treated as a function defined on SO(3). The first example deals with unimodal ODFs and shows that there are pairs of ODFs such that the corresponding PDFs are both the uniform distribution on $\mathbb{S}^2/S_{\text{tric}} \times \mathbb{S}^2$ and such that the first ODF has an arbitrarily sharp peak at some rotation $\mathbf{g}_0 \in \text{SO}(3)$ and the second ODF is almost zero in a whole neighborhood of $\mathbf{g}_0$, i.e. does not have any peak at this orientation.

Example 4.9. Let $\kappa \in (0, 1)$. Then

$$f_\kappa(\mathbf{g}) = \sum_{l=0}^{\infty} \kappa^l \mathcal{U}_{2l}\left(\cos\frac{\measuredangle \mathbf{g}}{2}\right) = \frac{1+\kappa}{1 - 2\kappa\cos\frac{\measuredangle \mathbf{g}}{2} + \kappa^2}, \quad \mathbf{g} \in \text{SO}(3),$$

defines a triclinic, unimodal and radially symmetric ODF with center $\mathbf{g}_0 = \text{Id}$. The parameter κ determines the sharpness of the ODF and we have $f_\kappa(\text{Id}) \to \infty$ as $\kappa \to 1$. One verifies that

$$f_{\kappa,\text{even}}(\mathbf{g}) = \sum_{l \in 2\mathbb{N}_0} \kappa^l \mathcal{U}_{2l}\left(\cos\frac{\measuredangle \mathbf{g}}{2}\right) = \frac{1 + 2\kappa^2\cos\frac{\measuredangle \mathbf{g}}{2} + \kappa^2}{1 - 2\kappa^2\cos\measuredangle \mathbf{g} + \kappa^4}, \quad \mathbf{g} \in \text{SO}(3),$$

and

$$f_{\kappa,\text{even}} - f_{\kappa,\text{odd}} = \sum_{l=0}^{\infty} (-\kappa)^l \mathcal{U}_{2l}\left(\cos\frac{\measuredangle \mathbf{g}}{2}\right) = \frac{1-\kappa}{1 + 2\kappa\cos\frac{\measuredangle \mathbf{g}}{2} + \kappa^2}, \quad \mathbf{g} \in \text{SO}(3),$$

are non–negative and hence represent valid ODFs that define identical PDFs

$$\mathcal{X} f_{\kappa,\text{even}} = \mathcal{X}(f_{\kappa,\text{even}} - f_{\kappa,\text{odd}}) = \mathcal{X} f_\kappa.$$

At the center $\mathbf{g}_0 = \text{Id}$ we obtain

$$(f_{\kappa,\text{even}} - f_{\kappa,\text{odd}})(\text{Id}) = \sum_{l=0}^{\infty} (-\kappa)^l (2l+1) = \frac{1-\kappa}{(1+\kappa)^2}.$$

Since $\lim_{\kappa\to 1} \frac{1-\kappa}{(1+\kappa)^2} = 0$ we conclude that $f_{\kappa,\text{even}} - f_{\kappa,\text{odd}}$ has no peak at $\mathbf{g}_0 = \text{Id}$ for $\kappa \to 1$.

Plots of the three ODF's f_κ, $f_{\kappa,\text{even}}$ and $f_{\kappa,\text{even}} - f_{\kappa,\text{odd}}$ are given in Figure 4.3 for $\kappa = 0.5$ and $\kappa = 0.9$.

The second example deals with radially symmetric ODFs such that the corresponding PDFs are all the uniform distribution on $\mathbb{S}^2/S_{\text{tric}} \times \mathbb{S}^2$. A similar example was already given by Matthies et al. (1987, Sec. 13.5).

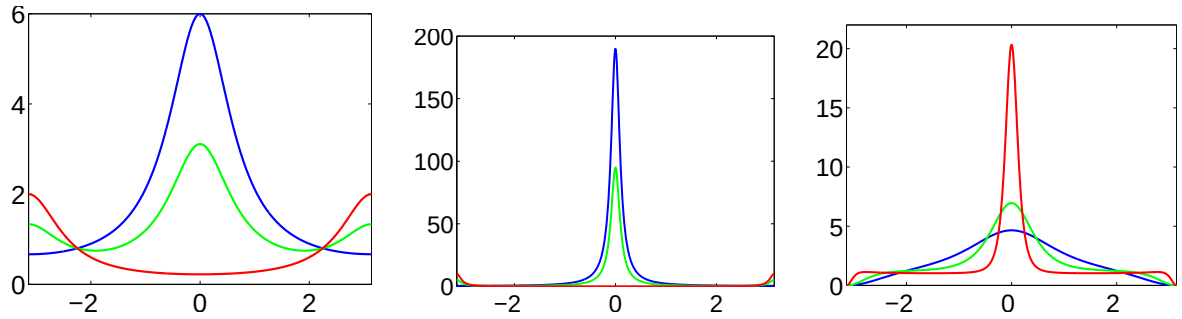

Figure 4.3: Each plot contains the graphs of three radially symmetric ODFs with identical PDFs plotted as functions of the rotational angle from the center. The functions f_κ (blue), $f_{\kappa,\text{even}}$ (green), and $f_{\kappa,\text{even}} - f_{\kappa,\text{odd}}$ (red) defined in Example 4.9 are plotted in the two left most diagrams for $\kappa = 0.5$ (left) and $\kappa = 0.9$ (middle). The functions f_κ defined in Example 4.10 are plotted in the right diagram for $\kappa = 0.5$ (blue), $\kappa = 0.7$ (green) and $\kappa = 0.9$ (red).

Example 4.10. Let $\kappa > 0$ and denote $K_\kappa^{\text{odd}}(\omega)$, $\omega \in [0, \pi]$ the odd part of the Abel–Poisson kernel (cf. Section 3.4)

$$\begin{aligned} K_\kappa^{\text{odd}}(\omega) &= \sum_{l \in 2\mathbb{N}_0+1} (2l+1)\kappa^{2l} \mathcal{U}_{2l}(\cos\tfrac{\omega}{2}) \\ &= \frac{\kappa^2\Big(3 + 7\kappa^4 - 5\kappa^8 - \kappa^{12} + 2(3 + \kappa^4 - 5\kappa^8)\cos\omega + 2\kappa^4(1 - 3\kappa^4)\cos 2\omega + \cos 3\omega\Big)}{(1 - 2\kappa^4\cos 2\omega + \kappa^8)^2}. \end{aligned}$$

We define a triclinic, radially symmetric ODF with center in $\mathbf{g}_0 = \text{Id}$ that defines a uniformly distributed PDF by setting

$$f_\kappa(\mathbf{g}) = 1 + \Big(\min_{\omega\in[0,\pi]} K_\kappa^{\text{odd}}(\omega)\Big)^{-1} K_\kappa^{\text{odd}}(\measuredangle \mathbf{g}) = 1 + \frac{(\kappa^4-1)^2}{\kappa^2(3+\kappa^4)} K_\kappa^{\text{odd}}(\measuredangle \mathbf{g}), \quad \mathbf{g} \in \text{SO}(3).$$

The discrepancy between the ODFs f_κ and the uniformly distributed ODF $f_{\text{unif}} = 1$ is

$$\|f_{\text{unif}} - f_\kappa\|_{L^2(\text{O}(3))} = \frac{(\kappa^4-1)^2}{\kappa^2(3+\kappa^4)} \sum_{l\in 1+2\mathbb{N}_0} (2l+1)^2\kappa^{2l} = \frac{9\kappa^2 + 22\kappa^{10} + \kappa^{18}}{(1+\kappa^4)^3(3 - 2\kappa^4 - \kappa^8)}$$

in the L^2–norm and

$$\|f_{\text{unif}} - f_\kappa\|_{L^\infty} = \frac{(\kappa^4-1)^2}{\kappa^2(3+\kappa^4)} \sum_{l\in 1+2\mathbb{N}_0} (2l+1)^2\kappa^{l} = \frac{9 + 22\kappa^4 + \kappa^8}{3 - 2\kappa^4 - \kappa^8}$$

in the maximum norm. Both quantities tend to infinity for $\kappa \to 1$. The ODF f_κ is plotted in Figure 4.3 for $\kappa = 0.5$, $\kappa = 0.7$ and $\kappa = 0.9$.

The following proposition is a direct consequence of Example 4.10.

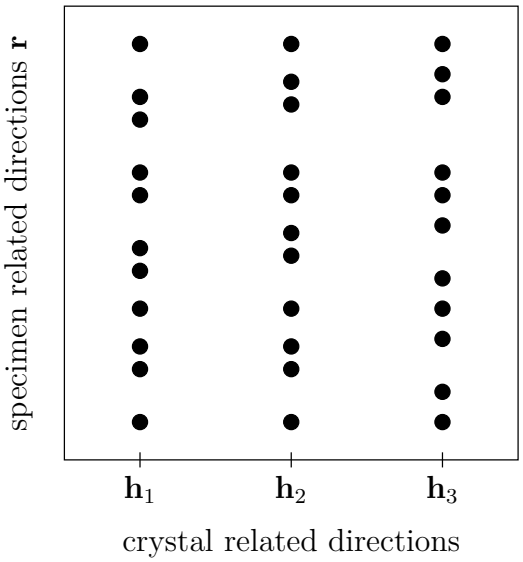

Figure 4.4: Scheme of a PDF sampling grid.

Proposition 4.11. *Let $S_{\text{Laue}} \subseteq \mathrm{O}(3)$ be some Laue group and let $f \in L^2(\mathrm{O}(3)/S_{\text{Laue}})$ be some ODF with $f \geq \varepsilon > 0$. Then the range*

$$\Omega_f = \{\, \tilde{f} \in L^2(\mathrm{O}(3)/S_{\text{Laue}}) \mid \mathcal{X}\tilde{f} = \mathcal{X}f \text{ and } \tilde{f} \geq 0 \,\}$$

of all ODF defining the same PDF as f is unbounded with respect to the L^2–norm and with respect to the L^∞–norm.

Proposition 4.11 indicates that it is in general not a good idea to look for the maximum value of an estimated ODF, since it varies arbitrarily within the range of ODFs corresponding to a given PDF. It should be noted that Proposition 4.11 does not apply to finite dimensional subspaces of $L^2(\mathrm{O}(3)/S_{\text{Laue}})$, e.g. if only ODFs with a certain bandwidth or resolution are considered. However, the range of Ω_f restricted to those finite dimensional subspaces remains still remarkable in practice (cf. Schaeben, 1994).

The Ambiguity Due to the Clustered Data Layout. As it was already pointed out in Section 4.2 the true PDF $P_{\text{true}} \in C(\mathbb{S}^2/S_{\text{Laue}} \times \mathbb{S}^2)$ is sampled in an irregular, strongly clustered way, i.e. the sampling grid $(S_{\text{Laue}}\mathbf{h}_i, \mathbf{r}_{ij}) \in \mathbb{S}^2/S_{\text{Laue}} \times \mathbb{S}^2$, $i = 1, \ldots, N$, $j = 1, \ldots, N_i$ of the PDF contains only a few different crystal directions $\mathbf{h}_i$ but many specimen directions $\mathbf{r}_{ij}$. A schematic illustration of a typical sampling grid used in diffraction experiments is plotted Figure 4.4.

Let $f_{\text{true}} \in C(\mathrm{O}(3)/S_{\text{Laue}})$ be the true ODF of a specimen and let $\hat{f}_{\text{true}}$ be its Fourier coefficients. Then in view of Equation (4.1) and Theorem 3.24 the true PDF has the

Fourier representation

$$P_{\text{true}}(\mathbf{h},\mathbf{r}) = \sum_{l\in 2\mathbb{N}} \sum_{k,k'=-l}^{l} \frac{1}{(l+\frac{1}{2})^{\frac{1}{2}}} \hat{f}_{\text{true}}(l,k,k') \mathcal{Y}_l^{k'}(\mathbf{h}) \overline{\mathcal{Y}_l^k(\mathbf{r})}.$$

Consequently every single pole figure $P(\mathbf{h}_i, \circ)$, $i = 1,\dots,N$ with respect to a fixed crystal direction $\mathbf{h}_i \in \mathbb{S}^2$ has a Fourier representation of the form

$$P(\mathbf{h}_i,\mathbf{r}) = \sum_{l=0}^{\infty} \sum_{k=-l}^{l} \hat{P}_{\mathbf{h}_i}(l,k) \overline{\mathcal{Y}_l^k(\mathbf{r})}, \quad i = 1,\dots,N \tag{4.7}$$

where the Fourier coefficients $\hat{P}_{\mathbf{h}_i}(l,k)$ are related to the Fourier coefficients $\hat{f}_{\text{true}}(l,k,k')$ of the ODF by

$$\hat{P}_{\mathbf{h}_i}(l,k) = \sum_{k'=-l}^{l} \frac{1}{(l+\frac{1}{2})^{\frac{1}{2}}} \hat{f}_{\text{true}}(l,k,k') \mathcal{Y}_l^{k'}(\mathbf{h}_i), \quad (i = 1,\dots,N,\ l \in \mathbb{N}_0,\ k = -l,\dots,l). \tag{4.8}$$

Equation (4.7) describes for each pole figure a system of linear equations, each of which can be seen as an inverse Fourier transform with sample points $\big(\mathbf{r}_{ij}, P(\mathbf{h}_i,\mathbf{r}_{ij})\big)$, $j = 1,\dots,N_i$. Depending on the smoothness of the true PDF and the number of sample points N_i we have a minimum bandwidth $L_{\min}$ that is required to approximate the given sampling of the pole figures.

On the other hand equation (4.8) describes for any $l \in \mathbb{N}_0$ and $k = -l,\dots,l$ a system of linear equations with a fixed number N of equations but an increasing number of free variables. The systems of linear equations (4.8) define a maximum bandwidth $L_{\max}$ up to which all systems have a unique solution. Obviously, the bandwidth $L_{\max}$ depends on the number of sampled crystal directions $\mathbf{h}_i \in \mathbb{S}^2/S_{\text{Laue}}$, $i = 1,\dots,N$ and the Laue group S_{Laue}. If, as it is the case in practice, the number of sample nodes per pole figure is much larger then the number of pole figures, then the minimum number $L_{\min}$ of Fourier coefficients that is required to approximate the pole figures is smaller then the maximum number $L_{\max}$ of Fourier coefficients that can be calculated from a fixed number of measured pole figures. In other words, if we are going to estimate the true ODF at the desired bandwidth $L_{\min}$ the subspace of possible solutions does not only contain harmonic functions of odd degree but also harmonic functions with even degree between $L_{\max}$ and $L_{\min}$.

A more detailed analysis of this source of ambiguity can be found in Bunge (1969, Sec. 1.4.1). An impressive illustration of this issue represents the pair of sample ODFs by Boogaart (cf. Bernstein et al., 2005) which are totally different but define six identical pole figures. Remember that six is a common total number of pole figures to be measured.

As an additional difficulty we have the fact that many experimental settings result in incomplete pole figure coverages, i.e. the specimen directions do not lie uniformly

dense in the hemisphere $\mathbb{S}^2_+$. Since the inversion of the Radon transform is not local (cf. Theorem 3.19) a consistent estimator of the value of the true ODF at a single orientation requires information about the PDF on its complete domain $\mathbb{S}^2/S_{\text{Laue}} \times \mathbb{S}^2$.

The Ambiguity Due to Superposed Pole Figures. In the case of superposed pole figures equation (4.7) and equation (4.8) change to

$$P(H_i, \mathbf{r}) = \sum_{l=0}^{\infty} \sum_{k=-l}^{l} \hat{P}_{H_i}(l,k)\overline{\mathcal{Y}_l^k(\mathbf{r})}, \quad i = 1, \dots, N$$

and

$$\hat{P}_{H_i}(l,k) = \sum_{k'=-l}^{l} \frac{1}{(l+\frac{1}{2})^{\frac{1}{2}}} \hat{f}_{\text{true}}(l,k,k') \sum_{\mathbf{h} \in H_i} \rho_i(\mathbf{h}) \mathcal{Y}_l^{k'}(\mathbf{h}),$$

where $i = 1, \dots, N$, $l \in \mathbb{N}_0$, $k = -l, \dots, l$. Hence, there are less constraints on the Fourier coefficients of f_{true} in comparison to the case that the crystal directions in H_i have been measured independently. In general this results in a smaller bandwidth $L_{\max}$ up to which the Fourier coefficients of the true ODF can be estimated.

The Ambiguity Due to the Unknown Normalization Coefficients. An additional source of ambiguity are the unknown normalization coefficients $\boldsymbol{\alpha}_{\text{true}} \in \mathbb{R}^N$ of the measured diffraction counts. In the case of complete pole figures, i.e. the sampling grids $\mathbf{r}_i = (\mathbf{r}_{i1}, \dots, \mathbf{r}_{iN_i})$ provide complete coverages of the hemisphere $\mathbb{S}^2_+$, the normalization coefficients can be directly estimated from the diffraction counts (cf. Proposition 4.31).

However, in practice the measured specimen directions usually do not provide a complete coverage the hemisphere but contain sparse areas. In those cases estimation of the normalization coefficients is only promising if the ratio of mass of the density function $\mathcal{X} f_{\text{true}}(H_i, \circ)$ is known that is concentrated in the region covered by the sampling grid $\mathbf{r}_i$. Hence, the ambiguity of the unknown normalization coefficients can be seen as the lack of knowledge about this ratio.

The following example gives an illustration of this issue. We consider an ODF that is the superposition of two unimodal not overlapping peaks. We want to retrieve this ODF from two given pole figures of this ODF, which are incomplete in such a way that each peak of the ODF is visible only at one pole figure. Then the lack of information about the normalization coefficients of the pole figures corresponds to the lack of information about the ratio of the two ODF components.

An additional difficulty connected with the unknown normalization coefficients is the fact that the corresponding estimation problem is in general not convex (cf. Section 4.5) in contrast to the case of known normalization coefficients where quadratic estimation functionals exist.

The Ambiguity Due to the Ill–Posedness of the Radon Transform. The inversion of the planar Radon transform is a classical example of an ill–posed problem. In Section 3.2 we have characterized the one–dimensional Radon transform on O(3) as an isomorphism between the Sobolev spaces $\mathcal{H}_0(\mathrm{O}(3))$ and $\mathcal{H}_{\frac{1}{2}}(\mathbb{S}^2 \times \mathbb{S}^2)$. Hence, the inversion of the one–dimensional Radon transform on O(3) is an ill–posed problem of order $\frac{1}{2}$ (cf. Louis, 1989, Sec. 3.2). Since the measured diffraction counts are in general effected by measurement errors one has to apply regularization techniques to avoid amplification of errors (cf. Bernier and Miller, 2006; van den Boogaart et al., 2006).

4.4 The Reproducibility of the ODF

We are concerned with the following simplified problem. Let $S_{\mathrm{Laue}} \subseteq \mathrm{O}(3)$ be a Laue group and let $P_i \in L^2(\mathbb{S}^2)$, $i = 1, \ldots, N$, be a list of pole figures with respect to the crystal directions $\mathbf{h}_i \in \mathbb{S}^2$. We are interested in the range of ODFs $f \in L^2(\mathrm{O}(3)/S_{\mathrm{Laue}})$ that satisfy

$$\mathcal{X}f(\mathbf{h}_i, \circ) = P_i, \quad i = 1, \ldots, N. \tag{4.9}$$

In other words, here we focus on the ambiguity of the ODF estimation problem neglecting the ambiguity due to incomplete or superposed pole figures and unknown normalization coefficients. This problem was first formulated by Matthies (cf. Matthies, 1982, Sec. 31) and is central in QTA (Schaeben, 1994). Remember that for $f \in L^2(\mathrm{O}(3)/S_{\mathrm{Laue}})$ the partial pointwise evaluation $\mathcal{X}f(\mathbf{h}, \circ) \in L^2(\mathbb{S}^2)$ is well defined (cf. Remark 3.12) for any crystal direction $\mathbf{h} \in \mathbb{S}^2$.

In Proposition 4.11 we have shown that the range of such ODFs is in general unbounded with respect to the maximum norm and with respect to the L^2–norm. However, there exist ODFs $f \in C(\mathrm{O}(3)/S_{\mathrm{Laue}})$ such that there is an one to one relation to the corresponding PDF. A class of such ODFs is described by the next proposition. For simplicity we restrict ourself to the triclinic case, i.e. to $S_{\mathrm{Laue}} = S_{\mathrm{tric}} = \{\mathrm{Id}, -\mathrm{Id}\}$. Then the orientation space simplifies to $\mathrm{O}(3)/S_{\mathrm{tric}} = \mathrm{SO}(3)$.

Proposition 4.12. *Let $f_{true} \in C(\mathrm{SO}(3))$ be a triclinic ODF localized within a ball of diameter $\frac{\pi}{2}$ around a certain orientation $\mathbf{g}_0 \in \mathrm{SO}(3)$, i.e. $f_{true}(\mathbf{g}) = 0$ for all $\mathbf{g} \in \mathrm{SO}(3)$ with $\measuredangle(\mathbf{g}_0^{-1}\mathbf{g}) \geq \frac{\pi}{2}$. Then f_{true} is uniquely determined by the corresponding pole density function $P_{true} = \mathcal{X}f_{true}$.*

Proof. First of all we notice that the condition $f_{\mathrm{true}}(\mathbf{g}) = 0$ for all $\mathbf{g} \in \mathrm{SO}(3)$ with $\measuredangle(\mathbf{g}_0^{-1}\mathbf{g}) \geq \frac{\pi}{2}$ is equivalent to the condition $P(\mathbf{h}, \mathbf{r}) = 0$ for all $\mathbf{h}, \mathbf{r} \in \mathbb{S}^2$ with $\measuredangle(\mathbf{g}_0\mathbf{h}, \mathbf{r}) = \frac{\pi}{2}$. This is due to the identity of the sets

$$\left\{ \mathbf{g} \in \mathrm{SO}(3) \;\middle|\; \measuredangle(\mathbf{g}, \mathbf{g}_0) \geq \frac{\pi}{2} \right\} = \left\{ \mathbf{g} \in G(\mathbf{h}, \mathbf{r}) \;\middle|\; \mathbf{h}, \mathbf{r} \in \mathbb{S}^2, \measuredangle(\mathbf{g}_0\mathbf{h}, \mathbf{r}) = \frac{\pi}{2} \right\}$$

and the non–negativity of f_{true}. Consequently, the assumptions of the proposition can be derived from the pole density function P_{true} directly.

Let $\mathbf{h}, \mathbf{r} \in \mathbb{S}^2$ such that $\measuredangle(\mathbf{g}_0\mathbf{h}, \mathbf{r}) = \frac{\pi}{2}$. By inequality (2.5) any rotation $\mathbf{g} \in \mathrm{SO}(3)$ with $\mathbf{g}\mathbf{g}_0\mathbf{h} = \mathbf{r}$ satisfies $\measuredangle(\mathbf{g}_0, \mathbf{g}) \geq \frac{\pi}{2}$. Hence, the condition $f_{\mathrm{true}}(\mathbf{g}) = 0$ for all rotations $\mathbf{g} \in \mathrm{SO}(3)$ with $\measuredangle(\mathbf{g}_0, \mathbf{g}) \geq \frac{\pi}{2}$ implies $f_{\mathrm{true}}(\mathbf{g}) = 0$ for all rotations $\mathbf{g} \in G(\mathbf{h}, \mathbf{r})$. Consequently $\mathcal{R}f(\mathbf{h}, \mathbf{r}) = 0$ and we conclude that the Radon transform of the true ODF f_{true} is uniquely determined by the true PDF P_{true} thanks to

$$\mathcal{R}f_{\mathrm{true}}(\mathbf{g}_0\mathbf{h}, \mathbf{r}) = \begin{cases} P_{\mathrm{true}}(\mathbf{g}_0\mathbf{h}, \mathbf{r}) & \text{if } \measuredangle(\mathbf{g}_0\mathbf{h}, \mathbf{r}) \leq \frac{\pi}{2}, \\ 0 & \text{otherwise,} \end{cases}$$

for any $\mathbf{h}, \mathbf{r} \in \mathbb{S}$. By Theorem 3.10 the Radon transform is injective and hence the ODF f_{true} is uniquely determined by the PDF P_{true}. □

Our purpose in this section is to relax the assumptions of Proposition 4.12 such that it applies to arbitrary ODFs and to single pole figures $P_i = P(\mathbf{h}_i, \circ)$, $i = 1, \ldots, N$.

General Framework.

Definition 4.13. Let $\psi\colon [0, \pi] \to \mathbb{R}_+$ be some non–negative, square integrable function and let $S \subseteq \mathbb{S}^2$ be an arbitrary subset. We define the *concentration* of a non–negative, square integrable function $P\colon \mathbb{S}^2 \to \mathbb{R}_+$ with respect to the set S and the weighting function ψ as

$$\sigma_\psi(P, S) = \frac{1}{4\pi} \int_{\mathbb{S}^2} \psi(\measuredangle(S, \mathbf{r}))P(\mathbf{r})\, \mathrm{d}\mathbf{r}.$$

Here, $\measuredangle(\mathbf{r}, S)$ denoted the angular distance between the vector $\mathbf{r}$ and the set S.

Analogously we define the *concentration* of any non–negative, square integrable function $f\colon \mathrm{O}(3) \to \mathbb{R}_+$ in some subset $Q \subseteq \mathrm{O}(3)$ with respect to the weighting function ψ by

$$\sigma_\psi(f, Q) = \frac{1}{16\pi^2} \int_{\mathrm{O}(3)} \psi(\measuredangle(Q, \mathbf{g}))f(\mathbf{g})\, \mathrm{d}\mathbf{g}.$$

Let $P\colon \mathbb{S}^2 \to \mathbb{R}_+$ and $f\colon \mathrm{O}(3) \to \mathbb{R}_+$ be probability density functions. Then there are two important special cases for the choice of the function ψ which allow for a statistical interpretation of the concentrations $\sigma_\psi(P, S)$ and $\sigma_\psi(f, Q)$. If $\psi(t) = \mathbf{1}_{[0,\varepsilon]}$ is the indicator function then $\sigma_\psi(P, S)$ and $\sigma_\psi(f, Q)$ represent the mass located within the distance $\varepsilon > 0$ to the sets S and Q, respectively. If $\psi(t) = t^2$ and S and Q are single elements which correspond to the mean values of P and f then $\sigma_\psi(P, S)$ and $\sigma_\psi(f, Q)$ are the variances of P and f, respectively. It is emphasized that Definition 4.13 allows for the presence of crystal symmetries, i.e. for ODFs defined on factor spaces $\mathrm{O}(3)/S_{\mathrm{Laue}}$. In this case the set Q has to be chosen such that $Q = QS_{\mathrm{Laue}}$. Since any Laue group contains the inversion $-\mathrm{Id} \in \mathrm{O}(3)$ we have $Q = -Q$ in all cases of interest.

Now we are ready to formulate the main theorem of this section relating the concentrations of an ODF and its pole figures.

Theorem 4.14. *Let $Q \subseteq \mathrm{O}(3)$ with $-\mathrm{Id} \in Q$ and let $\psi : [0,\pi] \to \mathbb{R}_+$ be some non–negative, square integrable function. Then we define for any list $\mathbf{h} = (\mathbf{h}_1, \dots, \mathbf{h}_N)$ of crystal directions $\mathbf{h}_i \in \mathbb{S}^2$ and for any coefficients $\boldsymbol{\lambda} \in \mathbb{R}_+^N$ with $\sum_{i=1}^N \lambda_i = 1$ the function*

$$\Psi_{Q,\mathbf{h},\boldsymbol{\lambda}} \colon \mathrm{O}(3) \to \mathbb{R}_+, \quad \Psi_{Q,\mathbf{h},\boldsymbol{\lambda}}(\mathbf{g}) = \sum_{i=1}^N \lambda_i \psi(\measuredangle(\mathbf{g}\mathbf{h}_i, Q\mathbf{h}_i)). \tag{4.10}$$

Let $\psi_1, \psi_2 \colon [0,\pi] \to \mathbb{R}_+$ be two non–negative, square integrable functions satisfying the inequality

$$\psi_1(\measuredangle(\mathbf{g}, Q)) \leq \Psi_{Q,\mathbf{h},\boldsymbol{\lambda}}(\mathbf{g}) \leq \psi_2(\measuredangle(\mathbf{g}, Q)), \quad \mathbf{g} \in \mathrm{O}(3). \tag{4.11}$$

Then we have for any square integrable ODF $f \colon \mathrm{O}(3) \to \mathbb{R}_+$ the inequality

$$\sigma_{\psi_1}(f, Q) \leq \sum_{i=1}^N \lambda_i \sigma_\psi(\mathcal{X}f(\mathbf{h}_i, \circ), Q\mathbf{h}_i) \leq \sigma_{\psi_2}(f, Q). \tag{4.12}$$

Proof. Since $\bigcup_{\mathbf{r}\in\mathbb{S}^2} G(\mathbf{h}_i, \mathbf{r}) = \mathrm{SO}(3)$ defines a disjoint coverage of $\mathrm{SO}(3)$ for any $\mathbf{h}_i \in \mathbb{S}^2$, $i = 1, \dots, N$, we have

$$\begin{aligned}
\sigma_\psi(\mathcal{X}f(\mathbf{h}_i, \circ), Q\mathbf{h}_i) &= \frac{1}{4\pi} \int_{\mathbb{S}^2} \psi(\measuredangle(\mathbf{r}, Q\mathbf{h}_i)) \frac{1}{4\pi} \int_{G(\mathbf{h}_i,\mathbf{r}) \cup -G(-\mathbf{h}_i,\mathbf{r})} f(\mathbf{g}) \, \mathrm{d}\mathbf{g} \, \mathrm{d}\mathbf{r} \\
&= \frac{1}{16\pi^2} \int_{\mathrm{O}(3)} \psi(\measuredangle(\mathbf{g}\mathbf{h}_i, Q\mathbf{h}_i)) f(\mathbf{g}) \, \mathrm{d}\mathbf{g}.
\end{aligned}$$

Consequently, we can state for any function ψ_1 satisfying $\psi_1(\measuredangle(\mathbf{g}, Q)) \leq \Psi_{Q,\mathbf{h},\lambda}(\mathbf{g})$ that

$$\begin{aligned}
\sum_{i=1}^N \lambda_i \sigma_\psi(\mathcal{X}f(\mathbf{h}_i, \circ), Q\mathbf{h}_i) &= \sum_{i=1}^N \lambda_i \frac{1}{16\pi^2} \int_{\mathrm{O}(3)} \psi(\measuredangle(\mathbf{g}\mathbf{h}_i, Q\mathbf{h}_i)) f(\mathbf{g}) \, \mathrm{d}\mathbf{g} \\
&= \frac{1}{16\pi^2} \int_{\mathrm{O}(3)} \sum_{i=1}^N \lambda_i \psi(\measuredangle(\mathbf{g}\mathbf{h}_i, Q\mathbf{h}_i)) f(\mathbf{g}) \, \mathrm{d}\mathbf{g} \geq \sigma_{\psi_1}(f, Q).
\end{aligned}$$

In the last inequality we have made use of the non–negativity of the functions f and ψ. This proves the inequality (4.12) for ψ_1. The proof for ψ_2 is analogous. □

The crucial point of Theorem 4.14 is that it provides a relationship between the concentration $\sigma_{\psi_1}(f, Q)$ of an ODF f and the concentrations $\sigma_\psi(\mathcal{X}f(\mathbf{h}_i, \circ), Q\mathbf{h}_i)$, $i = 1, \dots, N$ of some of its pole figures while making use of the non–negativity of the ODF. However, the application of Theorem 4.14 to practical problems is not straight forward but involves an interplay between presumptions about the true ODF and the desired results in mind. In general we have the following recipe.

1. Choose a region of concentration Q.

2. Choose a weighting function ψ appropriate to the sharpness of the ODF.
3. Choose weighting coefficients λ_i, $i = 1, \dots, N$ with $\sum_{i=1}^{N} \lambda_i = 1$.
4. Determine $\Psi_{Q,\mathbf{h},\boldsymbol{\lambda}}$, $\Psi^{\inf}_{Q,\mathbf{h},\boldsymbol{\lambda}}$ and $\Psi^{\sup}_{Q,\mathbf{h},\boldsymbol{\lambda}}$.
5. Choose ψ_1, ψ_2 according to condition (4.11).
6. Apply Theorem 4.14.

Since the weighting coefficients λ_i, $i = 1, \dots, N$ can be chosen arbitrarily it makes sense to look for those weighting coefficients which lead to a maximum sharp inequality (4.12). The sharpness of inequality (4.12) depends on the difference between the functions ψ_1 and ψ_2 which have to be chosen according to condition (4.11). Moreover, the criteria of maximum sharpness of inequality (4.12) can be used as a rule for choice of the pole figure $P(\mathbf{h}_i, \circ)$ to be measured for texture determination.

In the following we restrict ourself to the case $\lambda_i = 1/N$, $i = 1, \dots, N$ and write $\Psi_{Q,\mathbf{h}}$ instead of $\Psi_{Q,\mathbf{h},\boldsymbol{\lambda}}$.

Triclinic Crystal Symmetry. Let us start with the simple case of a triclinic crystal symmetry and concentration in a single crystal orientation $\mathbf{g}_0 S_{\text{tric}} = \{\text{Id}, -\text{Id}\} = Q$. Fixing $\psi(t) = t^2$ and crystal directions $\mathbf{h} = (\mathbf{h}_1, \dots, \mathbf{h}_N)$, $\mathbf{h}_i \in \mathbb{S}^2$ we can plot $\Psi_{Q,\mathbf{h}}$ as follows. For any angle $\omega \in [0, \pi]$ we plot the range of $\Psi_{Q,\mathbf{h}}(\mathbf{g})$, where $\measuredangle(\mathbf{g}, Q) = \omega$. This has been done in Figure 4.5 for a single crystal direction $\mathbf{h} = (\mathbf{e}_1)$, for the three crystal directions $\mathbf{h} = (\mathbf{e}_1, \mathbf{e}_2, \mathbf{e}_3)$, and for the seven crystal directions

$$\mathbf{h} = \left(\begin{pmatrix} 1 \\ 0 \\ 0 \end{pmatrix}, \begin{pmatrix} 0 \\ 1 \\ 0 \end{pmatrix}, \begin{pmatrix} 0 \\ 0 \\ 1 \end{pmatrix}, \begin{pmatrix} 1 \\ 1 \\ 1 \end{pmatrix}, \begin{pmatrix} 1 \\ 1 \\ -1 \end{pmatrix}, \begin{pmatrix} 1 \\ -1 \\ 1 \end{pmatrix}, \begin{pmatrix} -1 \\ 1 \\ 1 \end{pmatrix}, \begin{pmatrix} 1 \\ -1 \\ -1 \end{pmatrix} \right).$$

Additionally the function

$$\tilde{\Psi}_Q(\mathbf{g}) = \frac{1}{4\pi} \int_{\mathbb{S}^2} \psi(\measuredangle(\mathbf{g}\mathbf{h}, Q\mathbf{h}))\, \mathrm{d}\mathbf{h}, \tag{4.13}$$

is plotted which can be interpreted as the limit of $\Psi_{Q,\mathbf{h}}$ when the total number of crystal directions N increases to infinity.

We define for abbreviation the functions $\Psi^{\inf}_{Q,\mathbf{h}} \colon [0, \pi] \to \mathbb{R}_+$ and $\Psi^{\sup}_{Q,\mathbf{h}} \colon [0, \pi] \to \mathbb{R}_+$ as

$$\begin{aligned} \Psi^{\inf}_{Q,\mathbf{h}}(\omega) &:= \inf\{\, \Psi_{Q,\mathbf{h}}(\mathbf{g}) \mid \mathbf{g} \in \mathrm{O}(3), \measuredangle(\mathbf{g}, Q) = \omega \,\}, \\ \Psi^{\sup}_{Q,\mathbf{h}}(\omega) &:= \sup\{\, \Psi_{Q,\mathbf{h}}(\mathbf{g}) \mid \mathbf{g} \in \mathrm{O}(3), \measuredangle(\mathbf{g}, Q) = \omega \,\} \end{aligned} \tag{4.14}$$

and give some interpretations of graphs plotted in Figure 4.5.

1. The observation that $\Psi^{\inf}_{Q,\mathbf{h}}(\pi) = 0$ in the case of the three crystal directions $\mathbf{h}_i = \mathbf{e}_i$, $i = 1, \dots, 3$ relates to the fact that there are crystal orientations $\mathbf{g} S_{\text{tric}} \in \mathrm{O}(3)/S_{\text{tric}}$, e.g. $\mathbf{g} = \mathrm{Rot}_{\mathbf{e}_i}(\pi)$, with $\mathbf{g} S_{\text{tric}} \mathbf{h}_i = S_{\text{tric}} \mathbf{h}_i$, $i = 1, \dots, 3$. In other words an ODF concentrated in $\mathrm{Rot}_{\mathbf{e}_i}(\pi) S_{\text{tric}}$, $i = 1, \dots, 3$, causes identical pole figures $P(\mathbf{e}_1, \circ)$, $P(\mathbf{e}_2, \circ)$, $P(\mathbf{e}_3, \circ)$ as an ODF concentrated in $\mathrm{Id} S_{\text{tric}}$.

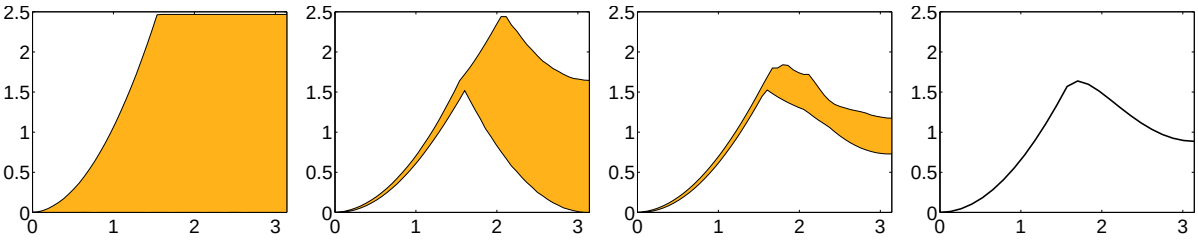

Figure 4.5: The graphs of the function $\Psi_{Q,\mathbf{h}}$ for $Q = \{\mathrm{Id}, -\mathrm{Id}\}$ and for one, three and seven crystal directions $\mathbf{h}$, and the function $\tilde{\Psi}_Q$.

2. The observation $\Phi_{\mathrm{inf}}(\omega) \geq a > 0$ for $\omega > \omega_0 > 0$ and some $a, \omega_0 \in \mathbb{R}_+$ in the case of the seven crystal directions $\mathbf{h}_i$ as chosen above, implies that the pole figures $P(\mathbf{h}_i, \circ)$, $i = 1, \ldots, 7$ are sufficient to distinguish between an ODF sufficiently well concentrated in $\mathbf{g}_0 = \mathrm{Id} \in \mathrm{SO}(3)$ and any other ODF.

3. Figure 4.5 indicates that the range of $\Psi_{Q,\mathbf{h}}(\mathbf{g})$ with $\measuredangle(\mathbf{g}, Q) = \omega$ shrinks when the number of crystal directions increases and that $\Psi_{Q,\mathbf{h}}$ eventually converges to the function $\tilde{\Psi}_Q$ as plotted in right most graph. This behavior is more formally described by the next proposition.

Proposition 4.15. *Let $\psi\colon [0,\pi] \to \mathbb{R}_+$ be some non–negative, square integrable function, let $\mathbf{h} = (\mathbf{h}_1, \ldots, \mathbf{h}_N)$, $\mathbf{h}_i \in \mathbb{S}^2$ be a list of $N \in \mathbb{N}$ crystal directions and let $Q = \{-\mathbf{g}_0, \mathbf{g}_0\}$ for some rotation $\mathbf{g}_0 \in \mathrm{SO}(3)$. Furthermore, denote $\Psi_{Q,\mathbf{h}}, \tilde{\Psi}_Q, \Psi^{inf}_{Q,\mathbf{h}}$ and $\Psi^{sup}_{Q,\mathbf{h}}$ the functions as defined in the equations (4.10), (4.13) and (4.14). Then $\mathbf{g} \mapsto \tilde{\Psi}_Q(\mathbf{g})$ is a function depending only on the angle $\measuredangle(\mathbf{g}, Q)$ and we have*

$$\Psi^{inf}_{Q,\mathbf{h}}(\measuredangle(\mathbf{g}, Q)) \leq \tilde{\Psi}_Q(\mathbf{g}) \leq \Psi^{sup}_{Q,\mathbf{h}}(\measuredangle(\mathbf{g}, Q)), \quad (\mathbf{g} \in \mathrm{O}(3)). \tag{4.15}$$

Proof. Without loss of generality, we may assume $Q = \{-\mathrm{Id}, \mathrm{Id}\}$. Then we have for all $\mathbf{g}, \mathbf{q} \in \mathrm{O}(3)$

$$\tilde{\Psi}_Q(\mathbf{q}^{-1}\mathbf{g}\mathbf{q}) = \frac{1}{4\pi} \int_{\tilde{\mathbf{h}} \in \mathbb{S}^2} \psi(\measuredangle(\mathbf{g}\mathbf{q}\tilde{\mathbf{h}}, Q\mathbf{q}\tilde{\mathbf{h}}))\, \mathrm{d}\tilde{\mathbf{h}} = \tilde{\Psi}_Q(\mathbf{g})$$

and hence $\tilde{\Psi}_Q$ depends only on the angle $\measuredangle(\mathbf{g}, Q)$.

Furthermore, we observe that the function

$$\tilde{\psi}(\omega) = \frac{1}{4\pi} \int_{\mathbb{S}^2} \psi(\measuredangle(\mathrm{Rot}_{\boldsymbol{\eta}}(\omega)\tilde{\mathbf{h}}, Q\tilde{\mathbf{h}}))\, \mathrm{d}\boldsymbol{\eta}$$

does not depend on the particular choice of $\tilde{\mathbf{h}} \in \mathbb{S}^2$. Consequently, we have for any list $\mathbf{h} = (\mathbf{h}_1, \ldots, \mathbf{h}_N)$, $\mathbf{h}_i \in \mathbb{S}^2$ of $N \in \mathbb{N}$ of crystal directions and any coefficients $\boldsymbol{\lambda} \in \mathbb{R}^N_+$, $\sum_{i=1}^N \lambda_i = 1$ the equality

$$\frac{1}{4\pi} \int_{\mathbb{S}^2} \Psi_{Q,\mathbf{h}}(\mathrm{Rot}_\eta(\omega))\, \mathrm{d}\boldsymbol{\eta} = \frac{1}{4\pi} \int_{\mathbb{S}^2} \sum_{i=1}^N \lambda_i \psi(\measuredangle(\mathrm{Rot}_{\boldsymbol{\eta}}(\omega)\mathbf{h}_i, Q\mathbf{h}_i))\, \mathrm{d}\boldsymbol{\eta} = \tilde{\psi}(\omega).$$

On the other hand we have for any $\mathbf{q} \in \mathrm{SO}(3)$ with $\measuredangle \mathbf{q} = \omega$,

$$\tilde{\Psi}_Q(\mathbf{q}) = \frac{1}{4\pi} \int_{\mathbb{S}^2} \tilde{\Psi}_Q(\mathrm{Rot}_{\boldsymbol{\eta}}(\omega))\, \mathrm{d}\boldsymbol{\eta} = \frac{1}{4\pi} \int_{\mathbb{S}^2} \frac{1}{4\pi} \int_{\mathbb{S}^2} \psi(\measuredangle(\mathrm{Rot}_{\boldsymbol{\eta}}(\omega)\mathbf{h}_i, Q\mathbf{h}_i))\, \mathrm{d}\mathbf{h}\, \mathrm{d}\boldsymbol{\eta} = \tilde{\psi}(\omega)$$

and hence

$$\frac{1}{4\pi} \int_{\mathbb{S}^2} \Psi_{Q,\mathbf{h}}(\mathrm{Rot}_{\boldsymbol{\eta}}(\omega))\, \mathrm{d}\boldsymbol{\eta} = \tilde{\Psi}_Q(\mathbf{q}), \quad \mathbf{q} \in \mathrm{SO}(3), \measuredangle \mathbf{q} = \omega$$

Together with the non–negativity of $\Psi_{Q,\mathbf{h}}$ this proves equation (4.15). □

Remark 4.16. Proposition 4.15 states that for a fixed function $\psi\colon [0,\pi] \to \mathbb{R}_+$ there is an upper and a lower bound for the functions ψ_1 and ψ_2 as specified in Theorem 4.14. In particular, we have for any square integrable ODF $f\colon \mathrm{O}(3)/S_{\mathrm{tric}} \to \mathbb{R}$ the equality

$$\sigma_{\tilde{\Psi}_Q}(f, Q) = \frac{1}{4\pi} \int_{\mathbb{S}^2} \sigma_{\psi}(\mathcal{X} f(\mathbf{h}, \circ), Q)\, \mathrm{d}\mathbf{h}.$$

General Crystal Symmetries. Proposition 4.15 does not apply to arbitrary Laue groups and arbitrary choices of Q. Nevertheless, setting $\psi(t) = t^2$ the function $\tilde{\Psi}_Q$ gives an impression about the preservation of localization also for non–triclinic crystal symmetries. The functions $\tilde{\Psi}_Q$ is plotted in Figure 4.6 for all Laue groups $Q = S_{\mathrm{Laue}}$.

Remark 4.17. One recognizes a qualitative difference between the functions $\tilde{\Psi}_Q^{\mathrm{inf}}$ of those Laue group that do not contain two perpendicular symmetry axes (top row) and those containing perpendicular symmetry axes (bottom row). For the Laue groups displayed in the top row the function $\tilde{\Psi}_Q^{\mathrm{inf}}$ seems to be decreasing beginning with a certain angle whereas for the Laue group displayed at bottom row the function $\tilde{\Psi}_Q^{\mathrm{inf}}$ seems to be monotonously increasing. In view of Theorem 4.14 one would therefore expect a better preservation of localization in the case of Laue groups containing two perpendicular symmetry axes.

In the following we demonstrate the application of Theorem 4.14 with two practical examples. In particular we give estimates for weak and sharp orthorhombic textures based on three pole figures. The purpose of these estimates is to show that in contrast to Example 4.9 and Example 4.10 the general type of ODFs can be determined by diffraction experiments, i.e. weak pole figures correspond to weak ODFs and sharp pole figures correspond to sharp ODFs.

The orthorhombic crystal symmetry is described by the Laue group

$$S_{\mathrm{orth}} = \langle -\mathrm{Id}, \mathrm{Rot}_{\mathbf{e}_1}(\pi), \mathrm{Rot}_{\mathbf{e}_2}(\pi) \rangle\,.$$

Here the notation $G = \langle \mathbf{g}_1, \ldots, \mathbf{g}_N \rangle$ defines the group generated by the elements $\mathbf{g}_1, \ldots, \mathbf{g}_N$. Furthermore, we denote for any unit vector $\boldsymbol{\eta} \in \mathbb{S}^2$ the set of antipodal vectors $\{\boldsymbol{\eta}, -\boldsymbol{\eta}\}$ by $\pm\boldsymbol{\eta}$. In the case of orthorhombic crystal symmetry the maximum rotational angle of a crystal orientation $\mathbf{g}S_{\mathrm{orth}} \in \mathrm{O}(3)/S_{\mathrm{orth}}$ is $\frac{2}{3}\pi$ as it is shown in the next lemma.

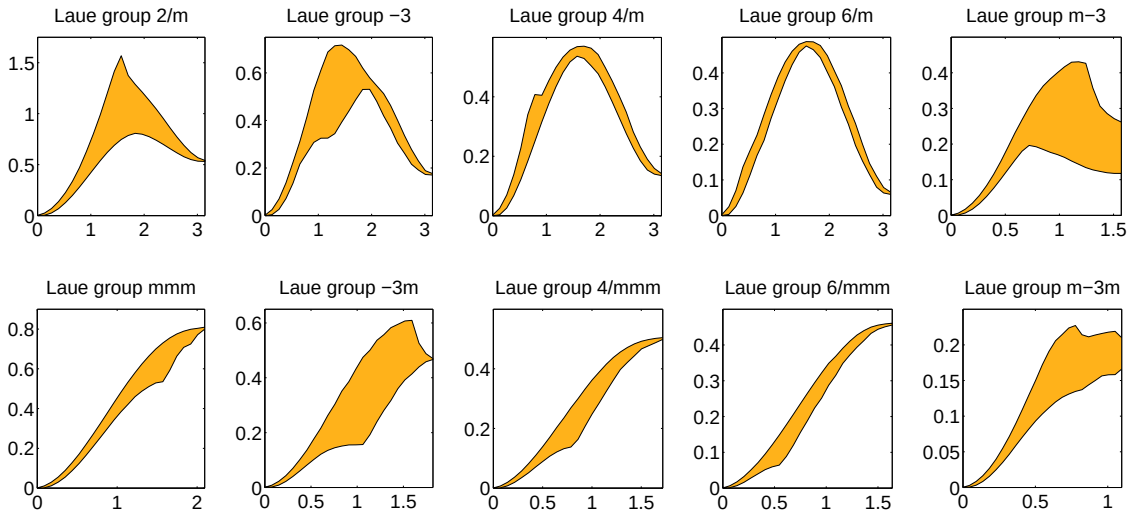

Figure 4.6: The function $\tilde{\Psi}_{Q,\mathbf{h}}$ for all Laue groups.

Lemma 4.18. *Let* $\mathbf{g} \in \mathrm{O}(3)$. *Then there is a rotation* $\mathrm{Rot}_{\boldsymbol{\eta}}(\omega) \in \mathbf{g}S_{orth}$ *with*

$$\omega \le 2 \operatorname{arccot}\bigl(\cos \max_{i=1,\dots,3} \measuredangle(\boldsymbol{\eta}, \pm\mathbf{e}_i)\bigr). \tag{4.16}$$

In particular $\measuredangle(\mathbf{g}, S_{orth}) \le \frac{2}{3}\pi$.

Proof. For any $\omega \in [0,\pi]$ and $\boldsymbol{\eta} \in \mathbb{S}^2$ we have by equation (2.4)

$$\cos \frac{\measuredangle\bigl(\mathrm{Rot}_{\boldsymbol{\eta}}(\omega), \mathrm{Rot}_{\mathbf{e}_i}(\frac{\pi}{2})\bigr)}{2} = \sin\tfrac{\omega}{2} \cos \measuredangle(\boldsymbol{\eta}, \mathbf{e}_i), \quad i = 1,\dots,3.$$

Let $\omega > 2 \operatorname{arccot}\bigl(\cos \measuredangle(\boldsymbol{\eta}, \mathbf{e}_1)\bigr)$. Then $\cos \measuredangle(\boldsymbol{\eta}, \mathbf{e}_1) > \cot \frac{\omega}{2}$ and hence

$$\measuredangle(\mathrm{Rot}_{\boldsymbol{\eta}}(\omega), \mathrm{Rot}_{\mathbf{e}_1}(\tfrac{\pi}{2})) < 2 \arccos(\sin\tfrac{\omega}{2} \cot\tfrac{\omega}{2}) = \omega.$$

In other words, for every rotation $\mathrm{Rot}_{\boldsymbol{\eta}}(\omega) \in \mathbf{g}S_{\mathrm{orth}}$ that does not satisfy the condition (4.16) there is a crystallographically equivalent rotation with smaller rotational angle. Since the symmetry group S_{orth} is finite there is at least one rotation $\mathrm{Rot}_{\boldsymbol{\eta}}(\omega) \in \mathbf{g}S_{\mathrm{orth}}$ that satisfies the condition (4.16). For $\boldsymbol{\eta} = \frac{1}{\sqrt{3}}(1,1,1)^T$ we obtain $2 \operatorname{arccot} \boldsymbol{\eta} \cdot \mathbf{e}_i = \frac{2}{3}\pi$, $i = 1,\dots,3$. □

Lemma 4.19. *Let* $\psi(t) = t^2$. *Then the concentration* $\sigma_\psi(f_{unif}, S_{orth})$ *of the uniform distribution* $f_{unif} = 1$ *on* $\mathrm{O}(3)/S_{orth}$ *is given by the integral*

$$\sigma_\psi(f_{unif}, S_{orth}) = \frac{24}{\pi^2} \int_0^\pi \sin^2\frac{\omega}{2} \int_0^{\frac{\pi}{4}} \int_0^{\operatorname{arccot}\cos\rho} \sin\theta \min\bigl\{\omega, 2\arccos(\sin\tfrac{\omega}{2}\cos\theta)\bigr\}^2 \,\mathrm{d}\omega\,\mathrm{d}\theta\,\mathrm{d}\rho. \tag{4.17}$$

Proof. Using spherical trigonometry one verifies that

$$\Delta = \Big\{ \boldsymbol{\eta} = (\theta, \rho) \in \mathbb{S}^2 \;\Big|\; \rho \in [0, \tfrac{\pi}{4}],\, \theta \in [0, \operatorname{arccot} \cos \rho] \Big\}$$

defines the spherical triangle that contains all points $\boldsymbol{\eta} = (\theta, \rho) \in \mathbb{S}^2$ with $\rho \in [0, \frac{\pi}{4}]$ such that $\measuredangle(\boldsymbol{\eta}, \mathbf{e}_3) = \min_{i=1,\dots,3} \measuredangle(\boldsymbol{\eta}, \pm\mathbf{e}_i)$. Moreover, the triangle Δ allows for a decomposition of the sphere into 48 symmetric copies.

Let $\omega \in [0, \pi]$ and $\boldsymbol{\eta} \in \mathbb{S}^2$. Then

$$\measuredangle\big(\mathrm{Rot}_{\boldsymbol{\eta}}(\omega), \mathrm{Rot}_{\mathbf{e}_i}(\tfrac{\pi}{2})\big) = 2 \arccos\big(\sin \tfrac{\omega}{2} \cos \measuredangle(\boldsymbol{\eta}, \mathbf{e}_i)\big)$$

and consequently

$$\measuredangle\big(\mathrm{Rot}_{\boldsymbol{\eta}}(\omega), S_{\mathrm{orth}}\big) = \min_{i=1,\dots,3} \Big\{ \omega, 2 \arccos\big(\sin \tfrac{\omega}{2} \cos \measuredangle(\boldsymbol{\eta}, \pm\mathbf{e}_i)\big) \Big\}.$$

Hence, $\measuredangle\big(\mathrm{Rot}_{\boldsymbol{\eta}}(\omega), S_{\mathrm{orth}}\big)$ depends only on the angular distances $\measuredangle(\boldsymbol{\eta}, \pm\mathbf{e}_i)$, $i = 1, \dots, 3$ and the rotational angle ω. By symmetry arguments we obtain

$$\begin{aligned}
&\frac{1}{8\pi^2} \int_{\mathrm{SO(3)}} \measuredangle(\mathbf{g}, S_{\mathrm{orth}})^2 \,\mathrm{d}\mathbf{g} \\
&= \frac{1}{2\pi^2} \int_0^{\pi} \sin^2 \tfrac{\omega}{2} \int_{\mathbb{S}^2} \measuredangle(\mathrm{Rot}_{\boldsymbol{\eta}}(\omega), S_{\mathrm{orth}})^2 \,\mathrm{d}\boldsymbol{\eta} \,\mathrm{d}\omega \\
&= \frac{24}{\pi^2} \int_0^{\pi} \sin^2 \tfrac{\omega}{2} \int_{\Delta} \min\Big\{ \omega, 2 \arccos\big(\sin \tfrac{\omega}{2} \cos \measuredangle(\boldsymbol{\eta}, \mathbf{e}_3)\big) \Big\}^2 \,\mathrm{d}\boldsymbol{\eta} \,\mathrm{d}\omega \\
&= \frac{24}{\pi^2} \int_0^{\pi} \sin^2 \tfrac{\omega}{2} \int_0^{\frac{\pi}{4}} \int_0^{\operatorname{arccot} \cos \rho} \sin\theta \min\Big\{ \omega, 2 \arccos\big(\sin \tfrac{\omega}{2} \cos\theta\big) \Big\}^2 \,\mathrm{d}\theta \,\mathrm{d}\rho \,\mathrm{d}\omega.
\end{aligned}$$

□

Remark 4.20. The integral (4.17) can be evaluated numerically. Using the computer algebra system `Mathematica` we obtained for the concentration $\sigma_\psi(f_{\mathrm{unif}}, S_{\mathrm{orth}})$ of the uniformly distributed ODF $f_{\mathrm{unif}} = 1$ on $\mathrm{O(3)}/S_{\mathrm{orth}}$ with respect to the function $\psi(t) = t^2$ the estimate

$$1.85 < \sigma_\psi(f_{\mathrm{unif}}, S_{\mathrm{orth}}) < 1.86.$$

The following proposition states that if the pole figures $P_{\mathbf{e}_i}$, $i = 1, \dots, 3$ of an orthorhombic texture are almost uniformly distributed the corresponding ODF is so, too.

Proposition 4.21. *Denote $f_{unif} = 1$ the ODF uniformly distributed on $\mathrm{O(3)}/S_{orth}$ and $P_{unif} = 1$ the corresponding PDF uniformly distributed on $\mathbb{S}^2/S_{orth} \times \mathbb{S}^2$. Furthermore, let $\psi(t) = t^2$, $\varepsilon > 0$ and let $P_{\mathbf{e}_i} \in L^2(\mathbb{S}^2)$, $i = 1, \dots, 3$ be three pole figures such that*

$$\Big| \sigma_\psi(P_{\mathbf{e}_i}, \pm\boldsymbol{\eta}) - \sigma_\psi(P_{unif}, \pm\boldsymbol{\eta}) \Big| \leq \varepsilon$$

for any $\boldsymbol{\eta} \in \mathbb{S}^2$. *Then any ODF* $f \in L^2(\mathrm{O}(3)/S_{orth})$ *with* $\mathcal{X}f(\mathbf{e}_i, \circ) = P_{\mathbf{e}_i}$, $i = 1, \dots, 3$ *satisfies the inequality*

$$\sigma_\psi(f, \mathbf{q}S_{orth}) \geq \frac{3}{2}(\pi - 2 - \varepsilon) \geq 0.9\, \sigma_\psi(f_{unif}, S_{orth}) - \frac{3}{2}\varepsilon \tag{4.18}$$

for any $\mathbf{q} \in \mathrm{O}(3)$.

Proof. First of all we show that $t \mapsto \arccos^2 t$ defines a convex mapping on $[-1, 1]$. Its derivatives are given by

$$\frac{\mathrm{d}}{\mathrm{d}t} \arccos^2 t = -\frac{2 \arccos t}{\sqrt{1-t^2}} \quad \text{and} \quad \frac{\mathrm{d}^2}{\mathrm{d}t^2} \arccos^2 t = \frac{2\sqrt{1-t^2} - 2t \arccos t}{(1-t^2)^{\frac{3}{2}}}.$$

Observing

$$\sqrt{1-t^2} - t \arccos t = 0 \quad \text{for } t = 1$$

and

$$\frac{\mathrm{d}}{\mathrm{d}t}(\sqrt{1-t^2} - t \arccos t) = -\arccos t \leq 0 \quad \text{for } t \in [-1, 1]$$

we conclude

$$\frac{\mathrm{d}^2}{\mathrm{d}t^2} \arccos^2 t \geq 0, \quad t \in [-1, 1]$$

and hence the function $t \mapsto \arccos^2 t$ is convex.

Let $\omega \in [0, \pi]$ and $\boldsymbol{\eta} \in \mathbb{S}^2$. Then by equation (2.1) we have

$$\measuredangle(\mathrm{Rot}_{\boldsymbol{\eta}}(\omega)\mathbf{e}_i, \mathbf{e}_i)^2 = \arccos^2\Big((\boldsymbol{\eta} \cdot \mathbf{e}_i)^2 + \big(1 - (\boldsymbol{\eta} \cdot \mathbf{e}_i)^2\big) \cos\omega\Big).$$

In view of the first part of this proof $\measuredangle(\mathrm{Rot}_{\boldsymbol{\eta}}(\omega)\mathbf{e}_i, \mathbf{e}_i)^2$ is a convex function with respect to $(\boldsymbol{\eta} \cdot \mathbf{e}_i)^2$ and hence $\frac{1}{3}\sum_{i=1}^3 \measuredangle(\mathrm{Rot}_{\boldsymbol{\eta}}(\omega)\mathbf{e}_i, \mathbf{e}_i)^2$ is a convex function with respect to $(\boldsymbol{\eta} \cdot \mathbf{e}_i)^2$, $i = 1, \dots, 3$.

For any $\boldsymbol{\eta} \in \mathbb{S}^2$ we have $(\boldsymbol{\eta} \cdot \mathbf{e}_1)^2 + (\boldsymbol{\eta} \cdot \mathbf{e}_2)^2 + (\boldsymbol{\eta} \cdot \mathbf{e}_3)^2 = 1$ and hence the domain

$$\left\{ \big((\boldsymbol{\eta} \cdot \mathbf{e}_1)^2, (\boldsymbol{\eta} \cdot \mathbf{e}_2)^2, (\boldsymbol{\eta} \cdot \mathbf{e}_3)^2\big)^T \in \mathbb{R}^3_+ \;\middle|\; \boldsymbol{\eta} \in \mathbb{S}^2 \right\}$$

is convex. Since a convex function on a convex domain has its maximum value at one of the edges of the domain we obtain

$$\frac{1}{3}\sum_{i=1}^3 \measuredangle(\mathrm{Rot}_{\boldsymbol{\eta}}(\omega)\mathbf{e}_i, \mathbf{e}_i)^2 \leq \frac{1}{3}\sum_{i=1}^3 \measuredangle(\mathrm{Rot}_{\mathbf{e}_1}(\omega)\mathbf{e}_i, \mathbf{e}_i)^2 = \frac{2}{3}\omega^2.$$

Let $\mathbf{g}_0, \mathbf{g} \in \mathrm{O}(3)$ and $\mathbf{q} \in \mathbf{g}S_{\mathrm{orth}}$ such that $\measuredangle(\mathbf{g}, S_{\mathrm{orth}}) = \measuredangle\mathbf{q}$. Then

$$\frac{1}{3}\sum_{i=1}^3 \measuredangle(\mathbf{g}\mathbf{e}_i, \mathbf{g}_0 S_{\mathrm{orth}}\mathbf{e}_i)^2 = \frac{1}{3}\sum_{i=1}^3 \measuredangle(\mathbf{q}\mathbf{e}_i, \pm\mathbf{g}_0\mathbf{e}_i)^2 \leq \frac{2}{3}\measuredangle(\mathbf{q}, \mathbf{g}_0)^2 = \frac{2}{3}\measuredangle(\mathbf{g}, \mathbf{g}_0 S_{\mathrm{orth}})^2.$$

Setting $\mathbf{h} = (\mathbf{e}_1, \mathbf{e}_2, \mathbf{e}_3)$, $\psi(t) = t^2$ and $\psi_2(t) = \frac{2}{3}t^2$ the condition

$$\Psi_{\mathbf{g}_0 S_{\mathrm{orth}}, \mathbf{h}}(\mathbf{g}) \leq \psi_2(\measuredangle(\mathbf{g}, \mathbf{g}_0 S_{\mathrm{orth}}))$$

of Theorem 4.14 is satisfied for any $\mathbf{g} \in \mathrm{O}(3)$ and we obtain

$$\frac{1}{3}\sum_{i=1}^{3} \sigma_\psi(P_{\mathbf{e}_i}, \mathbf{g}_0 S_{\mathrm{orth}} \mathbf{e}_i) \leq \sigma_{\psi_2}(f, \mathbf{g}_0 S_{\mathrm{orth}}) = \frac{2}{3}\sigma_\psi(f, \mathbf{g}_0 S_{\mathrm{orth}}).$$

On the other hand we have assumed

$$|\sigma_\psi(P_{\mathbf{e}_i}, S_{\mathrm{orth}}\boldsymbol{\eta}) - \sigma_\psi(P_{\mathrm{unif}}, S_{\mathrm{orth}}\boldsymbol{\eta})| \leq \varepsilon$$

for any $\boldsymbol{\eta} \in \mathbb{S}^2$. Since $\sigma_\psi(P_{\mathrm{unif}}, \pm\boldsymbol{\eta}) = \pi - 2$ independently of the choice of $\boldsymbol{\eta} \in \mathbb{S}^2$ we obtain for any $\mathbf{g}_0 \in \mathrm{O}(3)$

$$\sigma_\psi(f, \mathbf{g}_0 S_{\mathrm{orth}}) \geq \frac{3}{2}(\pi - 2 - \varepsilon) \geq 0.9\, \sigma_\psi(f_{\mathrm{unif}}, \mathbf{g}_0 S_{\mathrm{orth}}) - \frac{2}{3}\varepsilon.$$

The last estimate is due to Remark 4.20. □

The second example deals with three complete pole figures $P_{\mathbf{e}_i}$, $i = 1, \ldots, 3$ each of which is concentrated in some ball $B(\pm\mathbf{g}_0\mathbf{e}_i, \varepsilon)$ where $\mathbf{g}_0 S_{\mathrm{orth}} \in \mathrm{O}(3)/S_{\mathrm{orth}}$ is an arbitrary crystal orientation and $\varepsilon \in (0, \pi)$ is the radius. We show that under these assumptions any ODF $f \in L^2(\mathrm{O}(3)/S_{\mathrm{orth}})$ with $\mathcal{X}f(\mathbf{e}_i, \circ) = P_{\mathbf{e}_i}$ is concentrated in a slightly larger ball with center $\mathbf{g}_0 S_{\mathrm{orth}}$.

Proposition 4.22. *Let $\varepsilon \in (0, \frac{\pi}{3})]$, $\alpha \in [0, \frac{2}{3}]$, $\mathbf{g}_0 \in \mathrm{O}(3)$ and let $P_{\mathbf{e}_i} \in L^2(\mathbb{S}^2)$, $i = 1, \ldots, 3$ be three pole figures such that*

$$\frac{1}{4\pi}\int_{B(\mathbf{g}_0\mathbf{e}_i, \varepsilon)} P_{\mathbf{e}_i}(\mathbf{r})\, \mathrm{d}\mathbf{r} \geq 1 - \alpha.$$

Then any ODF $f \in L^2(\mathrm{O}(3)/S_{orth})$ with $\mathcal{X}f(\mathbf{e}_i, \circ) = P_{\mathbf{e}_i}$, $i = 1, \ldots, 3$ satisfies the inequality

$$\frac{1}{16\pi^2}\int_{B(\mathbf{g}_0 S_{orth}, \varepsilon')} f(\mathbf{g})\, \mathrm{d}\mathbf{g} \geq 1 - \tfrac{3}{2}\alpha \tag{4.19}$$

where ε' is defined by $\cos\varepsilon' = 2\cos\varepsilon - 1$.

Proof. Let $\omega \in (0, \pi)$ and let $\boldsymbol{\eta} \in \mathbb{S}^2$ such that $\measuredangle(\boldsymbol{\eta}, \mathbf{e}_i) \leq \frac{\pi}{2}$, $i = 1, \ldots, 3$. Then we have by equation (2.1) for the angular distance between $\mathrm{Rot}_{\boldsymbol{\eta}}(\omega)\mathbf{e}_i$ and $\mathbf{e}_i$ the equality

$$\cos\measuredangle(\mathrm{Rot}_{\boldsymbol{\eta}}(\omega)\mathbf{e}_i, \mathbf{e}_i) = \cos^2\measuredangle(\boldsymbol{\eta}, \mathbf{e}_i) + \sin^2\measuredangle(\boldsymbol{\eta}, \mathbf{e}_i)\cos\omega.$$

In particular, the angular distance $\measuredangle(\mathrm{Rot}_{\boldsymbol{\eta}}(\omega)\mathbf{e}_i, \mathbf{e}_i)$ is a monotonously increasing function of $\measuredangle(\boldsymbol{\eta}, \mathbf{e}_i) \in [0, \frac{\pi}{2}]$.

For any vector $\boldsymbol{\eta} \in \mathbb{S}^2$ with $\measuredangle(\boldsymbol{\eta}, \mathbf{e}_i) \leq \frac{\pi}{2}$, $i = 1, \dots, 3$ the angular distance to at least two of the vectors $\mathbf{e}_i$, $i = 1, \dots, 3$ satisfies $\measuredangle(\boldsymbol{\eta}, \mathbf{e}_i) \geq \frac{\pi}{4}$. Let $\mathbf{e}_1$ and $\mathbf{e}_2$ be these vectors. Using the monotony of $\measuredangle(\mathrm{Rot}_{\boldsymbol{\eta}}(\omega)\mathbf{e}_i, \mathbf{e}_i)$ as a function of $\measuredangle(\boldsymbol{\eta}, \mathbf{e}_i)$ we conclude that

$$\measuredangle(\mathrm{Rot}_{\boldsymbol{\eta}}(\omega)\mathbf{e}_i, \mathbf{e}_i) \geq \arccos(\tfrac{1}{2} + \tfrac{1}{2}\cos\omega), \quad i = 1, 2.$$

Let $\varepsilon \in (0, \frac{\pi}{3}]$ and set $\varepsilon' = \arccos(2\cos\varepsilon - 1)$. Then we have for for all $\omega \in [\varepsilon', \frac{2}{3}\pi]$ the inequality

$$\pi - \varepsilon \geq \tfrac{2}{3}\pi \geq \measuredangle(\mathrm{Rot}_{\boldsymbol{\eta}}(\omega)\mathbf{e}_i, \mathbf{e}_i) \geq \varepsilon, \quad i = 1, 2$$

and consequently

$$\measuredangle(\mathrm{Rot}_{\boldsymbol{\eta}}(\omega)\mathbf{e}_i, S_{\mathrm{orth}}\mathbf{e}_i) \geq \varepsilon, \quad i = 1, 2. \tag{4.20}$$

The above argumentation generalizes to arbitrary rotational axes $\boldsymbol{\eta} \in \mathbb{S}^2$ by replacing $\mathbf{e}_i$ by $-\mathbf{e}_i$ for some $i = 1, \dots, 3$ in the initial constrains on $\boldsymbol{\eta}$. Eventually, we obtain that for any rotation $\mathbf{q} \in \mathrm{SO}(3)$ with rotational angle $\measuredangle(\mathbf{q}) \in [\varepsilon', \frac{2}{3}\pi]$ the inequality

$$\measuredangle(\mathbf{q}\mathbf{e}_i, S_{\mathrm{orth}}\mathbf{e}_i) \geq \varepsilon$$

is satisfied for at least two of the vectors $\mathbf{e}_i$, $i = 1, \dots, 3$.

Let $\mathbf{g}S_{\mathrm{orth}} \in \mathrm{O}(3)/S_{\mathrm{orth}}$ such that $\measuredangle(\mathbf{g}, S_{\mathrm{orth}}) \geq \varepsilon'$. By Lemma 4.18 we can assume without lost of generality that $\measuredangle\mathbf{g} \in [\varepsilon', \frac{2}{3}\pi]$. Together with equation (4.20) this implies that

$$\measuredangle(\mathbf{g}\mathbf{e}_i, S_{\mathrm{orth}}\mathbf{e}_i) \geq \varepsilon$$

for at least two of the vectors $\mathbf{e}_i$, $i = 1, \dots, 3$.

Setting $\psi(t) = \mathbf{1}_{[\varepsilon,\pi]}$, $\psi_1(t) = \frac{2}{3}\mathbf{1}_{[\varepsilon',\frac{2}{3}\pi]}$ and $\mathbf{h} = (\mathbf{e}_1, \mathbf{e}_2, \mathbf{e}_3)$ we obtain for any $\mathbf{g} \in \mathrm{O}(3)$

$$\psi_1(\measuredangle(\mathbf{g}, S_{\mathrm{orth}})) \leq \frac{1}{3}\sum_{i=1}^{3} \psi(\measuredangle(\mathbf{g}\mathbf{e}_i, S_{\mathrm{orth}}\mathbf{e}_i)) = \Psi_{S_{\mathrm{orth}},\mathbf{h}}(\mathbf{g})$$

and hence the condition of Theorem 4.14 is satisfied. We conclude that any ODF $f \in L^2(\mathrm{O}(3)/S_{\mathrm{orth}})$ with $\mathcal{X}f(\mathbf{e}_i, \circ) = P_{\mathbf{e}_i}$, $i = 1, \dots, 3$ satisfies

$$\sigma_{\psi_1}(f, S_{\mathrm{orth}}) \leq \frac{1}{3}\sum_{i=1}^{3} \sigma_{\psi}(P_{\mathbf{e}_i}, S_{\mathrm{orth}}\mathbf{e}_i) \leq \alpha.$$

For $\mathbf{g}_0 = \mathrm{Id}$ the assertion of Proposition 4.22 follows from

$$\frac{1}{16\pi^2}\int_{B(S_{\mathrm{orth}},\omega)} f(\mathbf{g})\,\mathrm{d}\mathbf{g} = 1 - \frac{3}{2}\sigma_{\psi_1}(f, S_{\mathrm{orth}}) \geq 1 - \frac{3}{2}\alpha.$$

The general case is due to symmetry reasons. □

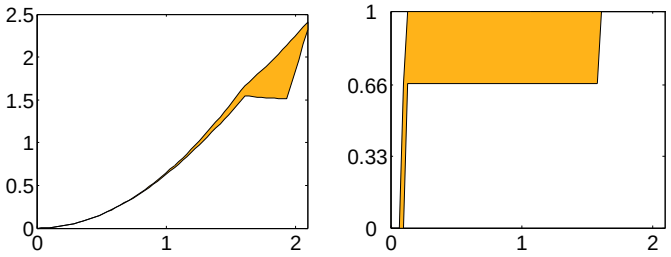

Figure 4.7: The function $\Psi_{S_{\mathrm{orth}},\mathbf{h}}$ for $\mathbf{h} = (\mathbf{e}_1, \mathbf{e}_2, \mathbf{e}_3)$ and $\psi(t) = t^2$ (left) and for $\psi(t) = \mathbf{1}_{[5\frac{\pi}{180}, \frac{2}{3}\pi]}$ (right).

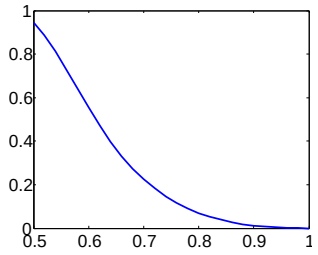

Figure 4.8: Mass located withih the halfwidth of the ODF f_κ in dependency of κ.

Plots of the functions $\Psi_{S_{\mathrm{orth}},\mathbf{h}}$ for $\mathbf{h} = (\mathbf{e}_1, \mathbf{e}_2, \mathbf{e}_3)$ and $\psi(t) = t^2$ and for $\psi(t) = \mathbf{1}_{[\varepsilon, \frac{2}{3}\pi]}$ are given in Figure 4.7.

It remains the question how Proposition 4.21 and Proposition 4.22 agree with the family of ODFs f_κ constructed in Example 4.9 and 4.10. The point is that in both examples the mass located under the peak of f_κ tends to zero as the peak becomes more sharp. Let f_κ be the family of sample ODFs as defined in Example 4.10. Using formula (3.15) for the halfwidth of the Abel–Poisson kernel depending on the parameter κ we calculated the mass of f_κ located within a ball with center $\mathbf{g}_0 = \mathrm{Id}$ and a radius specified by the halfwidth of the Abel–Poisson kernel. The numerical result is plotted in Figure 4.8.

4.5 ODF Estimation

Throughout all of this section we denote by $S_{\mathrm{Laue}} \subseteq \mathrm{O}(3)$, $\mathbf{I}^b \in \mathbb{R}^{\bar{N}}_+$, $H_i \subseteq \mathbb{S}^2/S_{\mathrm{Laue}}$, $\rho_i \colon H_i \to \mathbb{R}$ and $\mathbf{r}_{ij} \in \mathbb{S}^2$, $i = 1, \ldots, N$, $j = 1, \ldots, N_i$ the known parameters of a diffraction experiment as described in Section 4.2 and by $\mathbf{I} \in \mathbb{R}^{\bar{N}}$ the measured diffraction counts. According to Section 4.2 we interpret the diffraction counts $\mathbf{I} \in \mathbb{R}^{\bar{N}}$ as an one–element random sample of the family of Poisson distributions

$$\mathcal{I}_{ij} = \mathrm{Poiss}\Big(\mathbf{I}^b_{ij} + [\boldsymbol{\alpha}_{\mathrm{true}}]_i \, \mathcal{X} f_{\mathrm{true}}(H_i, \mathbf{r}_{ij})\Big), \quad i = 1, \ldots, N, \; j = 1, \ldots, N_i, \tag{4.21}$$

where the true ODF $f_{\mathrm{true}} \in C(\mathrm{O}(3)/S_{\mathrm{Laue}})$ and the true normalization coefficients $\boldsymbol{\alpha}_{\mathrm{true}} \in \mathbb{R}^N_+$ are the unknown model parameters.

In this section we are going to introduce and compare estimators of the true ODF $f_{\mathrm{true}} \in C(\mathrm{O}(3)/S_{\mathrm{Laue}})$ from given diffraction counts $\mathbf{I} \in \mathbb{R}^{\bar{N}}$. However, before we do so we shortly discuss the relevance of ODF estimation in texture analysis in general.

General Discussion. As a first point we remember that even for complete and exact data there is in general no uniquely defined ODF associated with the data. In particular,

the range of ODFs that correspond to a given PDF is in general unbounded with respect to the maximum norm and with respect to the L^2–norm (cf. Proposition 4.11). The consequence of this observation is that it makes in general no sense to ask for pointwise estimates of the true ODF.

A second point is that in practice one is typically not interested in a pointwise estimate of the true ODF f_{true}, but in integrals of the form

$$\int_{\mathrm{O}(3)} f_{\text{true}}(\mathbf{g})\psi(\mathbf{g})\,\mathrm{d}\mathbf{g},$$

where $\psi\colon \mathrm{O}(3) \to \mathbb{R}$ is a some integrable function, e.g.

- $\psi = T_l^{kk'}$, $l = 1, \ldots, 4$ for the lower order Fourier coefficients of the true ODF,
- $\psi = \mathbf{1}_Q$ for the ratio of mass of the true ODF concentrated in a certain subset $Q \subseteq \mathrm{O}(3)$,
- $\psi = f_{\text{true}}$ for the texture index $\|f_{\text{true}}\|_{L^2(\mathrm{O}(3))}$,
- $\psi = \ln(f_{\text{true}})$ for the entropy of the true ODF f_{true},
- $\psi = \delta_{G(\mathbf{h},\mathbf{r})}$, $\mathbf{h}, \mathbf{r} \in \mathbb{S}^2$ for the corresponding PDF $\mathcal{X} f_{\text{true}}$.

For all these characteristics one can think of direct estimators that do not rely on a pointwise estimate of the true ODF. However, the drawback of those estimators is that they do not incorporate the prior information of the non–negativity of ODFs, which has been proven to have a great impact on the correctness of the estimated ODF (cf. Section 4.4). We conclude that incorporation of the non–negativity constraint leads not only to more accurate estimators for the true ODF but also for the integrals mentioned above.

From this point of view pointwise ODF estimation can be seen as a method to combine the data obtained by a diffraction experiment with the a priori information about the non–negativity of ODFs. In a second step the estimate of the ODF can be used to determine estimates of various integrals of the ODF.

The Bayesian Maximum a Posteriori Estimator. Bayesian estimation is a framework that allows to combine prior information on unknown parameters with random samples in oder to obtain an a posteriori probability distribution of the unknown parameters. For a comprehensive introduction to Bayesian estimation see Kaipio and Somersalo (2004, Section 3.1).

Let us denote in a general setting the probability space of possible observations by (O, ω) and the probability space of model parameters by (M, μ). Furthermore, let both probability measures ω, μ be representable by probability density functions $p_O\colon M \to \mathbb{R}_+$ and $p_M\colon M \to \mathbb{R}_+$, respectively and let us assume that there is a joint probability density function $p_{O,M}\colon O \times M \to \mathbb{R}_+$. Then the conditional probability density function

$p_{O|M}(o \mid m)$ of an observations $o \in O$ given model parameters $m \in M$ is defined by the Bayesian law as

$$p_{O|M}(o \mid m) = \frac{p_{O,M}(o, m)}{p_M(m)}. \tag{4.22}$$

Analogously, the conditional probability density function $p_{M|O}(m \mid o)$ of a model parameter $m \in M$ given the observation $o \in O$ is defined as

$$p_{M|O}(m \mid o) = \frac{p_{M,O}(m, o)}{p_O(o)}. \tag{4.23}$$

Based on these notations the Bayesian maximum a posteriori estimator is defined as

Definition 4.23. Let $o \in O$ be some observation. Then any solution of the maximization problem

$$m_{\mathrm{BE}} = \operatorname*{argmax}_{m \in M} p_{M|O}(m \mid o) \tag{4.24}$$

is called *Bayesian maximum a posteriori estimator* of the model parameters m given the observations o.

The Bayesian maximum a posteriori estimator can be interpreted as the model parameters that are most likely given the observations o compared to any other model parameters. The next theorem describes the Bayesian maximum a posteriori estimator applied to the ODF estimation problem.

Proposition 4.24. *Let $\lambda \in \mathbb{R}_+$, $s > \frac{3}{2}$ and let the prior information on the true ODF be given by the restriction of the Gaussian distribution*

$$\begin{aligned} p_M &\colon \mathcal{H}_s(\mathrm{O}(3)/S_{\mathrm{Laue}}) \to \mathbb{R}_+ \\ p_M(f) &= \exp(-\lambda \left\| f \right\|^2_{\mathcal{H}_s(\mathrm{O}(3)/S_{\mathrm{Laue}})}) \end{aligned} \tag{4.25}$$

to the subset of ODFs in $\mathcal{H}_s(\mathrm{O}(3)/S_{\mathrm{Laue}})$. Then any solution $(f_{BE}, \boldsymbol{\alpha}_{BE})$ of the minimization problem

$$\begin{aligned} (f_{BE}, \boldsymbol{\alpha}_{Be}) = &\operatorname*{argmin}_{f \in \mathcal{H}_s(\mathrm{O}(3)/S_{\mathrm{Laue}}), \boldsymbol{\alpha} \in \mathbb{R}^N_+} J_{BE}(f, \boldsymbol{\alpha}) \\ \text{subject to } f \geq 0 \text{ and } &\int_{\mathrm{O}(3)} f(\mathbf{g} S_{\mathrm{Laue}}) \, \mathrm{d}\mathbf{g} = 16\pi^2 \end{aligned} \tag{4.26}$$

where

$$J_{BE}(f, \boldsymbol{\alpha}) = \sum_{i=1}^{N} \sum_{j=1}^{N_i} \mathbf{I}_{ij} \ln\bigl(\boldsymbol{\alpha}_i \mathcal{X} f(H_i, \mathbf{r}_{ij}) + \mathbf{I}^b_{ij}\bigr) - \boldsymbol{\alpha}_i \mathcal{X} f(H_i, \mathbf{r}_{ij}) + \lambda \left\| f \right\|^2_{\mathcal{H}_s(\mathrm{O}(3)/S_{\mathrm{Laue}})}$$

is a Bayesian maximum a posteriori estimator of the true ODF f_{true} and the true normalization coefficients $\boldsymbol{\alpha}_{true}$ given the diffraction counts $\mathbf{I} \in \mathbb{R}^{\bar{N}}_+$ with respect to the model (4.6).

Proof. Let $f \in \mathcal{H}_s(\mathrm{O}(3)/S_{\mathrm{Laue}})$, $s > \frac{3}{2}$ be an ODF and let $\boldsymbol{\alpha} \in \mathbb{R}^N$ be some normalization coefficients. Then we can assume by Lemma 2.22 that $f \in C(\mathrm{O}(3)/S_{\mathrm{Laue}})$. According to equation (4.21) the distributions $\mathcal{I}_{ij}$, $i = 1, \dots, N$, $j = 1, \dots, N_i$ of the diffractions counts have the probability density functions

$$\varphi_{ij}(\mathbf{I}_{ji}) = \frac{(\boldsymbol{\alpha}_i \mathcal{X} f(H_i, \mathbf{r}_{ij}) + \mathbf{I}_{ij}^b)^{\mathbf{I}_{ij}}}{\mathbf{I}_{ij}!} e^{-\boldsymbol{\alpha}_i \mathcal{X} f(H_i, \mathbf{r}_{ij}) + \mathbf{I}_{ij}^b}.$$

Since the measurements of the diffraction counts are statistically independent we obtain the following probability density function for the vector $\mathcal{I}$ of diffraction counts given the ODF f and the normalization coefficients $\boldsymbol{\alpha}$,

$$p_{O|M}(\mathbf{I} \mid f, \boldsymbol{\alpha}) = \prod_{i=1}^{N} \prod_{j=1}^{N_i} \frac{(\boldsymbol{\alpha}_i \mathcal{X} f(H_i, \mathbf{r}_{ij}) + \mathbf{I}_{ij}^b)^{\mathbf{I}_{ij}}}{\mathbf{I}_{ij}!} \exp - \left(\boldsymbol{\alpha}_i \mathcal{X} f(H_i, \mathbf{r}_{ij}) + \mathbf{I}_{ij}^b\right).$$

Using the Bayesian law we obtain

$$p_{M|O}(f, \boldsymbol{\alpha} \mid \mathbf{I}) = \frac{p_{O|M}(\mathbf{I} \mid f, \boldsymbol{\alpha}) p_M(f, \boldsymbol{\alpha})}{p_O(\mathbf{I})} = C \exp J_{\mathrm{BE}}(f, \boldsymbol{\alpha})$$

where $C = p_O(\mathbf{I})$ is some constant independent of the model parameters $f, \boldsymbol{\alpha}$. Consequently any solution of minimization problem (4.26) is a solution of the maximization problem (4.24) and vice versa. □

Remark 4.25. The prior information specified in Proposition 4.24 may be interpreted as assumed smoothness of the true ODF, i.e. if there are two ODFs both fitting the given observations with the same error we expect the smoother ODF to be the "right" one. The parameter $\lambda \in \mathbb{R}_+$ of the Gaussian distribution p_M specifies the discrepancy between the probability of smooth and non–smooth ODFs.

The minimization problem (4.26) is in general hard to solve. However, if we fix a certain ODF $f \in L^2(\mathrm{O}(3)/S_{\mathrm{Laue}})$ the Bayesian maximum a posteriori estimator of the corresponding normalization coefficients $\boldsymbol{\alpha} \in \mathbb{R}_+^N$ can be easily determined.

Proposition 4.26. *Let $s > \frac{3}{2}$ and let the functional J_{BE} be as defined in equation* (4.26). *Then the minimization problem*

$$\boldsymbol{\alpha}_{BE}(f) = \operatorname*{argmax}_{\boldsymbol{\alpha} \in \mathbb{R}^N} J_{BE}(f, \boldsymbol{\alpha})$$

has for any ODF $f \in \mathcal{H}_s(\mathrm{O}(3)/S_{\mathrm{Laue}})$ a unique solution given by

$$[\boldsymbol{\alpha}_{BE}]_i(f) = \frac{\sum_{j=1}^{N_i} \frac{\mathbf{I}_{ij} \mathcal{X} f(H_i, \mathbf{r}_{ij})}{\mathcal{X} f(H_i, \mathbf{r}_{ij}) + \mathbf{I}_{ij}^b}}{\sum_{j=1}^{N_i} \mathcal{X} f(H_i, \mathbf{r}_{ij})}. \tag{4.27}$$

In particular, we have $\boldsymbol{\alpha}_{BE}(f) \geq 0$.

Proof. Calculating the derivative of the logarithm of $J_{\mathrm{BE}}(f, \circ)$

$$\begin{aligned}\frac{\mathrm{d}}{\mathrm{d}\boldsymbol{\alpha}_i} \ln J_{\mathrm{BE}}(f, \boldsymbol{\alpha}) &= \frac{\mathrm{d}}{\mathrm{d}\boldsymbol{\alpha}_i} \left(\sum_{j=1}^{N_i} \mathbf{I}_{ij} \ln\bigl(\boldsymbol{\alpha}_i \mathcal{X} f(H_i, \mathbf{r}_{ij}) + \mathbf{I}_{ij}^b\bigr) - \mathcal{X} f(H_i, \mathbf{r}_{ij}) \right) \\ &= \frac{1}{\boldsymbol{\alpha}_i} \sum_{j=1}^{N_i} \frac{\mathbf{I}_{ij} \mathcal{X} f(H_i, \mathbf{r}_{ij})}{\mathcal{X} f(H_i, \mathbf{r}_{ij}) + \mathbf{I}_{ij}^b} - \sum_{j=1}^{N_i} \mathcal{X} f(H_i, \mathbf{r}_{ij})\end{aligned}$$

we see that it has exactly one zero point given by equation (4.27). □

The Weighted Least Squares Estimator.

Definition 4.27. Let $\lambda \geq 0$, $s > \frac{3}{2}$ and let $W_i \in \mathbb{R}^{N_i \times N_i}$, $i = 1, \ldots, N$ some positive definite weighting matrices. Then we call any solution of the minimization problem

$$\begin{aligned}(f_{\mathrm{LS}}, \boldsymbol{\alpha}_{\mathrm{LS}}) = &\operatorname*{argmin}_{f \in \mathcal{H}_s(\mathrm{O}(3)/S_{\mathrm{Laue}}), \boldsymbol{\alpha} \in \mathbb{R}_+^N} J_{\mathrm{LS}}(f, \boldsymbol{\alpha}) \\ \text{subject to } f \geq 0 \text{ and } &\int_{\mathrm{O}(3)} f(\mathbf{g} S_{\mathrm{Laue}}) \, \mathrm{d}\mathbf{g} = 16\pi^2,\end{aligned} \tag{4.28}$$

where

$$J_{\mathrm{LS}}(f, \boldsymbol{\alpha}) = \frac{1}{\bar{N}} \sum_{i=1}^{N} \left\| \boldsymbol{\alpha}_i \mathcal{X} f(H_i, \mathbf{r}_i) + \mathbf{I}_i^b - \mathbf{I}_i \right\|_W^2 + \lambda \left\| f \right\|_{\mathcal{H}_s(\mathrm{O}(3)/S_{\mathrm{Laue}})}^2,$$

regularized, weighted least squares estimator of the true ODF f_{true} given the diffraction counts $\mathbf{I} \in \mathbb{R}^{\bar{N}}$.

Remark 4.28. Denote $C_i \in \mathbb{R}^{N_i \times N_i}$ the covariance matrices of the random vectors $\mathcal{I}_i$, $i = 1, \ldots, N$ of diffraction counts and let $W_i = \mathrm{diag}(\mathbf{I}_i)^{-1}$ be the inverse of its one point estimator. Then the least squares estimator (4.28) can be interpreted as the Bayesian maximum a posteriori estimator where the Poisson distribution was approximated by a Gaussian distribution with same mean and a variance given by the estimate W (cf. Feller, 1971, pp. 190 and 245). In particular, there is a correspondence between the regularization term in equation (4.28) and the prior information used in the Bayesian maximum a posteriori estimator (cf. Vogel, 2002, Sec. 4.2).

As in the Bayesian case the minimization problem (4.28) has an unique solution for any fixed ODF.

Proposition 4.29. *Let $s > \frac{3}{2}$, $W_i = diag(\mathbf{I}_i)^{-1}$ and let $f \in \mathcal{H}_s(\mathrm{O}(3)/S_{\mathrm{Laue}})$ be some arbitrary ODF. Then the minimization problem*

$$\boldsymbol{\alpha}_{LS}(f) = \operatorname*{argmin}_{\boldsymbol{\alpha} \in \mathbb{R}^N} J_{LS}(f, \boldsymbol{\alpha})$$

has an unique solution given by

$$[\boldsymbol{\alpha}_{LS}]_i(f) = \frac{\sum_{j=1}^{N_i} \mathcal{X}f(H_i, \mathbf{r}_{ij})\mathbf{I}_{ij}^{-1}(\mathbf{I}_{ij} - \mathbf{I}_{ij}^b)}{\sum_{j=1}^{N_i} \mathcal{X}f(H_i, \mathbf{r}_{ij})^2\mathbf{I}_{ij}^{-1}}, \quad i = 1, \ldots, N. \tag{4.29}$$

Unfortunately, the Bayesian maximum a posteriori estimator $\boldsymbol{\alpha}_{\mathrm{BE}}(f)$ as well as the least squares estimator $\boldsymbol{\alpha}_{\mathrm{LS}}(f)$ of the normalization coefficients are very sensitive with respect to the fixed ODF f.

Example 4.30. Assume that only two diffraction counts $\mathbf{I}_{11} = 500$ and $\mathbf{I}_{12} = 1800$ have been measured with respect to a certain set of crystal directions H_1 and with respect to the specimen directions $\mathbf{r}_{11}, \mathbf{r}_{12} \in \mathbb{S}^2$. Assume furthermore that the corresponding background intensities are $\mathbf{I}_{11}^b = \mathbf{I}_{11}^b = 300$ and that the true normalization coefficient is $\boldsymbol{\alpha}_{\mathrm{true}} = 1000$.

Let f be an arbitrary ODF such that $\mathcal{X}f(H_1, \mathbf{r}_{11}) = 1.9$ and $\mathcal{X}f(H_1, \mathbf{r}_{12}) = 0.1$. Then the Bayesian maximum a posteriori estimator of the normalization coefficient is $\boldsymbol{\alpha}_{\mathrm{BE}}(f) = 1.9$, whereas the least squares estimator of the normalization coefficient is $\boldsymbol{\alpha}_{\mathrm{LS}}(f) = 117$. We see that both estimators strongly underestimates the true normalization coefficient.

Altering Example 4.30 such that the diffraction counts are even more unbalanced and such that the presumed ODF f fits them even worse one obtains estimates of the normalization coefficients that are close to zero. Observing furthermore that for $\boldsymbol{\alpha}_i(f)$ close to zero the functionals J_{BE} and J_{LS} do not depend on the fitting of the ODF f to the vector of diffraction counts $\mathbf{I}_i$ of the i–th pole figure we conclude that solving the minimization problems (4.26) and (4.32) leads to unstable algorithms.

Stable Estimation of the Normalization Coefficients. In order to develop a numerically efficient and robust method for ODF estimation we propose the following estimator of the normalization coefficients $\boldsymbol{\alpha}$ given an estimated ODF f

$$[\boldsymbol{\alpha}_{\mathrm{QR}}]_i(f) = \frac{\sum_{j=1}^{N_i} \omega_{ij}(\mathbf{I}_{ij} - \mathbf{I}_{ij}^b)}{\sum_{j=1}^{N_i} \omega_{ij}\mathcal{X}f(H_i, \mathbf{r}_{ij})}, \quad i = 1, \ldots, N, \tag{4.30}$$

where $\omega_{ij} \in \mathbb{R}_+$, $i = 1, \ldots, N$, $j = 1, \ldots, N_i$, are some positive quadrature weights to be chosen according to the specimen directions $\mathbf{r}_{ij} \in \mathbb{S}^2$. We refer to $\boldsymbol{\alpha}_{\mathrm{QR}}$ as the *quadrature rule estimator* of the unknown normalization coefficients $\boldsymbol{\alpha}$. We mention that the quadrature rule estimator of the normalization coefficients coincides with the Bayesian maximum a posteriori estimator of the normalization coefficients if the background intensities $\mathbf{I}^b$ are zero and the quadrature weights ω_{ij}, $i = 1, \ldots, N$, $j = 1, \ldots, N_i$ are set to one.

In the case of specimen directions $\mathbf{r}_{ij}$, , $i = 1, \ldots, N$, $j = 1, \ldots, N_i$, that provide a complete coverage of the hemisphere $\mathbb{S}^2_+$ estimation of the normalization coefficients is possible without relying on an estimated ODF.

Proposition 4.31. *Let $i \in 1, \dots, N$ and let $\mathbf{r}_i = (\mathbf{r}_{i1}, \dots, \mathbf{r}_{iN_i})$ be a set of specimen directions in the hemisphere $\mathbb{S}^2_+$ such that there exist quadrature weights $\omega_{ij} \in \mathbb{R}_+$ that allow for an exact quadrature formula for all even functions up to a certain bandwidth $L \in \mathbb{N}$. Let furthermore $S_{\mathrm{Laue}} \subseteq \mathrm{O}(3)$ be an arbitrary Laue group. Then the quadrature rule estimator $[\boldsymbol{\alpha}_{QR}]_i(f)$ does not depend on the specific choice of an ODF $f \in C(\mathrm{O}(3)/S_{\mathrm{Laue}})$ with bandwidth L.*

Proof. In Lemma 3.25 we have shown that $\mathcal{X}f(\mathbf{h}, \circ) \in C(\mathbb{S}^2)$ defines a even function for any ODF $f \in C(\mathrm{O}(3)/S_{\mathrm{Laue}})$ and any crystal direction $\mathbf{r} \in \mathbb{S}^2$. Consequently, the denominator of the quadrature rule estimator $[\boldsymbol{\alpha}_{\mathrm{QR}}]_i(f)$ satisfies

$$\sum_{j=1}^{N_i} \omega_{ij} \mathcal{X}f(H_i, \mathbf{r}_{ij}) = \sum_{\mathbf{h} \in H_i} \rho_i(\mathbf{h}) \int_{\mathbb{S}^2} \mathcal{X}f(\mathbf{h}, \mathbf{r}) \, \mathrm{d}\mathbf{r} = 4\pi.$$

□

However, complete grids of specimen direction are only rarely used in practical diffraction experiment. For this reason and for the sake of simplicity we restrict ourself from now on to the case $\omega_{ij} = 1$, $i = 1, \dots, N$, $j = 1, \dots, N_i$. For this setting we show that the quadrature rule estimator $\boldsymbol{\alpha}_{\mathrm{QR}}(f)$ converges in the mean value to the true normalization coefficients as f converges to the true ODF.

Proposition 4.32. *Let $\boldsymbol{\alpha}_{true} \in \mathbb{R}^N_+$ be some normalization coefficients, let $f \in C(\mathrm{O}(3)/S_{\mathrm{Laue}})$ be some arbitrary ODF satisfying $\|\mathcal{X}f(H_i, \mathbf{r}_i)\|_1 > 0$, $i = 1, \dots, N$ and denote*

$$\mathcal{I}_{ij} = Poiss\big([\boldsymbol{\alpha}_{true}]_i \mathcal{X}f_{true}(H_i, \mathbf{r}_{ij}) + \mathbf{I}^b_{ij}\big), \quad i = 1, \dots, N, \ j = 1, \dots, N_i,$$

the random variables describing the distribution of the diffraction counts.

Then there is for any $\varepsilon > 0$ a $\delta > 0$ such that for any $f \in \mathcal{H}_s(\mathrm{O}(3)/S_{\mathrm{Laue}})$ with

$$\|f_{true} - f\|_\infty \leq \delta$$

we have

$$\|\mathbb{E}\boldsymbol{\alpha}_{QR}(f) - \boldsymbol{\alpha}_{true}\|_\infty \leq \varepsilon.$$

Moreover, the relative mean square errors $\mathbb{E}\Big(1 - \frac{[\boldsymbol{\alpha}_{QR}]_i(f)}{[\boldsymbol{\alpha}_{true}]_i}\Big)^2$, $i = 1, \dots, N$ of the quadrature rule estimator $\boldsymbol{\alpha}_{QR}(f)$ become arbitrary small as the true normalization coefficients converge to infinity and f converges to f_{true}.

Proof. In view of $\|\mathcal{X}f_{\mathrm{true}}(H_i, \mathbf{r}_i)\|_1 > 0$, $i = 1, \dots, N$ and the continuity of the functional $f \mapsto \mathcal{X}f(H_i, \mathbf{r}_{ij})$ there is for every $\varepsilon > 0$ a $\delta > 0$ such that for any ODF $f \in C(\mathrm{O}(3)/S_{\mathrm{Laue}})$ with $\|f_{\mathrm{true}} - f\|_\infty \leq \delta$ we have

$$\left| \sum_{j=1}^{N_i} \mathcal{X}f(H_i, \mathbf{r}_{ij}) - \sum_{j=1}^{N_i} \mathcal{X}f_{\mathrm{true}}(H_i, \mathbf{r}_{ij}) \right| \leq \varepsilon \, \|\mathcal{X}f(H_i, \mathbf{r}_i)\|_1, \quad i = 1, \dots, N.$$

For those ODFs f we obtain

$$\left|\mathbb{E}\boldsymbol{\alpha}_{\mathrm{QR}}(f) - \boldsymbol{\alpha}_{\mathrm{true}}\right| = \left|\boldsymbol{\alpha}_{\mathrm{true}} \frac{\sum_{j=1}^{N_i} \mathcal{X} f_{\mathrm{true}}(H_i, \mathbf{r}_{ij})}{\sum_{j=1}^{N_i} \mathcal{X} f(H_i, \mathbf{r}_{ij})} - \boldsymbol{\alpha}_{\mathrm{true}}\right| \leq \boldsymbol{\alpha}_{\mathrm{true}}\varepsilon$$

$i = 1, \ldots, N$. This proves the first assertion of Proposition 4.32.

Let $\varepsilon > 0$ and let $f \in C(\mathrm{O}(3)/S_{\mathrm{Laue}})$ be an arbitrary ODF such that

$$\left|\sum_{j=1}^{N_i} \mathcal{X} f(H_i, \mathbf{r}_{ij}) - \sum_{j=1}^{N_i} \mathcal{X} f_{\mathrm{true}}(H_i, \mathbf{r}_{ij})\right| \leq \varepsilon. \tag{4.31}$$

In order to prove the convergence of the relative mean square error we calculate

$$\begin{aligned}
&\mathbb{E}\left(1 - \frac{[\boldsymbol{\alpha}_{\mathrm{QR}}]_i(f)}{[\boldsymbol{\alpha}_{\mathrm{true}}]_i}\right)^2 \\
&= [\boldsymbol{\alpha}_{\mathrm{true}}]_i^{-2}\, \mathbb{E}\left(\frac{\sum_{j=1}^{N_i} \mathcal{I}_i - \mathbf{I}_i^b - [\boldsymbol{\alpha}_{\mathrm{true}}]_i \mathcal{X} f(H_i, \mathbf{r}_{ij})}{\sum_{j=1}^{N_i} \mathcal{X} f(H_i, \mathbf{r}_{ij})}\right)^2 \\
&= \frac{\mathbb{E}\Big(\sum_{j=1}^{N_i} \mathrm{Poiss}\big([\boldsymbol{\alpha}_{\mathrm{true}}]_i \mathcal{X} f_{\mathrm{true}}(H_i, \mathbf{r}_{ij}) + \mathbf{I}_{ij}^b\big) - [\boldsymbol{\alpha}_{\mathrm{true}}]_i \mathcal{X} f(H_i, \mathbf{r}_{ij}) + \mathbf{I}_{ij}^b\Big)^2}{[\boldsymbol{\alpha}_{\mathrm{true}}]_i^2 \left(\sum_{j=1}^{N_i} \mathcal{X} f(H_i, \mathbf{r}_{ij})\right)^2} \\
&= \frac{\varepsilon^2 [\boldsymbol{\alpha}_{\mathrm{true}}]_i^2 + [\boldsymbol{\alpha}_{\mathrm{true}}]_i \sum_{j=1}^{N_i} \mathcal{X} f(H_i, \mathbf{r}_{ij}) + \mathbf{I}_{ij}^b}{[\boldsymbol{\alpha}_{\mathrm{true}}]_i^2 \left(\sum_{j=1}^{N_i} \mathcal{X} f(H_i, \mathbf{r}_{ij})\right)^2}.
\end{aligned}$$

Substituting back ε from equation (4.31) we obtain

$$\lim_{[\boldsymbol{\alpha}_{\mathrm{true}}]_i \to \infty} \mathbb{E}\left(1 - \frac{[\boldsymbol{\alpha}_{\mathrm{QR}}]_i(f)}{[\boldsymbol{\alpha}_{\mathrm{true}}]_i}\right)^2 = \frac{\left\|\mathcal{X} f(H_i, \mathbf{r}_i) - \mathcal{X} f_{\mathrm{true}}(H_i, \mathbf{r}_{ij})\right\|_1^2}{\left\|\mathcal{X} f(H_i, \mathbf{r}_i)\right\|_1}, \quad i = 1, \ldots, N.$$

The right hand term converges to zero as f converges to f_{true} in $\mathcal{H}_s(\mathrm{O}(3)/S_{\mathrm{Laue}})$. □

Based on the quadrature rule estimator of the normalization coefficients we end up with the following ODF estimator.

Definition 4.33. Let $s > \frac{3}{2}$, $\lambda > 0$ and let f_{MLS} be a solution of the minimization problem

$$f_{\mathrm{MLS}} = \operatorname*{argmin}_{f \in \mathcal{H}_s(\mathrm{O}(3)/S_{\mathrm{Laue}})} J_{\mathrm{MLS}}(f) \quad \text{subject to } f \geq 0, \int_{\mathrm{O}(3)} f(\mathbf{g} S_{\mathrm{Laue}})\, \mathrm{d}\mathbf{g} = 16\pi^2$$

$$\text{where } J_{\mathrm{MLS}}(f) = \sum_{i=1}^{N} \left\| \frac{\|\mathbf{I}_i - \mathbf{I}_i^b\|_1}{\left\|\mathcal{X} f(H_i, \mathbf{r}_i)\right\|_1} \mathcal{X} f(H_i, \mathbf{r}_i) + \mathbf{I}_i^b - \mathbf{I}_i \right\|_{\mathrm{diag}(\mathbf{I}_i)^{-1}}^2 + \lambda \left\|f\right\|_{\mathcal{H}_s(\mathrm{O}(3)/S_{\mathrm{Laue}})}^2. \tag{4.32}$$

Then we refer to f_{MLS} as the *modified least squares ODF estimator* (MLS ODF estimator).

The modified least squares ODF estimator is similar to other ODF estimators mentioned so far in the literature. In fact, the only difference to the regularized least squares approach (cf. Bernier and Miller, 2006) are the weighting matrix $\mathrm{diag}(\mathbf{I}_i)^{-1}$ which more precisely model our prior knowledge about the distribution of the measurement errors. The impact of these weights on the accuracy of estimation is demonstrated with an example in Section 5.4. A second difference is the direct incorporation of the unknown normalization coefficients $\boldsymbol{\alpha}$ into the minimization functional.

5 Implementation of the MLS ODF Estimator

In this chapter we describe a fast algorithm for the calculation of the MLS ODF estimator as introduced in Section 4.5. The algorithm we present relies on fast Fourier algorithms on the two-dimensional sphere $\mathbb{S}^2$ and on the rotational group $\mathrm{SO}(3)$. These Fourier algorithms are introduced in Section 5.1. In the subsequent sections we discretize the MLS ODF estimator and apply the modified steepest descent algorithm to solve the minimization problem associated to the discretized MLS ODF estimator. We complete this chapter with some numerical tests and a discussion of two practical applications of the presented algorithm.

5.1 Fast Fourier Transforms on $\mathbb{S}^2$ and SO(3)

The Fourier Transform on $\mathbb{S}^2$. Let $P \in L^2(\mathbb{S}^2)$ be a band limited function on $\mathbb{S}^2$ with bandwidth $L \in \mathbb{N}_0$. Then P has a well defined Fourier expansion of the form

$$P = \sum_{l=0}^{L} \sum_{k=-l}^{l} \hat{P}(l,k) \mathcal{Y}_l^k,$$

with Fourier coefficients $\hat{P}(l,k)$, $l = 0, \ldots, L$, $k = -l, \ldots, l$ (cf. Section 2.3). For the Fourier coefficients we use the vector notation $\hat{\mathbf{P}} \in \mathbb{C}^{(2L+1)^2}$ with $\hat{\mathbf{P}}_{lk} = \hat{P}(l,k)$ for $l = 0, \ldots, L$ and $k = -l, \ldots, l$. Conform to Potts and Kunis (2002 – 2006) we call the evaluation of the function P at a list of arbitrary nodes given its vector of Fourier coefficients (direct) discrete spherical Fourier transform. More precisely, we define.

Definition 5.1 (discrete spherical Fourier transform)**.** Let $\mathbf{r} = (\mathbf{r}_1, \ldots, \mathbf{r}_N)$ be a vector of $N \in \mathbb{N}_0$ arbitrary nodes $\mathbf{r}_j \in \mathbb{S}^2$ and let $\hat{\mathbf{P}} \in \mathbb{C}^{(2L+1)^2}$ be a vector of Fourier coefficients with bandwidth $L \in \mathbb{N}_0$. Then the linear operator

$$\mathcal{F}_{\mathbf{r},L} \colon \mathbb{C}^{(2L+1)^2} \to \mathbb{C}^N, \quad [\mathcal{F}_{\mathbf{r},L} \hat{\mathbf{P}}]_j = \sum_{l=0}^{L} \sum_{k=-l}^{l} \hat{\mathbf{P}}_{lk} \mathcal{Y}_l^k(\mathbf{r}_j), \quad j = 1, \ldots, N$$

is called *discrete spherical Fourier transform*. Its adjoint operator

$$\mathcal{F}_{\mathbf{r},L}^H\colon \mathbb{C}^N \to \mathbb{C}^{(2L+1)^2}, \quad [\mathcal{F}_{\mathbf{r},L}^H \mathbf{c}]_{lk} = \sum_{j=1}^{N} \mathbf{c}_j \overline{\mathcal{Y}_l^k(\mathbf{r}_j)}, \quad l = 1,\dots,L,\ k = -l,\dots,l$$

is called *adjoint discrete spherical Fourier transform*.

A naive implementation of the (adjoint) discrete spherical Fourier transform for $N \in \mathbb{N}_0$ arbitrary nodes with bandwidth $L \in \mathbb{N}_0$ requires $\mathcal{O}(NL^2)$ numerical operations. However, there exist much faster algorithms. The algorithm described by Kunis and Potts (2003) and (Keiner and Potts, 2006) calculates both transforms with numerical complexity $\mathcal{O}(L^2 \ln^2 L + N)$. We refer to this algorithm as the *non–equispaced fast spherical Fourier transform* (NFSFT). An implementation of this algorithm is availably as a part of the `NFFT`–library (Potts and Kunis, 2002 – 2006).

The Fourier Transform on SO(3). Let $f \in L^2(\mathrm{SO}(3))$ be a band limited function on SO(3) with bandwidth $L \in \mathbb{N}_0$. Then f has a well defined Fourier expansion of the form (cf. Section 2.5)

$$f = \sum_{l=0}^{L} \sum_{k,k'=-l}^{l} \frac{(l+\frac{1}{2})^{\frac{1}{2}}}{2\pi} \hat{f}(l,k,k') T_l^{kk'}$$

with Fourier coefficients $\hat{f}(l,k,k)$, $l = 0,\dots,L$, $k,k' = -l,\dots,l$. The vector of Fourier coefficients has the dimension

$$\dim \bigoplus_{l=0}^{L} \mathrm{Harm}_l(\mathrm{SO}(3)) = \frac{1}{3}(L+1)(2L+1)(2L+3) \tag{5.1}$$

and we abbreviate it by $\hat{\mathbf{f}}_{lkk'} = \hat{f}(l,k,k')$ for $l = 0,\dots,L$ and $k,k' = -l,\dots,l$. Now we define the discrete Fourier transform on SO(3) analogously to the spherical counterpart.

Definition 5.2 (discrete Fourier transform on SO(3))**.** Let $\mathbf{g} = (\mathbf{g}_1,\dots,\mathbf{g}_M)$ be a vector of $M \in \mathbb{N}$ arbitrary nodes $\mathbf{g}_i \in \mathrm{SO}(3)$ and let $\hat{\mathbf{f}} \in \mathbb{C}^{\frac{1}{3}(L+1)(2L+1)(2L+3)}$ be a vector of Fourier coefficients with bandwidth $L \in \mathbb{N}_0$. Then the linear operator

$$\mathcal{F}_{\mathbf{g},L}\colon \mathbb{C}^{\frac{1}{3}(L+1)(2L+1)(2L+3)} \to \mathbb{C}^M,$$
$$[\mathcal{F}_{\mathbf{g},L}\hat{\mathbf{f}}]_m = \sum_{l=0}^{L} \sum_{k,k'=-l}^{l} \frac{(l+\frac{1}{2})^{\frac{1}{2}}}{2\pi} \hat{\mathbf{f}}_{lkk'} T_l^{kk'}(\mathbf{g}_m), \quad m = 1,\dots,N$$

is called *discrete Fourier transform on* SO(3). Its adjoint operator

$$\mathcal{F}_{\mathbf{g},L}^H\colon \mathbb{C}^m \to \mathbb{C}^{\frac{1}{3}(L+1)(2L+1)(2L+3)}, \quad [\mathcal{F}_{\mathbf{g},L}^H \mathbf{c}]_{lkk'} = \sum_{m=1}^{M} \frac{(l+\frac{1}{2})^{\frac{1}{2}}}{2\pi} \mathbf{c}_m \overline{T_l^{kk'}(\mathbf{g}_m)},$$

$l = 1,\dots,L$, $k,k' = -l,\dots,l$, is called *adjoint discrete Fourier transform on* SO(3).

By equation (5.1) we notice that a naive implementation of the (adjoint) discrete Fourier transform at $M \in \mathbb{N}_0$ arbitrary nodes with bandwidth $L \in \mathbb{N}_0$ has the numerical complexity $\mathcal{O}(ML^3)$. An $\mathcal{O}(L^4)$ algorithm for the case of regular aligned nodes in SO(3) was proposed by Kostelec and Rockmore (2003). This algorithm was generalized by Vollrath (2006) to an $\mathcal{O}(M + L^3 \log^2 L)$ algorithm that works for arbitrary nodes.

Applications to Radially Symmetric Functions. The fast discrete Fourier transform is the cornerstone of almost all fast algorithms dealing with functions given as the superposition of radially symmetric functions (cf. Potts and Steidl, 2003; Keiner, 2005). This is due to the fact that the adjoined Fourier transform as defined in Definition 5.2 maps the coefficient vector of a function given as the superposition of radially symmetric, band limited functions to the vector of Fourier coefficients of this function. More precisely we have

Proposition 5.3. *Let*

$$\psi(\mathbf{g}) = \sum_{l=0}^{L} \hat{\psi}(2l) \mathcal{U}_{2l}\left(\cos \frac{\measuredangle \mathbf{g}}{2}\right)$$

be a radially symmetric function in $L^2(\mathrm{SO}(3))$ with bandwidth $L \in \mathbb{N}_0$ and even order Chebyshev coefficients $\hat{\psi}(2l)$, $l = 0, \dots, L$. Let furthermore, $\mathbf{g} = (\mathbf{g}_1, \dots, \mathbf{g}_M)$, $\mathbf{g}_m \in \mathrm{SO}(3)$ be a list of $M \in \mathbb{N}_0$ arbitrary rotations. Then for any coefficient vector $\mathbf{c} \in \mathbb{R}^M$ the vector $\hat{\mathbf{f}}$ of Fourier coefficients of the function

$$f(\mathbf{q}) = \sum_{m=1}^{M} \mathbf{c}_m \psi(\mathbf{q}\mathbf{g}_m^{-1}).$$

is given by

$$\hat{\mathbf{f}}_{lkk'} = \mathbf{w} \odot \mathcal{F}_{\mathbf{g},L}^H \mathbf{c}, \quad \mathbf{w}_{lkk'} = \frac{4\pi^2}{l + \frac{1}{2}} \hat{\psi}(2l), \tag{5.2}$$

where $\mathbf{w}$ is a $\frac{1}{3}(L+1)(2L+1)(2L+3)$–dimensional vector and $\odot$ denotes the componentwise multiplication. In particular, the Fourier coefficients of f can be calculated with numerical complexity $\mathcal{O}(M + L^3 \log^2 L)$ using the fast adjoint Fourier transform on SO(3).

Proof. By the addition theorem 2.14 on SO(3) we obtain

$$\begin{aligned} f(\mathbf{q}) &= \sum_{m=1}^{M} \mathbf{c}_m \sum_{l=0}^{L} \hat{\psi}(2l) \sum_{k,k'=-l}^{l} \overline{T_l^{kk'}(\mathbf{g}_m)} T_l^{kk'}(\mathbf{q}) \\ &= \sum_{l=0}^{L} \sum_{k,k'=-l}^{l} \frac{(l+\frac{1}{2})^{\frac{1}{2}}}{2\pi} \left(\hat{\psi}(2l) \sum_{m=1}^{M} \frac{2\pi}{(l+\frac{1}{2})^{\frac{1}{2}}} \mathbf{c}_m \overline{T_l^{kk'}(\mathbf{g}_m)} \right) T_l^{kk'}(\mathbf{q}). \end{aligned}$$

By equation (2.27) we have for all $l \ni \mathbb{N}_0$, $k, k' = -l, \ldots,$

$$\hat{f}(l,k,k') = \frac{2\pi}{(l+\frac{1}{2})^{\frac{1}{2}}}\hat{\psi}(2l)\sum_{m=1}^{M}\mathbf{c}_m\overline{T_l^{kk'}}(\mathbf{g}_m) = \frac{4\pi^2}{l+\frac{1}{2}}\hat{\psi}(2l)\left[\mathcal{F}_{\mathbf{g},L}^H\mathbf{c}\right]_{lkk'}.$$

This proves equation (5.2). □

Once there is a fast algorithm for the calculation of the Fourier coefficients of a function given as the superposition of radially symmetric, band limited functions we immediately obtain fast algorithms for its pointwise evaluation, for the pointwise evaluation of its convolution with an arbitrary radially symmetric function or the calculation of its Sobolev norm.

Corollary 5.4. *Let $f \in L^2(\mathrm{SO}(3))$ be as defined in Proposition 5.3. Then we have for any vector $\mathbf{q} = (\mathbf{q}_1, \ldots, \mathbf{q}_N)$ of rotations $\mathbf{q}_i \in \mathrm{SO}(3)$*

$$f(\mathbf{q}) = \mathcal{F}_{\mathbf{q},L}\left(\mathbf{w} \odot \mathcal{F}_{\mathbf{g},L}^H\mathbf{c}\right), \quad \mathbf{w}_{lkk'} = \frac{4\pi^2}{l+\frac{1}{2}}\hat{\psi}(2l). \tag{5.3}$$

Let furthermore, $\phi \in L^2(\mathrm{SO}(3))$ be a radially symmetric function with bandwidth $L \in \mathbb{N}$ and even order Chebyshev coefficients $\hat{\psi}(2l) \in \mathbb{R}$, $l = 0, \ldots, L$. Then we have for any vector $\mathbf{q} = (\mathbf{q}_1, \ldots, \mathbf{q}_N)$ of rotations $\mathbf{q}_i \in \mathrm{SO}(3)$

$$f * \phi(\mathbf{q}) = \mathcal{F}_{\mathbf{q},L}\left(\mathbf{w} \odot \mathcal{F}_{\mathbf{g},L}^H\mathbf{c}\right), \quad \mathbf{w}_{lkk'} = \frac{4\pi^2}{l+\frac{1}{2}}\hat{\psi}(2l)\hat{\phi}(2l). \tag{5.4}$$

In particular the non–equispaced fast Fourier transform for $\mathrm{SO}(3)$ allows for the pointwise evaluation of f or of its convolution with ϕ in N arbitrary rotations with numerical complexity $\mathcal{O}(M + N + L^3\log^2 L)$.

Moreover, the Sobolev norm $\|f\|_{\mathcal{H}_s(\mathrm{SO}(3))}$, $s > 1$, of f satisfies the equality

$$\|f\|_{\mathcal{H}_s(\mathrm{SO}(3))} = \|\mathbf{w} \odot \mathcal{F}_{\mathbf{g},L}^H\mathbf{c}\|_2, \quad \mathbf{w}_{lkk'} = 4\pi^2(l+\tfrac{1}{2})^{s-1} \tag{5.5}$$

and the numerical complexity to calculate $\|f\|_{\mathcal{H}_s(\mathrm{SO}(3))}$ is $\mathcal{O}(M + L^3\log^2 L)$.

Proof. Equation (5.3) follows from Proposition 5.3 and the definition of the discrete Fourier transform for SO(3). Equation (5.4) is a consequence of equation (2.32), and equation (5.5) is a consequence of the definition of the Sobolev norm 2.20. □

5.2 Discretisation of the MLS ODF Estimator

Throughout all of this section let $S_{\mathrm{Laue}} \subseteq \mathrm{O}(3)$, $\mathbf{I}_i, \mathbf{I}_i^b \in \mathbb{R}_+^{N_i}$, $H_i \subseteq \mathbb{S}^2$, $\rho_i \colon H_i \to \mathbb{R}$ and $\mathbf{r}_i = (\mathbf{r}_{i1}, \ldots, \mathbf{r}_{iN_i})$, $\mathbf{r}_{ij} \in \mathbb{S}^2$, $i = 1, \ldots, N$ be the known parameters of a diffraction

experiment as described in Section 4.2. We introduce the following notations. Let $\mathbf{x}, \mathbf{y} \in \mathbb{R}^d$ be some arbitrary vectors and let $a \in \mathbb{R}$ be some number. Then we define the pointwise exponentiation of $\mathbf{x}$ with exponent a by

$$\mathbf{x}^a := (\mathbf{x}_1^a, \dots, \mathbf{x}_d^a)^T$$

and the weighted norm of $\mathbf{y}$ with weighs $\mathbf{x}$ by

$$\|\mathbf{y}\|_{\mathbf{x}} := \|\mathbf{y} \odot \mathbf{x}^{\frac{1}{2}}\|_2 \,,$$

where $\mathbf{y} \odot \mathbf{x}$ denotes the coordiantewise multiplication.

We are concerned with the modified least squares ODF estimator 4.33 as introduced in Section 4.5

$$\begin{aligned} \tilde{f} &= \operatorname*{argmin}_{f \in \mathcal{H}_s(\mathrm{O}(3)/S_{\mathrm{Laue}})} J(f) \quad \text{subject to } f \geq 0 \text{ and } \int_{\mathrm{O}(3)} f(\mathbf{g})\, \mathrm{d}\mathbf{g} = 16\pi^2 \\ \text{where } J(f) &= \sum_{i=1}^{N} \left\| \frac{\|\mathbf{I}_i - \mathbf{I}_i^b\|_1}{\|\mathcal{X}f(H_i, \mathbf{r}_i)\|_1} \mathcal{X}f(H_i, \mathbf{r}_i) + \mathbf{I}_i^b - \mathbf{I}_i \right\|_{\mathbf{I}_i^{-1}}^2 + \lambda \|f\|_{\mathcal{H}_s(\mathrm{O}(3)/S_{\mathrm{Laue}})} \,. \end{aligned} \tag{5.6}$$

Remember that $\lambda, s \geq 0$ are free parameters to be chosen accordingly to the assumed smoothness of the ODF and that $\mathcal{X}f(H_i, \mathbf{r}_i)$ denotes the vector of the theoretical diffraction intensities of the i-th pole figure as defined in equation (4.5).

Our purpose in this section is to formulate a finite dimensional minimization problem the solution of which approximates the solution of minimization problem (5.6), i.e. we want to discretize minimization problem (5.6). We will do so in two steps. First we construct a finite dimensional subspace of $\mathcal{H}_s(\mathrm{O}(3)/S_{\mathrm{Laue}})$ and second we restrict the functional J to this subspace.

Discretisation of the ODF Space. A finite dimensional subspace of $\mathcal{H}_s(\mathrm{O}(3)/S_{\mathrm{Laue}})$, $s > \frac{3}{2}$ that is well suited for a numerical solution of minimization problem (5.6) needs to satisfy the following requirements. First it should be rich enough to approximate a sufficiently large class of ODFs. Second the subspace should allow for fast calculation of the functional J for its elements, and third it should be easy to verify the non–negativity property of the ODFs. The second requirement is met best by a discretisation in the frequency domain, i.e. by approximation with Wigner–D functions (cf. Roe, 1965; Bunge, 1969), whereas the third requirement is met best by a discretisation in the spatial domain, i.e. by a finite element approach (cf. Bernier and Miller, 2006) or by approximation by indicator functions (cf. Schaeben, 1994). As a compromise between both objectives we propose a discretisation by radially symmetric functions. We prove that a discretisation by radially symmetric functions allows for fast computation of the functional J using Fourier techniques as well as for easy handling of the non–negativity constraint.

Definition 5.5. Let $S_{\text{Laue}} \subseteq \mathrm{O}(3)$ be some Laue group and let $\psi\colon \mathrm{SO}(3) \to \mathbb{R}_+$ be some non–negative, radially symmetric function with finite bandwidth $L \in \mathbb{N}$. Then we define its symmetrised counterpart as

$$\psi_{S_{\text{Laue}}}(\mathbf{q}) = \frac{1}{|S_{\text{Laue}}|} \sum_{\mathbf{q}' \in S_{\text{Laue}}} \psi(\mathbf{q}\mathbf{q}'). \tag{5.7}$$

Moreover, we define for any list $\mathbf{g} = (\mathbf{g}_1, \ldots, \mathbf{g}_M)$ of $M \in \mathbb{N}_0$ rotations $\mathbf{g}_m \in \mathrm{SO}(3)$ the M–dimensional cone $V(\psi, \mathbf{g}) \subseteq \mathcal{H}_s(\mathrm{O}(3)/S_{\text{Laue}})$ as

$$V(\psi, \mathbf{g}) = \left\{ f = \sum_{m=1}^{M} \mathbf{c}_m \psi_{S_{\text{Laue}}}(\circ\, \mathbf{g}_m^{-1}) \;\middle|\; \mathbf{c} \geq 0 \right\}. \tag{5.8}$$

Let $\psi\colon \mathrm{SO}(3) \to \mathbb{R}_+$ be a radially symmetric function. Then it is reasonable to choose the grid $\mathbf{g} = (\mathbf{g}_1, \ldots, \mathbf{g}_M)$ in $\mathrm{SO}(3)$ such that the orientations $\mathbf{g}_m S_{\text{Laue}}$, $m = 1, \ldots, M$ are almost uniformly distributed in $\mathrm{O}(3)/S_{\text{Laue}}$ and the minimum distance between two orientations is about the halfwidth of ψ. The issue of an optimal choice of the grid $\mathbf{g}$ and the ansatz function ψ is addressed in Section 5.4.

Obviously, all function $f \in V(\psi, \mathbf{g})$ are non–negative. Moreover, we immediately obtain by Lemma 3.7

Proposition 5.6. *Let $\psi\colon \mathrm{SO}(3) \to \mathbb{R}$ be some radially symmetric function of bandwidth $L \in \mathbb{N}_0$. Then the application of the operator $\mathcal{X}$ as defined in equation (4.5) on the ansatz functions $\psi_{S_{\text{Laue}}}(\circ\, \mathbf{q}^{-1})$, $\mathbf{q} \in \mathrm{SO}(3)$ is given by*

$$\left(\mathcal{X}\psi_{S_{\text{Laue}}}(\circ\, \mathbf{q}^{-1})\right)(H_i, \mathbf{r}_{ij}) = \sum_{l=0}^{L} \hat{\psi}(2l) \sum_{\mathbf{h} \in H_i} \rho_i(\mathbf{h}) \mathcal{P}_l(\mathbf{q}\mathbf{h}_i \cdot \mathbf{r}_{ij}). \tag{5.9}$$

Here $\hat{\psi}(2l)$, $l = 0, \ldots, L$ denotes the even order Chebyshev coefficients of ψ (cf. Section 2.5 and Section 3.4).

Proof. By Lemma 3.7 we have

$$\begin{aligned}
\mathcal{X}\psi_{S_{\text{Laue}}}(\circ \mathbf{q}^{-1})(H_i, \mathbf{r}_{ij}) &= \frac{1}{|S_{\text{point}}|} \sum_{\mathbf{p} \in S_{\text{Laue}}} \mathcal{X}\psi(\circ(\mathbf{q}\mathbf{p})^{-1})(H_i, \mathbf{r}_{ij}) \\
&= \sum_{l=0}^{L} \hat{\psi}(2l) \frac{1}{|S_{\text{point}}|} \sum_{\mathbf{p} \in S_{\text{Laue}}} \sum_{\mathbf{h} \in H_i} \rho_i(\mathbf{h}) \mathcal{P}_l(\mathbf{q}\mathbf{p}\mathbf{h} \cdot \mathbf{r}_{ij}).
\end{aligned}$$

Since by Remark 4.6 the symmetry properties $H_i = S_{\text{Laue}} H_i$ and $\rho_i(\mathbf{h}) = \rho_i(\mathbf{p}\mathbf{h})$ holds true for all $\mathbf{h} \in H_i$ and $\mathbf{p} \in S_{\text{Laue}}$ the middle sum can be omitted. □

Restriction of the Functional J to $V(\psi, \mathbf{g})$. Next we are going to restrict the functional J to the finite dimensional space $V(\psi, \mathbf{g})$.

Proposition 5.7. *Let $s > \frac{3}{2}$ and let $V(\psi, \mathbf{g})$ be a discretisation of $\mathcal{H}_s(\mathrm{O}(3)/S_{\mathrm{Laue}})$ as defined in equation 5.8. Then the minimization problem (5.6) restricted to $V(\psi, \mathbf{g})$ is equivalent to the minimization problem*

$$\begin{aligned} \mathbf{c}_{est} &= \operatorname*{argmin}_{\mathbf{c}\in\mathbb{R}^M} J(\mathbf{c}), \quad \textit{subject to } \mathbf{c} \geq 0, \mathbf{c} \neq 0 \\ \textit{with} \quad J(\mathbf{c}) &= \sum_{i=1}^{M} \left\| \frac{\Psi_i \mathbf{c}}{\mathbf{c}^T \mathbf{a}_i} + \mathbf{I}_i^b - \mathbf{I}_i \right\|_{\mathbf{I}_i^{-1}}^2 + \left\| \frac{\mathcal{F}_{\mathbf{g},L}^H \mathbf{c}}{\mathbf{c}^T \mathbf{a}_0} \right\|_{\mathbf{w}_{\lambda,s}^2}^2 . \end{aligned} \tag{5.10}$$

The matrices $\Psi_i \in \mathbb{R}^{M,N_i}$ and the vectors $\mathbf{a}_0, \mathbf{a}_i \in \mathbb{R}^M$, $i = 1, \ldots, N$ are defined as

$$\Psi_{ij,m} = \left(\mathcal{X}\psi_{S_{\mathrm{Laue}}}(\circ\, \mathbf{g}_m^{-1})\right)(H_i, \mathbf{r}_{ij}), \quad \mathbf{a}_0 = \mathbf{1}_M, \ \mathbf{a}_i = \frac{\Psi_i^T \mathbf{1}_{N_i}}{\|\mathbf{I}_{ij} - \mathbf{I}_{ij}^b\|_1} \tag{5.11}$$

and the weights $\mathbf{w}_{\lambda,s} \in \mathbb{R}^{\frac{1}{3}(L+1)(2L+1)(2L+3)}$,

$$[\mathbf{w}_{\lambda,s}]_{lkk'} = \sqrt{\lambda} 4\pi^2 (l + \tfrac{1}{2})^{s-1}. \tag{5.12}$$

are chosen accordingly to the Sobolev space $\mathcal{H}_s(\mathrm{O}(3)/S_{\mathrm{Laue}})$.

Proof. By Corollary 5.4 and Proposition 5.6 we have for any $\mathbf{c} \in \mathbb{R}_+^M$ with $\|\mathbf{c}\|_1 = 1$

$$J(\mathbf{c}) = J\left(\sum_{m=1}^{M} \mathbf{c}_m \psi_{S_{\mathrm{Laue}}}(\circ \mathbf{g}_m^{-1}) \right).$$

Hence, the restriction of minimization problem (5.6) to $V(\psi, \mathbf{g})$ is equivalent to the restriction of minimization problem (5.13) to $\{\, \mathbf{c} \in \mathbb{R}_+^M \mid \|\mathbf{c}\|_1 = 1 \,\}$. Since the discretized functional J is scaling invariant, i.e. $J(\mathbf{c}) = J(\mu\mathbf{c})$ for all $\mu > 0$, the constraint $\|\mathbf{c}\|_1 = 1$ can be replaced by the constrained $\mathbf{c} \neq 0$. □

Proposition 5.8. *Let a discretisation $V(\psi, \mathbf{g})$ of $\mathcal{H}_s(\mathrm{O}(3)/S_{\mathrm{Laue}})$, $s > \frac{3}{2}$ be chosen such that for any $\mathbf{c} \neq 0$ we have $\Psi_i \mathbf{c} \neq 0$. Then the functional J is differentiable on the domain $\mathbb{R}_+^M \backslash \{0\}$ and the minimization problem (5.10) has a (in general not unique) solution.*

Proof. Continuity and differentiability of J follows from the assertion that $\Psi_i \mathbf{c} \neq 0$ and hence $\mathbf{a}_i^T \mathbf{c} > 0$ for all $\mathbf{c} \neq 0$ and $i = 1, \ldots, N$. In order to prove existence of a solution we apply Weierstrass theorem on the functional J restricted to the compact domain $\{\, \mathbf{c} \in \mathbb{R}_+^M \mid \|\mathbf{c}\|_1 = 1 \,\}$ and make use of the scaling invariance of J. □

In general the functional J in minimization problem 5.10 is a rational function of second order and therefore convexity of J and uniqueness of a solution cannot be guaranteed. The next example shows that non–convexity may occur also within the constraints of minimization problem 5.10.

Example 5.9. Let us consider four diffraction counts $\mathbf{I}_1 = \mathbf{I}_2 = (5,1)^T$ with respect to two crystal directions $\mathbf{h}_1, \mathbf{h}_2 \in \mathbb{S}^2$ and with respect to four specimen directions $\mathbf{r}_{12}, \mathbf{r}_{22}, \mathbf{r}_{21}, \mathbf{r}_{22} \in \mathbb{S}^2$. Let furthermore, ψ_1, ψ_2 be two ODFs such that the corresponding diffraction intensities are

$$\mathcal{X}\psi_1 \left(\mathbf{h}_1, \begin{pmatrix} \mathbf{r}_{12} \\ \mathbf{r}_{22} \end{pmatrix} \right) = \mathcal{X}\psi_2 \left(\mathbf{h}_2, \begin{pmatrix} \mathbf{r}_{21} \\ \mathbf{r}_{22} \end{pmatrix} \right) = \begin{pmatrix} 2 \\ 1 \end{pmatrix}$$

and

$$\mathcal{X}\psi_1 \left(\mathbf{h}_2, \begin{pmatrix} \mathbf{r}_{21} \\ \mathbf{r}_{22} \end{pmatrix} \right) = \mathcal{X}\psi_2 \left(\mathbf{h}_1, \begin{pmatrix} \mathbf{r}_{11} \\ \mathbf{r}_{12} \end{pmatrix} \right) = \begin{pmatrix} 2 \\ 4 \end{pmatrix}.$$

Restricting the functional J to all convex combinations $f_\tau = \tau\psi_1 + (1-\tau)\psi_2$ of ψ_1 and ψ_2 the functional J becomes a rational function in τ. More precisely, we calculate

$$J(\tau) = \sum_{i=1}^{2} \sum_{j=1}^{2} \mathbf{I}_{ij}^{-1} \Big(\alpha_i(\tau) \big(\tau \mathcal{X}\psi_1(\mathbf{h}_i, \mathbf{r}_{ij}) + (1-\tau)\mathcal{X}\psi_2(\mathbf{h}_i, \mathbf{r}_{ij}) \big) - \mathbf{I}_{ij} \Big)^2,$$

where we have set

$$\alpha_1(\tau) := \frac{\|\mathbf{I}_1\|_1}{\tau \|\mathcal{X}\psi_1(\mathbf{h}_1, \mathbf{r}_1)\|_1 + (1-\tau) \|\mathcal{X}\psi_2(\mathbf{h}_1, \mathbf{r}_1)\|_1} = \frac{2}{2-\tau}$$
$$\text{and } \alpha_2(\tau) = \frac{\|\mathbf{I}_2\|_1}{\tau \|\mathcal{X}\psi_1(\mathbf{h}_2, \mathbf{r}_2)\|_1 + (1-\tau) \|\mathcal{X}\psi_2(\mathbf{h}_2, \mathbf{r}_2)\|_1} = \frac{2}{1+\tau}.$$

accordingly to equation (4.30). One verifies that the functional $J(\tau)$ is not convex on the interval $[0,1]$. The graph of $\tau \mapsto J(\tau)$ is plotted in Figure 5.1. and shows evidence of this conjecture.

Finally we give a fast algorithm for the calculation of the matrix vector products $\Psi_i \mathbf{c}$ and $\Psi_i^T \mathbf{d}$ which are involved in the representation of the functional J in Proposition 5.7.

Lemma 5.10. *Let $\Psi_i \in \mathbb{R}^{N_i, M}$ be defined as in Proposition 5.7 and denote $\hat{\boldsymbol{\psi}} \in \mathbb{R}^{L+1}$, $\hat{\boldsymbol{\psi}}_l = \hat{\psi}(2l)$, $l = 1, \ldots, L$, the vector of the even order Chebyshev coefficients of the ansatz function ψ up to the bandwidth L. Moreover, we consecutively number the elements of the list H_i by $\mathbf{h}_{in}$, $n = 1, \ldots, |H_i|$ and introduce the notation $\boldsymbol{\rho}_{in} = \rho_i(\mathbf{h}_{in})$. Then for any vectors $\mathbf{c} \in \mathbb{R}^M$ and $\mathbf{d} \in \mathbb{R}^{N_i}$ the matrix vector products $\Psi_i \mathbf{c}$ and $\Psi_i^T \mathbf{d}$ are calculated by Algorithm 1 and Algorithm 5.2, respectively, with numerical complexity $\mathcal{O}(M + N_i + L^3 \log^2 L)$.*

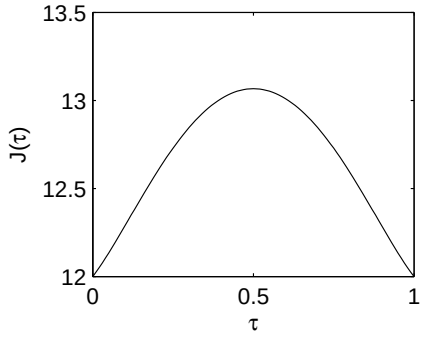

Figure 5.1: The functional $J(\tau)$ as defined in Example 5.9.

Algorithm 5.1: Fast matrix vector multiplication $\Psi_i \mathbf{c}$

input : $\mathbf{c} \in \mathbb{R}^M$
$\hat{\boldsymbol{\psi}} \in \mathbb{R}^L$
$\mathbf{r}_{ij} \in \mathbb{S}^2$,$j = 1, \ldots, N_i$
$\mathbf{g}_m \mathbf{h}_n \in \mathbb{S}^2$, $m = 1, \ldots, M$, $n = 1, \ldots, |H_i|$
$\boldsymbol{\rho} \in \mathbb{R}^{|H_i|}$
output: $\mathbf{d} = \Psi_i \mathbf{c} \in \mathbb{R}^{N_i}$

for $l \leftarrow 0, \ldots, L$ **do** **for** $k \leftarrow -l, \ldots, l$ **do** $\mathbf{F}_{lk} = 0$
for $n \leftarrow 1, \ldots, |H_i|$ **do** $\mathbf{F} \leftarrow \mathbf{F} + \boldsymbol{\rho}_{in} \mathcal{F}^H_{\mathbf{g}\mathbf{h}_{in}, L} \mathbf{c}$
for $l \leftarrow 0, \ldots, L$ **do** **for** $k \leftarrow -l, \ldots, l$ **do** $\mathbf{F}_{lk} \leftarrow \hat{\boldsymbol{\psi}}_l \mathbf{F}_{lk}$
$\mathbf{d} \leftarrow \mathcal{F}^H_{\mathbf{r}_i, L} \mathbf{F}$

Proof. By Lemma 5.6 and the addition theorem we have for $i = 1, \ldots, N$, $j = 1, \ldots, N_i$,

$$\begin{aligned}
[\Psi_i \mathbf{c}]_j &= \sum_{m=1}^{M} \mathbf{c}_m \Psi_{ij,m} \\
&= \sum_{m=1}^{M} \mathbf{c}_m \sum_{\mathbf{h} \in H_i} \rho(\mathbf{h}) \sum_{l=0}^{L} \hat{\psi}(2l) \mathcal{P}_l(\mathbf{g}_m \mathbf{h} \cdot \mathbf{r}_{ij}) \\
&= \sum_{m=1}^{M} \mathbf{c}_m \sum_{n=1}^{|H_i|} \rho_{in} \sum_{l=0}^{L} \hat{\boldsymbol{\psi}}_l \sum_{k=-l}^{l} \overline{\mathcal{Y}_l^k(\mathbf{g}_m \mathbf{h}_{in})} \mathcal{Y}_l^k(\mathbf{r}_{ij}) \\
&= \sum_{l=0}^{L} \sum_{k=-l}^{l} \mathcal{Y}_l^k(\mathbf{r}_{ij}) \hat{\boldsymbol{\psi}}_l \sum_{n=1}^{|H_i|} \rho_{in} \sum_{m=1}^{M} \mathbf{c}_m \overline{\mathcal{Y}_l^k(\mathbf{g}_m \mathbf{h}_{in})}.
\end{aligned}$$

Evaluation of the most inner sum for all even $l = 0, \ldots, L$ and all $k = -l, \ldots, l$ corre-

Algorithm 5.2: Fast matrix vector multiplication $\Psi_i^T \mathbf{d}$

input : $\mathbf{d} \in \mathbb{R}^{N_i}$
$\hat{\boldsymbol{\psi}} \in \mathbb{R}^L$
$\mathbf{r}_{ij} \in \mathbb{S}^2, j = 1, \ldots, N_i$
$\mathbf{g}_m \mathbf{h}_n \in \mathbb{S}^2,\ m = 1, \ldots, M,\ n = 1, \ldots, |H_i|$
$\boldsymbol{\rho} \in \mathbb{R}^{|H_i|}$
output: $\mathbf{c} = \Psi_i^H \mathbf{d} \in \mathbb{R}^M$

$F \leftarrow \mathcal{F}^H_{\mathbf{r}_i, L} \mathbf{d}$
for $l \leftarrow 0, \ldots, L$ **do** **for** $k \leftarrow -l, \ldots, l$ **do** $\mathbf{F}_{lk} \leftarrow \hat{\boldsymbol{\psi}}_l \mathbf{F}_{lk}$
$\mathbf{c} \leftarrow \mathbf{0}_M$
for $n \leftarrow 1, \ldots, |H_i|$ **do** $\mathbf{c} \leftarrow \mathbf{c} + \boldsymbol{\rho}_{in} \mathcal{F}_{\mathbf{g}\mathbf{h}_{in}, L} \mathbf{F}$

sponds to the adjoint discrete spherical Fourier transform, i.e.

$$f_{lk}(\mathbf{h}_{in}) = \sum_{m=1}^{M} \mathbf{c}_m \overline{\mathcal{Y}_l^k(\mathbf{g}_m \mathbf{h}_{in})} = \left[\mathcal{F}^H_{\mathbf{g}\mathbf{h}_{in}, L} \mathbf{c}\right]_{lk}, \quad i = 1, \ldots, N,\ n = 1, \ldots, |H_i|.$$

Let the Fourier vector $\mathbf{F} \in \mathbb{C}^{(2L+1)^2}$ be given by

$$\mathbf{F}_{lk} = \sum_{n=1}^{|H_i|} \hat{\boldsymbol{\psi}}_l \rho_{in} f_{lk}(\mathbf{h}_{in}), \quad l = 0, \ldots, L,\ k = -l, \ldots, l.$$

Then the evaluation of the most outer sum for all $j = 1, \ldots, N_i$ is the discrete spherical Fourier transform applied to the vector $\mathbf{F}$, i.e.

$$[\Psi_i \mathbf{c}]_j = \sum_{l=0}^{L} \sum_{k=-l}^{l} \mathbf{F}_{lk} \mathcal{Y}_l^k(\mathbf{r}_{ij}) = \left[\mathcal{F}_{\mathbf{r}_i, L} \mathbf{F}\right]_j.$$

□

5.3 The MLS ODF Estimation Algorithm

In this section we describe a numerical algorithm to solve minimization problem (5.10). Therefore we first recall the modified steepest descent algorithm for the solution of non–negatively constraint minimization problems.

The Modified Steepest Descent Algorithm. There are several algorithms for non–linear, non–negatively constrained minimization e.g. projected steepest descent, modified steepest descent, gradient projection residual norm conjugated gradients (GPRNCG),

etc. (cf. Vogel, 2002). In this work we restrict ourself to the *modified steepest descent algorithm* (cf. Kim (2002, Section 4.2.1), Bardsley and Nagy (2005)) since it is appropriate to large scale problems and combines simplicity and fast convergence. Moreover, it is especially well suited for problems where the unknown vector is sparse (cf. Bardsley and Nagy, 2005).

Let J be some arbitrary differentiable function on $\mathbb{R}^M$. We are looking for solutions of the non–negatively constrained minimization problem

$$\mathbf{c}_{\text{est}} = \operatorname*{argmin}_{\mathbf{c}\in\mathbb{R}^M_+} J(\mathbf{c}). \tag{5.13}$$

The modified steepest descent algorithm is an iterative method based on the fix point iteration

$$\mathbf{c}^{(n+1)} = \mathbf{c}^{(n)} + \tau^{(n)}\tilde{\mathbf{c}}^{(n)} \tag{5.14}$$

where $\tilde{\mathbf{c}}^{(n)} \in \mathbb{R}^M$ is some descent direction and $\tau > 0$ is the step size. In contrast to the ordinary steepest descent algorithm the descent direction $\tilde{\mathbf{c}}^{(n)}$ is fixed as the negative gradient of $J(\mathbf{c}^{(n)})$ componentwise multiplied with the current estimate $\mathbf{c}^{(n)}$, i.e.

$$\tilde{\mathbf{c}}^{(n)} = -\mathbf{c}^{(n)} \odot \operatorname{grad} J(\mathbf{c}^{(n)}). \tag{5.15}$$

This descent direction is motivated by the facts that $\mathbf{c}^{(n)} \odot \operatorname{grad} J(\mathbf{c}^{(n)}) = 0$ is the Kuhn-Tucker condition for the minimization problem (5.13).

The step length $\tau^{(n)}$ is calculated by a line search. In order to ensure the non–negativity of $\mathbf{c}^{(n+1)}$ at each iteration $n \in \mathbb{N}$ the step size has to be restricted to $[0, \tau^{(n)}_{\max}]$ with

$$\begin{aligned} \tau^{(n)}_{\max} &= \max\Big\{ \tau > 0 \;\Big|\; \mathbf{c}^{(n)} + \tau\tilde{\mathbf{c}}^{(n)} \geq 0 \Big\} \\ &= \min\Bigg\{ -\frac{[\mathbf{c}^{(n)}]_m}{[\tilde{\mathbf{c}}^{(n)}]_m} \;\Bigg|\; m = 1,\dots,M,\ [\tilde{\mathbf{c}}^{(n)}]_m < 0 \Bigg\}. \end{aligned} \tag{5.16}$$

Algorithm 5.3 outlines the modified steepest descent algorithm.

Adaption to Functional J. Now we want to apply the modified steepest descent algorithm to minimization problem (5.10). Therefore we fix for the remainder of this section a certain Laue group $S_{\text{Laue}} \subseteq \mathrm{O}(3)$ and an arbitrary discretisation $V(\psi, \mathbf{g})$ of $\mathcal{H}_s(\mathrm{O}(3)/S_{\text{Laue}})$, $s > \frac{3}{2}$ as defined in Definition 5.5. Furthermore, we assume the diffraction counts and the background intensities to be $\mathbf{I}_i, \mathbf{I}_i^b \in \mathbb{R}^{N_i}_+$ and rely on the matrices $\Psi_i \in \mathbb{R}^{N_i \times M}$ and the vectors $\mathbf{a}_0, \mathbf{a}_i \in \mathbb{R}^M$, $i = 1,\dots,N$ as defined in Proposition 5.7.

We will use the following abbreviations.

Definition 5.11. Let $n \in \mathbb{N}$ and $\mathbf{c}^{(n)}, \tilde{\mathbf{c}}^{(n)} \in \mathbb{R}^M$. Then we define for $i = 0,\dots,N$ the coefficients $\boldsymbol{\alpha}_i^{(n)}, \tilde{\boldsymbol{\alpha}}_i^{(n)} \in \mathbb{R}$ as

$$\boldsymbol{\alpha}_i^{(n)} = \frac{1}{\mathbf{a}_i^T\mathbf{c}^{(n)}} \quad \text{and} \quad \tilde{\boldsymbol{\alpha}}_i^{(n)} = \frac{1}{\mathbf{a}_i^T\tilde{\mathbf{c}}^{(n)}}. \tag{5.17}$$

Algorithm 5.3: Modified steepest descent algorithm

input : $\mathbf{c}_0 \in \mathbb{R}_+^M$ /* initial guess */
output: $\mathbf{c} \in \mathbb{R}_+^M$ /* minimizer */

$k \leftarrow 0$
while *no convergence* **do**
  $\mathbf{u}^{(n)} \leftarrow \operatorname{grad} J(\mathbf{c}^{(n)})$ /* calculate gradient */
  $\tilde{\mathbf{c}}^{(n)} \leftarrow -\mathbf{c}^{(n)} \odot \mathbf{u}^{(n)}$ /* calculate descent direction */
  $\tau_{\text{opt}} \leftarrow \operatorname{argmin} J(\mathbf{c}^{(n)} + \tau\tilde{\mathbf{c}}^{(n)})$ /* line search */
  $\tau_{\text{bndry}} \leftarrow \min\{ -\frac{[\mathbf{c}^{(n)}]_m}{[\tilde{\mathbf{c}}^{(n)}]_m} \mid m = 1, \dots, M,\ [\tilde{\mathbf{c}}^{(n)}]_m < 0 \}$
  $\tau^{(n)} \leftarrow \min\{\tau_{\text{opt}}, \tau_{\text{bndry}}\}$
  $\mathbf{c}^{(n+1)} \leftarrow \mathbf{c}^{(n)} + \tau^{(n)}\tilde{\mathbf{c}}^{(n)}$ /* update $\mathbf{c}$ */
  $k \leftarrow k + 1$
end
$\mathbf{c} \leftarrow \mathbf{c}^{(n)}$

Moreover, we define the residuals $\mathbf{u}_i^{(n)}, \tilde{\mathbf{u}}_i^{(n)} \in \mathbb{R}^{N_i}$, $i = 1, \dots, N$ as

$$\mathbf{u}_i^{(n)} = \mathbf{I}^{-\frac{1}{2}} \odot \left(\boldsymbol{\alpha}_i^{(n)} \Psi_i \mathbf{c}^{(n)} + \mathbf{I}_i^b - \mathbf{I}_i \right), \quad \text{and} \quad \tilde{\mathbf{u}}_i^{(n)} = \mathbf{I}^{-\frac{1}{2}} \odot \left(\tilde{\boldsymbol{\alpha}}_i^{(n)} \Psi_i \tilde{\mathbf{c}}_i^{(n)} + \mathbf{I}_i^b - \mathbf{I}_i \right)$$

and set for completeness the vectors $\mathbf{u}_0^{(n)}, \tilde{\mathbf{u}}_0^{(n)} \in \mathbb{C}^{\frac{1}{3}(L+1)(2L+1)(2L+3)}$ to

$$\mathbf{u}_0^{(n)} = \boldsymbol{\alpha}_0^{(n)} \mathbf{w}_{\lambda,s} \odot \mathcal{F}_{\mathbf{g},L}^H \mathbf{c}^{(n)} \quad \text{and} \quad \tilde{\mathbf{u}}_0^{(n)} = \tilde{\boldsymbol{\alpha}}_0^{(n)} \mathbf{w}_{\lambda,s} \odot \mathcal{F}_{\mathbf{g},L}^H \tilde{\mathbf{c}}^{(n)}. \tag{5.18}$$

Here we make use of the Fourier weights $\mathbf{w}_{\lambda,s} \in \mathbb{R}^{\frac{1}{3}(L+1)(2L+1)(2L+3)}$ as defined in Proposition 5.7.

With these abbreviations we have

Proposition 5.12. *Let $n \in \mathbb{N}$ and $\mathbf{c}^{(n)} \in \mathbb{R}^M$. Then the functional J as defined in Proposition 5.7 simplifies to*

$$J(\mathbf{c}^{(n)}) = \sum_{i=0}^{N} \left\| \mathbf{u}_i^{(n)} \right\|_2^2. \tag{5.19}$$

Let furthermore $\tilde{\mathbf{c}}^{(n)} \in \mathbb{R}^M$ and $\mathbf{c}^{(n+1)} = \mathbf{c}^{(n)} + \tau^{(n)}\tilde{\mathbf{c}}^{(n)}$ for some $\tau^{(n)} \in \mathbb{R}$. Then we have for all $i = 0, \dots, N$ the recurrence formulae

$$\boldsymbol{\alpha}_i^{(n+1)} = \frac{\boldsymbol{\alpha}_i^{(n)} \tilde{\boldsymbol{\alpha}}_i^{(n)}}{\tau^{(n)} \boldsymbol{\alpha}_i^{(n)} + \tilde{\boldsymbol{\alpha}}_i^{(n)}} \quad \textit{and} \quad \mathbf{u}_i^{(n+1)} = \frac{\tilde{\boldsymbol{\alpha}}_i^{(n)} \mathbf{u}_i^{(n)} + \tau^{(n)} \boldsymbol{\alpha}_i^{(n)} \tilde{\mathbf{u}}_i^{(n)}}{\tau^{(n)} \boldsymbol{\alpha}_i^{(n)} + \tilde{\boldsymbol{\alpha}}_i^{(n)}}. \tag{5.20}$$

Proof. By Definition 5.11 we obtain for any $i = 0, \dots, N$ the relationship

$$\boldsymbol{\alpha}_i^{(n+1)} = \frac{1}{\mathbf{a}_i^T(\mathbf{c}^{(n)} + \tau^{(n)}\tilde{\mathbf{c}}^{(n)})} = \frac{1}{\frac{1}{\boldsymbol{\alpha}_i^{(n)}} + \frac{\tau^{(n)}}{\tilde{\boldsymbol{\alpha}}_i^{(n)}}} = \frac{\boldsymbol{\alpha}_i^{(n)}\tilde{\boldsymbol{\alpha}}_i^{(n)}}{\tau^{(n)}\boldsymbol{\alpha}_i^{(n)} + \tilde{\boldsymbol{\alpha}}_i^{(n)}}.$$

and for any $i = 1, \dots, N$ the equality

$$\begin{aligned}
\mathbf{u}_i^{(n+1)} \odot \mathbf{I}_i^{\frac{1}{2}} &= \boldsymbol{\alpha}_i^{(n+1)}\Psi_i\left(\mathbf{c}^{(n)} + \tau^{(n)}\tilde{\mathbf{c}}^{(n)}\right) + \mathbf{I}_i^b - \mathbf{I}_i \\
&= \frac{\boldsymbol{\alpha}_i^{(n)}\tilde{\boldsymbol{\alpha}}_i^{(n)}}{\tau^{(n)}\boldsymbol{\alpha}_i^{(n)} + \tilde{\boldsymbol{\alpha}}_i^{(n)}}\Psi_i\left(\mathbf{c}^{(n)} + \tau^{(n)}\tilde{\mathbf{c}}^{(n)}\right) + \mathbf{I}_i^b - \mathbf{I}_i \\
&= \frac{\tilde{\boldsymbol{\alpha}}_i^{(n)}(\boldsymbol{\alpha}_i^{(n)}\Psi_i\mathbf{c}^{(n)} + \mathbf{I}_i^b - \mathbf{I}_i) + \tau^{(n)}\boldsymbol{\alpha}_i^{(n)}(\tilde{\boldsymbol{\alpha}}_i^{(n)}\Psi_i\tilde{\mathbf{c}}^{(n)} + \mathbf{I}_i^b - \mathbf{I}_i)}{\tau^{(n)}\boldsymbol{\alpha}_i^{(n)} + \tilde{\boldsymbol{\alpha}}_i^{(n)}} \\
&= \frac{\tilde{\boldsymbol{\alpha}}_i^{(n)}\mathbf{u}_i^{(n)} + \tau^{(n)}\boldsymbol{\alpha}_i^{(n)}\tilde{\mathbf{u}}_i^{(n)}}{\tau^{(n)}\boldsymbol{\alpha}_i^{(n)} + \tilde{\boldsymbol{\alpha}}_i^{(n)}} \odot \mathbf{I}_i^{\frac{1}{2}}.
\end{aligned}$$

For $i = 0$ the proof of equation (5.20) is analogous. □

With the abbreviations of Definition 5.11 we find the following expression for the gradient of the functional J.

Lemma 5.13. *Let $n \in \mathbb{N}$. Then the gradient of the functional $J(\mathbf{c}^{(n)}) = \sum_{i=0}^{N}\left\|\mathbf{u}_i^{(n)}\right\|_2^2$. is given by*

$$\begin{aligned}
&\frac{1}{2}\operatorname{grad} J(\mathbf{c}^{(n)}) = \boldsymbol{\alpha}_0^{(n)}\left(\mathcal{F}_{\mathbf{g},L}\left(\mathbf{u}_0^{(n)} \odot \mathbf{w}_{\lambda,s}\right) - \|\mathbf{u}_0^{(n)}\|_2^2\,\mathbf{a}_0\right) + \sum_{i=1}^{N}\boldsymbol{\alpha}_i^{(n)}\left(\mathbf{v}_i - \boldsymbol{\alpha}_i^{(n)}\mathbf{v}_i^T\mathbf{c}^{(n)}\mathbf{a}_i\right), \\
&\quad \textit{where } \mathbf{v}_i = \Psi_i^T\left(\mathbf{u}_i^{(n)} \odot \mathbf{I}_i^{-\frac{1}{2}}\right).
\end{aligned} \tag{5.21}$$

Proof. By the chain rule we obtain

$$\begin{aligned}
\frac{1}{2}\frac{\mathrm{d}}{\mathrm{d}\mathbf{c}^{(n)}}\left\|\frac{\Psi_i\mathbf{c}^{(n)}}{\mathbf{a}_i^T\mathbf{c}^{(n)}} + \mathbf{I}_i^b - \mathbf{I}_i\right\|_{\mathbf{I}_i^{-1}}^2 &= \frac{\mathbf{a}_i^T\mathbf{c}^{(n)}\Psi_i^T - \mathbf{a}_i\left(\Psi_i\mathbf{c}^{(n)}\right)^T}{\left(\mathbf{a}_i^T\mathbf{c}^{(n)}\right)^2}\left(\left(\frac{\Psi_i\mathbf{c}^{(n)}}{\mathbf{a}_i^T\mathbf{c}^{(n)}} + \mathbf{I}_i^b - \mathbf{I}_i\right) \odot \mathbf{I}_i^{-1}\right) \\
&= \frac{\Psi_i^T\left(\mathbf{u}_i^{(n)} \odot \mathbf{I}_i^{-1}\right)}{\mathbf{a}_i^T\mathbf{c}^{(n)}} - \frac{\left(\mathbf{u}_i^{(n)} \odot \mathbf{I}_i^{-\frac{1}{2}}\right)^T\Psi_i\mathbf{c}^{(n)}}{\left(\mathbf{a}_i^T\mathbf{c}^{(n)}\right)^2}\mathbf{a}_i.
\end{aligned}$$

On the other hand the gradient of the regularization term is

$$\begin{aligned}
\frac{1}{2}\frac{\mathrm{d}}{\mathrm{d}\mathbf{c}^{(n)}}\left\|\frac{\mathbf{w}_{\lambda,s} \odot \mathcal{F}_{\mathbf{g},L}^H\mathbf{c}^{(n)}}{\mathbf{a}_0^T\mathbf{c}^{(n)}}\right\|_2^2 &= \frac{\mathbf{a}_0^T\mathbf{c}^{(n)}\mathcal{F}_{\mathbf{g},L} - \mathbf{a}_0\left(\mathcal{F}_{\mathbf{g},L}^H\mathbf{c}^{(n)}\right)^T}{(\mathbf{a}_0^T\mathbf{c})^2}\frac{\mathbf{w}_{\lambda,s}^2 \odot \mathcal{F}_{\mathbf{g},L}^H\mathbf{c}\mathcal{F}_{\mathbf{g},L}}{\mathbf{a}_0^T\mathbf{c}^{(n)}} \\
&= \boldsymbol{\alpha}_0^{(n)}\left(\mathcal{F}_{\mathbf{g},L}\left(\mathbf{u}_0^{(n)} \odot \mathbf{w}_{\lambda,s}\right) - \|\mathbf{u}_0^{(n)}\|_2^2\,\mathbf{a}_0\right).
\end{aligned}$$

□

We will also need the following representation of the function $\tau \mapsto J(\mathbf{c}^{(n)} + \tau\tilde{\mathbf{c}}^{(n)})$ as a simple rational function based on the quantities $\mathbf{u}_0^{(n)}$ and $\tilde{\mathbf{u}}_0^{(n)}$ as defined in Definition 5.11.

Lemma 5.14. *Let $\mathbf{c}^{(n)}, \tilde{\mathbf{c}}^{(n)} \in \mathbb{R}^M$. Then $\tau \mapsto J(\mathbf{c}^{(n)} + \tau\tilde{\mathbf{c}}^{(n)})$ is a rational function in τ. More precisely, we have*

$$J\big(\mathbf{c}^{(n)} + \tau\tilde{\mathbf{c}}^{(n)}\big) = \sum_{i=0}^{N} \frac{A_i + 2\tau B_i + \tau^2 C_i}{\Big(\tau\boldsymbol{\alpha}_i^{(n)} + \tilde{\boldsymbol{\alpha}}_i^{(n)}\Big)^2}, \tag{5.22}$$

where we have set for any $i = 0, \ldots, N$,

$$A_i = \big\|\tilde{\boldsymbol{\alpha}}_i^{(n)}\mathbf{u}_i^{(n)}\big\|_2^2,\ B_i = \Big\langle \tilde{\boldsymbol{\alpha}}_i^{(n)}\mathbf{u}_i^{(n)}, \boldsymbol{\alpha}_i^{(n)}\tilde{\mathbf{u}}_i^{(n)} \Big\rangle,\ C_i = \big\|\boldsymbol{\alpha}_i^{(n)}\tilde{\mathbf{u}}_i^{(n)}\big\|_2^2. \tag{5.23}$$

Proof. By Proposition 5.12 the function $\tau \mapsto J(\mathbf{c} + \tau\tilde{\mathbf{c}})$ can be rewritten as

$$\begin{aligned} J\big(\mathbf{c}^{(n)} + \tau\tilde{\mathbf{c}}^{(n)}\big) &= \sum_{i=0}^{N} \Big\| \frac{\tilde{\boldsymbol{\alpha}}_i^{(n)}\mathbf{u}_i^{(n)} + \tau\boldsymbol{\alpha}_i^{(n)}\tilde{\mathbf{u}}_i^{(n)}}{\tau\boldsymbol{\alpha}_i^{(n)} + \tilde{\boldsymbol{\alpha}}_i^{(n)}} \Big\|_2^2 \\ &= \sum_{i=1}^{N} \frac{\big\|\tilde{\boldsymbol{\alpha}}_i^{(n)}\mathbf{u}_i^{(n)}\big\|_2^2 + 2\tau\Big\langle \tilde{\boldsymbol{\alpha}}_i^{(n)}\mathbf{u}_i^{(n)}, \boldsymbol{\alpha}_i^{(n)}\tilde{\mathbf{u}}_i^{(n)} \Big\rangle + \tau^2\big\|\boldsymbol{\alpha}_i^{(n)}\tilde{\mathbf{u}}_i^{(n)}\big\|_2^2}{\big(\tau\boldsymbol{\alpha}_i^{(n)} + \tilde{\boldsymbol{\alpha}}_i^{(n)}\big)^2}. \end{aligned}$$

□

Corollary 5.15. *Line search of the functional J can be performed with numerical complexity $\mathcal{O}(\bar{N} + M + L^3 \log^2 L)$. A simple line search algorithm that makes use of formula* (5.22) *is given in Algorithm 4.*

The next lemma shows that one can choose the upper bound $\tau_{\max}^{(n)}$ as defined in equation (5.16) as the maximum stepsize.

Lemma 5.16. *Let $\mathbf{c}^{(n)} \in \mathbb{R}^M$ and let $\tilde{\mathbf{c}}^{(n)} = \mathbf{c}^{(n)} \odot \operatorname{grad} J(\mathbf{c}^{(n)})$ be the modified gradient of the functional J. Then the maximum step length as defined in equation* (5.16)

$$\tau_{max}^{(n)} = \min\left\{ -\frac{\big[\mathbf{c}^{(n)}\big]_i}{\big[\tilde{\mathbf{c}}^{(n)}\big]_i} \;\middle|\; m = 1, \ldots, M,\ \big[\tilde{\mathbf{c}}^{(n)}\big]_i < 0 \right\}.$$

is finite.

Proof. Since $J(\mathbf{c}^{(n)})$ does not depend on the scale of $\mathbf{c}^{(n)}$, i.e. $J(\mathbf{c}^{(n)}) = J(\mu\mathbf{c}^{(n)})$ for all $\mu > 0$, the gradient of $J(\mathbf{c}^{(n)})$ is orthogonal to $\mathbf{c}^{(n)}$. Taking into account that $\mathbf{c}^{(n)} \geq 0$ we conclude that the modified descent search direction $\tilde{\mathbf{c}}^{(n)} = -\operatorname{grad} J(\mathbf{c}^{(n)}) \odot \mathbf{c}^{(n)}$ is either zero or has at least one negative component. Hence, $\tau_{\max}^{(n)}$ is finite. □

Algorithm 5.4: Line Search

input : $\tau_{\max}^{(n)} \in \mathbb{R}$ /* maximum step length */
$\mathbf{u}_0^{(n)} \in \mathbb{R}^{\frac{1}{3}(L+1)(2L+1)(2L+3)}$
$\tilde{\mathbf{u}}_0^{(n)} \in \mathbb{R}^{\frac{1}{3}(L+1)(2L+1)(2L+3)}$
$\mathbf{u}_i^{(n)} \in \mathbb{R}^{N_i}$, $i = 1, \ldots, N$
$\tilde{\mathbf{u}}_i^{(n)} \in \mathbb{R}^{N_i}$, $i = 1, \ldots, N$
$\boldsymbol{\alpha}^{(n)} \in \mathbb{R}^{N+1}$
$\tilde{\boldsymbol{\alpha}}^{(n)} \in \mathbb{R}^{N+1}$

output: $\tau^{(n)} \in \mathbb{R}_+$ /* optimum step length */

for $i \leftarrow 0, \ldots, N$ **do** /* precomputation */
$A_i \leftarrow \left\| \tilde{\boldsymbol{\alpha}}_i^{(n)} \mathbf{u}_i^{(n)} \right\|_2^2$
$B_i \leftarrow \left\langle \tilde{\boldsymbol{\alpha}}_i^{(n)} \mathbf{u}_i^{(n)}, \boldsymbol{\alpha}_i^{(n)} \tilde{\mathbf{u}}_i^{(n)} \right\rangle$
$C_i \leftarrow \left\| \boldsymbol{\alpha}_i^{(n)} \tilde{\mathbf{u}}_i^{(n)} \right\|_2^2$
end
$J_0 \leftarrow \sum_{i=0}^{N} A_i \left(\tilde{\boldsymbol{\alpha}}_i^{(n)} \right)^{-2}$ /* current value of $J(\mathbf{c}^{(n)})$ */
$\tau \leftarrow \tau_{\max}^{(n)}$
$J \leftarrow \sum_{i=0}^{N} \frac{A_i + 2\tau B_i + \tau^2 C_i}{\left(\tau \boldsymbol{\alpha}_i^{(n)} + \tilde{\boldsymbol{\alpha}}_i^{(n)} \right)^2}$ /* value of $J(\mathbf{c}^{(n)} + \tau \tilde{\mathbf{c}}^{(n)})$ */
while $J > J_0$ **do**
$\tau \leftarrow \frac{1}{2}\tau$ /* reduce step length */
$J \leftarrow \sum_{i=0}^{N} \frac{A_i + 2\tau B_i + \tau^2 C_i}{\left(\tau \boldsymbol{\alpha}_i^{(n)} + \tilde{\boldsymbol{\alpha}}_i^{(n)} \right)^2}$ /* update value of $J(\mathbf{c} + \tau \tilde{\mathbf{c}})$ */
end
$\tau^{(n)} \leftarrow \tau$

Merging Proposition 5.12, Lemma 5.13, Corollary 5.15 and Lemma 5.16 we obtain the following Theorem.

Theorem 5.17. *Algorithm 5 implements the MSD algorithm for minimization problem* (5.10). *Every iteration step has the numerical complexity* $\mathcal{O}(\bar{N} + M + L^3 \log^2 L)$.

Proof. Algorithm 5 implements the modified steepest descent Algorithm 5.3.

In lines 1 – 5 the vectors $\mathbf{a}_i \in \mathbb{R}^M$, $i = 1, \ldots, N$ needed for the calculation of the normalization coefficients (cf. Proposition 5.7), the initial values of the residuals $\mathbf{u}_i^{(0)}$ and the normalization coefficients $\boldsymbol{\alpha}_i^{(0)}$, $i = 1, \ldots, N$ (cf. Definition 5.11) are calculated. These calculations require the matrix vector multiplications $\Psi_i^T \mathbf{1}_{N_i}$ (cf. Algorithm 5.2) and $\Psi_i \mathbf{c}$, $i = 1, \ldots, N$ (cf. Algorithm 1). Both algorithms have the numerical complexity $\mathcal{O}(N_i + M + L^3 \log^2 L)$ (cf. Lemma 5.10).

Algorithm 5.5: Modified Least Squares ODF Estimator

input : $\mathbf{c}^{(0)} \in \mathbb{R}^M$ /* initial vector */
$\mathbf{I}_i \in \mathbb{R}^{N_i}$, $i = 1, \ldots, N$ /* diffraction counts */
$\mathbf{I}_i^b \in \mathbb{R}^{N_i}$, $i = 1, \ldots, N$ /* background intensities */
$\mathbf{w}_{\lambda,s} \in \mathbb{R}^{\frac{1}{3}(L+1)(2L+1)(2L+3)}$ /* regularization weights */
output: $\mathbf{c} \in \mathbb{R}^M$

$\mathbf{a}_0 \leftarrow \mathbf{1}_M$
for $i \leftarrow 1, \ldots, N$ **do** $\mathbf{a}_i \leftarrow \frac{\Psi_i^T \mathbf{1}_{N_i}}{(\mathbf{I}_i^T - \mathbf{I}_i^b)^T \mathbf{1}_{N_i}}$
for $i \leftarrow 0, \ldots, N$ **do** $\boldsymbol{\alpha}_i^{(0)} \leftarrow \frac{1}{\mathbf{a}_i^T \mathbf{c}^{(0)}}$; /* normalization coefficients */
$\mathbf{u}_0^{(0)} \leftarrow \boldsymbol{\alpha}_0^{(0)} \mathbf{w}_{\lambda,s} \odot \mathcal{F}_{\mathbf{g},L} \mathbf{c}^{(0)}$
for $i \leftarrow 1, \ldots, N$ **do** $\mathbf{u}_i^{(0)} \leftarrow \left(\boldsymbol{\alpha}_i^{(0)} \Psi_i \mathbf{c}^{(0)} + \mathbf{I}_i^b - \mathbf{I}_i\right) \odot \mathbf{I}_i^{-\frac{1}{2}}$
$n \leftarrow 1$
while *no convergence* **do**
  $\tilde{\mathbf{v}}_0^{(n)} \leftarrow -\boldsymbol{\alpha}_0^{(n)} \left(\mathcal{F}_{\mathbf{g},L}\left(\mathbf{w}_{\lambda,s} \odot \mathbf{u}_0^{(n)}\right) - \|\mathbf{u}_0^{(n)}\|_2^2 \, \mathbf{a}_0 \right)$
  for $i \leftarrow 1, \ldots, N$ **do** $\tilde{\mathbf{v}}_i^{(n)} \leftarrow -\boldsymbol{\alpha}_i^{(n)} \Psi_i^T \left(\mathbf{u}_i^{(n)} \odot \mathbf{I}_i^{-\frac{1}{2}} \right)$
  $\mathbf{v}^{(n)} \leftarrow \tilde{\mathbf{v}}_0^{(n)} + \sum_{i=1}^N \tilde{\mathbf{v}}_i^{(n)} - \boldsymbol{\alpha}_i^{(n)} \left\langle \tilde{\mathbf{v}}_i^{(n)}, \mathbf{c}^{(n)} \right\rangle \mathbf{a}_i$ /* gradient */
  $\tilde{\mathbf{c}}^{(n)} \leftarrow \mathbf{v}^{(n)} \odot \mathbf{c}^{(n)}$ /* descent direction */
  for $i \leftarrow 0, \ldots, N$ **do** $\tilde{\boldsymbol{\alpha}}_i^{(n)} \leftarrow \frac{1}{\mathbf{a}_i^T \tilde{\mathbf{c}}^{(n)}}$
  $\tilde{\mathbf{u}}_0^{(n)} \leftarrow \tilde{\boldsymbol{\alpha}}_0^{(n)} \mathbf{w}_{\lambda,s} \odot \mathcal{F}_{\mathbf{g},L} \tilde{\mathbf{c}}^{(n)}$
  for $i \leftarrow 1, \ldots, N$ **do** $\tilde{\mathbf{u}}_i^{(n)} \leftarrow \left(\tilde{\boldsymbol{\alpha}}_i^{(n)} \Psi_i \tilde{\mathbf{c}}^{(n)} + \mathbf{I}_i^b - \mathbf{I}_i\right) \odot \mathbf{I}_i^{-\frac{1}{2}}$
  $\tau_{\max}^{(n)} \leftarrow \min_{m=1,\ldots,M} \left\{ -\frac{\mathbf{c}_m^{(n)}}{\tilde{\mathbf{c}}_m^{(n)}} \;\middle|\; \tilde{\mathbf{c}}_m^{(n)} < 0, m = 1, \ldots, M \right\}$
  $\tau^{(n)} \leftarrow \mathrm{LineSearch}\left(\tau_{\max}^{(n)}, \boldsymbol{\alpha}_i^{(n)}, \tilde{\boldsymbol{\alpha}}_i^{(n)}, \mathbf{u}_i^{(n)}, \tilde{\mathbf{u}}_i^{(n)}, i = 0, \ldots, N\right)$
  $\mathbf{c}^{(n)} \leftarrow \mathbf{c}^{(n)} + \tau^{(n)} \tilde{\mathbf{c}}^{(n)}$ /* update solution */
  for $i \leftarrow 0, \ldots, N$ **do** $\mathbf{u}_i^{(n)} \leftarrow \frac{\tilde{\boldsymbol{\alpha}}_i^{(n)}}{\tau^{(n)} \boldsymbol{\alpha}_i^{(n)} + \tilde{\boldsymbol{\alpha}}_i^{(n)}} \mathbf{u}_i^{(n)} + \frac{\tau^{(n)} \boldsymbol{\alpha}_i^{(n)}}{\tau^{(n)} \boldsymbol{\alpha}_i^{(n)} + \tilde{\boldsymbol{\alpha}}_i^{(n)}} \tilde{\mathbf{u}}_i^{(n)}$
  for $i \leftarrow 0, \ldots, N$ **do** $\boldsymbol{\alpha}_i^{(n)} \leftarrow \frac{\boldsymbol{\alpha}_i^{(n)} \tilde{\boldsymbol{\alpha}}_i^{(n)}}{\tau^{(n)} \boldsymbol{\alpha}_i^{(n)} + \tilde{\boldsymbol{\alpha}}_i^{(n)}}$
  $n \leftarrow n + 1$
end
$\mathbf{c} \leftarrow \mathbf{c}^{(n)}$

In lines 8 – 10 the gradient of the functional J in $\mathbf{c}^{(n)}$ is calculated according to Lemma 5.13. This essentially requires the matrix vector multiplications $\Psi_i^T \mathbf{u}_i^{(n)}$, $i = 1, \dots, N$, which have the numerical complexity $\mathcal{O}(N_i + M + L^3 \log^2 L)$.

In line 11 the modified descent direction of the MSD – algorithm is calculated according to equation (5.15).

In lines 12 – 14 the updates $\tilde{\mathbf{u}}_i^{(n)}$ and $\tilde{\boldsymbol{\alpha}}_i^{(n)}$, $i = 1, \dots, N$ of the residuals and the normalization coefficients are calculated (cf. Definition 5.11). Again this requires the matrix vector multiplications $\Psi_i \mathbf{c}$, $i = 1, \dots, N$.

In lines 15 and 16 the step size is calculated using Algorithm 4 and the initial step length as approved in Lemma 5.16.

The updating of the coefficient vector is done in line 17. Whereas the residuals and the normalization coefficients are updated in lines 18 and 19 (cf. Proposition 5.12).

We conclude that a single iteration of algorithm 5 has numerical complexity $\mathcal{O}(\bar{N} + M + L^3 \log^2 L)$. □

Calculations on the Estimated ODF. Once an estimate of the true ODF has been calculated one is typically interested in several characteristics of this estimate, e.g. its pointwise evaluation for specific orientations, the pointwise evaluation of the corresponding PDF for specific crystal and specimen directions, the calculation of its Fourier coefficients, or its convolution with a radially symmetric function on SO(3). We gave a fast algorithm for the calculation of the Fourier coefficients of the estimated ODF in Proposition 5.3. Combining this algorithm with the fast Fourier transform on SO(3) we obtained in Corollary 5.4 fast algorithms for the pointwise evaluation of the ODF and its convolution with a radially symmetric function. Pointwise evaluation of the corresponding PDF was already described in Lemma 5.10.

5.4 Numerical Tests

In this section we are going to perform some basic tests on the convergence and robustness of Algorithm 5. A second goal is to study the interplay between the estimation error, the arbitrary parameters of Algorithm 5, and the parameters of the PDF–to–ODF inversion problem itself (cf. Table 4.1).

The Default Setting. For a concise representation we first define three sample ODFs and a default setting for the PDF–to–ODF inversion problem and alter this setting gradually in the subsequent paragraphs to analyze the specific impact of single parameters.

The first sample ODF f_1 is defined as a composition of two Abel–Poisson radially symmetric functions with halfwidth 12° and halfwidth 6°, respectively and follows orthorhombic crystal symmetry, i.e.

$$S_{\text{Laue}} = S_{\text{orth}} = \langle -\text{Id}, \text{Rot}_{\mathbf{e}_1}(\pi), \text{Rot}_{\mathbf{e}_2}(\pi) \rangle .$$

Sample ODF f_1		component 1		component 2	
crystal symmetry	orth.	kernel	Abel–Poisson	kernel	Abel–Poisson
specimen symmetry	triclinic	halfwidth	12°	halfwidth	6°
uniform portion	0	center	Id	center	$\mathrm{Rot}_{\mathbf{e}_3}(25°)$
texture components	2	weight	5	weight	1

Sample ODF f_2		component 1		component 2	
crystal symmetry	orth.	kernel	v. M. Fischer	kernel	v. M. Fischer
specimen symmetry	triclinic	halfwidth	7°	halfwidth	3°
uniform portion	0	center	Id	center	$\mathrm{Rot}_{\mathbf{e}_1}(10°)$
texture components	2	weight	10	weight	1

Sample ODF f_3		component 1	
crystal symmetry	trigonal	kernel	fibre v. M. Fischer
specimen symmetry	triclinic	halfwidth	7°
uniform portion	0	center	$G(\mathbf{e}_1, \mathbf{e}_1)$

Table 5.1: The parameters of the three sample ODFs f_1, f_2 and f_3.

Here we have again used the notation $G = \langle \mathbf{g}_1, \ldots, \mathbf{g}_N \rangle$ for the group G generated by the elements $\mathbf{g}_1, \ldots, \mathbf{g}_N$. The second sample ODF f_2 follows the same crystal symmetry but consists of two von Mises–Fischer radially symmetric components with halfwidth 7° and halfwidth 3°, respectively. The third sample ODF f_3 follows trigonal crystal symmetry, i.e. the corresponding Laue group is

$$S_{\mathrm{Laue}} = S_{\mathrm{trig}} = \left\langle -\mathrm{Id}, \mathrm{Rot}_{\mathbf{e}_3}(\tfrac{2\pi}{3}), \mathrm{Rot}_{\mathbf{e}_1}(\pi) \right\rangle,$$

and is fibre symmetric. More precisely, we have

$$f_3(\mathbf{g}) = \frac{\kappa}{\sinh \kappa} \exp\bigl(\kappa \cos \measuredangle(\mathbf{g}\mathbf{e}_1, \mathbf{e}_1)\bigr), \quad \mathbf{g} \in \mathrm{SO}(3).$$

The function f_3 is called *fibre von Mises–Fischer kernel* (cf. Schaeben and v.d. Boogaart, 2003). For the third sample ODF f_3 we have fixed the free parameter κ such that the halfwidth of f_3 is 7°. A summary of all three sample ODFs is given in Table 5.4. Displays of their graphs can be found in the appendix in the Figures A.7, A.8, and A.9.

In order to simulate a diffraction experiment we have to specify all the parameters listed in Table 4.1. Having no specific practical setting in mind we choose $N = 7$ crystal directions

$$\mathbf{h} = \left(\begin{pmatrix} 1 \\ 0 \\ 0 \end{pmatrix}, \begin{pmatrix} 0 \\ 1 \\ 0 \end{pmatrix}, \begin{pmatrix} 0 \\ 0 \\ 1 \end{pmatrix}, \begin{pmatrix} 1 \\ 1 \\ 0 \end{pmatrix}, \begin{pmatrix} 1 \\ 0 \\ 1 \end{pmatrix}, \begin{pmatrix} 0 \\ 1 \\ 1 \end{pmatrix}, \begin{pmatrix} 1 \\ 1 \\ 1 \end{pmatrix} \right)$$

and assume that the corresponding diffraction intensities do not interfere with other crystal directions, i.e. $H_i = S_{\text{Laue}}\mathbf{h}_i$, $i = 1, \dots, 7$. For each fixed specimen direction $\mathbf{h}_i \in \mathbb{S}^2$ we construct a grid of $N_i = 13,201$ specimen directions $\mathbf{r}_i = (\mathbf{r}_{i1}, \dots, \mathbf{r}_{iN_i})$ that forms an equidistribution on the hemisphere $\mathbb{S}^2_+$ such that the distance between two neighboring nodes is about 1.25° (cf. Freeden, 1998, Example 7.1.9). We say grid $\mathbf{r}$ has the resolution $\delta = 1.25°$. Neglecting measurement errors we simulate diffraction counts $\mathbf{I} \in \mathbb{R}^{\bar{N}}$ by setting

$$\mathbf{I}_{ij} = \mathcal{X} f(H_i, \mathbf{r}_{ij}), \quad i = 1, \dots, N,\ j = 1, \dots, N_i,$$

where f is one of the three sample ODFs f_1, f_2 or f_3. In particular, we set $\boldsymbol{\alpha}_i = 1$ and $\mathbf{I}^b_{ij} = 0$, $i = 1, \dots, N$, $j = 1, \dots, N_i$. The simulated diffraction counts $\mathbf{I}_1, \dots, \mathbf{I}_7$ of the three sample ODFs are plotted in the Figures A.1,A.2, and A.3.

Finally, we have to specify the default values for the parameters of Algorithm 5, as they are the discretisation $V(\mathbf{g}, \psi)$ (cf. Definition 5.5), the default regularization parameters $\lambda, s \in \mathbb{R}$ (cf. Proposition 5.7) and the convergence criterion.

Let us fix $s = 2$. Then we choose for the discretisation $V(\mathbf{g}, \psi)$ of $\mathcal{H}_s(\mathrm{O}(3)/S_{\text{Laue}})$ an equidistribution $\mathbf{g} = (\mathbf{g}_1, \dots, \mathbf{g}_M)$ on $\mathrm{O}(3)/S_{\text{Laue}}$ with a resolution of $\delta = 2.5°$. In the case of orthorhombic crystal symmetry the grid $\mathbf{g}$ contains $M = 237,600$ nodes and in the case of trigonal crystal symmetry it contains $M = 158,400$ nodes. As the ansatz function $\psi\colon \mathrm{SO}(3) \to \mathbb{R}$ we chose the de la Vallée Poussin kernel with halfwidth $b = 1.875°$ restricted to the bandwidth $L = 325$.

Since we work with exact data in the default setting we do not apply regularization be default but set $\lambda = 0$. As convergence criteria we use the criterion to stop if 32 iterations has been exceeded or if the relative improvement of the residual error becomes less then the largest relative improvement that occurred so far in the iteration process divided by 100, i.e. if

$$\frac{\|\mathbf{u}^{(n-1)}\|^2 - \|\mathbf{u}^{(n)}\|^2}{\|\mathbf{u}^{(n)}\|^2} < 10^{-4} \max_{k=1,\dots,n-1} \frac{\|\mathbf{u}^{(k-1)}\|^2 - \|\mathbf{u}^{(k)}\|^2}{\|\mathbf{u}^{(k)}\|^2}.$$

The complete list of all default parameters is given in Table 5.2.

Convergence. First of all we are going to check Algorithm 5 for convergence. As a measure of the estimation error between the true ODF and the estimated ODF we propose the following quantity.

Definition 5.18. Let $f_{\text{true}}, f_{\text{est}} \in L^1(\mathrm{O}(3)/S_{\text{Laue}})$ be the true and the estimated ODF, respectively. Then we define the *estimation error* $\varepsilon(f_{\text{true}}, f_{\text{est}})$ as

$$\varepsilon(f_{\text{true}}, f_{\text{est}}) = \frac{1}{32\pi^2} \int_{\mathrm{O}(3)} |f_{\text{true}}(\mathbf{g}) - f_{\text{est}}(\mathbf{g})| \, \mathrm{d}\mathbf{g}. \tag{5.24}$$

parameter	default value
number of pole figures	$N = 7$
number of specimen directions	$N_i = 13201$, $i = 1, \dots, N$
crystal directions	$\mathbf{h} = \left(\begin{pmatrix}1\\0\\0\end{pmatrix}, \begin{pmatrix}0\\1\\0\end{pmatrix}, \begin{pmatrix}0\\0\\1\end{pmatrix}, \begin{pmatrix}1\\1\\0\end{pmatrix}, \begin{pmatrix}1\\0\\1\end{pmatrix}, \begin{pmatrix}0\\1\\1\end{pmatrix}, \begin{pmatrix}1\\1\\1\end{pmatrix}\right)$
superposition of crystal directions	$H_i = S_{\text{Laue}}\mathbf{h}_i$, $i = 1, \dots, N$
specimen directions	$\mathbf{r}$ = equidistribution on $\mathbb{S}^2_+$, resolution 1.25°
diffraction counts	$\mathbf{I}_{ij} = \mathcal{X}f(\mathbf{h}_i, \mathbf{r}_{ij})$
background intensities	$\mathbf{I}^b_{ij} = 0$, $i = 1, \dots, N$, $j = 1, \dots, N_i$
normalization coefficients	$\boldsymbol{\alpha}_i = 0$, $i = 1, \dots, N$,
discretisation of $\mathrm{O}(3)/S_{\text{Laue}}$	$\mathbf{g}$ = equidistribution on $\mathrm{SO}(3)/S_{\text{Laue}}$, resolution 2.5°
ansatz function	ψ = de la Vallée Poussin kernel, $b = 1.875°$
bandwidth	$\mathrm{L} = 325$
regularization parameter	$\lambda = 0$

Table 5.2: Default parameters of the numerical experiments.

Remark 5.19. The estimation error $\varepsilon(f_{\text{true}}, f_{\text{est}})$ can be interpreted as the percentage of mass that is dislocated between the two density functions f_{true} and f_{est}. In particular, we have

$$0 \leq \varepsilon(f_{\text{true}}, f_{\text{est}}) \leq 1,$$

and $\varepsilon(f_{\text{true}}, f_{\text{est}}) = 0$ if and only if the ODFs f_{true} and f_{est} are identical and $\varepsilon(f_{\text{true}}, f_{\text{est}}) = 1$ if and only if they have disjoint support.

In our numerical tests we do not calculate the estimation error $\varepsilon(f_{\text{true}}, f_{\text{est}})$ exactly but evaluate f_{true} and f_{est} at an equidistribution on $\mathrm{O}(3)/S_{\text{Laue}}$ with resolution 1.25° and approximate the integral in equation (5.24) by a quadrature formula. Furthermore, we do not apply the fast algorithms based on the fast Fourier transform on SO(3) as described in Corollary 5.4 for the evaluation of the functions f_{true} and f_{est} but use the direct algorithm.

Beside the weighted residual norm

$$\mathrm{RN} = \|\mathbf{I}\|_1^{-1} \left(\sum_{i=1}^{N} \left\| [\boldsymbol{\alpha}_{\text{est}}]_i \mathcal{X} f_{\text{est}}(H_i, \mathbf{r}_i) + \mathbf{I}^b_i - \mathbf{I}_i \right\|^2_{\mathbf{I}_i^{-1}} \right)^{\frac{1}{2}}$$

that is minimized by Algorithm 5 for the default setting there is a second, in texture community more established measure for the goodness of fit between the estimated diffraction intensities and the measured diffraction counts.

Definition 5.20. Let $\mathbf{I} \in \mathbb{R}^{\bar{N}}$ be the measured diffraction counts with respect to the diffraction parameters as summarized in Table 4.1 and let $f_{\text{est}} \in C(\mathrm{O}(3)/S_{\text{Laue}})$ and

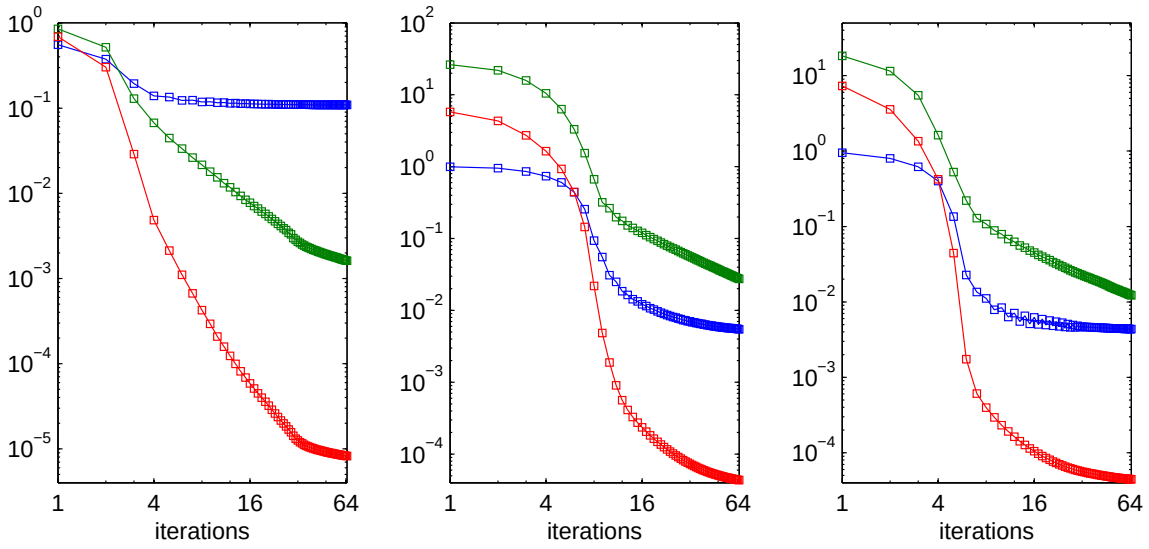

(a) sample ODF f_1 **(b)** sample ODF f_2 **(c)** sample ODF f_3

Figure 5.2: The estimation error $\varepsilon(f_{\text{true}}, f_{\text{est}})$ (blue graph), the weighted residual norm RN (red graph) and the RP values RP_μ, $\mu = 0.01$ (green graph) against the iteration steps of Algorithm 5.

$\boldsymbol{\alpha}_{\text{est}} \in \mathbb{R}_+^N$ be an estimated ODF and estimated normalization coefficients, respectively. Then for any $\mu > 0$ the RP_μ - value is defined as (cf. Matthies et al., 1987, sec. 14.4)

$$\text{RP}_\mu = \frac{1}{|V_\mu|} \sum_{(i,j)\in V_\mu} \frac{\left| [\boldsymbol{\alpha}_{\text{est}}]_i \mathcal{X} f_{\text{est}}(H_i, \mathbf{r}_i) + \mathbf{I}_i^b - \mathbf{I}_i \right|}{\mathbf{I}_i - \mathbf{I}_i^b} \tag{5.25}$$

where $V_\mu = \{\, (i,j) \mid i = 1,\dots,N,\ j = 1,\dots,N_i,\ \mathbf{I}_i - \mathbf{I}_i^b > [\boldsymbol{\alpha}_{\text{est}}]_i \mu \,\}$ and $|V_\mu|$ denotes the number of elements in V_μ.

The estimation error $\varepsilon(f_{\text{true}}, f_{\text{est}})$, the weighted residual norm RN and the RP values RP_μ, $\mu = 0.001$ are plotted in Figure 5.2 versus the iteration steps of Algorithm 5 applied to the default setting.

We mention that the estimation error for the sharp ODF f_2 is much smaller then for the weaker ODF f_1 which is conform to Section 4.4. Moreover, the decrease of the estimation error is very small between iteration 32 and iteration 64. This approves our restriction to the maximum iteration depth 32.

We have plotted the estimated ODFs in the Figures A.10, A.11, and A.12 in the Appendix A for a morphological comparison with the original ODFs.

Discretisation. In a second experiment we alter the parameters of the discretisation $V(\mathbf{g}, \psi)$ and keep track of the estimation error. Therefore we construct a list of equidistributions in $\text{O}(3)/S_{\text{Laue}}$ with resolution δ as given in Table 5.3a and vary the halfwidth

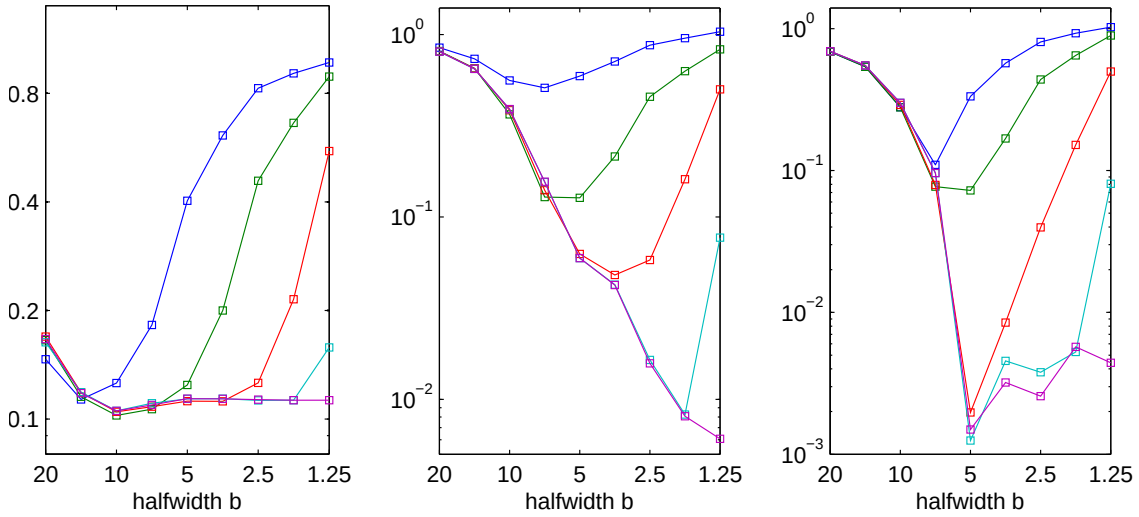

(a) sample ODF f_1 **(b)** sample ODF f_2 **(c)** sample ODF f_3

Figure 5.3: The estimation error in dependency of the discretisation parameters (b, δ). The blue graphs corresponds to $\delta = 20°$, the green graph to $\delta = 10°$, the red graph to $\delta = 5°$, the cyan graph to $\delta = 2.5°$ and the magenta graph to $\delta = 1.875°$.

b and the bandwidth L of the de la Vallée Poussin ansatz function ψ as described in Table 5.3b. The bandwidth L of the ansatz function ψ has been chosen such that for any $l > L$ the Chebyshev coefficients of ψ satisfy

$$\hat{\psi}(l) < 10^{-15}.$$

resolution δ (°)	20	10	5	2.5	1.875
number of nodes for S_{orth}	576	3,708	29,736	237,600	563,232
number of nodes for S_{trig}	384	2,472	19,824	158,400	375,488

(a) Parameters of the equidistribution $\mathbf{g} = (\mathbf{g}_1, \ldots, \mathbf{g}_M)$ in $\mathrm{O}(3)/S_{\text{Laue}}$.

halfwidth b (°)	20	15	10	7,5	5	3.75	2.5	1.875	1.25
bandwidth L	23	33	52	70	107	143	215	325	432

(b) Halfwidths and bandwidth of the ansatz function ψ.

Table 5.3: Tested discretisation parameters.

We calculate the estimation error for the three sample ODFs f_1, f_2, and f_3 for all combinations of the parameters (b, δ). The results are visualized in Figure 5.3.

One recognizes that for a fixed resolution δ of the grid $\mathbf{g}$ in $\mathrm{O}(3)/S_{\text{Laue}}$ the estimation error as a function of the halfwidth b of the ansatz function ψ is decreasing until $b \approx \frac{3}{2}\delta$

and increasing for $b > \frac{3}{2}\delta$. For $b < \frac{3}{2}\delta$ the halfwidth of the ansatz function ψ is clearly to small for a good approximation. For $b > \frac{3}{2}\delta$ we loose in approximation of sharp textures (cf. Figure 5.3b). For weak textures however, a halfwidth close to the actual halfwidth of the ODF components could result in a better estimations (cf. Figure 5.3a, 5.3c).

Noisy Data. Until to now we have tested Algorithm 5 for exact data only. According to Section 4.2 the measured intensity counts $\mathbf{I}_{ij}$ can be modeled as a random sample of the family of Poisson distributions

$$\mathcal{I}_{ij} = \mathrm{Poiss}\Big(\mathbf{I}^b_{ij} + [\boldsymbol{\alpha}_{\mathrm{true}}]_i \, \mathcal{X} f_{\mathrm{true}}(H_i, \mathbf{r}_{ij})\Big), \quad i = 1, \dots, N, j = 1, \dots, N, \tag{5.26}$$

which depend on the normalization coefficients $\boldsymbol{\alpha}_{\mathrm{true}} \in \mathbb{R}^N$ and the background intensities $\mathbf{I}^b_{ij} \in \mathbb{R}$.

Fixing the second sample ODF $f_{\mathrm{true}} = f_2$ as the as the true ODF we select normalization coefficients $[\boldsymbol{\alpha}_{\mathrm{true}}]_i$ and background intensities $\mathbf{I}^b_{ij}$, $i = 1, \dots, N$, $j = 1, \dots, N_i$ from the list $(10, 40, 60, 640, 2560)$ and simulate diffraction counts $\mathbf{I}_{ij} \in \mathbb{R}_+$ as random samples of the family of Poisson distributions (5.26). Applying Algorithm 5 to the simulated diffraction counts we obtain estimates of the second sample ODF f_2. The corresponding estimation errors are plotted in Figure 5.4a.

One recognizes that the estimation error decreases for decreasing background intensities and for increasing normalization coefficients. More interestingly, we note that the estimation error also decreases in the case that the background intensities and the normalization coefficients increase simultaneously. In practice this relates to the case that the measure time is increased.

Regularization. In Section 4.3 we have already discussed that the ODF estimation problem is ill–posed and hence regularization techniques are supposed to increase the accuracy of estimation. In the case of Algorithm 5 we have three independent sources regularization. First the implemented MLS ODF estimator itself includes explicit regularization which is controlled by the regularization parameter λ. A second origin of regularization is the chosen discretisation $V(\psi, \mathbf{g})$ as defined in Definition 5.5. Since $V(\psi, \mathbf{g})$ contains only linear combinations of translates of the ansatz function ψ with non–negative coefficients the halfwidth of ψ directly controls the smoothness of the functions in $V(\psi, \mathbf{g})$. Third the maximum iteration depth of Algorithm 5 can be interpreted as a regularization parameter.

In order to analyze the impact of these three independent sources of regularization we simulate noisy diffraction data as in the previous experiment, setting $[\boldsymbol{\alpha}_{\mathrm{true}}]_i = 10$, and $\mathbf{I}^b_{ij} = 2560$, $i = 1, \dots, N$, $j = 1, \dots, N_i$. We apply Algorithm 5 first using the default setting of parameters, second with the ansatz function ψ with halfwidth 2.5°, and third with explicit regularization enabled, i.e. with $\lambda = 10^{-4.25}$. The corresponding estimation errors are plotted in Figure 5.4b in dependency of the iteration count.

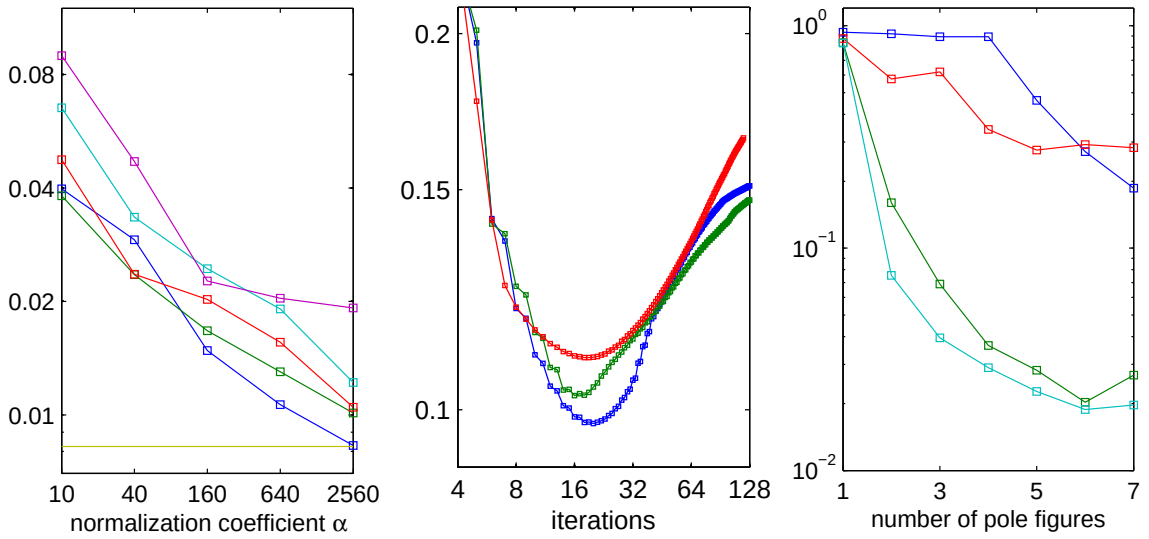

(a) noisy data **(b)** regularization **(c)** incomplete data

Figure 5.4: Plot (a) displays the estimation error in dependency of normalization coefficient α and the background intensity $\mathbf{I}^b$. The blue graph corresponds to $\mathbf{I}^b = 10$, the green graph to $\mathbf{I}^b = 40$, the red graph to $\mathbf{I}^b = 160$, the cyan graph to $\mathbf{I}^b = 640$, and the magenta graph to $\mathbf{I}^b = 2560$. The bottom yellow line corresponds to the estimation error for exact data. Plot (b) displays the estimation error in dependency of the iteration count for noisy data with $\boldsymbol{\alpha} = 10$ and $\mathbf{I}^b = 2560$. The blue line corresponds to the default setting without regularization, the green line corresponds to the default setting with regularization parameter $\lambda = 10^{-4.25}$, and the red line corresponds to the default setting but with halfwidth $b = 2.5°$ of the ansatz function. Plot (c) displays the estimation error in dependency of the number of pole figures and for the following configurations of specimen directions: blue graph – configuration A, green graph – configuration B, red graph – configuration C, and cyan graph – default configuration.

According to Figure 5.4b regularization by the maximum iteration depth leads to the best estimation error. However, it requires a much more detailed analysis to derive reliable results about the effect of regularization to Algorithm 5. The general problem of selecting an optimum regularization parameter has been exhaustively studied in literature (e.g. in Vogel, 2002; Wahba, 1990; Bernier and Miller, 2006).

Incomplete Data. In the next experiment we are going to apply Algorithm 5 to incomplete pole figure data, i.e. to configurations of specimen directions that do not provide a complete coverage of the hemisphere $\mathbb{S}^2_+$. For this purpose, we use three configurations that typically arise in practical diffraction experiments. Configuration A and B represent regular $1.25° \times 2.5°$ grids on the hemisphere that contain only specimen directions with $\theta < 80°$ or $\theta > 10°$, respectively. Configuration C contains 12,000 nodes at a resolution of $\delta = 1°$ and is taken from a real world diffraction experiment with an area detector (cf.

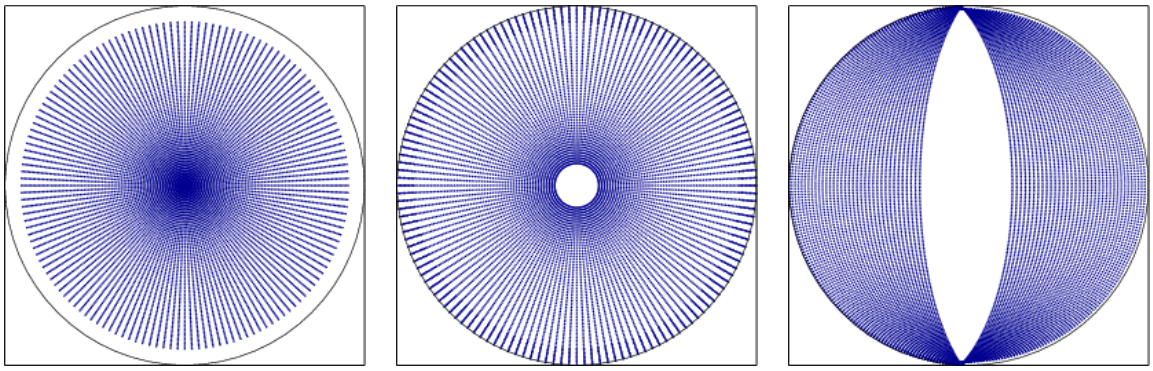

(a) configuration A **(b)** configuration B **(c)** configuration C

Figure 5.5: The three sample configuration of specimen directions.

Section 5.5). The three sample configurations A, B and C are visualized in Figure 5.5.

Next we simulate diffraction counts with respect to the configurations of specimen directions A, B, and C following the same recipe as in the previous experiment and setting the background intensities and the normalization coefficients to $\mathbf{I}^b_{ij} = [\boldsymbol{\alpha}_{\text{true}}]_i = 160$, $i = 1, \ldots, N$, $j = 1, \ldots, N_i$. We apply Algorithm 5 to the simulated diffraction data and reduce in a second step successively the number N of pole figures to be used by Algorithm 5. The resulting estimation errors in dependency of the number of pole figures and the specific configuration of specimen directions are plotted in Figure 5.4c. Additionally, the estimation error for the default configuration of specimen directions is plotted in dependency of the number of pole figures.

For configuration A the estimation error is close to one until the fifth pole figure has been included for ODF estimation. This is due to the fact that for configuration A the pole figures with respect to the crystal directions $\mathbf{e}_2, \ldots, \mathbf{e}_4$ are all empty, i.e. almost all the mass is concentrated in the regions that are not covered by configuration A (cf. Figure A.2). Consequently, the estimated ODF is concentrated along the fibre $G(\mathbf{e}_3, \mathbf{e}_3)$. The peaks of the fifth pole figure are located within the range of configuration A and hence the estimation error decreases.

In the case of configuration C the peaks of the second and the third pole figure are almost not contained in the diffraction data and hence the estimated ODF is concentrated along the fibre $G(\mathbf{e}_1, \mathbf{e}_1)$. In the case of configuration B only the peak of the third pole figure is not contained in the diffraction data and hence the first two pole figures already narrow the range of possible ODF.

Unknown Background Intensities. In texture analysis it is a well established practice to determine only the differences $\mathbf{I}^d_{ij} = \mathbf{I}_{ij} - \mathbf{I}^b_{ij}$ between the measured diffraction counts and the estimated background intensities. In order to apply Algorithm 5 to those data one can guess an arbitrary background intensity $\tilde{\mathbf{I}}^b = \tilde{\mathbf{I}}^b_{ij}$, $i = 1, \ldots, N$, $j = 1, \ldots, N_i$

and define diffraction counts $\tilde{\mathbf{I}}_{ij} = \mathbf{I}^d_{ij} + \tilde{\mathbf{I}}^b$, $i = 1, \dots, N$, $j = 1, \dots, N_i$.

In this paragraph we are going to check Algorithm 5 for its sensitivity against the guessed background intensity $\tilde{\mathbf{I}}^b$. For this purpose we simulate diffraction counts $\mathbf{I}_{ij}$ analogously to the previous experiments with normalization coefficients and background intensities given by $[\boldsymbol{\alpha}_{\text{true}}]_i = \mathbf{I}^b_{ij} = 160$, $i = 1, \dots, N$, $j = 1, \dots, N_i$. Based on these diffraction counts we calculate the differences $\mathbf{I}^d_{ij} = \mathbf{I}_{ij} - \mathbf{I}^b_{ij}$ and apply Algorithm 5 to the modified intensity counts $\tilde{\mathbf{I}}_{ij} = \mathbf{I}^d_{ij} + \tilde{\mathbf{I}}^b$ generated for guessed background intensities $\tilde{\mathbf{I}}^b = 1$, $\tilde{\mathbf{I}}^b = 40$, $\tilde{\mathbf{I}}^b = 160$, $\tilde{\mathbf{I}}^b = 640$ and $\tilde{\mathbf{I}}^b = 2560$. The estimation errors in dependency of the guessed background intensity $\tilde{\mathbf{I}}^b$ are given in Table 5.4.

guessed background intensity $\tilde{\mathbf{I}}^b$	1	40	160	640	2560	no weights
estimation error ε	0.215	0.125	0.020	0.025	0.030	0.045

Table 5.4: The estimations error in dependency of the guessed background intensity.

The last column corresponds to the minimizer of the functional

$$\tilde{J}(\mathbf{c}) = \sum_{i=1}^{M} \left\| \frac{\Psi_i \mathbf{c}}{\mathbf{c}^T \mathbf{a}_i} + \mathbf{I}^b_i - \mathbf{I}_i \right\|^2 + \left\| \frac{\mathcal{F}^H_{\mathbf{g},L} \mathbf{c}}{\mathbf{c}^T \mathbf{a}_0} \right\|^2_{\mathbf{w}^2_{\lambda,s}},$$

which differs from the functional minimized by Algorithm 5 by the absence of the weights $\mathbf{I}_i^{-1}$ in the first sum. In fact this is the functional that is minimized by the HHSM method (Bernier and Miller, 2006). We recognize that the weighted functional performs for the specific test problem at 50% better then the functional without weights. On the other hand it is quit sensitive against underestimated background intensities. The loss of accuracy due to an overestimated background intensity is less notable.

5.5 Applications

We end our study of the MLS ODF estimator with a short discussion of its application to two real world problems.

Area Detectors. The data for the first example were measured by Dr. U. Garbe at FRM II at the Technische Universität München. He analyzed an AL_3O_3 specimen with trigonal crystal symmetry using a neutron diffractometer and an area detector. He extracted diffraction counts corresponding to seven crystal directions and the configuration C of specimen directions as introduced in Section 5.4. This configuration contains 12,600 specimen directions at a resolution of one degree. The measured diffraction counts are plotted in Figure A.4a.

Since the diffraction counts suggest a weak texture we use the following rough discretisation. As the ansatz function ψ we choose the de la Vallée Poussin kernel with halfwidth

$b = 7.5°$ and as the grid $\mathbf{g}$ on $\mathrm{SO}(3)/S_{\mathrm{trig}}$ we choose an equidistribution with resolution $\delta = 10°$. With this settings we obtain after 10 iterations the RP value $\mathrm{RP}_\mu = 0.11$, $\mu = 0.001$. The recalculated pole figures are plotted in Figure A.4b.

Adapptive Measurements. The second example is based on explorations of Dr. J. J. Fundenberger on the texture of a Nigel specimen. He used a Siemens X–ray goniometer with point detector which allows for the measurement of the diffraction intensity for only one pair of crystal direction and specimen direction per measurement cycle. Since each measurement cycle takes up to ten second the measurement of a sharp texture at high resolution is a time critical problem. In the current experiment it were measured four pole figures with respect to the crystal directions (110), (200), (211) and (321) at a resolution of 1.25°. In contrast to ordinary measurements the grid of specimen directions was not chosen to be regularly distributed on the hemisphere, but to be clustered at regions of hight diffraction intensity and to be sparse at regions of low diffraction intensities. Compare to a regular $1.25° \times 1.25°$ grid the irregular grid contains only one fourth of the specimen directions and hence only one fourth of the measuring cycles are required. The irregular grid was constructed adaptively during the measurement process. The measured diffraction counts are plotted in Figure A.5.

For ODF estimation we fix an almost uniform grid of rotations $\mathbf{g}$ in $\mathrm{O}(3)/S_{\mathrm{cub}}$ with a resolution of 1.875°. Here the Laue group S_{cub} describes cubic crystal symmetry defined as

$$S_{\mathrm{Laue}} = S_{\mathrm{space}} = \left\langle -\mathrm{Id}, \mathrm{Rot}_{\mathbf{e}_1}(\tfrac{\pi}{2}), \mathrm{Rot}_{\mathbf{e}_1+\mathbf{e}_2+\mathbf{e}_3}(\tfrac{2\pi}{3}), \mathrm{Rot}_{\mathbf{e}_1+\mathbf{e}_2}(\pi) \right\rangle .$$

Together with the ansatz function ψ chosen as the de la Vallée Poussin kernel with halfwidth 1.25° restricted to bandwidth $L = 432$ the pair $(\mathbf{g}, \psi)$ defines the discretisation $V(\mathbf{g}, \psi)$ (cf. Definition 5.5). Using this discretisation we apply Algorithm 5 to the measured diffraction counts.

The RP value for the recalculated pole figures is $\mathrm{RP}_\mu = 0.19$, $\mu = 0.001$. Independently from the (110), (200), (211) and (321) pole figures J. Fundenberger has also measured the $(2, 2, 2)$ and $(3, 1, 0)$ pole figures. This time however for a regular $1.25° \times 2.5°$ grid of specimen directions. The corresponding diffraction intensities are plotted in Figure A.6b and can be compared with the pole figures recalculated from the estimated ODF which are plotted in Figure A.6a.

A PDF and ODF Plots

PDF Plots. Let $P \in C(\mathbb{S}^2/S_{\text{Laue}} \times \mathbb{S}^2)$ be an ODF with respect to the Laue group $S_{\text{Laue}} \subseteq \mathrm{O}(3)$. Then by Remark 3.25 each pole figure $P(\mathbf{h}, \circ) \in C(\mathbb{S}^2)$, $\mathbf{h} \in \mathbb{S}/S_{\text{Laue}}$ is an even function and hence it is sufficient to plot $P(\mathbf{h}, \mathbf{r})$ only for specimen directions $\mathbf{r} \in \mathbb{S}^2_+$ in the upper hemisphere. This requires a projection of the hemisphere $\mathbb{S}^2_+$ to the two dimensional plane. In this thesis we make use of the so called *equal area projection* defined by

$$\Pi \colon \mathbb{S}^2_+ \to \mathbb{R}^2, \quad (\theta, \rho) \mapsto \begin{pmatrix} \cos\rho\sqrt{2(1-\cos\theta)} \\ \sin\rho\sqrt{2(1-\cos\theta)} \end{pmatrix}, \tag{A.1}$$

which is also called *Schmidt projection* (cf. Bigalke, 1984, Sec. 5.5). According to the equal area projection the upper hemisphere is projected onto a circle in the two dimensional plane such that the specimen direction $\mathbf{e}_3 \in \mathbb{S}^2$ corresponds to its center, and the specimen directions $\mathbf{e}_1, \mathbf{e}_2 \in \mathbb{S}^2$ to the right and upper most points of the circle, respectively.

The color coding of the plotted pole figures we choose such that low values of P correspond to blue colors and high values of P correspond to red colors. The maximum and the minimum value of each pole figure is specified in the bottom line of each plot. The crystal direction relative to which the pole figure is plotted is specified in the upper left corner.

In the case of measured or simulated diffraction counts each data point $\mathbf{I}_{ij}$ corresponding to $P(\mathbf{h}_i, \mathbf{r}_{ij})$, $i = 1, \ldots, N$, $j = 1, \ldots, N_j$ is represented by a single dot at position $\Pi(\mathbf{r}_{ij}) \in \mathbb{R}^2$ with the corresponding color. In the case of pole figures calculated from an estimated ODF interpolated plots are given.

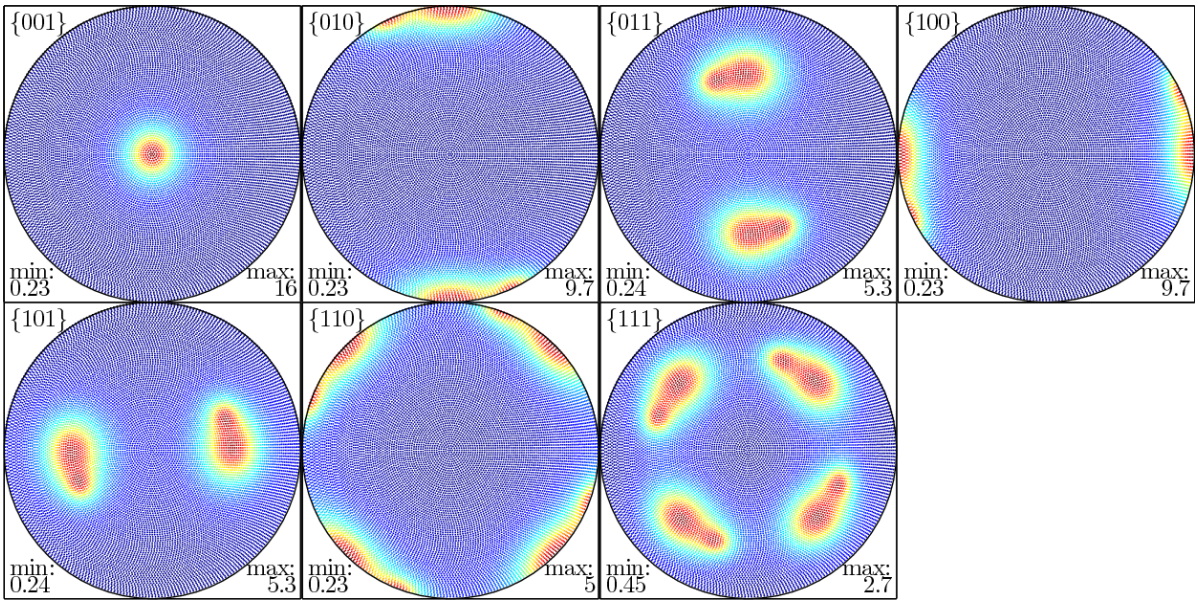

Figure A.1: Simulated diffraction counts of the sample ODF f_1 with respect to the default setting.

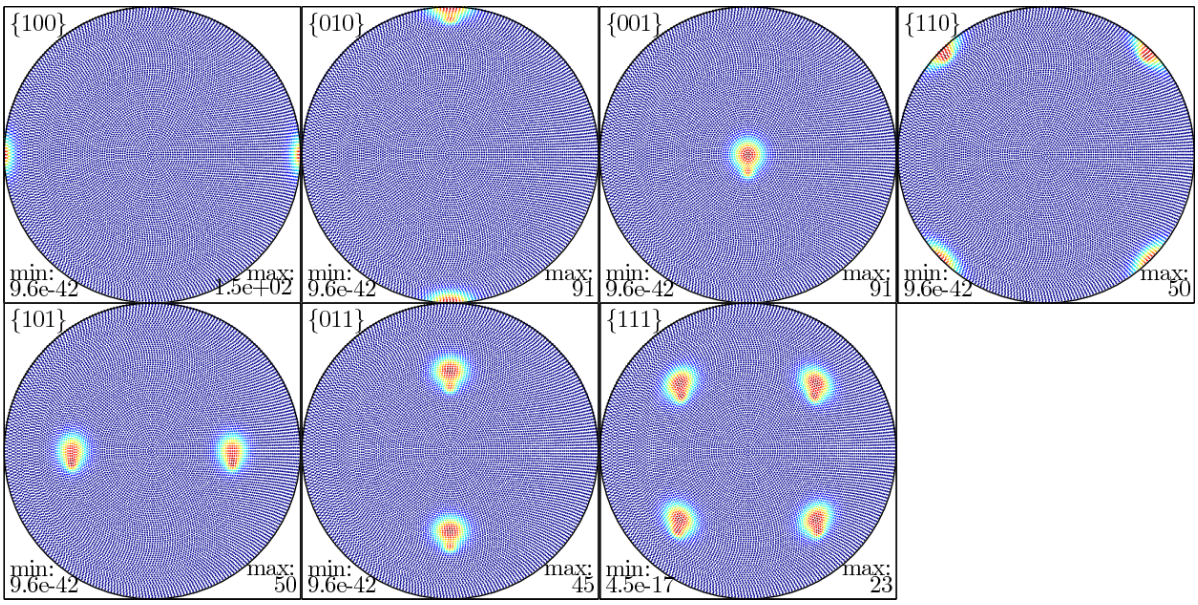

Figure A.2: Simulated diffraction counts of the sample ODF f_2 with respect to the default setting.

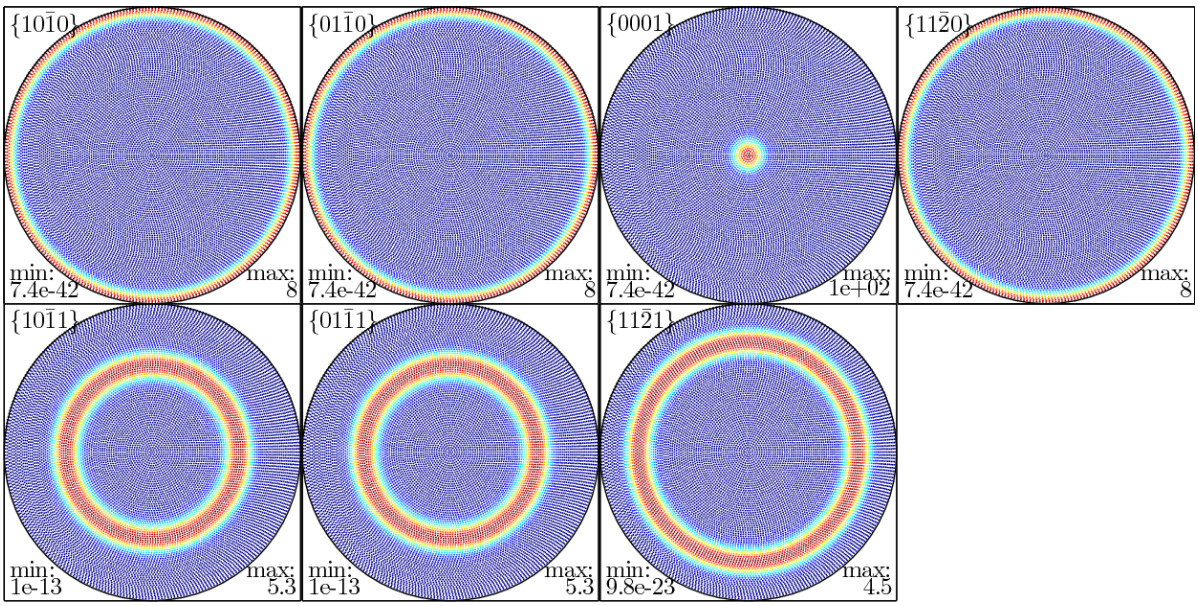

Figure A.3: Simulated diffraction counts of the sample ODF f_3 with respect to the default setting.

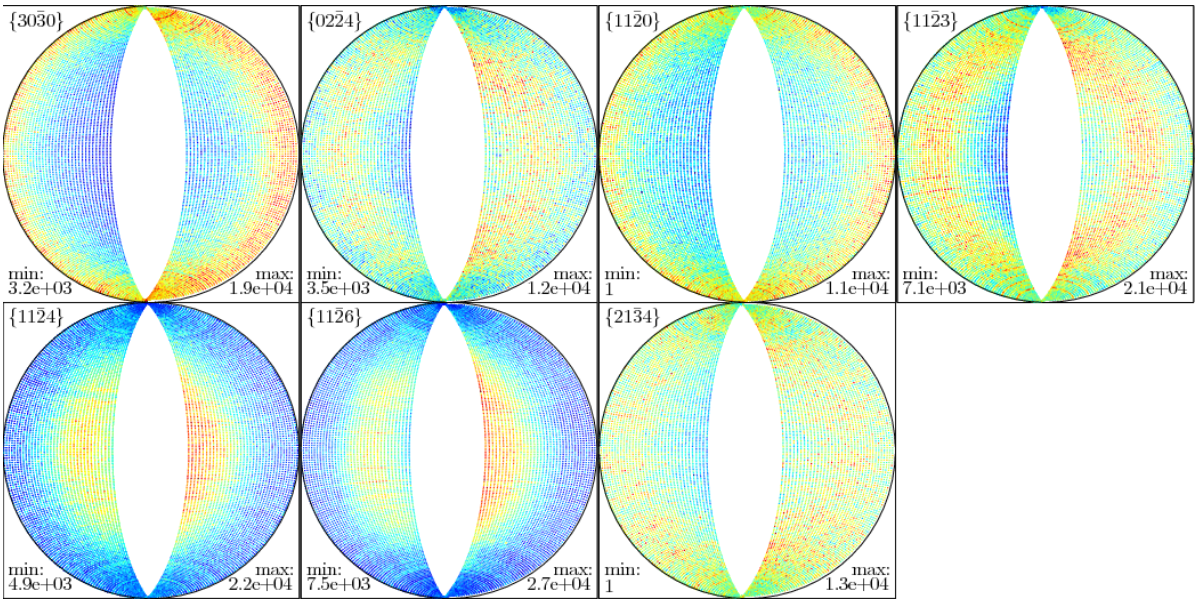

(a) Measured diffraction counts.

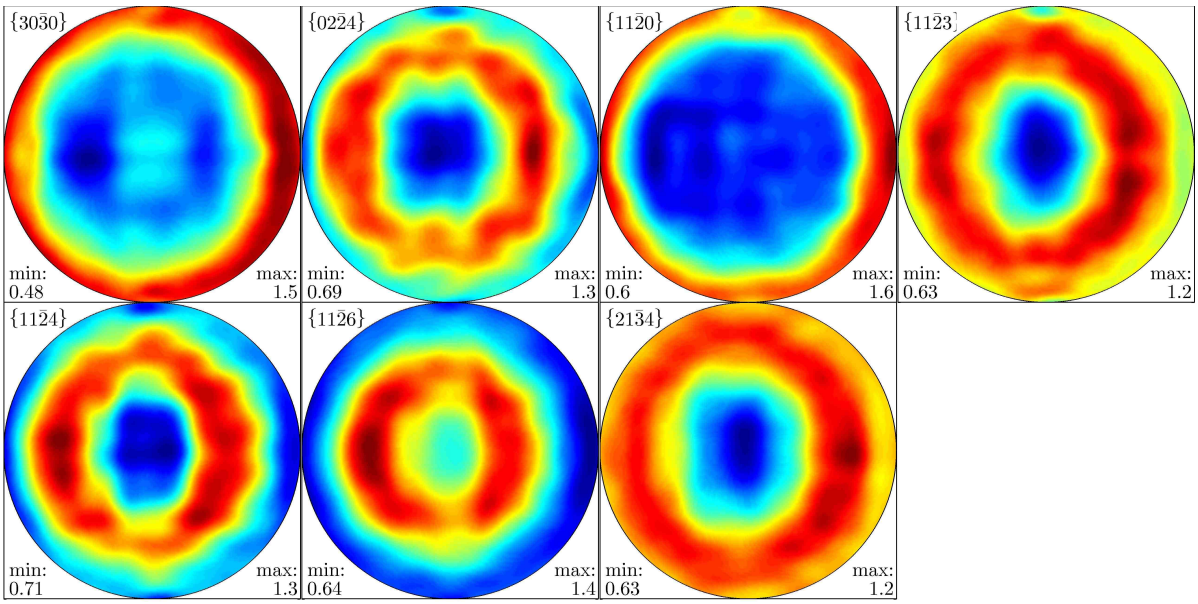

(b) Recalculated pole figures.

Figure A.4: Diffraction counts of an AL_3O_3 specimen with trigonal crystal symmetry measured by U. Garbe at FRM II at the Technische Universität München using a neutron diffractometer and an area detector (Figure (a)) and pole figures calculated from the ODF which was obtained by applying Algorithm 5 to the above diffraction data (Figure (b)).

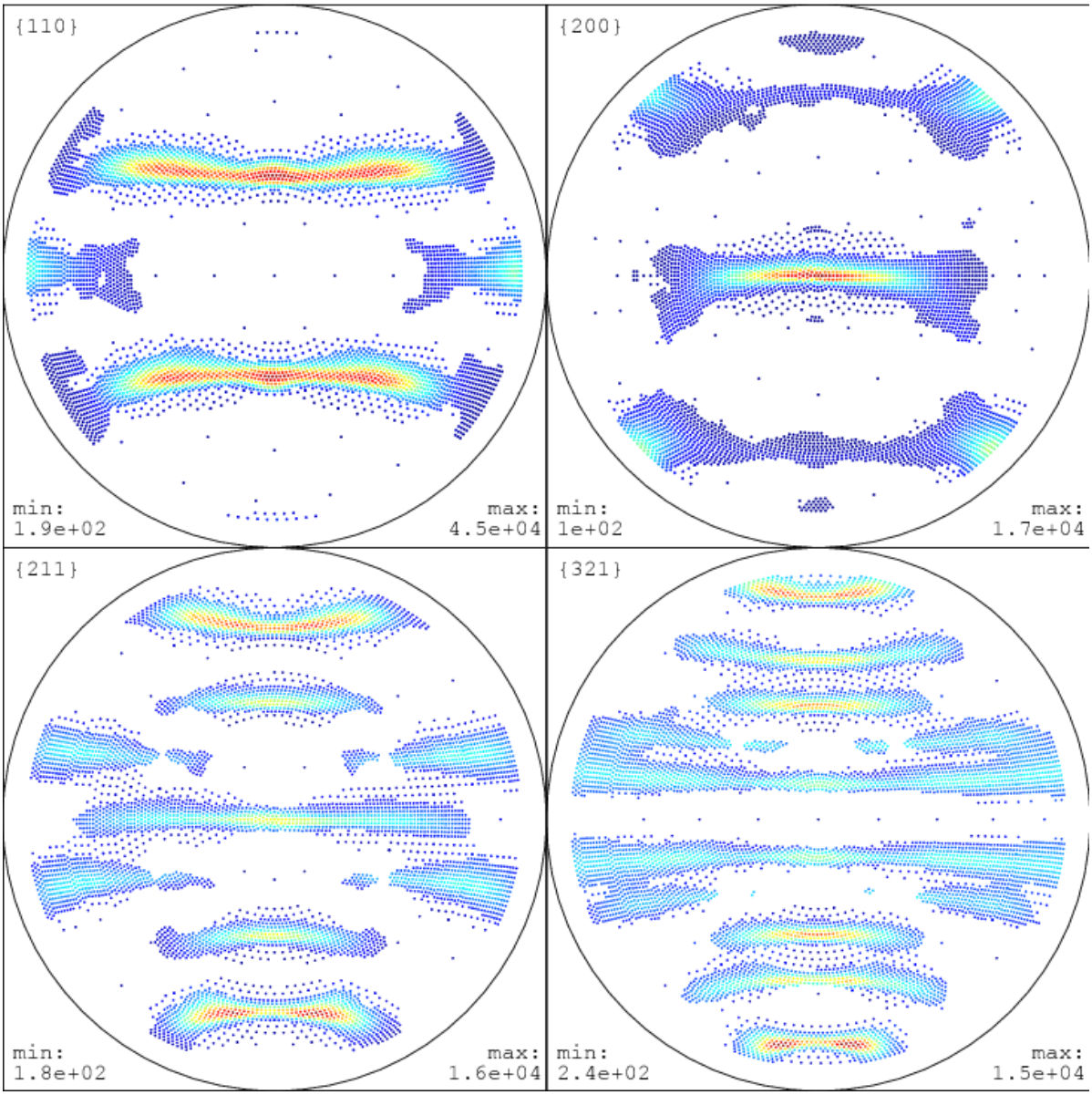

Figure A.5: Diffraction counts of a Nickel specimen with cubic crystal symmetry measured at an adaptively constructed grid of specimen directions by J. J. Fundenberger at the laboratoire détude des textures et application aux materiaux at Metz using an X-ray goniometer and a point detector.

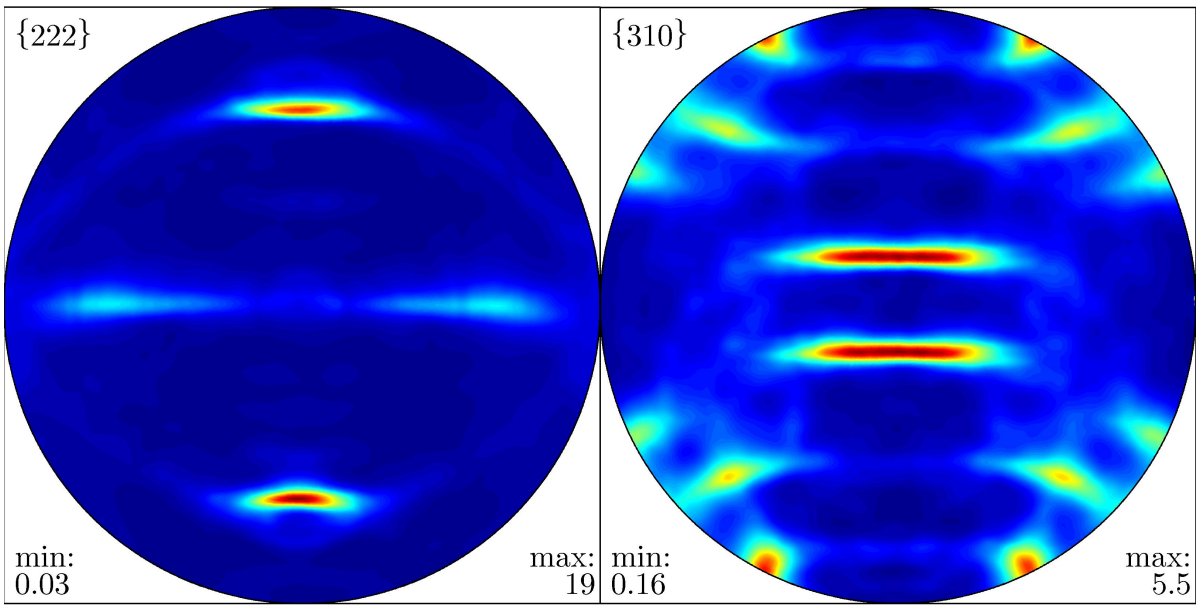

(a) Recalculated pole figures.

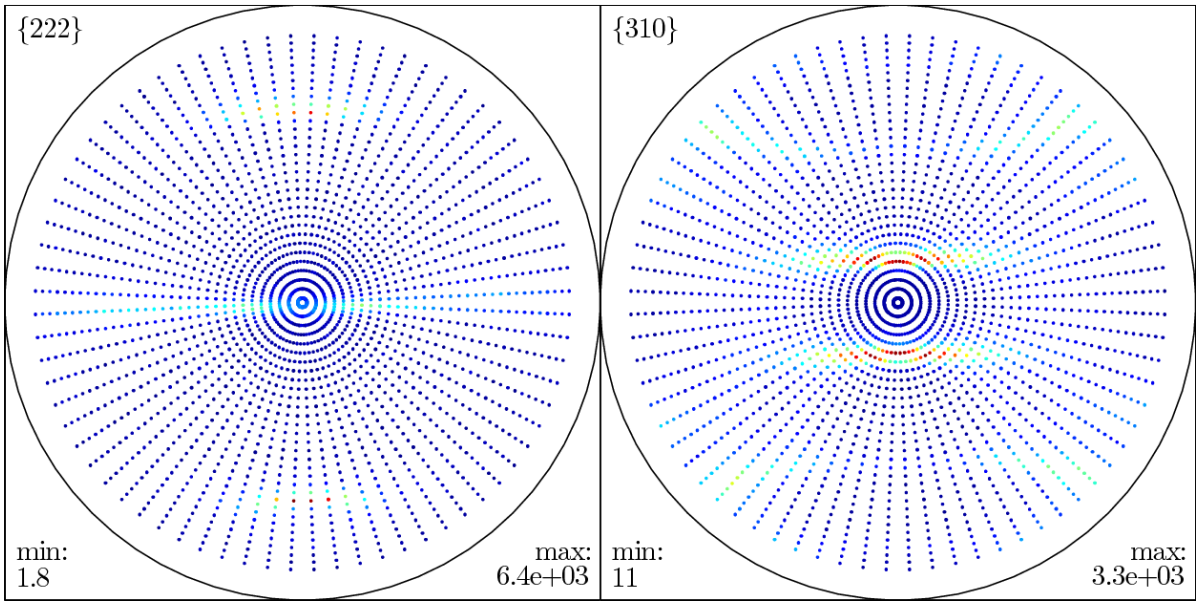

(b) Independently measured diffraction counts.

Figure A.6: Pole figures of the Nickel specimen measured by J. Fundenberger with respect of the crystal directions {222} and {310}. Figure (a) shows pole figures calculated from an ODF which was obtained by applying Algorithm 5 to the diffraction counts plotted in Figure A.5. Figure (b) shows the diffraction counts of an independent measurement of the same Nickel specimen but with a conventional configuration of specimen directions.

ODF Plots. In order to visualize an ODF $f\colon \mathrm{O}(3)/S_{\mathrm{Laue}} \to \mathbb{R}$ we plot sections of f along two dimensional submanifolds of SO(3). Let

$$\mathbf{g} = \mathrm{Rot}_{\mathbf{e}_3}(\alpha)\mathrm{Rot}_{\mathbf{e}_2}(\beta)\mathrm{Rot}_{\mathbf{e}_3}(\gamma)$$

be the Euler angle parameterization of the rotation $\mathbf{g} \in \mathrm{SO}(3)$. Then the angles (β, α) are the polar coordinates of the vector $\mathbf{g}\mathbf{e}_3 \in \mathbb{S}^2$ and the angle $\sigma = \alpha + \gamma$ describes the rotation of the vectors $\mathbf{g}\mathbf{e}_1$ and $\mathbf{g}\mathbf{e}_2$ relative to the vectors $\mathbf{e}_1$ and $\mathbf{e}_2$ in the $\mathbf{e}_1$-$\mathbf{e}_2$ plane. The sets

$$\Omega_\sigma = \{\, \mathbf{g} = \mathrm{Rot}_{\mathbf{e}_3}(\alpha)\mathrm{Rot}_{\mathbf{e}_2}(\beta)\mathrm{Rot}_{\mathbf{e}_3}(\gamma) \;\mid\; \alpha + \gamma = \sigma \,\}, \quad \sigma \in [0, 2\pi)$$

splits the three-dimensional manifold SO(3) into disjoint two-dimensional submanifolds, the so called σ-sections (cf. Helming et al., 1987).

In order to plot the ODF $f\colon \mathrm{SO}(3) \to \mathbb{R}$ we fix discrete values $\sigma = \sigma_1, \ldots, \sigma_K$ and plot the restrictions of f to the σ-sections Ω_{σ_k}, $k = 1, \ldots, K$ using the equal area projection with respect to the free variable (β, α). In fact, since (β, α) are the polar coordinates of $\mathbf{g}\mathbf{e}_3$ the plots of the σ-sections can be interpreted as the $\mathbf{e}_3$-pole figure of f split according the value of σ.

In the case of orthorhombic crystal symmetry σ-sections are plotted for $\sigma = 0°, 9°, \ldots, 171°$ and in the case of trigonal crystal symmetry for $\sigma = 0°, 6°, \ldots, 114°$. The value of σ is indicated in upper left corner of each plot. The color coding of the plots is handled analogously to the pole figure plots.

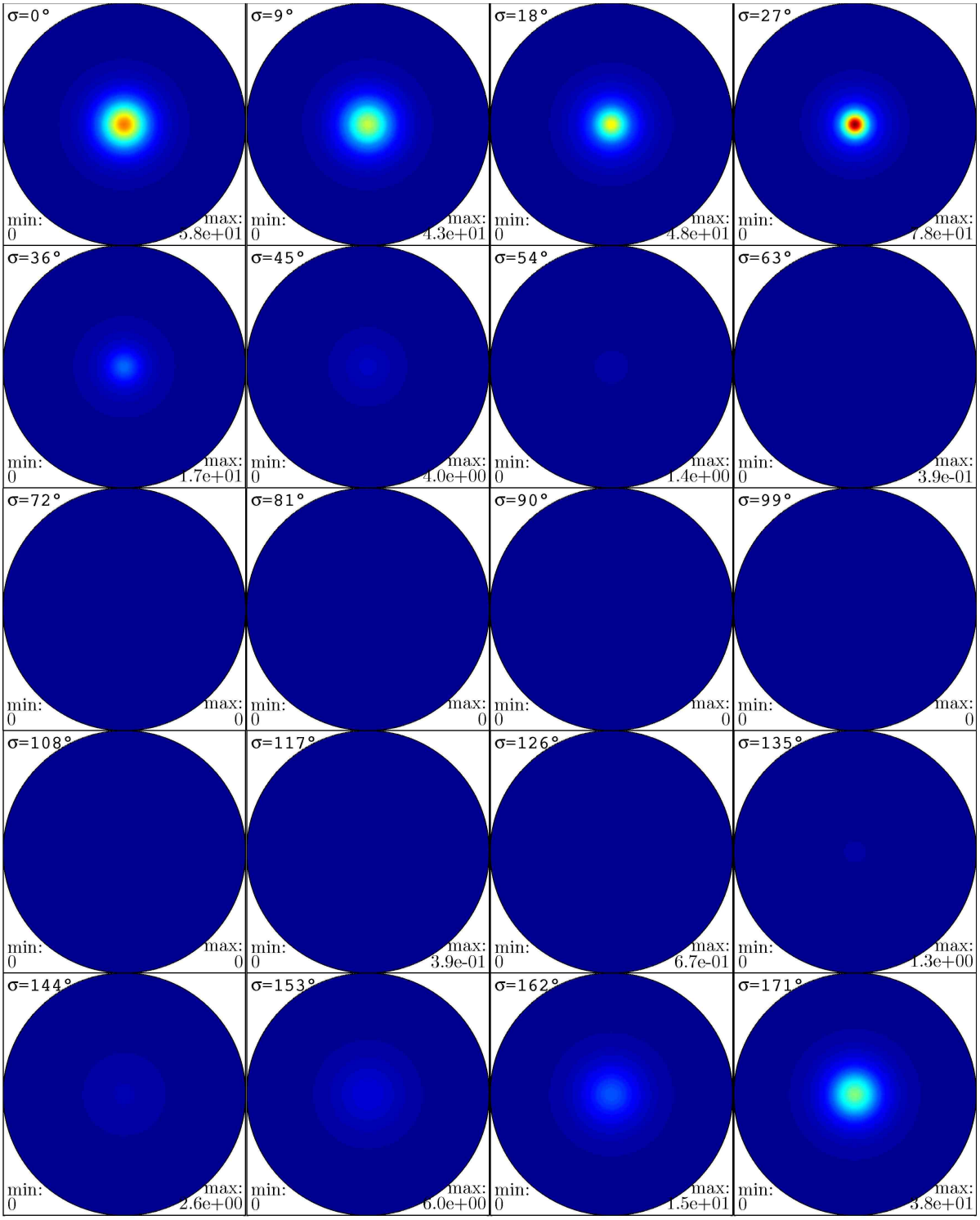

Figure A.7: The sample ODF f_1 plotted as sigma sections.

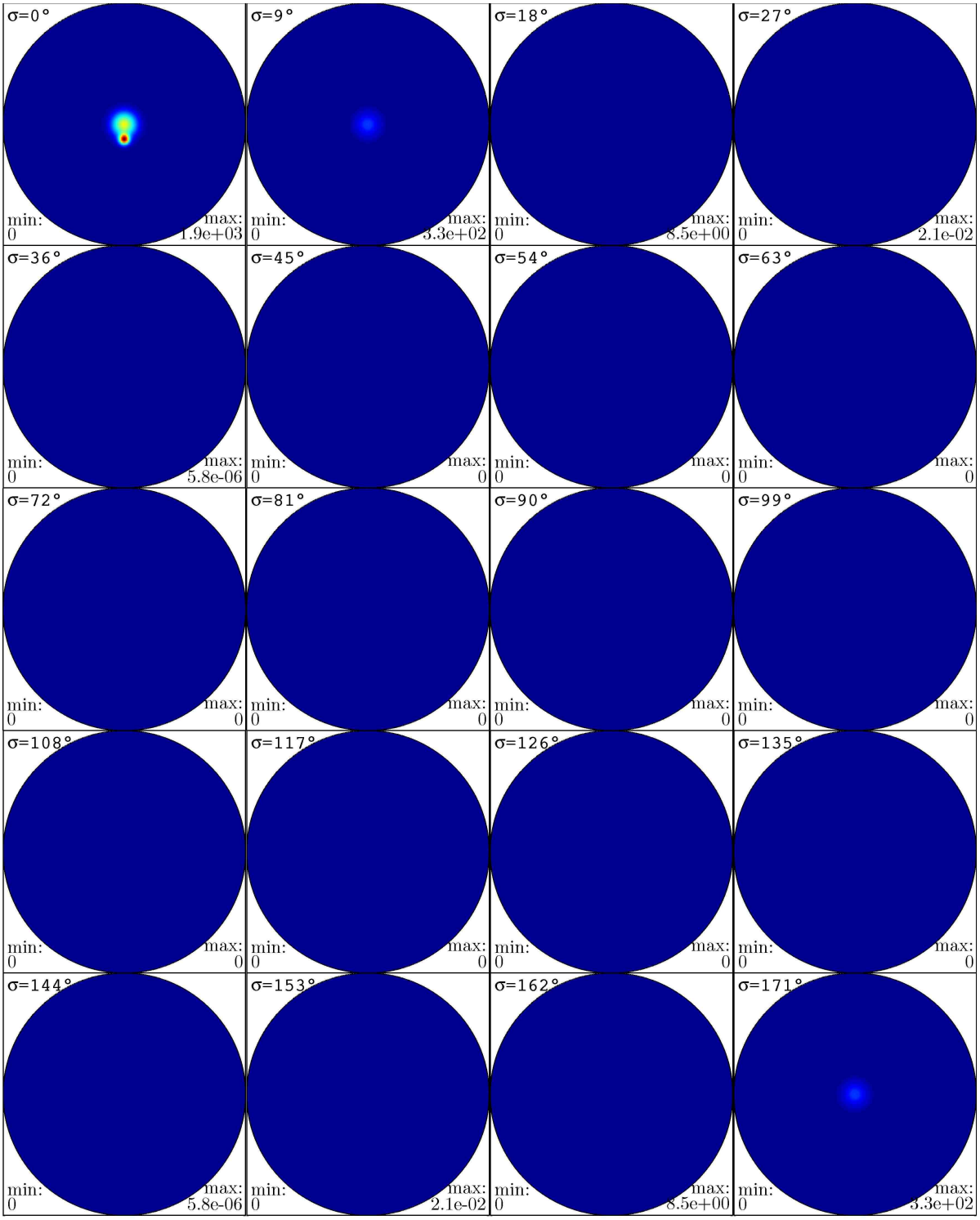

Figure A.8: The sample ODF f_2 plotted as sigma sections.

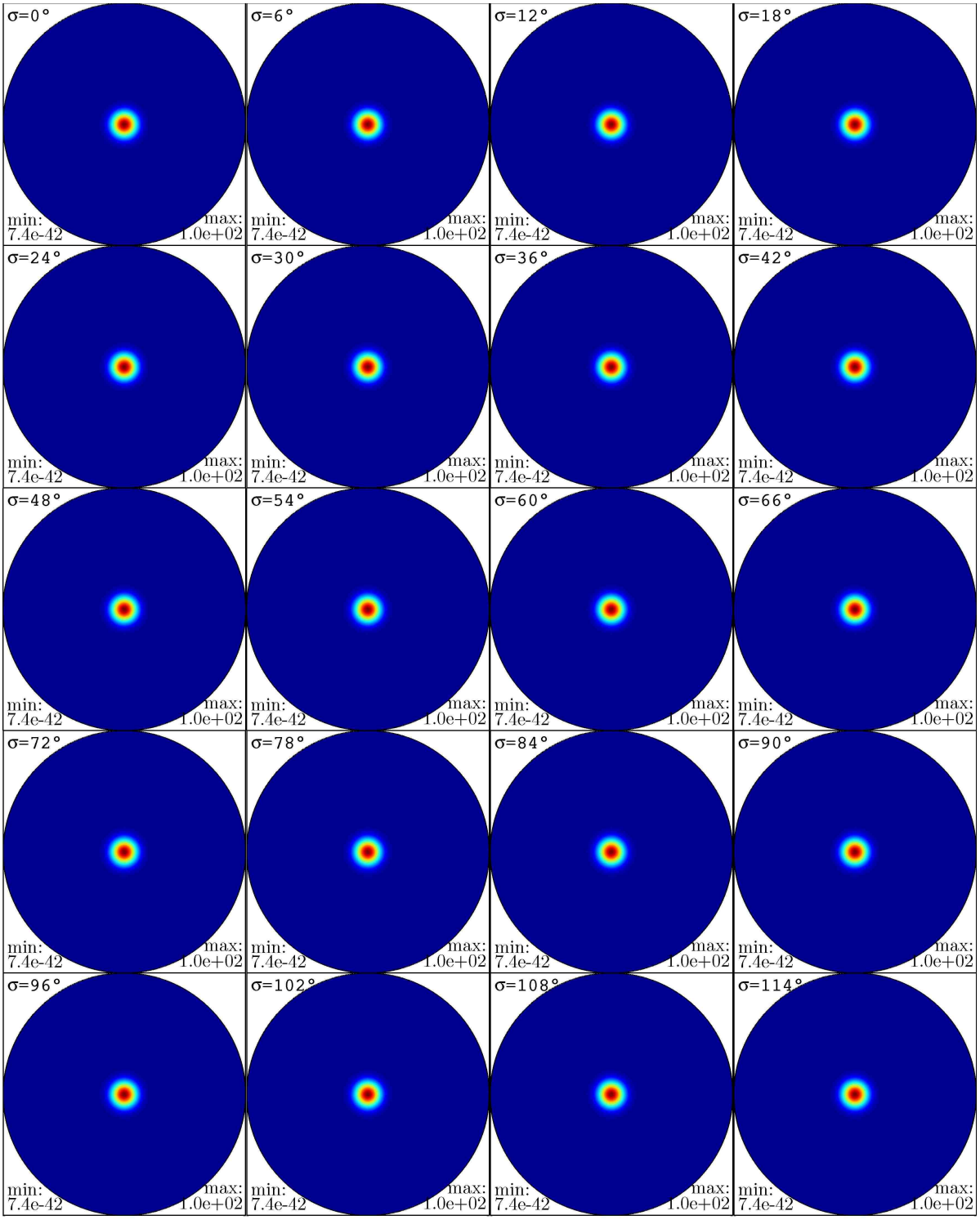

Figure A.9: The sample ODF f_3 plotted as sigma sections.

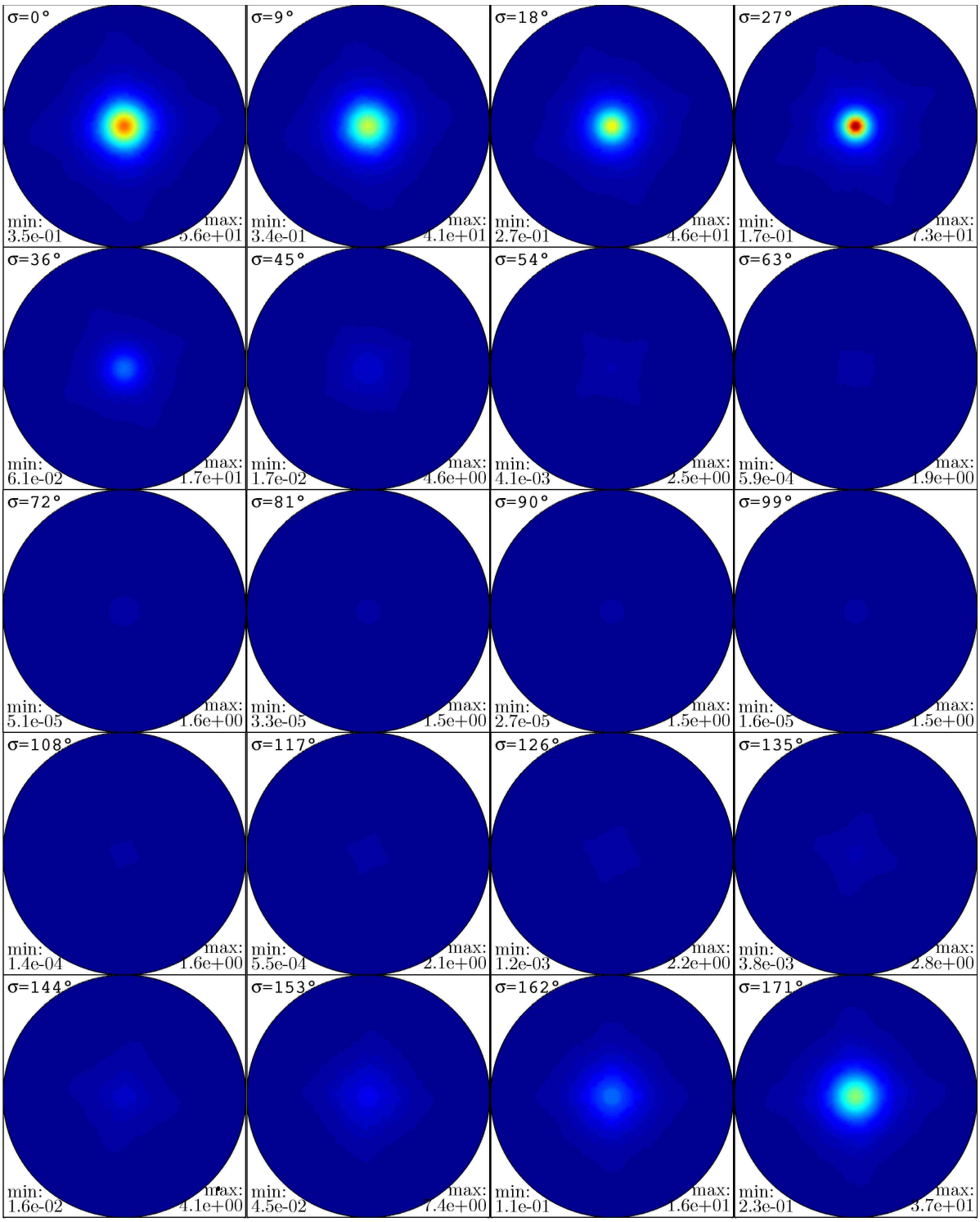

Figure A.10: The MLS ODF estimate of the sample ODF f_1 calculated by Algorithm 5 using the default setting as described in Section 5.4.

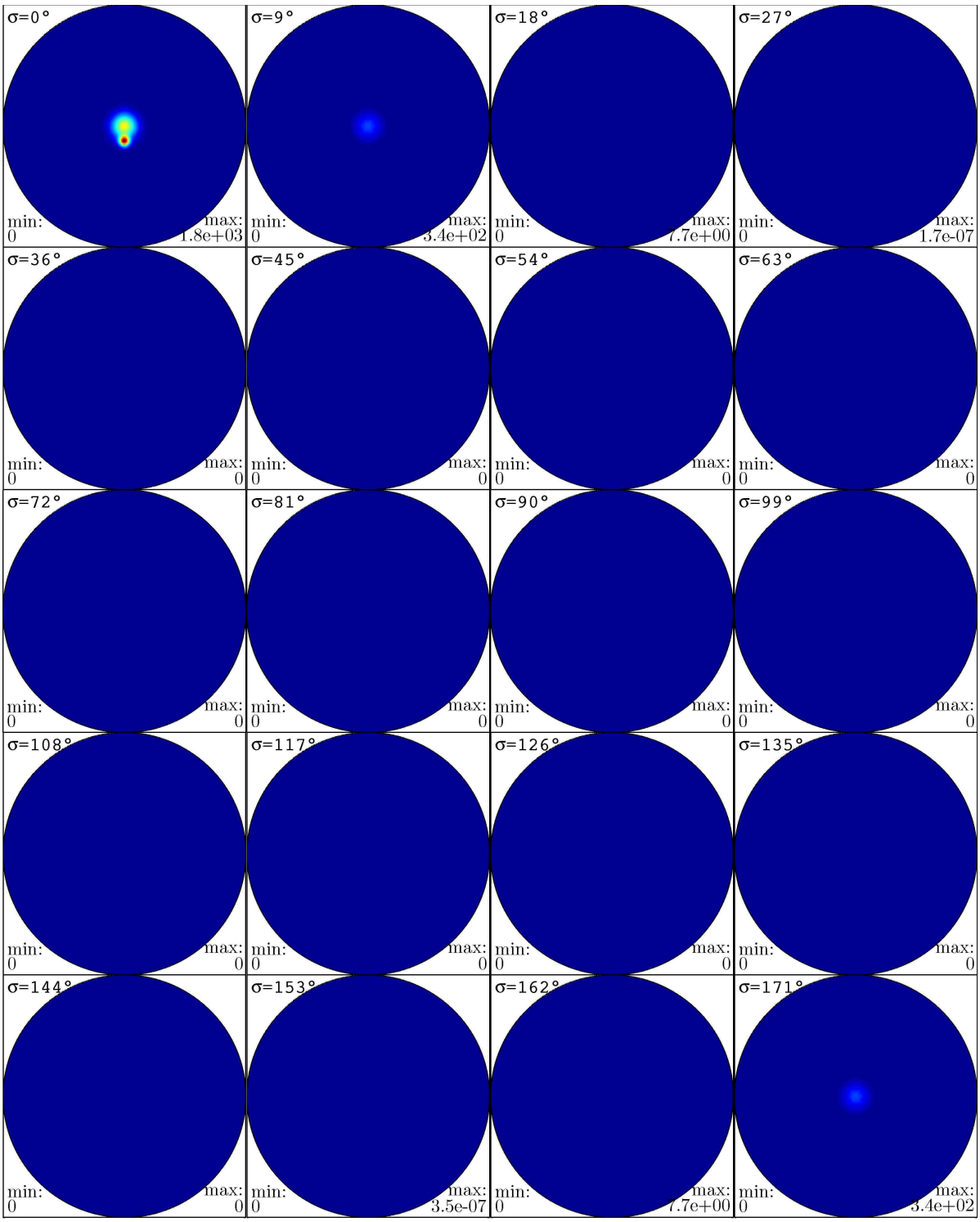

Figure A.11: The MLS ODF estimate of the sample ODF f_2 calculated by Algorithm 5 using the default setting as described in Section 5.4.

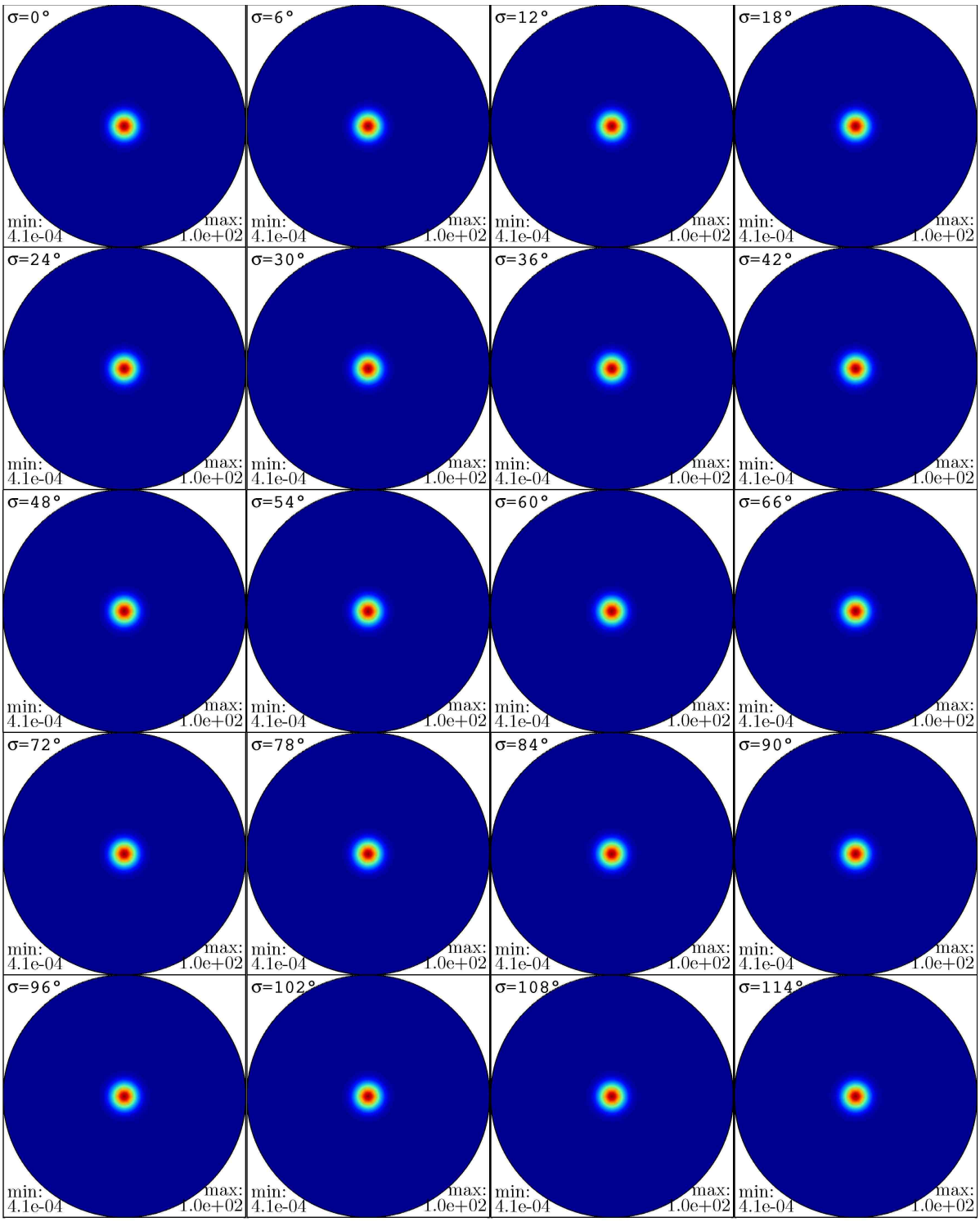

Figure A.12: The MLS ODF estimate of the sample ODF f_3 calculated by Algorithm 5 using the default setting as described in Section 5.4.

Bibliography

J. M. Bardsley and J. Nagy. Covariance-preconditioned iterative methods for nonnegatively constrained image reconstruction. *SIAM J. on Matrix Analysis and Applications*, 27:118–119, 2005.

J. V. Bernier and M. P. Miller. A novel optimization-based pole figure inversion method: comparison with WIMV and maximum entropy methods. *Journal of applied crystallography*, 39:697–713, 2006.

S. Bernstein and H. Schaeben. A one-dimensional radon transform on SO(3) and their application to texture goniometry. *Mathematical Methods in the Applied Science*, 28: 1269–1289, 2005.

S. Bernstein, R. Hielscher, and H. Schaeben. A brief survey of mathematical texture analysis with special emphasis on Radon transforms and their inverses. In L. H. Song, W. Tutschke, and S. Jain, editors, *Methods of Complex and Clifford Analysis*, pages 3–40, Hanoi, august 2005. SAS Internaional Publications, Delhi.

H.-G. Bigalke. *Kugelgeometrie*. Otto Salle Verlag, Verlag Sauerländer, 1984.

H. J. Bunge. Zur Darstellung allgemeiner Texturen. *Z. Metallk.*, 56:872–874, 1965.

H. J. Bunge. *Mathematische Methoden der Texturanalyse*. Akademie Verlag Berlin, 1969.

W. Cheney and W. Light. *A Course in Approximation Theory*. Brooks Cole, 1999.

J. M. Cowley. *Diffraction Physics*. North-Holland Personal Library, 3rd edition, 1995.

W. Feller. *An Introduction to Probability Theory and Its Applications*, volume 1. Wiley, New York, 1971.

W. Freeden. *Constructive Approximation on the Sphere*. Clarendon Press Oxford, 1998.

P. Funk. Über Flächen mit lauter geschlossenen geodätischen Linien. *Math.Ann.*, 74: 278–300, 1913.

P. Funk. Über eine geometrische Anwendung der Abelschen Integralgleichung. *Math. Ann.*, 77:129–135, 1916.

R. J. Gardner. *Geometric Tomography*. Cambridge University Press, 1995.

D. Gurarie. *Symmetries and Laplacian*. North-Holland, 1992.

C. Hammond. *The Basics of Crystallography and Diffraction*. Oxford University Press, 1997.

S. Helgason. *Groups and Geometric Analysis*. Academic Press, 1984.

S. Helgason. *The Radon Transform*. Birkhäuser, 2nd edition, 1999.

K. Helming, S. Matthies, and G. W. Vinel. ODF representation by means of σ-sections. In J. S. Kallend and G.Gottstein, editors, *ICOTOM 8*, pages 17–30, Santa Fee, September 1987.

K. Jähnich. *Vektoranalysis*. Springer Verlag, 1992.

J. Kaipio and E. Somersalo. *Statistical and Computational Inverse Problems*, volume 160 of *Applied mathematical scinces*. Springer, April 2004.

J. Keiner. Fast spherical Fourrier transform and applications, 2005.

J. Keiner and D. Potts. Fast evaluation of quadrature formulae on the sphere. Preprint A-06-07, Universität zu Lübeck, 2006.

B. Kim. *Numerical optimisation methods for image restoration*. PhD thesis, Stanford University, 2002.

P. J. Kostelec and D. N. Rockmore. FFTs on the rotation group. *Santa Fe Institute Working Papers Series Paper*, 03-11-060, 2003.

S. Kunis and D. Potts. Fast spherical Fourier algorithms. *J. Comput. Appl. Math.*, 161 (1):75 – 98, 2003.

A. K. Louis. *Inverse und schlecht gestellte Probleme*. B. G. Teubner Stuttgart, 1989.

S. Matthies. On the reproducibility of the orientation distribution function of texture samples from pole figures (ghost phenomena). *phys. stat. sol. (b)*, 92:K135–K138, 1979.

S. Matthies. *Aktuelle Probleme der quantitativen Texturanalyse*. Akademie der Wissenschaften der DDR, Zentralinstitut für Kernforschung Rossendorf bei Dresden, 1982.

S. Matthies, G. Vinel, and K. Helmig. *Standard Distributions in Texture Analysis*, volume 1. Akademie-Verlag Berlin, 1987.

L. Meister and H. Schaeben. A concise quaternion geometry of rotations. *MMAS*, 28: 101–126, 2004.

A. Morawiec. *Orientations and Rotations*. Springer-Verlag, 2004.

C. Müller. *Spherical Harmonics*. Springer, 1966.

F. Natterer. *The Mathematics of Computerized Tomography*. Wiley - Teubner Series in Computer Science, 1986.

D. I. Nikolayev and H. Schaeben. Characteristics of the ultrahyperbolic differential equation governing pole density functions. *Inverse Problems*, 15:1603–1619, 1999.

D. Potts and S. Kunis. *NFFT, Softwarepackage, C subroutine library*. TU Chemnitz, 2002 – 2006. URL `http://www.tu-chemnitz.de/~potts/nfft`.

D. Potts and G. Steidl. Fast summation at nonequispaced nodes by NFFTs. *SIAM J. on Sci. Comput.*, 24:2013–2037, 2003.

J. Radon. Über die Bestimmung von Funktionen durch ihre Integralwerte längs gewisser Mannigfaltigkeiten. *Ber. Verh. Sächs. Akad. Wiss. Leipzig. Math. Nat. Kl.*, 69:262–277, 1917.

A. G. Ramm and A. Katsevich. *The Radon Transform and Local Tomography*. CRC Press, 1996.

R. J. Roe. Description of crystallite orientation in polycrystal materials III. general solution to pole figure inversion. *J. Appl. Phys.*, 36:2024–2031, 1965.

H. Schaeben. Analogy and duality of texture analysis by harmonics or indicators. *Journal of Scientific Computing*, 9:173–195, 1994.

H. Schaeben. A simple standard orientation density function: The hyperspherical de la Vallée Poussin kernel. *phys. stat. sol. (b)*, 200:367–376, 1997.

H. Schaeben and K. G. v.d. Boogaart. Spherical harmonics in texture analysis. *Tectonophysics*, 370:253–268, 2003.

D. Schwarzenbach. *Kristallographie*. Springer, 2001.

G. Szegö. *Orthogonal Polynomials*. AMS, 4th edition, 1992.

K. van den Boogaart, R. Hielscher, J. Prestin, and H. Schaeben. Kernel-based methods for inversion of the Radon transform on SO(3) and their applications to texture analysis. *Journal of computational and applied mathematics*, 199(1):122–140, 2006.

D. Varshalovich, A. Moskalev, and V. Khersonski. *Quantum Theory of Angular Momentum*. World Scientifc Publishing,Singapore, 1988.

N. J. Vilenkin and A. U. Klimyk. *Representation of Lie Groups and Special Functions*, volume 1. Kluwer Academic Publishers, 1991.

C. R. Vogel. *Computational Methods for Inverse Problems*. Society for Industrial and Applied Mathematics (SIAM), Philadelphia, PA, 2002. ISBN 0-89871-507-5. Frontiers in Applied Mathematics.

A. Vollrath. Fast fourier transforms on the rotation group and applications. Diploma thesis, Universität zu Lübeck, 2006.

G. Wahba. *Spline models for observational data*, volume 59 of *CBMS-NSF Regional Conference Series in Applied Mathematics*. SIAM Philadelphia, 1990.

H. R. Wenk, H. Bunge, J. Kallend, K.Lücke, S.Matthies, J.Pospiech, and P. V. Houte. Orientation distributions: Representation and determination. In J. S. Kallend and G.Gottstein, editors, *ICOTOM 8*, pages 17–30, Santa Fee, September 1987.